

Appendix G:

Pre-failure Limit Equilibrium Analyses

Table of Contents

G1. Introduction	3
G2. Slump Location – 2D Stability Analysis	4
G2.1 Overview	4
G2.2 Model Setup	4
G2.2.1 Method of Analysis	4
G2.2.2 Geometry.....	4
G2.2.3 Pore-Water Pressure Conditions	5
G2.2.4 Material Properties	5
G2.3 Results of Analyses	6
G2.3.1 Screening Analysis	6
G2.3.2 Foundation Parametric Back Analysis	7
G3. Slump Location – 3D Stability Analysis	10
G3.1 Initial Analyses	10
G3.2 Detailed Analyses.....	11
G3.2.1 Overview	11
G3.2.2 Geometry.....	11
G3.2.3 Pore Water Pressure Conditions	12
G3.2.4 Material Properties	12
G3.3 Results of Analyses.....	13
G4. Site Wide - 2D Stability Analysis	14
G4.1 Model Setup	14
G4.1.1 Method of Analysis	14
G4.1.2 Sections Analysed	14
G4.1.3 Geometry.....	15
G4.1.4 Pore-Water Pressure Conditions	15
G4.1.5 Material Properties	15
G4.2 Results of Analysis	16
G5. References	17

List of Tables

Table G2-1: Material parameters for screening analyses	5
Table G2-2: Material parameters adopted for foundation parametric back analyses	6
Table G2-3: Screening Results Ch 1970 – Drained foundation parameters	7
Table G2-4: Screening Results Ch 1970 – Undrained foundation parameters	7
Table G3-1: Material parameters adopted for 3D LEA.....	13
Table G3-2: Effective stress analysis	13
Table G3-3: Undrained strength analysis	13
Table G3-4: Slide information for $\tau/\sigma'v = 0.22$ and tailings $\tau/\sigma'v = 0.06$	13
Table G4-1: Material parameters adopted for site wide analysis	15
Table G4-2: Cases analysed	16
Table G4-3: Site-wide stability results	16

List of Figures

Figure G2-1: Stability section model geometry	5
Figure G2-2: Foundation back analysis, drained tailings $\phi' = 34^\circ$	7
Figure G2-3: Foundation back analysis, drained tailings $\phi' = 40^\circ$	8
Figure G2-4: Foundation back analysis, undrained tailings $\tau/\sigma'v = 0.20$	8

Figure G2-5: Foundation back analysis, undrained tailings $\tau/\sigma_v' = 0.10$	9
Figure G3-1: Surfaces and enclosed volume mesh objects used in 3D numerical model.....	10
Figure G3-2: Cuckoo Search showing lowest FOS - Undrained parameters	11
Figure G3-3: Adopted failure surface geometry	12
Figure G3-4: Cross-section of slump showing modelled failure surface	12

List of Annexures

Annexure GA Figures

Annexure GB Slump - 2D LEA Screening Analyses

Annexure GC Slump - 2D LEA Foundation Back Analyses

Annexure GD Slump – 3D LEA

Annexure GE Site Wide – 2D LEA

G1. Introduction

This appendix summarises the static slope stability analyses undertaken at the slump (Chainage 1970) and selected other locations along the NTSF embankment prior to the failure on March 9, 2018. The analyses at the slump were completed using both 2D and 3D limit equilibrium analyses (LEA) while only 2D limit equilibrium analysis was adopted for the remainder of the NTSF embankment.

The purpose of the limit equilibrium analyses at the slump location was to understand what components of the embankment and foundations were critical in the analysis of the stability and to inform the selection of material parameters (in conjunction with laboratory testing) for deformation (FLAC) analyses reported in Appendix H. The analyses completed at selected locations along the remainder of the NTSF embankment were to understand the stability of the remainder of the NTSF embankment in the context of key learnings from the ITRB investigation and analysis of the slump.

The following appendices were used to provide the inputs to the stability analyses:

- Appendix B – embankment geometry and zoning, topography and pore water pressures;
- Appendix C – geological model of foundations;
- Appendix D – foundation and fill properties;
- Appendix E – tailings properties; and
- Appendix H – modelled phreatic surface for 3D LEA.

Sections G2 and G3, respectively, provide details of the 2D and 3D LEA at the slump, while Section G3 provides details of the site wide 2D LEA.

G2. Slump Location – 2D Stability Analysis

G2.1 Overview

A preliminary screening analysis was completed at the pre-failure slump location to understand the anticipated factors of safety for a range of material properties (both drained and undrained) and to gain an appreciation of the key drivers of the failure mechanism (circular vs. block sliding) and failure surface geometry.

Subsequent to the screening analysis, a back analysis of the foundation strength parameters was completed for various FOS, using the most probable failure mechanism and geometry identified from the field investigation. These analyses in conjunction with laboratory testing of foundation materials were used to inform the selection of foundation design parameters for the deformation analyses.

G2.2 Model Setup

G2.2.1 Method of Analysis

Slope/W from the GeoStudio geotechnical suite was used for the screening analysis, while Rocscience's 2D LEA program Slide 7.0 was used for the foundation parametric back analysis.

Cracking observed on the Stage 7 and Stage 8 crest on the day of the slump did not indicate vertical displacement across the crack. This provided a preliminary indication that the mode of failure was translational rather than circular. On this basis a 'block search mode' was used in conjunction with the Morgenstern and Price method of slices to identify the critical surface for the screening analyses. The screening analyses were also run 'with' and 'without' optimization.

Field investigations were complete before the foundation parametric back analysis was commenced. As the investigations (drillholes CE433 and CE435 and ERI traverses) indicated a relatively shallow failure surface, a planar basal failure surface was adopted for these analyses. Additionally, a tension crack located in the vicinity of the Stages 7 and Stage 8 crests that extended to the level of phreatic surface was added to the model. Optimization of the block sliding surface was not adopted for the analysis as this invariably 'forced' the failure surface and yielded results that did not honour the shallow failure surface indicated by the investigations.

G2.2.2 Geometry

The section analysed was located through the center of the failure, perpendicular to the dam set-out line at Ch 1970. The embankment geometry was determined from both the as-built model, as well as LiDAR completed on the day of the failure. This section is shown in plan on Figure G1 in Annexure GA and the geometry is shown in section on Figure G2-1.

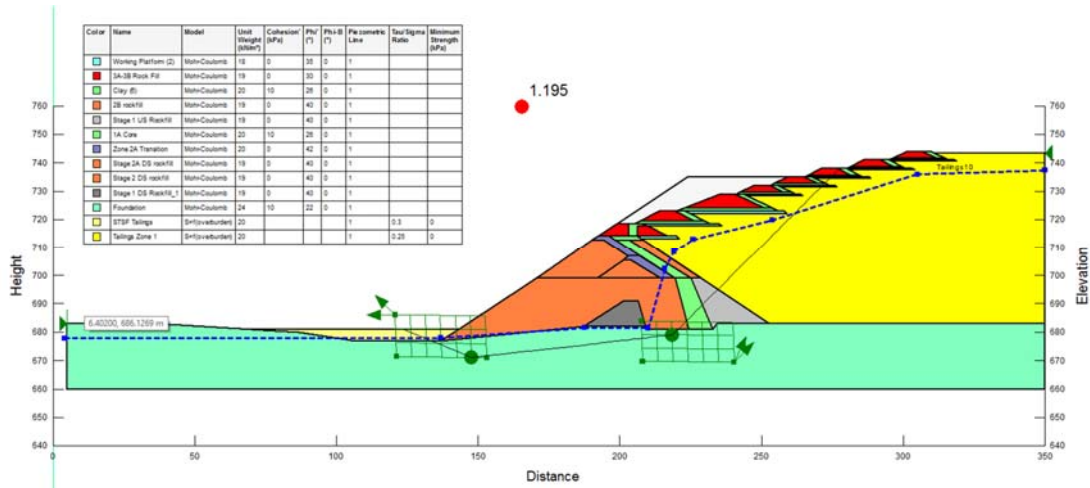


Figure G2-1: Stability section model geometry

G2.2.3 Pore-Water Pressure Conditions

The pore-water pressure conditions within the stability section were based on vibrating wire piezometers readings and pond level measurements taken before the failure. These readings are included in Appendix B and were used in part for the calibration of the 3D hydrogeological model described in Appendix H.

G2.2.4 Material Properties

Screening analyses were undertaken at a stage when only preliminary testing of foundation materials had been completed. The range in values adopted for these analyses and provided in Table G2-1 reflect the very formative nature of the analyses.

Table G2-1: Material parameters for screening analyses

Material	Bulk Density (kN/m ³)	Drained Parameters		Undrained Parameters	
		Cohesion c' (kPa)	Friction ϕ' (°)	Shear Strength Ratio τ/σ'	Minimum Strength (kPa)
Tailings (1)	20	0	34 to 40	0.18 to 0.24	0
Clay Fill (2)	20	10	22 to 26	-	-
Transition (3)	20	0	42	-	-
Rockfill (4)	19	0	40	-	-
Foundation	20	10	20 to 24 (6)	0.35 to 0.50 (5)	50

Notes:

- 1) Tailings undrained shear strength ratios (τ/σ') between 0.18 and 0.24 broadly cover the range in strength ratios determined by ATCW (2017) using vane shear tests. The range in drained strength parameters are based on CIU tests using values recommended by ATCW ($\phi' = 34^\circ$) and values at the peak stress ratio ($\phi' = 40^\circ$) (ATCW, 2017).
- 2) The strength of core materials was reduced from 26° to 22° following CIU triaxial tests completed on STSF samples completed in 2000.
- 3) Slightly higher effective strength parameters have been adopted for transition zones to reflect a finer particle size and higher placement density compared to general rockfill.
- 4) General rockfill strengths of $c' = 0\text{ kPa}$, $\phi' = 40^\circ$ have been adopted for all previous designs. These parameters are consistent with those reported by Leps (1970) for similar rock types

(quartz monzonite, diorite and andesite) to that used in the NTSF at a normal stress close to 1,000kPa.

- 5) Foundation undrained shear strength ratios (τ/σ'_v) between 0.35 and 0.50 cover the range of strength ratios determined from initial Direct Simple Shear (DSS) tests and those adopted by ATCW for the Stage 10 / Buttress design ($\tau/\sigma'_v = 0.51$). However, the latter value was calculated from remoulded triaxial tests where the maximum confining pressure ranged between 200kPa and 500kPa
- 6) Post peak friction angles determined by initial direct shear testing of foundation materials were used for drained strength parameters.

Parameters adopted for major material types and used for the foundation parametric back analyses are provided in Table G2-2. Effective stress strength parameters for the foundation materials (c' , ϕ') were varied to achieve a desired FOS (between 1.0 and 1.3).

Table G2-2: Material parameters adopted for foundation parametric back analyses

Material	Bulk Density (kN/m ³)	Drained Parameters		Undrained Parameters	
		Cohesion c' (kPa)	Friction ϕ' (°)	Shear Strength Ratio τ/σ'_v	Minimum Strength (kPa)
Tailings	20	0	34, 40	0.20, 0.10	0
Clay Fill	20	10	22		
Transition	20	0	42		
Rockfill	20	0	40		

G2.3 Results of Analyses

G2.3.1 Screening Analysis

The results of the screening analyses indicated that the block sliding mechanism adopted for the NTSF embankment failure provided the lowest FOS for the design section and a failure surface geometry that closely replicated the observed pre-failure cracking.

Further conclusions from the screening analyses were:

- For both undrained and drained foundation strength parameters, the FOS was relatively insensitive to the tailings strength parameters, varying by between 0.03 and 0.05 over the range of tailings undrained shear strength ratios adopted.
- A foundation shear strength ratio $\tau/\sigma'_v = 0.35$ provided a FOS that was closest to unity.
- The calculated FOS at the slump location is relatively insensitive to both the clay core and rockfill shear strength parameters, varying by 0.02 and 0.05 respectively, over the range of shear strength parameters analysed.
- For bedrock levels below RL 670, (equivalent to a clay depth of 6.5 m at the toe of the embankment), the calculated FOS varied by less than 0.01.

The results of this screening analysis for both drained and undrained foundation parameters is summarised in Table G2-3 and Table G2-4. Selected Slope/W plots for these analyses are included in Annexure GB.

Table G2-3: Screening Results Ch 1970 – Drained foundation parameters

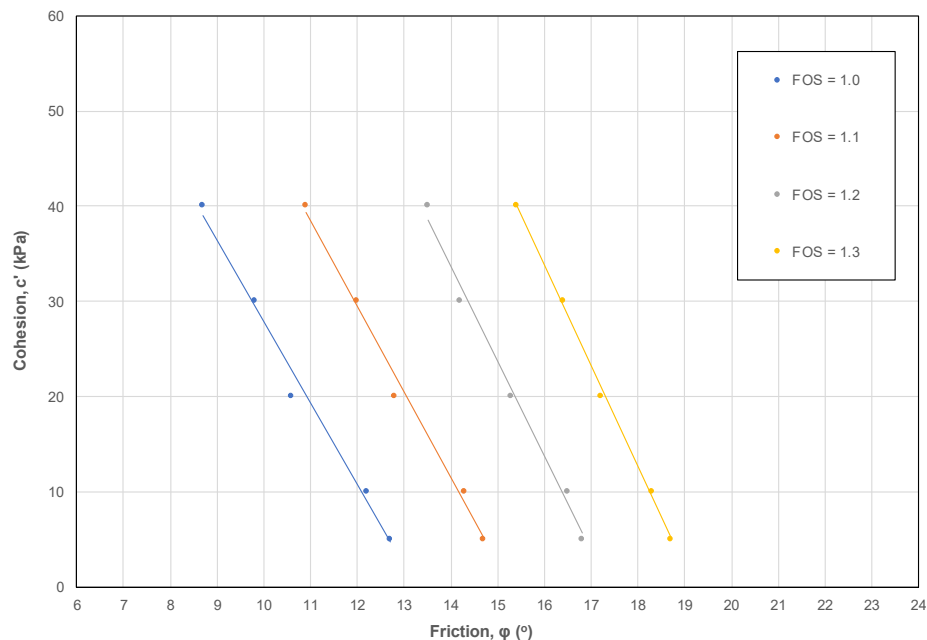
Tailings Strength (τ/sv')	Foundation Strength			
	$C'=10 \text{ kPa},$ $\varphi=20^\circ$	$C'=10 \text{ kPa},$ $\varphi=22^\circ$	$C'=10 \text{ kPa},$ $\varphi=24^\circ$	$C'=10 \text{ kPa},$ $\varphi=26^\circ$
0.20	1.06	1.14	1.19	1.25

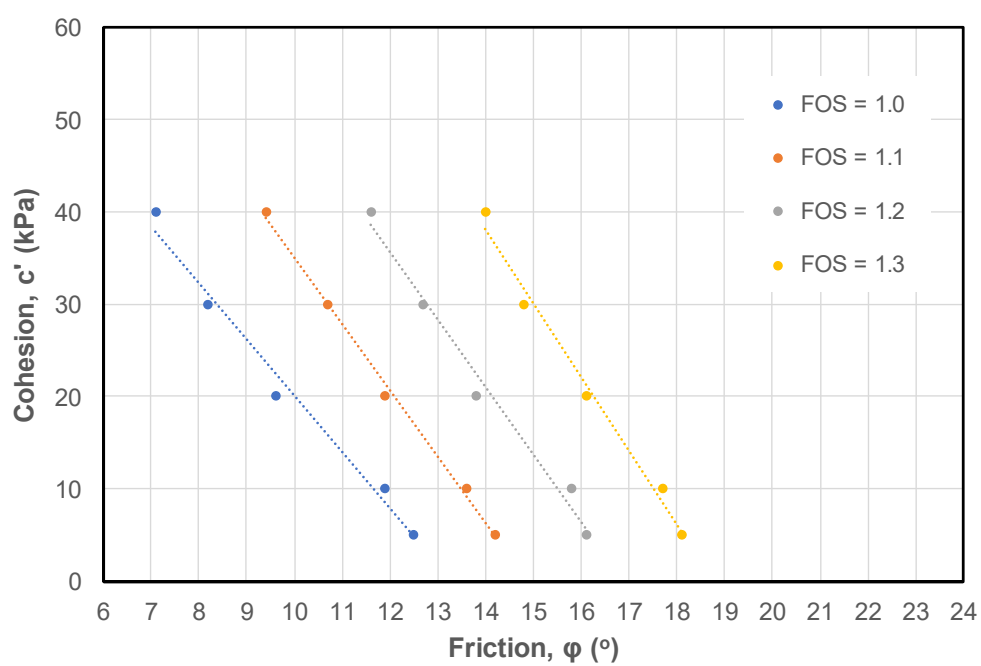
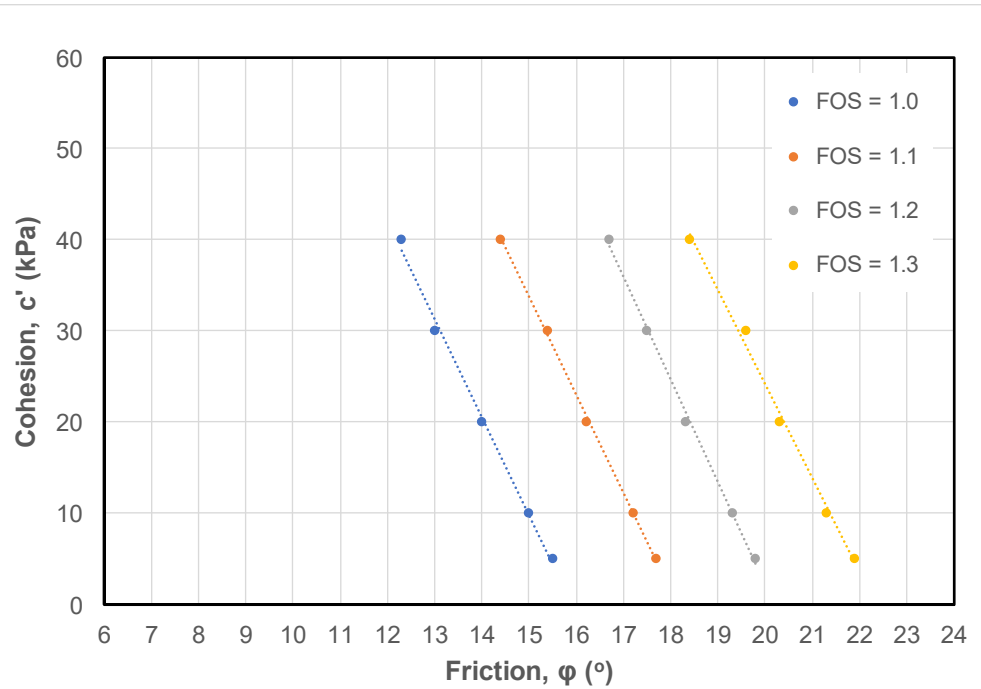
Table G2-4: Screening Results Ch 1970 – Undrained foundation parameters

Tailings Strength (t/sv')	Foundation Strength (t/sv')			
	0.35	0.40	0.45	0.5
0.20	1.00	1.10	1.18	1.26

G2.3.2 Foundation Parametric Back Analysis

Using the combination of material parameters provided in Table G2-2, the drained foundation parameters required to achieve a FOS = 1.0, 1.1, 1.2 and 1.3 were determined. This was achieved by first identifying the critical failure surface for $\varphi'=18^\circ$ and $c' = 5, 10, 20, 30$ and 40kPa . For the critical failure surfaces, φ' was varied (using a sensitivity function) to achieve the respective FOS. The results of the analyses are summarized in Figure G2-2 to Figure G2-5, while selected Slide 7.0 outputs are included in Annexure GC.

**Figure G2-2: Foundation back analysis, drained tailings $\varphi' = 34^\circ$**

Figure G2-3: Foundation back analysis, drained tailings $\phi' = 40^\circ$ Figure G2-4: Foundation back analysis, undrained tailings $\tau/\sigma_v' = 0.20$

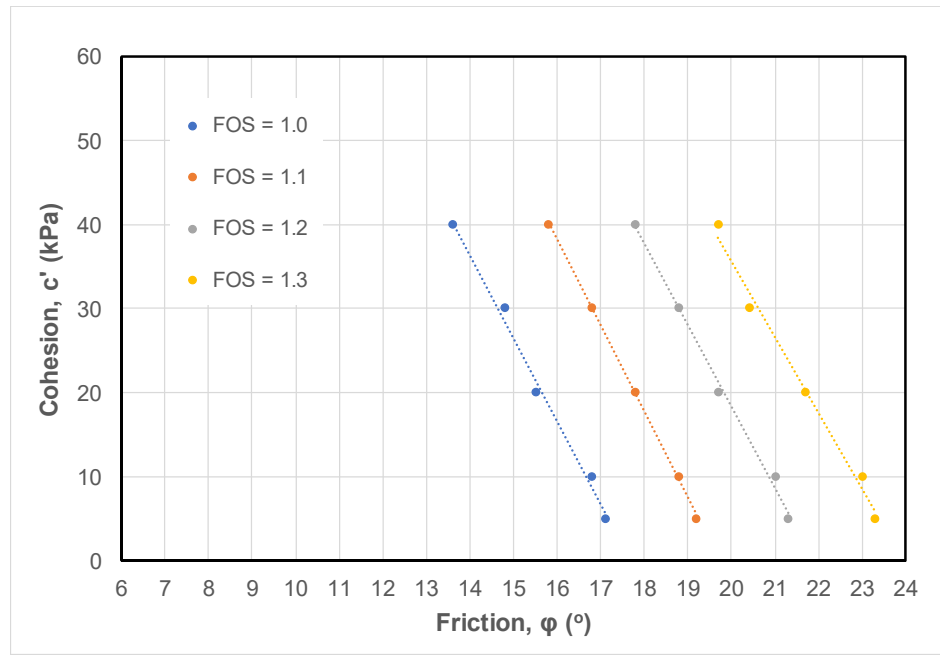


Figure G2-5: Foundation back analysis, undrained tailings $\tau/\sigma_v' = 0.10$

FOS determined in the earlier screening analyses are lower than those calculated in the foundation parametric back analyses. This is attributed to the 'optimisation routine' used in the earlier analyses which resulted in a deeper failure surface and a failure surface extending behind the Stage 10 crest for drained foundation strength parameters. Both these conditions were not consistent with the site observations.

G3. Slump Location – 3D Stability Analysis

G3.1 Initial Analyses

Initial 3D LEA stability runs for the NTSF embankment failure were undertaken directly by Soilvision Systems Ltd (Soilvision) (2018). The purpose of the 3D LEA was to undertake a calibration of the existing failure and assess the impact of 3D geometry on the calculated FOS.

Prior to the 3D model setup, 2D LEA was undertaken using 2D SVSLOPE to replicate the previous 2D SLOPE/W models and to ensure consistency between software packages. A comparison of the results indicated that for the ‘Block Search’ method, the results of Non-Optimization FOS were similar between SVSLOPE and SLOPE/W with an average difference of 1.8%. With optimization, SVSLOPE gave slightly lower FOS results compared to Slope/W with an average difference of 4.4%. ‘Cuckoo-Search’ and ‘Greco-Search’ methods were also undertaken by Soilvision. The Greco-Search often gave the lowest FOS, however values were generally within 1%. With Non-Optimization, the Greco-Search produced about 14% lower FOS than Block-Search in SLOPE/W and 7% with Optimization.

The Soilvision software package SVDESIGNER was used to build the 3D LEA model using the preconstruction ground surface, embankment zones, tailings surface and groundwater, all provided in 3D DXF format.

A comparison of FOS between 2D and 3D Cuckoo-Search results, without optimization, indicates that the 3D FOS is from 11% to 21% (average of 17.4%) greater than 2D FOS. With optimization, these numbers are reduced and range from 5% to 15% with an average of 8.8%.

When comparing 3D FOS values to 2D results, the 3D FOS values are typically greater due to 3D effects (Chaudhury, Domingos, Gitirana, Fredlund, & Lu, 2016). On a regular geometry, the 3D FOS could increase between 10% and 40% compared to 2D FOS, while for slopes with complex geometry, the difference can be significantly more (Stark & Eid, 1998).

The 3D model developed by Soilvision for the initial 3D LEA is shown as Figure G3-1, while a typical output is presented as Figure G3-2.

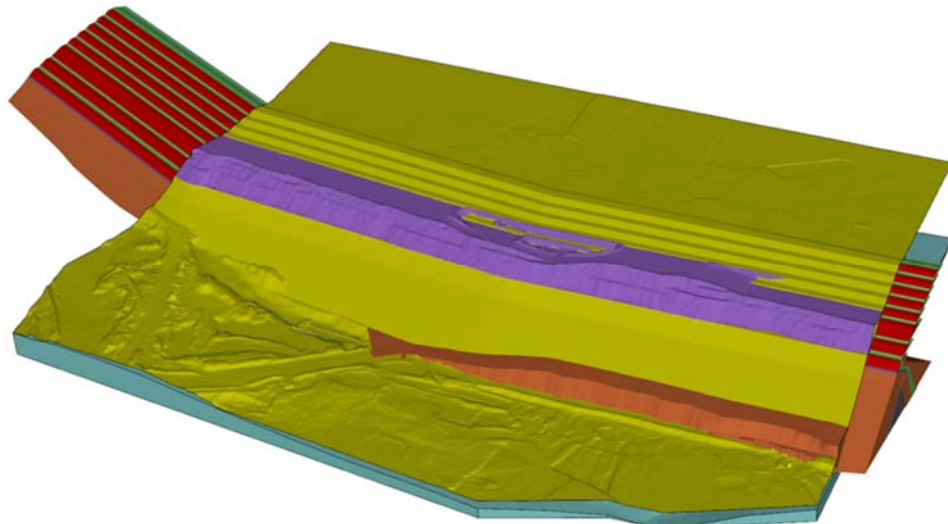


Figure G3-1: Surfaces and enclosed volume mesh objects used in 3D numerical model

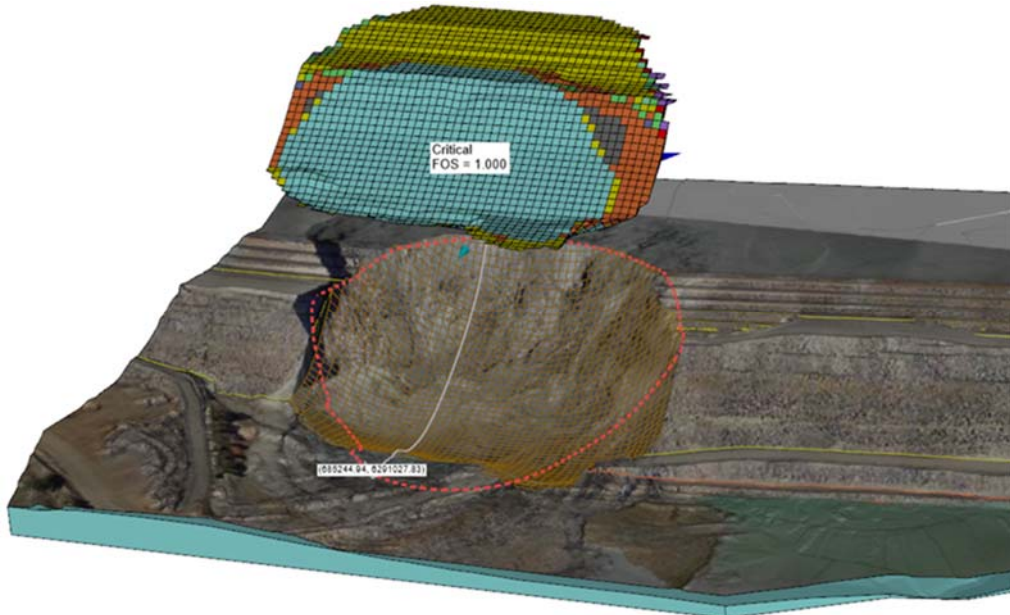


Figure G3-2: Cuckoo Search showing lowest FOS - Undrained parameters

G3.2 Detailed Analyses

G3.2.1 Overview

Following the investigations on the slump (CE433, CE435 and ERI) it became apparent that the search methods (Cuckoo and Greco) used by SVSLOPE to find the minimum FOS were only applicable to ellipsoidal failure surfaces. As it was considered that the ellipsoidal failure surface did not honour the field observations, the 3D LEA using SVSLOPE was completed using a fully specified failure surface. This is discussed in the following sections.

G3.2.2 Geometry

Hatch rebuilt the 3D model for the analysis using SVDESIGNER in a similar manner to that undertaken for the initial analyses. However, in the latter case the model was extended to the west and Stages 4 to 10 of the NTSF were modelled as a single solid volume rather than individual stages.

The failure surface adopted for the detailed analyses was modelled using twelve (12) planar surfaces as indicated on Figure G3-3. The tension cracks observed on Buttress 1 and Stage 8 crest were modelled as vertical planes extending to RL720. The arcuate nature of the tension crack was achieved using two vertical planes crossing Buttress 1 and orientated at 45° to the axis of the NTSF.

A section parallel to the axis of the NTSF and located near the outer edge of Buttress 1 shows the relationship between the modelled failure surface, 19th March 2018 topography and the pre-construction surface. A longitudinal section through the slump (showing the inferred failure surface) is presented as Figure C3 (Appendix C).

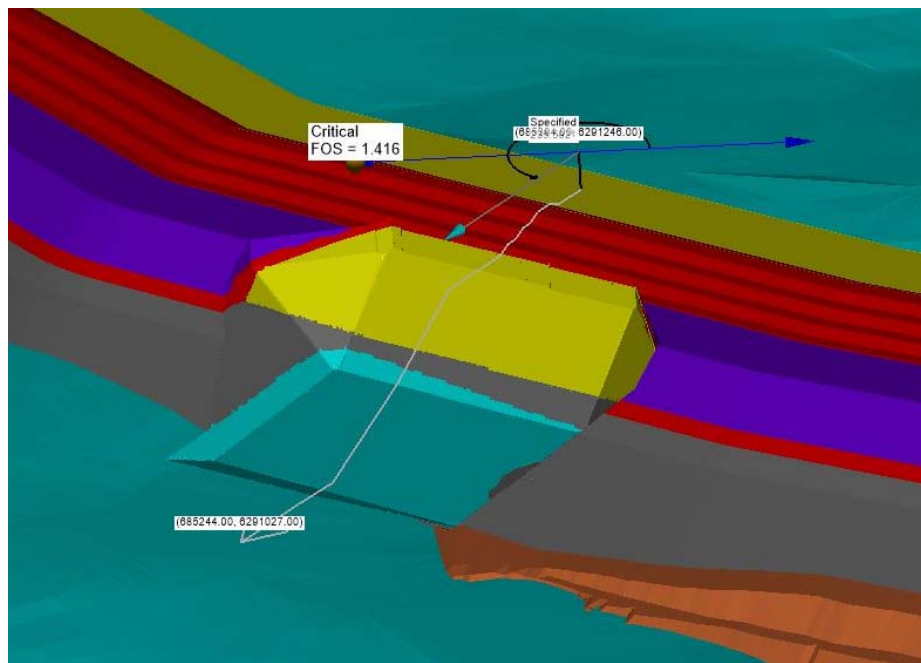


Figure G3-3: Adopted failure surface geometry

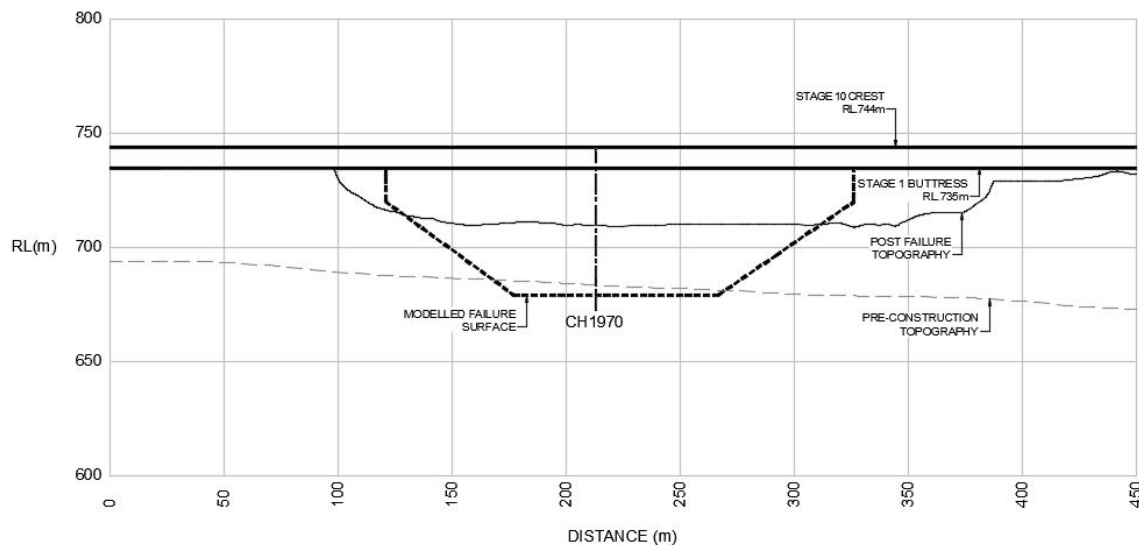


Figure G3-4: Cross-section of slump showing modelled failure surface

G3.2.3 Pore Water Pressure Conditions

A 3D model based on the results of vibrating wire piezometers readings and pond level measurements taken before the failure was used for the initial and detailed undrained strength analyses (USA) using the specified failure surface.

The phreatic surface output from the 3D FEFLOW model developed as part of the hydrogeological investigations (Appendix H) was incorporated into the effective stress analysis (ESA).

G3.2.4 Material Properties

Material properties adopted for the 3D LEA are similar to those adopted for the 2D LEA and are shown in Table G3-1. The strength of vertical planes in the failure surface (tension cracks) was nulled.

Table G3-1: Material parameters adopted for 3D LEA

Material	Bulk Density (kN/m ³)	Drained Parameters		Undrained Parameters	
		Cohesion c' (kPa)	Friction ϕ' (°)	Shear Strength Ratio t/sv'	Minimum Strength (kPa)
Tailings	20	0	32	0.20, 0.10, 0.06	0
Foundation	20	10, 0	16, 20	0.2	0
Clay Fill	20	10	22	0.34	0
Transition	20	0	42		
Rockfill	20	0	40		

G3.3 Results of Analyses

The results of the 3D LEA using SVSLOPE are summarized in Table G3-2 and Table G3-3, while selected SVSLOPE outputs are provided in Annexure GD.

Table G3-2: Effective stress analysis

Foundation Strength		Factors of Safety	
		Tailings Strength	
Cohesion c' (kPa)	Friction ϕ' (°)	Drained (c', ϕ')	Undrained t/sv' = 0.2
		1.385	1.216
10	20	1.567	1.398

Table G3-3: Undrained strength analysis

Foundation Strength t/sv'	Factors of Safety		
	Tailings Strength (t/sv')		
	0.20	0.10	0.06
0.2	1.041	0.968	0.939

Slide details for the case; foundation $\tau / \sigma v' = 0.2$ and tailings $\tau / \sigma v' = 0.06$ are provided in Table G3-4.

Table G3-4: Slide information for $\tau / \sigma v' = 0.2$ and tailings $\tau / \sigma v' = 0.06$

Slope Information	
Calculation Method:	M-P
Search Method:	Fully Specified Only
FOS:	0.939
Total Weight:	1.519E+007 (kN)
Total Volume:	7.681E+005 (m ³)
Total Activating Moment:	6.429E+008 (kNm)
Total Resisting Moment:	6.039E+008 (kNm)
Resisting Moment due to Vertical Side Shear:	-1.038E+006 (kNm)
Total Activating Force:	4.245E+006 (kN)
Total Resisting Force:	3.986E+006 (kN)
Resisting Force due to Vertical Side Shear:	-1.855E+004 (kN)
Total Active Columns:	2593
Total Sliding Surface Area:	3.54E+04 (m ²)
Center Point:	X: 685297.473 Y: 6291103.477 Z: 826.128 (m)
Rotated Center Point:	X*: 685221.868 Y*: 6291245.101 (m)
Slip Direction Angle:	55.592 (degrees)

G4. Site Wide - 2D Stability Analysis

G4.1 Model Setup

G4.1.1 Method of Analysis

Stability analyses were completed on a further five sections along the NTSF embankment. The sections analysed are shown in plan on Figure G1 in Annexure GA.

Rocscience's 2D LEA program Slide 7.0 utilizing Morgenstern and Price's method of slices (1965) was used for the analysis. With the exception of areas where the foundation was shallow and planar sliding was a potential failure mode, a 'circular search mode' was used to identify the critical failure surface. Where planar sliding was a potential failure mode (CH 1650), a 'block search mode' was used to define the critical failure surface.

As the purpose of the analysis was to assess the stability of the NTSF in the context of conditions contributing to the NTSF embankment failure, the analyses presented in this section have focused solely on potential slip failures through foundation materials. The analyses have not considered potential "intermediate" sliding surfaces through the embankment materials, the stability of upstream raised sections, nor the stability under seismic loading as these failure modes were beyond the scope of ITRB's brief.

G4.1.2 Sections Analysed

The NTSF embankment failure occurred adjacent to the margin of Tertiary basalt which was underlain by paleo-alluvium and low density weathering product of the Forest Reef Volcanics (FRV Unit A). An inspection of the NTSF geological map (Figure B1 Annexure BA) indicates that this is likely to be the only location where similar conditions exist along the NTSF embankment.

Notwithstanding the above, five sections were chosen for stability analysis which represent both critical and representative NTSF foundation conditions. The locations of the sections are shown on Figure G1 Annexure GA. A brief description of the geology and reference drillholes at each section is provided below.

- Section A - Chainage 990
 - Silurian Sediments (Cadia Coach Shale) – far right abutment; BH108
- Section B - Chainage 1650
 - Tertiary Basalt – adjacent to western side of slump; CE413, CE430
- Section C - Chainage 2210
 - Forest Reef Volcanics – adjacent to eastern side of slump; CE406, CE431, CE432
- Section D - Chainage 2500
 - Forest Reef Volcanics – maximum embankment height; BH017
- Section E - Chainage 2800
 - Forest Reef Volcanics – left abutment; CE403

G4.1.3 Geometry

The embankment geometry at each section was determined from both the as-built model, as well as LiDAR completed on 19 March 2018. The foundation elevation was inferred from construction drawings and pre-construction topography while the foundation stratigraphy was based on subsurface investigations undertaken in the vicinity of the NTSF on behalf of the ITRB and other parties as detailed in Appendix C.

G4.1.4 Pore-Water Pressure Conditions

The pore-water pressure conditions at each section were based on vibrating wire pore pressure measurements and hydrogeological modelling included in Appendix H.

G4.1.5 Material Properties

Parameters used in the analyses were based, where possible, on laboratory testing of foundation and fill materials and tailings described in Appendix D and Appendix E respectively. With the exception of tailings, parameters used in the analysis are effective stress parameters to replicate material behavior under long term drained conditions under static loading. A conservative approach has been adopted by using an undrained shear strength ratio (τ/σ_v' = 0.2) for the tailings.

Material properties used in the analyses are provided in Table G4-1, and supported with references in the following notes.

Table G4-1: Material parameters adopted for site wide analysis

Material	Bulk Density (kN/m ³)	Drained Parameters		Undrained Shear Strength Ratio, τ/σ_v'
		Cohesion c' (kPa)	Friction ϕ' (°)	
Tailings	20	0	32	0.2
Clay Fill (1)	20	10	22	-
Transition Fill (3)	20	0	42	-
Rockfill (3)	18-21	0	35-40	-
Residual Soil developed over Silurian Sedimentary Strata (4)	20	4	23	-
Silurian Sedimentary Strata (4)	20	4	27	-
Residual Soil developed over Basaltic (5)	20	30	21.3	-
Basalt (6)	25	1000	35	-
Paleo Alluvium (7)	20	38.5	27	-
Forest Reef Volcanics Unit A (8)	19	0	16	-
Forest Reef Volcanics Unit B (9)	20	43 - 55	22.5 – 24.6	-
Forest Reef Volcanics MW (10)	22	150	32	-

Notes:

- 1) Based on CIU testing completed as part of the ITRB investigation.
- 2) This remains unchanged from earlier assessments.
- 3) This remains unchanged from earlier assessments. The bulk density and friction angle vary slightly to accommodate change in maximum particle size as well as source material.
- 4) Based on CIU testing completed on Weemalla Formation, undertaken by GHD as part of the 2018 STSF investigation.

- 5) Based on DSS tests completed on samples retrieved as part of the ITRB investigation.
- 6) Parameters calculated using RocData using: UCS=20MPa, GSI=40 mi=5, Ei=25GPa.
- 7) Based on CIU testing completed as part of the ITRB investigation.
- 8) Based on CIU testing completed on samples as part of the ITRB investigation.
- 9) Lower bound and median parameters for Unit B are based on CIU testing completed on samples undertaken as part of ITRB and GHD investigation, detailed in Appendix D.
- 10) Parameters calculated using RocData using: UCS=3MPa, GSI=35, mi=20, Ei=500MPa.

G4.2 Results of Analysis

For each section up to four cases were analysed using either drained or undrained parameters for tailings and median or lower bound parameters for Unit B of the Forest Reef Volcanics as indicated in Table G4-2. The results of the analyses are summarised in Table G4-3, while graphical output is included in Annexure GE.

Table G4-2: Cases analysed

Case	Parameter Adopted	
	Tailings	Unit B FRV
1	Drained	Lower Bound
2	Drained	Median
3	Undrained	Lower Bound
4	Undrained	Median

Table G4-3: Site-wide stability results

Section	Factor of Safety			
	1	2	3	4
A (1)	2.097		1.655	
B (1)	1.791		1.605	
C	1.385	1.506	1.208	1.331
D	1.428	1.538	1.256	1.361
E	1.352	1.485	1.188	1.317

Notes:

- (1) Unit B FRV not intersected in these sections

G5. References

- Chaudhury, K., Domingos, V., Gitirana, G., Fredlund, M., & Lu, H. (2016). Three-dimensional slope stability: Geometry effects. *Tailings and Mine Waste*. Keystone, CO.
- Morgenstern, N. R., & Price, V. E. (1965). The analysis of the stability of general slip surfaces. *Geotech., London*, 15, 1, 79-93.
- SoilVision Systems Ltd. . (2018). SVOFFICE5 - Help Manual.
- Stark, T., & Eid, H. (1998). Performance of Three-Dimensional Slope Stability Methods in Practice. *Journal of Geotechnical and Geoenvironmental Engineering*, 1049-1060.

Annexure GA Figures

Figure G1 NTSF Stability Sections Location Plan



NOTES

1. ALL DIMENSIONS, ELEVATIONS AND COORDINATES ARE IN METERS, EXCEPT WHERE INDICATED OTHERWISE.
2. HORIZONTAL DATUM CORRESPONDS TO GDA 94 MGA ZONE 55.
3. VERTICAL DATUM CORRESPONDS TO AHD.
4. LIDAR SURVEY COMPLETED BY AAM ON THE 19TH OF MARCH 2018.

NTSF STABILITY SECTIONS LOCATION PLAN

CADIA NTSF FAILURE INDEPENDENT TECHNICAL REVIEW BOARD

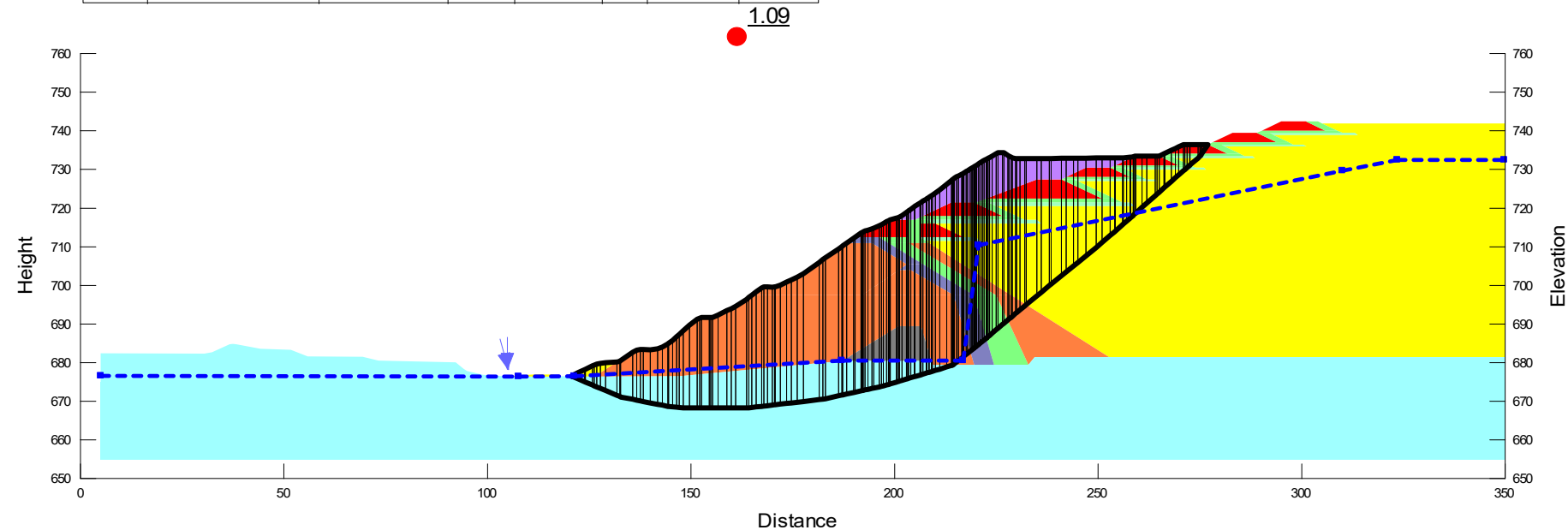
FIGURE G1

DESIGNED BM	DRAWN PK	APPROVED
DATE 20-12-2018	DWG. No. H356804-00000-22A-272-0007	

Annexure GB

Slump - 2D LEA Screening Analyses

Color	Name	Model	Unit Weight (kN/m³)	Cohesion' (kPa)	Phi' (°)	Tau/Sigma Ratio	Minimum Strength (kPa)
Red	Rock Fill	Mohr-Coulomb	21	0	40		
Light Green	Working Platform	Mohr-Coulomb	18	0	35		
Orange	2B rockfill	Mohr-Coulomb	19	0	40		
Light Green	Clay Core	Mohr-Coulomb	20	10	26		
Dark Blue	Zone 2A Transition	Mohr-Coulomb	20	0	42		
Grey	Stage 1 DS Rockfill_1	Mohr-Coulomb	21	0	40		
Purple	DS Berm	Mohr-Coulomb	19	0	40		
Yellow	Tailings su/p=0.20	S=f(overburden)	20			0.2	0
Cyan	Foundation su/p=0.40	S=f(overburden)	24			0.4	50



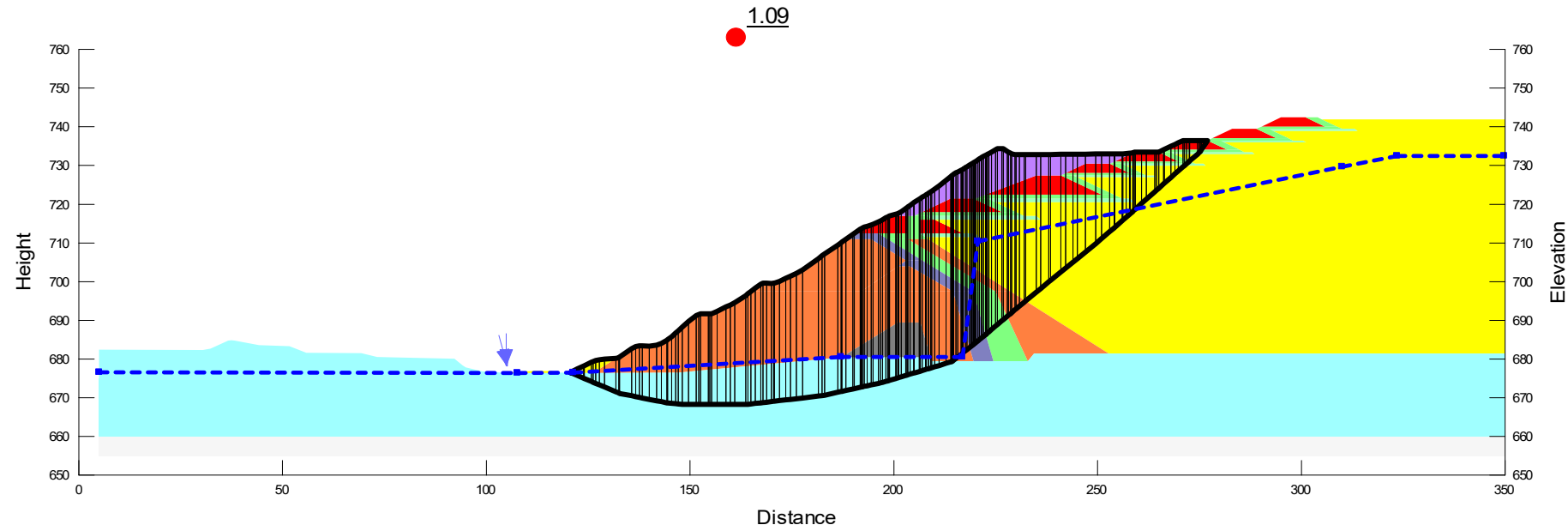
Project No.	H356804	
Prepared by:	ZY	
Checked by:	IG	13-Jun-18
Revision	A	13-Jun-18

CH 1950
Tailings $t/\sigma v' = 0.20$
Foundation $t/\sigma v' = 0.4$
Bedrock @ RL655m

HATCH

Cadia Mine
NTSF Failure Assessment
FIGURE 1

Color	Name	Model	Unit Weight (kN/m³)	Cohesion' (kPa)	Phi' (°)	Tau/Sigma Ratio	Minimum Strength (kPa)
Red	Rock Fill	Mohr-Coulomb	21	0	40		
Light Green	Working Platform	Mohr-Coulomb	18	0	35		
Orange	2B rockfill	Mohr-Coulomb	19	0	40		
Light Blue	Clay Core	Mohr-Coulomb	20	10	26		
Dark Blue	Zone 2A Transition	Mohr-Coulomb	20	0	42		
Grey	Stage 1 DS Rockfill_1	Mohr-Coulomb	21	0	40		
Purple	DS Berm	Mohr-Coulomb	19	0	40		
Yellow	Tailings su/p=0.20	S=f(overburden)	20			0.2	0
Cyan	Foundation su/p=0.40	S=f(overburden)	24			0.4	50



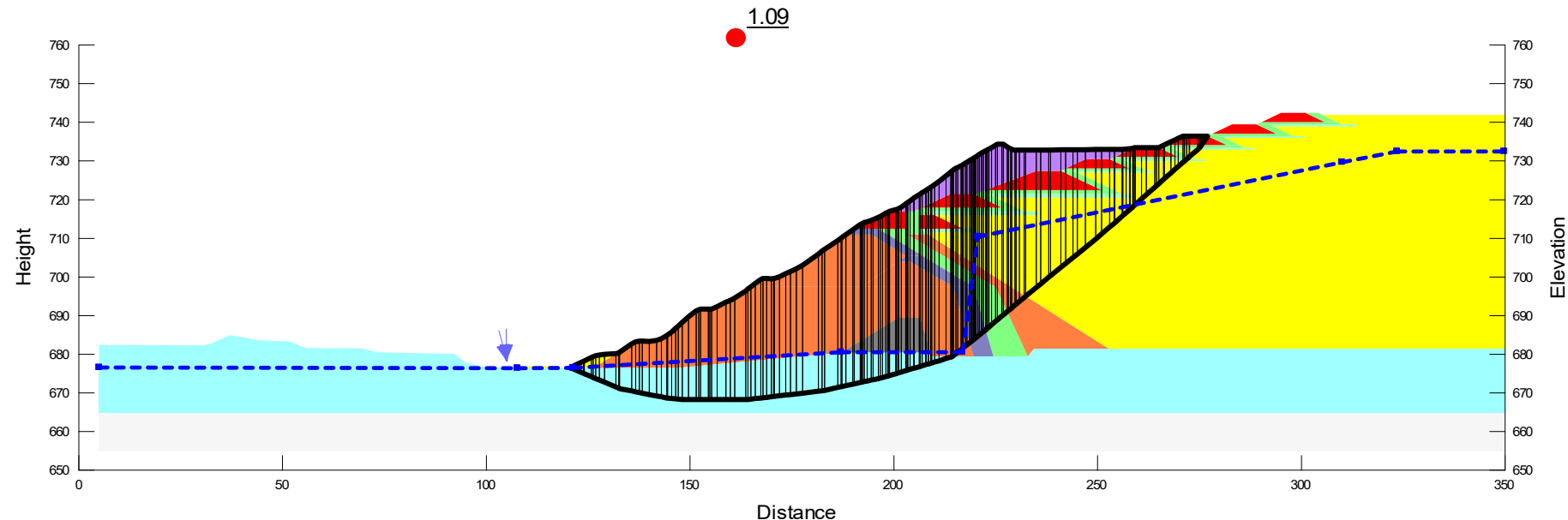
Project No.	H356804	
Prepared by:	ZY	
Checked by:	IG	13-Jun-18
Revision	A	13-Jun-18

CH 1950
Tailings $t/\sigma v' = 0.20$
Foundation $t/\sigma v' = 0.4$
Bedrock @ RL660m

HATCH

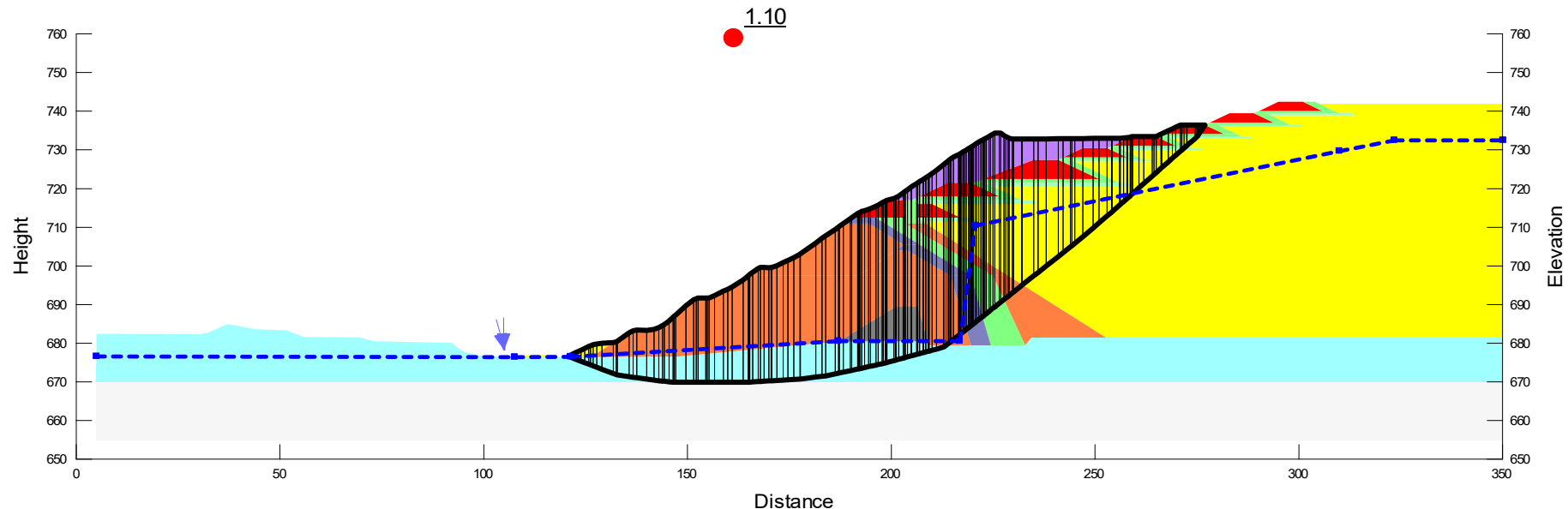
Cadia Mine
NTSF Failure Assessment
FIGURE 2

Color	Name	Model	Unit Weight (kN/m³)	Cohesion' (kPa)	Phi' (°)	Tau/Sigma Ratio	Minimum Strength (kPa)
Red	Rock Fill	Mohr-Coulomb	21	0	40		
Light Green	Working Platform	Mohr-Coulomb	18	0	35		
Orange	2B rockfill	Mohr-Coulomb	19	0	40		
Light Blue	Clay Core	Mohr-Coulomb	20	10	26		
Dark Blue	Zone 2A Transition	Mohr-Coulomb	20	0	42		
Grey	Stage 1 DS Rockfill_1	Mohr-Coulomb	21	0	40		
Purple	DS Berm	Mohr-Coulomb	19	0	40		
Yellow	Tailings su/p=0.20	S=f(overburden)	20			0.2	0
Cyan	Foundation su/p=0.40	S=f(overburden)	24			0.4	50



Project No.	H356804		CH 1950 Tailings $t/\sigma v' = 0.20$ Foundation $t/\sigma v' = 0.4$ Bedrock @ RL665m	Cadia Mine HATCH NTSF Failure Assessment
Prepared by:	ZY			
Checked by:	IG	13-Jun-18		
Revision	A	13-Jun-18		

Color	Name	Model	Unit Weight (kN/m³)	Cohesion' (kPa)	Phi' (°)	Tau/Sigma Ratio	Minimum Strength (kPa)
Red	Rock Fill	Mohr-Coulomb	21	0	40		
Light Green	Working Platform	Mohr-Coulomb	18	0	35		
Orange	2B rockfill	Mohr-Coulomb	19	0	40		
Light Green	Clay Core	Mohr-Coulomb	20	10	26		
Dark Blue	Zone 2A Transition	Mohr-Coulomb	20	0	42		
Grey	Stage 1 DS Rockfill_1	Mohr-Coulomb	21	0	40		
Purple	DS Berm	Mohr-Coulomb	19	0	40		
Yellow	Tailings su/p=0.20	S=f(overburden)	20			0.2	0
Cyan	Foundation su/p=0.40	S=f(overburden)	24			0.4	50



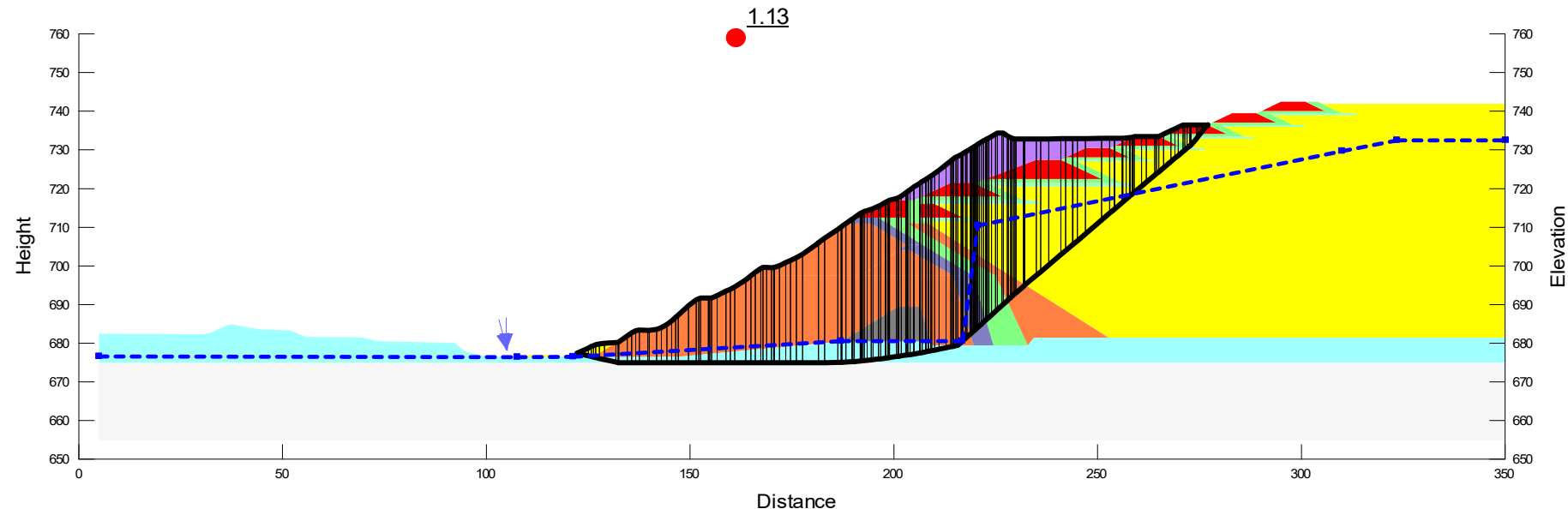
Project No.	H356804	
Prepared by:	ZY	
Checked by:	IG	13-Jun-18
Revision	A	13-Jun-18

CH 1950
Tailings $t/\sigma v' = 0.20$
Foundation $t/\sigma v' = 0.4$
Bedrock @ RL670m

HATCH

Cadia Mine
NTSF Failure Assessment
FIGURE 4

Color	Name	Model	Unit Weight (kN/m³)	Cohesion' (kPa)	Phi' (°)	Tau/Sigma Ratio	Minimum Strength (kPa)
Red	Rock Fill	Mohr-Coulomb	21	0	40		
Light Green	Working Platform	Mohr-Coulomb	18	0	35		
Orange	2B rockfill	Mohr-Coulomb	19	0	40		
Light Green	Clay Core	Mohr-Coulomb	20	10	26		
Dark Blue	Zone 2A Transition	Mohr-Coulomb	20	0	42		
Grey	Stage 1 DS Rockfill_1	Mohr-Coulomb	21	0	40		
Purple	DS Berm	Mohr-Coulomb	19	0	40		
Yellow	Tailings su/p=0.20	S=f(overburden)	20			0.2	0
Cyan	Foundation su/p=0.40	S=f(overburden)	24			0.4	50



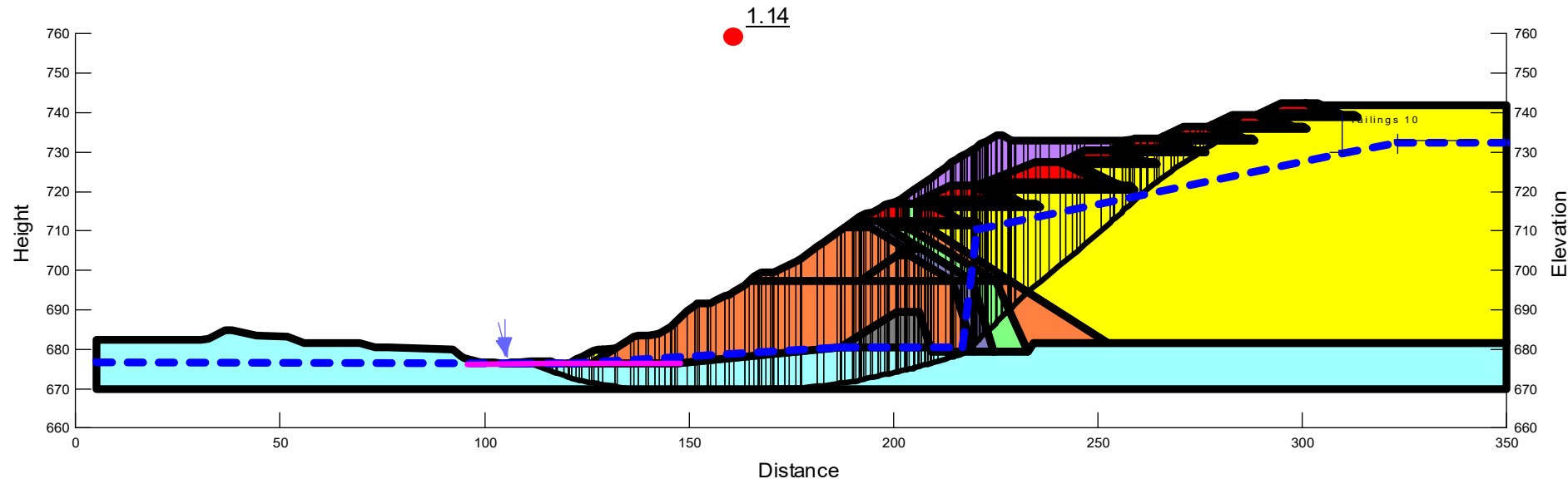
Project No.	H356804	
Prepared by:	ZY	
Checked by:	IG	13-Jun-18
Revision	A	13-Jun-18

CH 1950
Tailings $t/\sigma v' = 0.20$
Foundation $t/\sigma v' = 0.4$
Bedrock @ RL675m

HATCH

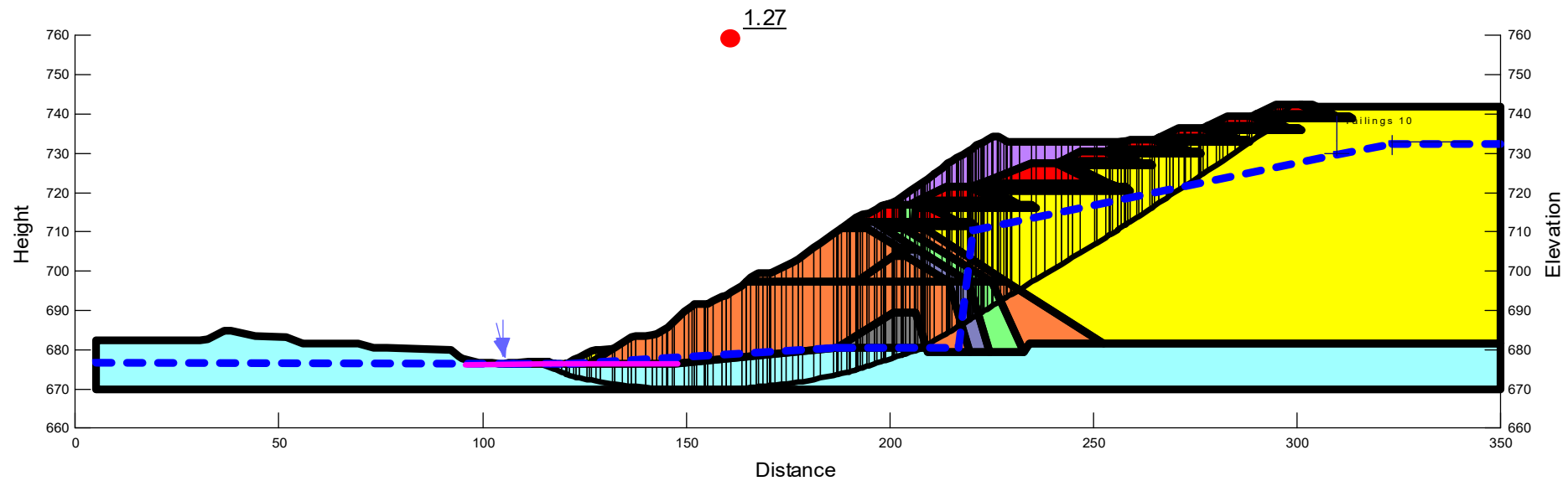
Cadia Mine
NTSF Failure Assessment
FIGURE 5

Color	Name	Model	Unit Weight (kN/m³)	Cohesion' (kPa)	Phi' (°)	Tau/Sigma Ratio	Minimum Strength (kPa)
Red	Rock Fill	Mohr-Coulomb	21	0	40		
Green	Working Platform	Mohr-Coulomb	18	0	35		
Orange	2B rockfill	Mohr-Coulomb	19	0	40		
Light Green	Clay Core	Mohr-Coulomb	20	10	26		
Blue	Zone 2A Transition	Mohr-Coulomb	20	0	42		
Grey	Stage 1 DS Rockfill_1	Mohr-Coulomb	21	0	40		
Purple	DS Berm	Mohr-Coulomb	19	0	40		
Yellow	Tailings su/p=0.20	S=f(overburden)	20			0.2	0
Cyan	Foundation Drained -22	Mohr-Coulomb	24	10	22		



Project No.	H356804		CH 1950 Tailings $t/\sigma v' = 0.20$ Foundation $c'=10, \phi' = 22^\circ$	HATCH 	Cadia Mine		
Prepared by:	ZY				NTSF Failure Assessment		
Checked by:	IG				FIGURE 6		
Revision	A						

Color	Name	Model	Unit Weight (kN/m³)	Cohesion' (kPa)	Phi' (°)	Tau/Sigma Ratio	Minimum Strength (kPa)
Red	Rock Fill	Mohr-Coulomb	21	0	40		
Green	Working Platform	Mohr-Coulomb	18	0	35		
Orange	2B rockfill	Mohr-Coulomb	19	0	40		
Light Green	Clay Core	Mohr-Coulomb	20	10	26		
Blue	Zone 2A Transition	Mohr-Coulomb	20	0	42		
Grey	Stage 1 DS Rockfill_1	Mohr-Coulomb	21	0	40		
Purple	DS Berm	Mohr-Coulomb	19	0	40		
Yellow	Tailings su/p=0.20	S=f(overburden)	20			0.2	0
Cyan	Foundation Drained -26	Mohr-Coulomb	24	10	26		



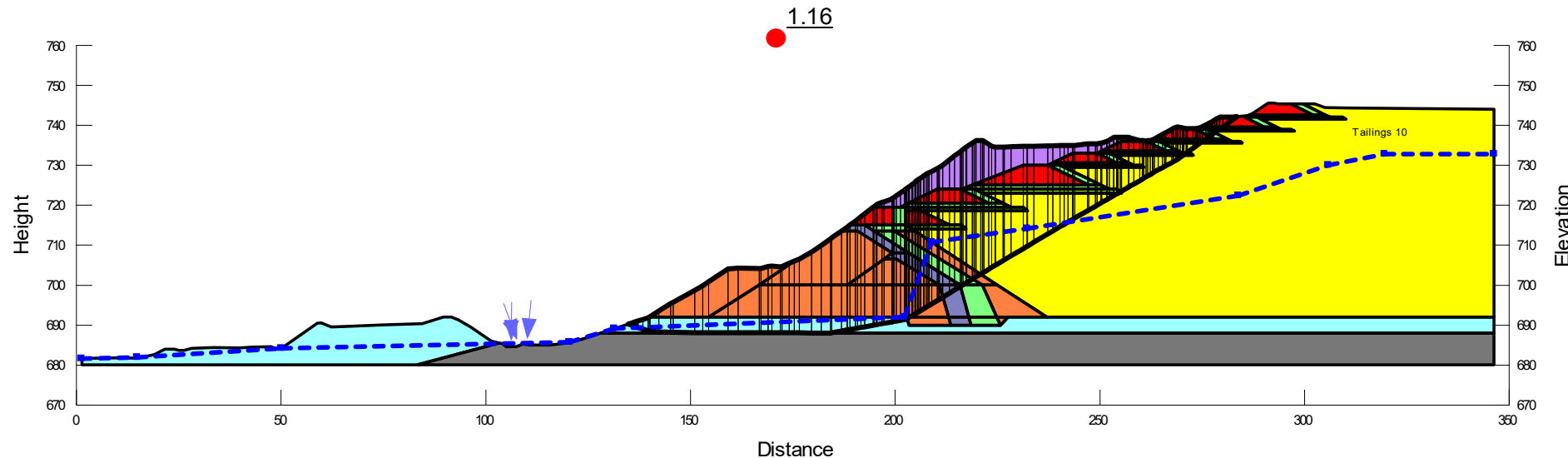
Project No.	H356804	
Prepared by:	ZY	
Checked by:	IG	13-Jun-18
Revision	A	13-Jun-18

CH 1950
Tailings $t/\sigma v' = 0.20$
Foundation $c'=10, \phi' = 26^\circ$

HATCH

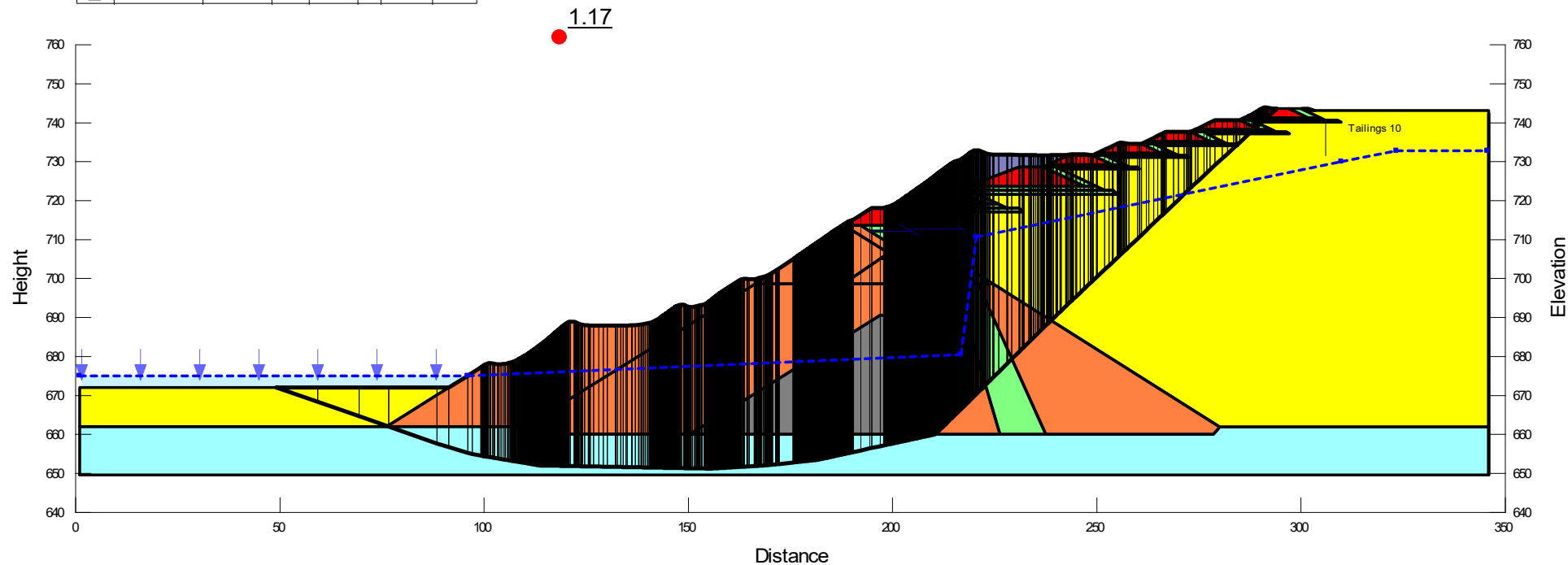
Cadia Mine
NTSF Failure Assessment
FIGURE 7

Color	Name	Model	Unit Weight (kN/m³)	Cohesion' (kPa)	Phi' (°)	Tau/Sigma Ratio	Minimum Strength (kPa)
Red	3A-3B Rock Fill	Mohr-Coulomb	19	0	30		
Green	4 Working Platform	Mohr-Coulomb	18	0	35		
Orange	2B rockfill	Mohr-Coulomb	19	0	40		
Light Green	1A Core	Mohr-Coulomb	20	10	26		
Dark Blue	Zone 2A Transition	Mohr-Coulomb	20	0	42		
Cyan	Foundation	S=f(overburden)	24			0.4	50
Purple	DS Berm	Mohr-Coulomb	19	0	40		
Grey	Weathered Basalt	Mohr-Coulomb	24	500	45		
Yellow	Tailings Su/p=0.2	S=f(overburden)	20			0.2	0



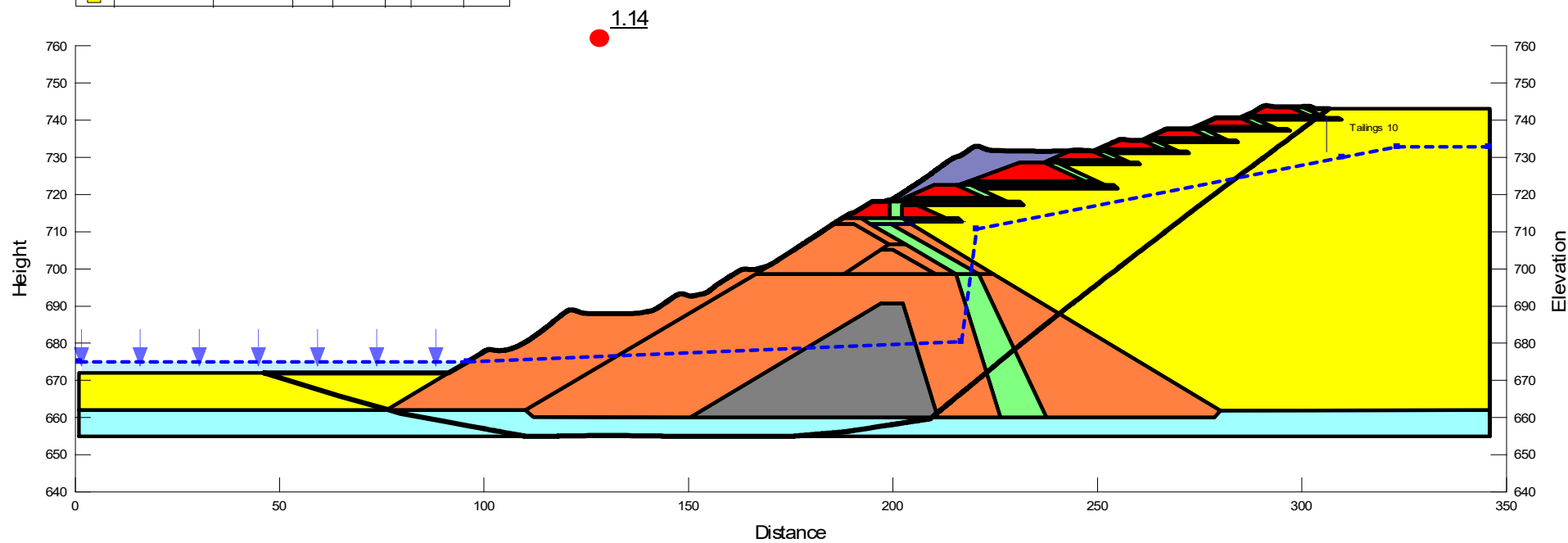
Project No.	H356804		CH 1700 Tailings $t/\sigma' = 0.20$ Foundation $t/\sigma' = 0.4$	HATCH Cadia Mine NTSF Failure Assessment FIGURE 8		
Prepared by:	ZY					
Checked by:	IG 13-Jun-18					
Revision	A	13-Jun-18				

Color	Name	Model	Unit Weight (kN/m³)	Cohesion (kPa)	Phi (°)	Tau/Sigma Ratio	Minimum Strength (kPa)
Red	3A-3B Rock Fill	Mohr-Coulomb	19	0	30		
Light Green	4 Working Platform	Mohr-Coulomb	18	0	35		
Light Green	1A Core	Mohr-Coulomb	20	10	26		
Light Blue	Zone 2B transition	Mohr-Coulomb	20	0	42		
Orange	Stage 2 DS rockfill	Mohr-Coulomb	19	0	40		
Grey	Stage 1 DS Rockfill_1	Mohr-Coulomb	19	0	40		
Cyan	Foundation Sur/p=0.4 $S=f(\sigma_{overburden})$		24			0.4	50
Yellow	Tailings sur/p=0.18 $S=f(\sigma_{overburden})$		20			0.18	0
Yellow	Tailings sur/p=0.2 $S=f(\sigma_{overburden})$		20			0.2	0

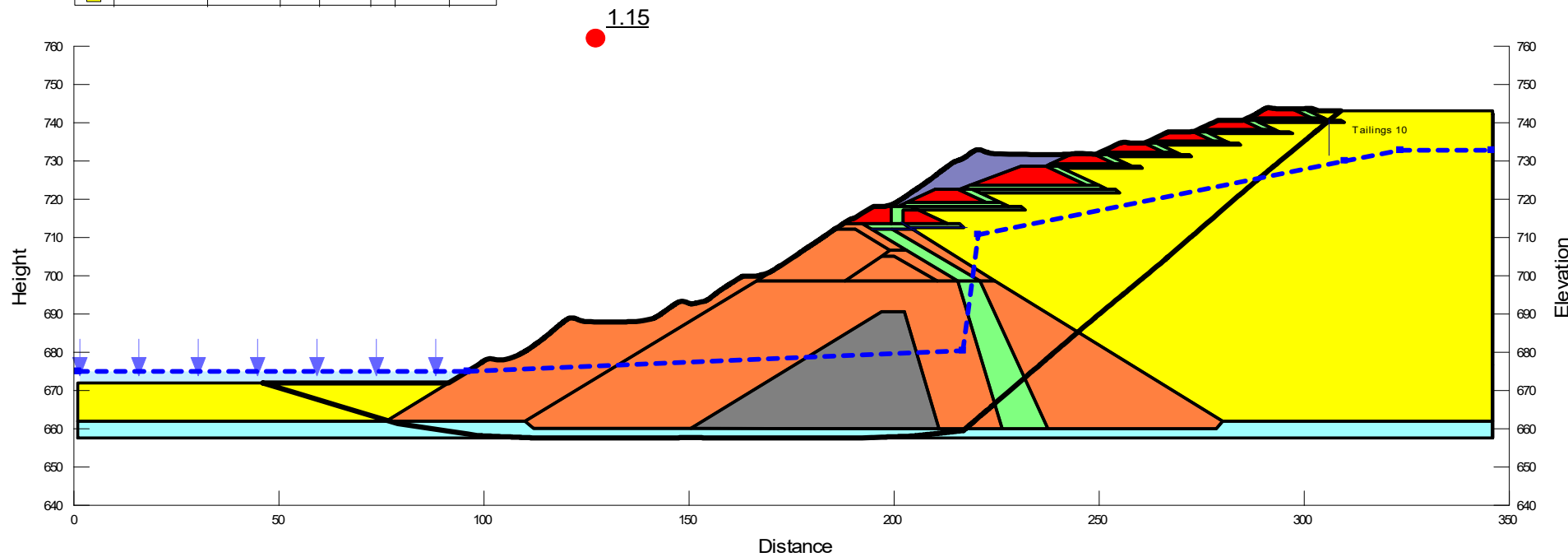


Project No.	H356804		CH 2400 Tailings $t/\sigma v' = 0.20$ Foundation $t/\sigma v' = 0.4$ Bedrock @ RL650	Cadia Mine HATCH NTSF Failure Assessment FIGURE 9
Prepared by:	ZY			
Checked by:	IG	13-Jun-18		
Revision	A	13-Jun-18		

Color	Name	Model	Unit Weight (kN/m^3)	Cohesion' (kPa)	Φ' ($^\circ$)	Tau/Sigma Ratio	Minimum Strength (kPa)
Red	3A-3B Rock Fill	Mohr-Coulomb	19	0	30		
Light Green	4 Working Platform	Mohr-Coulomb	18	0	35		
Dark Green	1ACore	Mohr-Coulomb	20	10	26		
Blue	Zone 2B transition	Mohr-Coulomb	20	0	42		
Orange	Stage 2 D Srock III	Mohr-Coulomb	19	0	40		
Grey	Stage 1 D Srock II_1	Mohr-Coulomb	19	0	40		
Cyan	Foundation Sub=0.4	$S=\ell(\text{overburden})$	24		0.4	50	
Yellow	Tailings $s/\ell=0.2$	$S=\ell(\text{overburden})$	20		0.2	0	



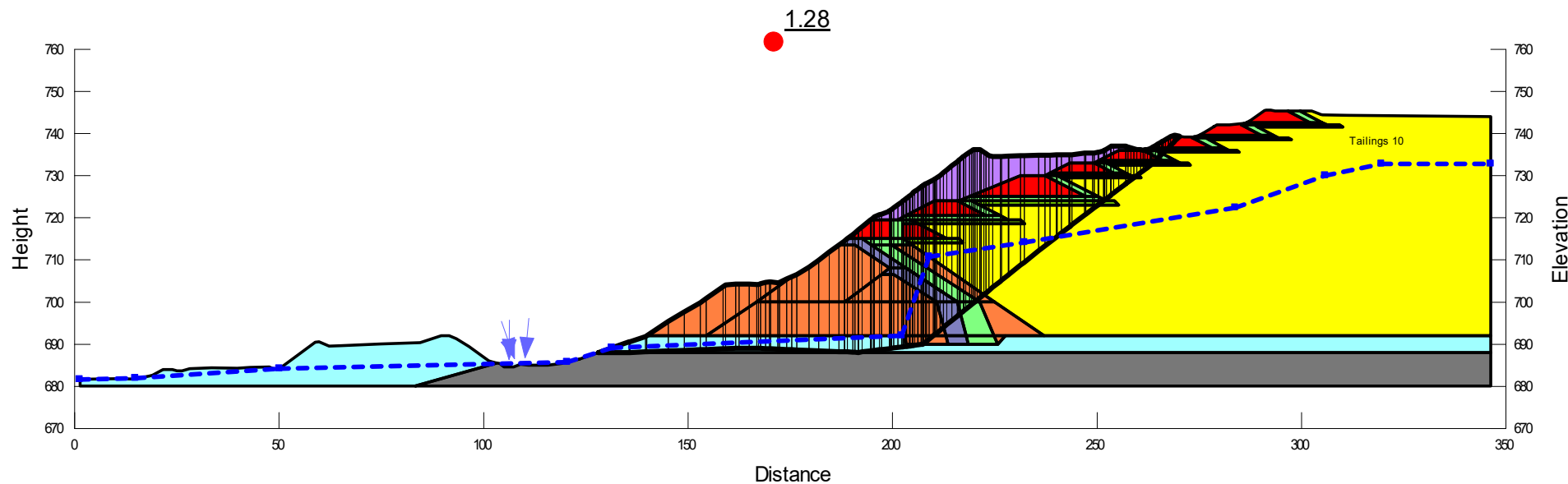
Color	Name	Model	Unit Weight (kN/m³)	Cohesion (kPa)	Phi (°)	Tau/Sigma Ratio	Minimum Strength (kPa)
Red	3A-3B Rock Fill	Mohr-Coulomb	19	0	30		
Green	4 Working Platform	Mohr-Coulomb	18	0	35		
Green	1A Core	Mohr-Coulomb	20	10	26		
Blue	Zone 2B transition	Mohr-Coulomb	20	0	42		
Orange	Stage 2 DS rockfill	Mohr-Coulomb	19	0	40		
Grey	Stage 1 DS Rockfill_1	Mohr-Coulomb	19	0	40		
Cyan	Foundation Su/p=0.4 S=f(overburden)	24			0.4	50	
Yellow	Tailings su/p=0.2 S=f(overburden)	20			0.2	0	



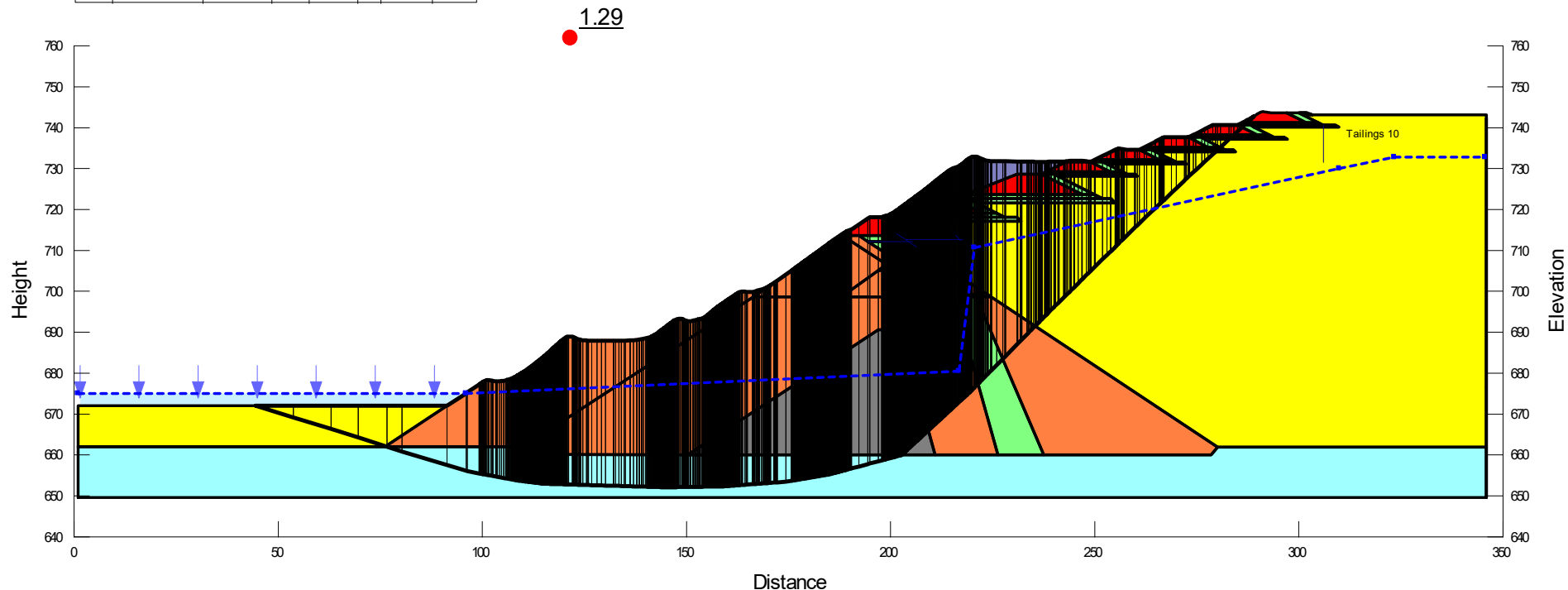
Project No.	H356804		CH 2400 Tailings $t/\sigma v' = 0.20$ Foundation $t/\sigma v' = 0.4$ Bedrock @ RL658	Cadia Mine HATCH NTSF Failure Assessment
Prepared by:	ZY			
Checked by:	IG	13-Jun-18		
Revision	A	13-Jun-18		

FIGURE 11

Color	Name	Model	Unit Weight (kN/m³)	Cohesion' (kPa)	Phi' (°)	Tau/Sigma Ratio	Minimum Strength (kPa)
Red	3A-3B Rock Fill	Mohr-Coulomb	19	0	30		
Green	4 Working Platform	Mohr-Coulomb	18	0	35		
Orange	2B rockfill	Mohr-Coulomb	19	0	40		
Light Green	1A Core	Mohr-Coulomb	20	10	26		
Blue	Zone 2A Transition	Mohr-Coulomb	20	0	42		
Purple	DS Berm	Mohr-Coulomb	19	0	40		
Grey	Weathered Basalt	Mohr-Coulomb	24	500	45		
Yellow	Tailings S _u /p=0.2	S=(overburden)	20			0.2	0
Cyan	Foundation Drained	Mohr-Coulomb	24	10	22		

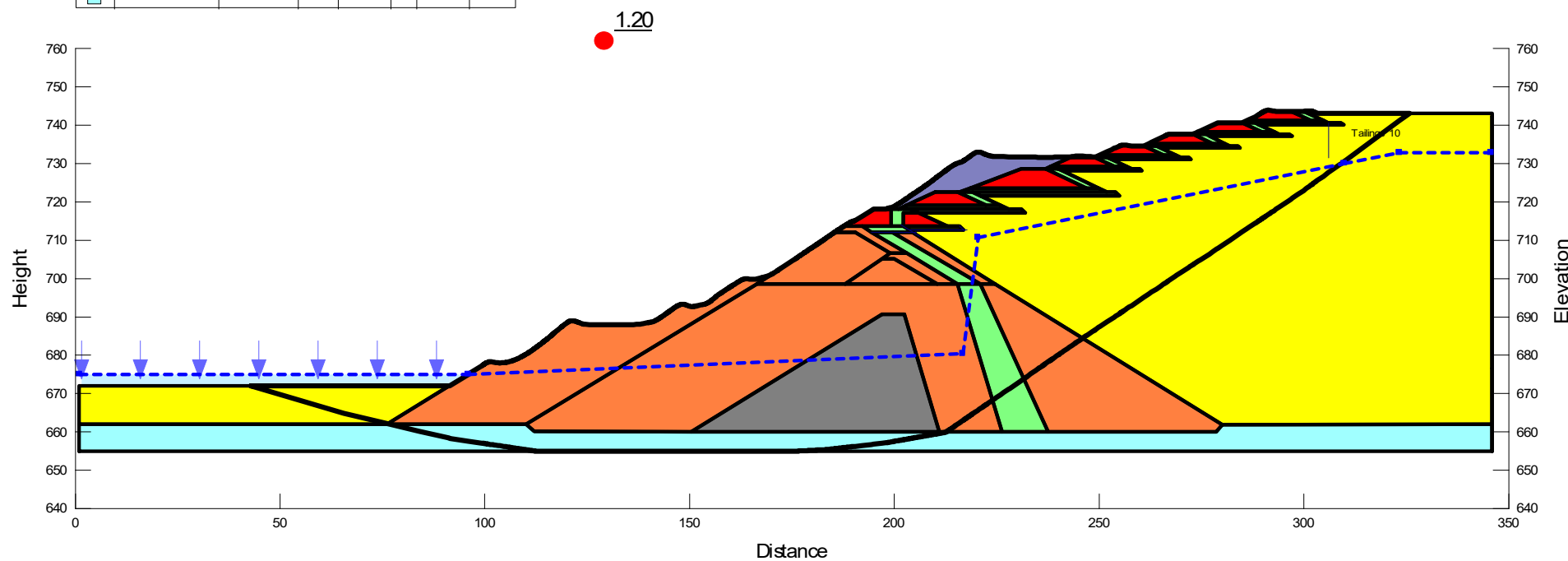


Color	Name	Model	Unit Weight (kN/m ³)	Cohesion' (kPa)	ϕ' (°)	Tau/Sigma Ratio	Minimum Strength (kPa)
Red	3A-3B Rock Fill	Mohr-Coulomb	19	0	30		
Light Green	4 Working Platform	Mohr-Coulomb	18	0	35		
Green	1A Core	Mohr-Coulomb	20	10	26		
Blue	Zone 2B transition	Mohr-Coulomb	20	0	42		
Orange	Stage 2 DS rockfill	Mohr-Coulomb	19	0	40		
Grey	Stage 1 DS Rockfill_1	Mohr-Coulomb	19	0	40		
Yellow	Tailings su/p=0.18	S=f(overburden)	20		0.18	0	
Yellow	Tailings su/p=0.2	S=f(overburden)	20		0.2	0	
Cyan	Foundation drained 22	Mohr-Coulomb	24	10	22		



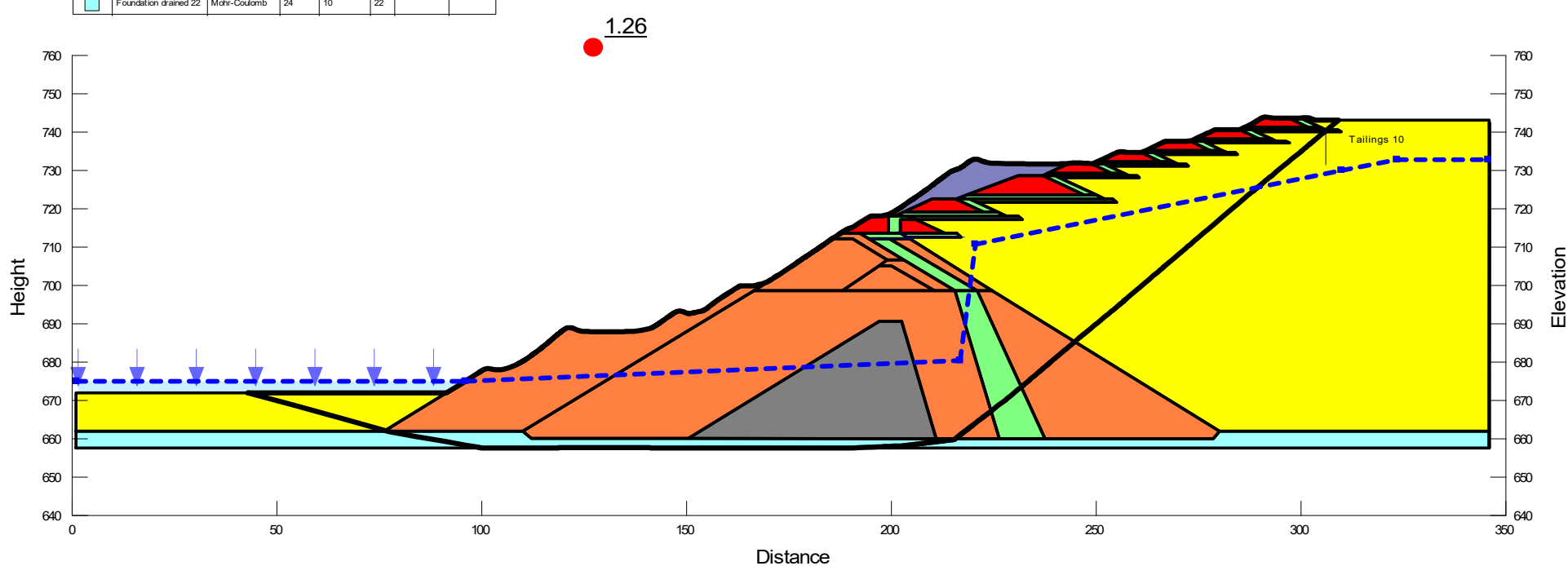
Project No.	H356804		CH 2400 Tailings $t/\sigma v' = 0.20$ Foundation $c'=10$, $\phi' = 22^\circ$ Bedrock at RL 650m	Cadia Mine
Prepared by:	ZY			NTSF Failure Assessment
Checked by:	IG	13-Jun-18		
Revision	A	13-Jun-18		FIGURE 13

Color	Name	Model	Unit Weight (kN/m³)	Cohesion' (kPa)	ϕ' (°)	Tau/Sigma Ratio	Minimum Strength (kPa)
Red	3A-3B Rock Fill	Mohr-Coulomb	19	0	30		
Green	4 Working Platform	Mohr-Coulomb	18	0	35		
Light Green	1ACore	Mohr-Coulomb	20	10	26		
Blue	Zone 2B transition	Mohr-Coulomb	20	0	42		
Orange	Stage 2 D Rockfill	Mohr-Coulomb	19	0	40		
Grey	Stage 1 D Rockfill_1	Mohr-Coulomb	19	0	40		
Yellow	Tailings $s_{ul}=0.2$	S=ff(overburden)	20		0.2	0	
Cyan	Foundation drained 22	Mohr-Coulomb	24	10	22		



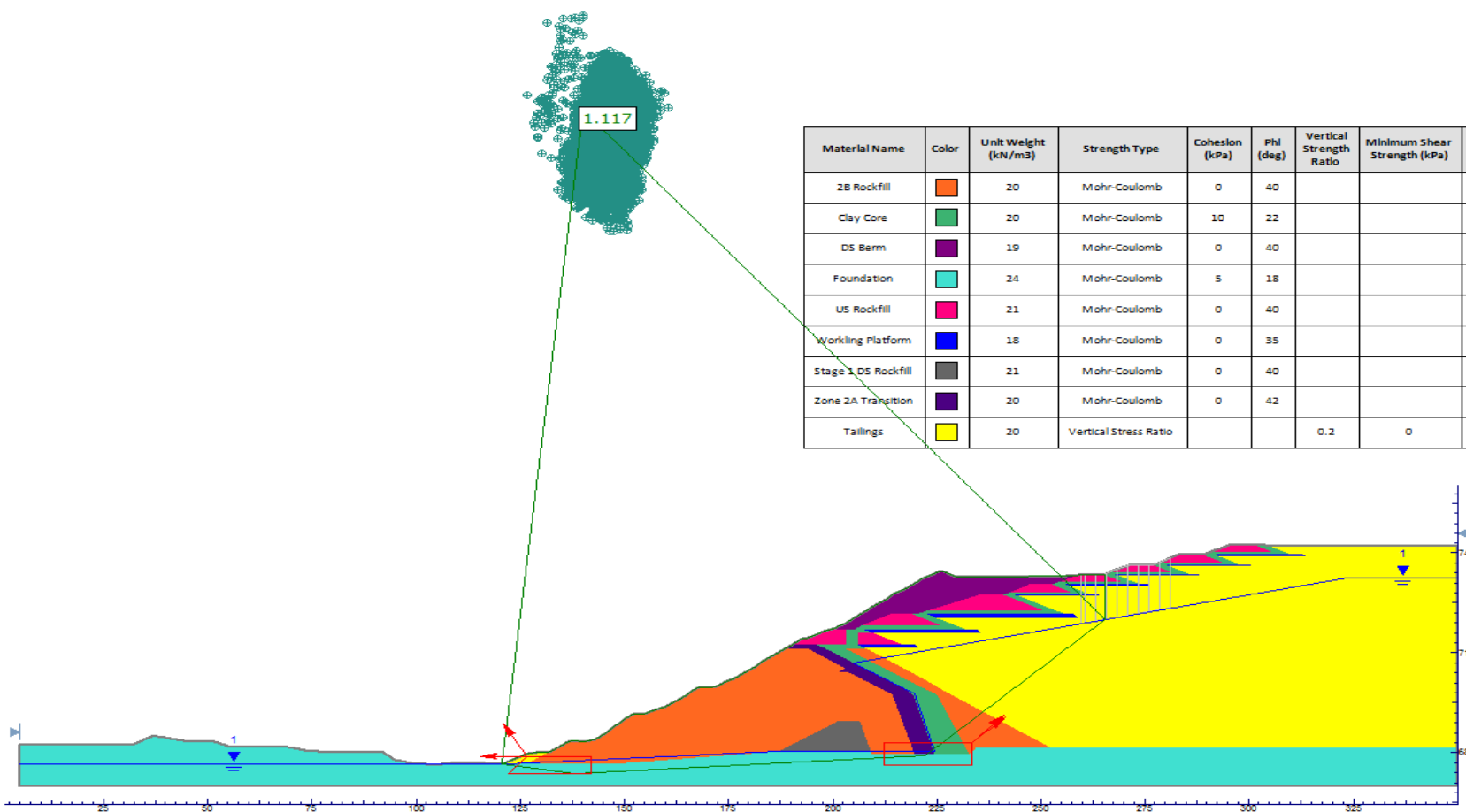
Project No.	H356804		CH 2400 Tailings $t/\sigma v' = 0.20$ Foundation $c'=10$, $\phi' = 22^\circ$ Bedrock at RL 655m	HATCH 	Cadia Mine
Prepared by:	ZY				NTSF Failure Assessment
Checked by:	IG	13-Jun-18			
Revision	A	13-Jun-18			FIGURE 14

Color	Name	Model	Unit Weight (kN/m³)	Cohesion' (kPa)	Phi' (°)	Tau/Sigma Ratio	Minimum Strength (kPa)
Red	3A-3B Rock Fill	Mahr-Coulomb	19	0	30		
Light Green	4 Working Platform	Mahr-Coulomb	18	0	35		
Dark Green	1A Core	Mahr-Coulomb	20	10	26		
Blue	Zone 2B transition	Mahr-Coulomb	20	0	42		
Orange	Stage 2 DS rockfill	Mahr-Coulomb	19	0	40		
Grey	Stage 1 DS Rockfill_1	Mahr-Coulomb	19	0	40		
Yellow	Tailings su/p=0.2 S=f(overburden)		20		0.2	0	
Cyan	Foundation drained 22	Mahr-Coulomb	24	10	22		



Project No.	H356804		CH 2400 Tailings $t/\sigma v' = 0.20$ Foundation $c'=10$, $\phi' = 22^\circ$ Bedrock at RL 658m	HATCH Cadia Mine NTSF Failure Assessment FIGURE 15
Prepared by:	ZY			
Checked by:	IG	13-Jun-18		
Revision	A	13-Jun-18		

Annexure GC
**Slump - 2D LEA Foundation Back
Analyses**



Project No.	H/356804	
Prepared by:	TMY	
Checked by:	IAG	
Revision	A	29-Oct-18

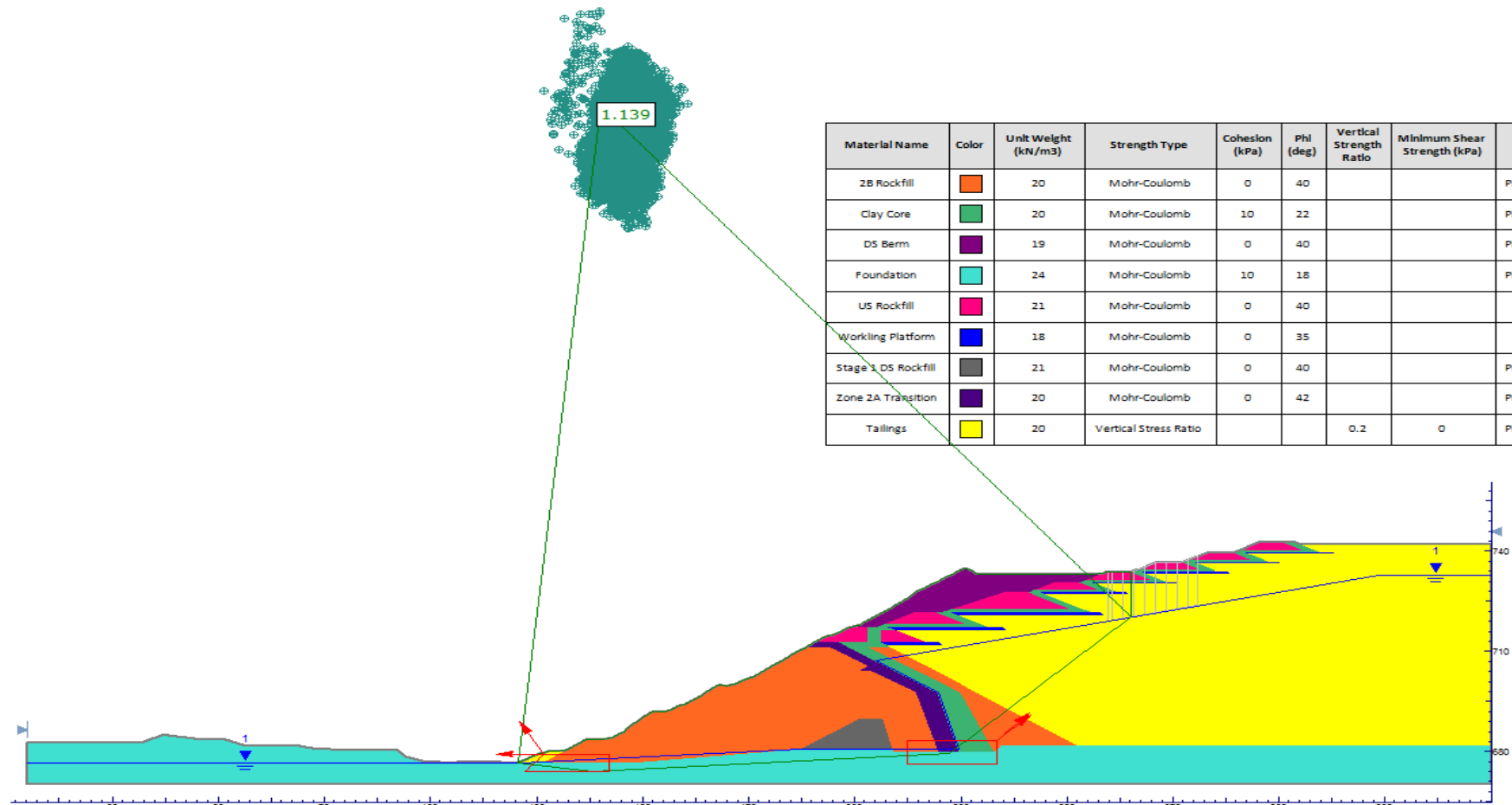
Foundation Sensitivity
Global Minimum Surface
Foundation $c'=5$ kPa

HATCH

ITRB

Cadia NTSF CH1950

FIGURE 1

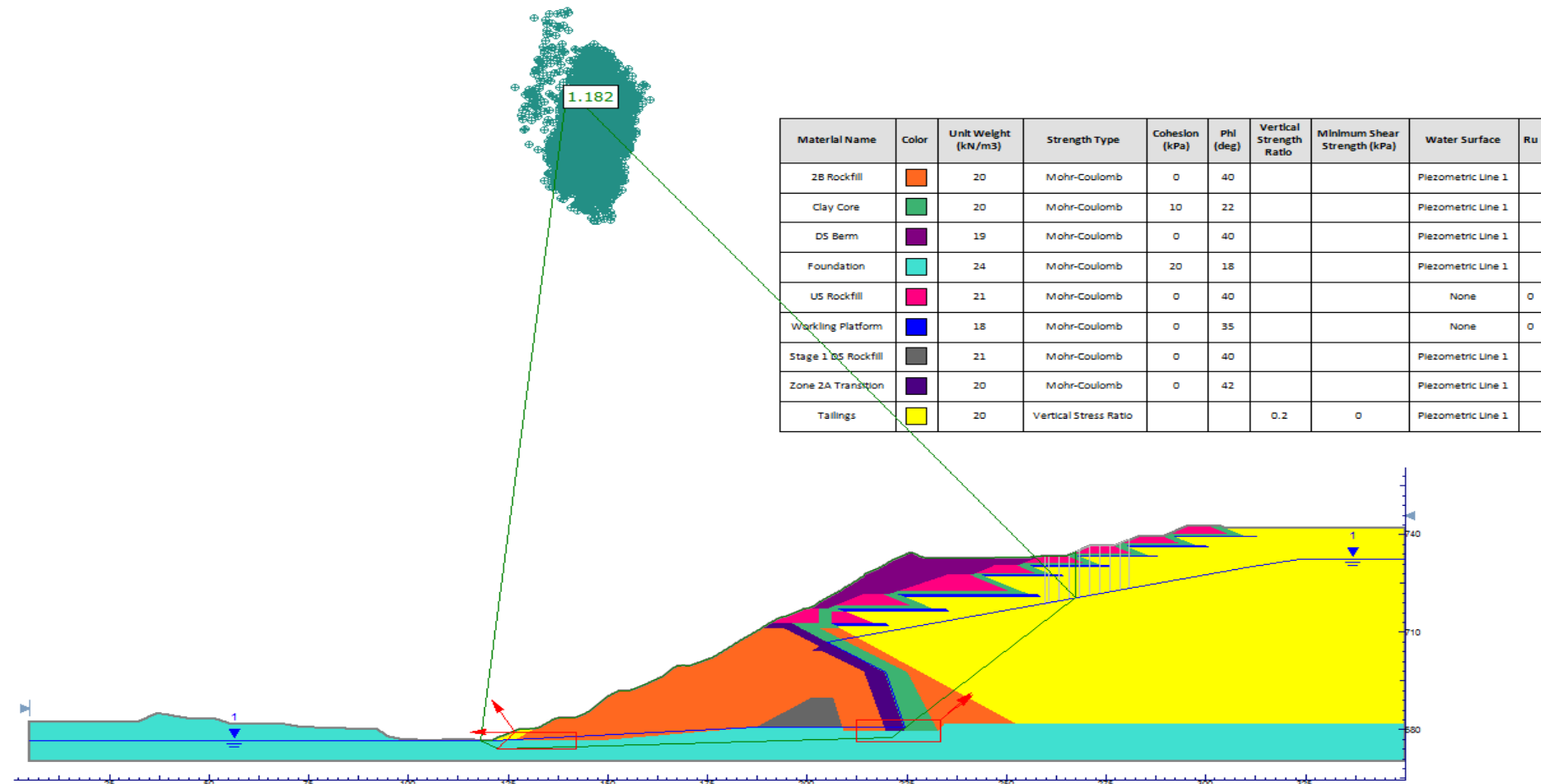


Project No.	H/356804	
Prepared by:	TMY	
Checked by:	IAG	
Revision	A	29-Oct-18

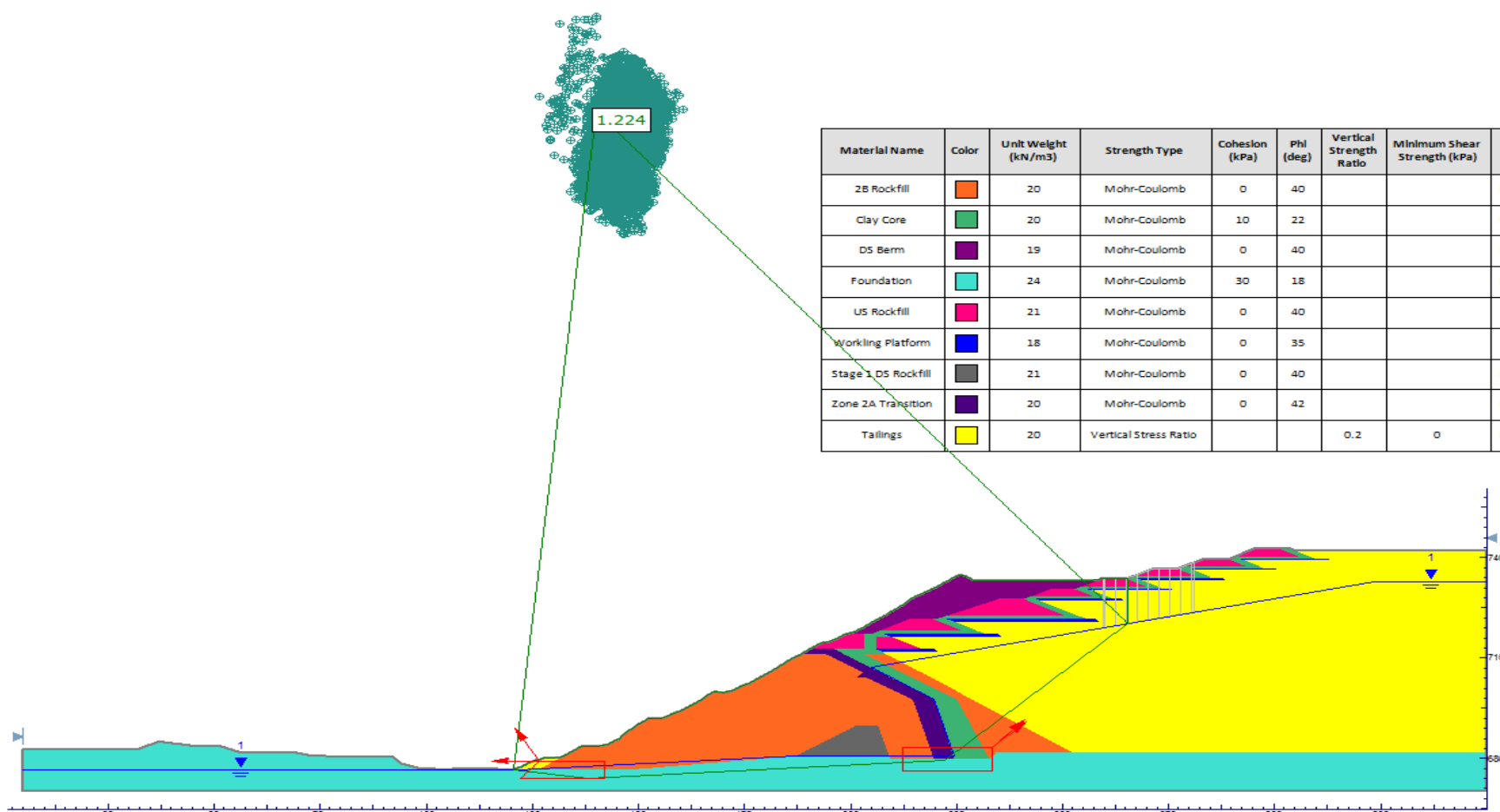
Foundation Sensitivity
Global Minimum Surface
Foundation $c'=10$ kPa

HATCH

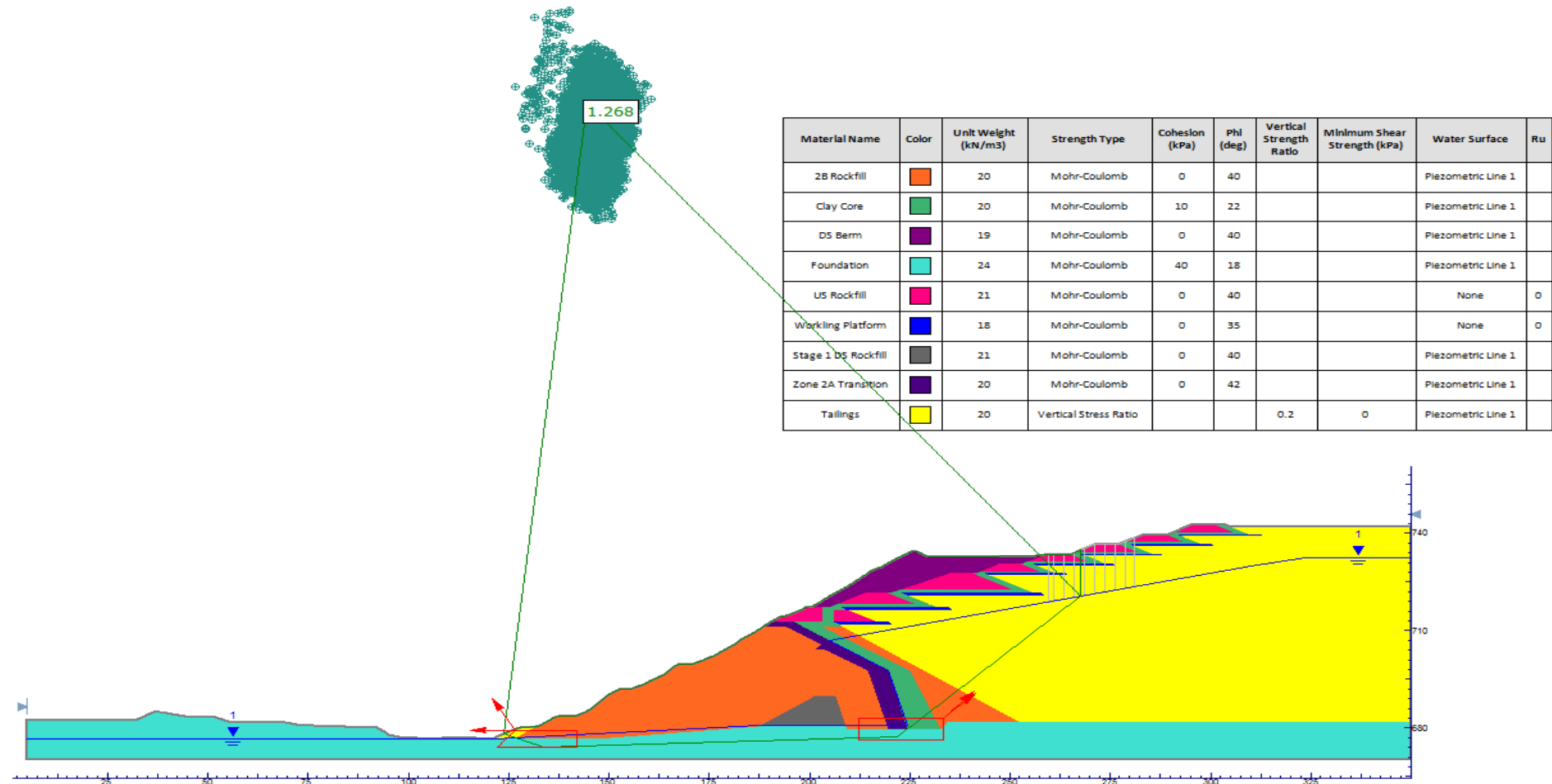
ITRB
Cadia NTSF CH1950
FIGURE 2



Project No.	H/356804		Foundation Sensitivity Global Minimum Surface Foundation $c'=20$ kPa	 ITRB Cadia NTSF CH1950 FIGURE 3		
Prepared by:	TMY					
Checked by:	IAG					
Revision	A	29-Oct-18				



Project No.	H/356804		Foundation Sensitivity Global Minimum Surface Foundation $c'=30$ kPa		ITRB		
Prepared by:	TMY						
Checked by:	IAG						
Revision	A	29-Oct-18			FIGURE 4		



Project No.	H/356804	
Prepared by:	TMY	
Checked by:	IAG	
Revision	A	29-Oct-18

Foundation Sensitivity
Global Minimum Surface
Foundation $c'=40$ kPa

HATCH

ITRB
Cadia NTSF CH1950
FIGURE 5

Annexure GD

Slump – 3D LEA

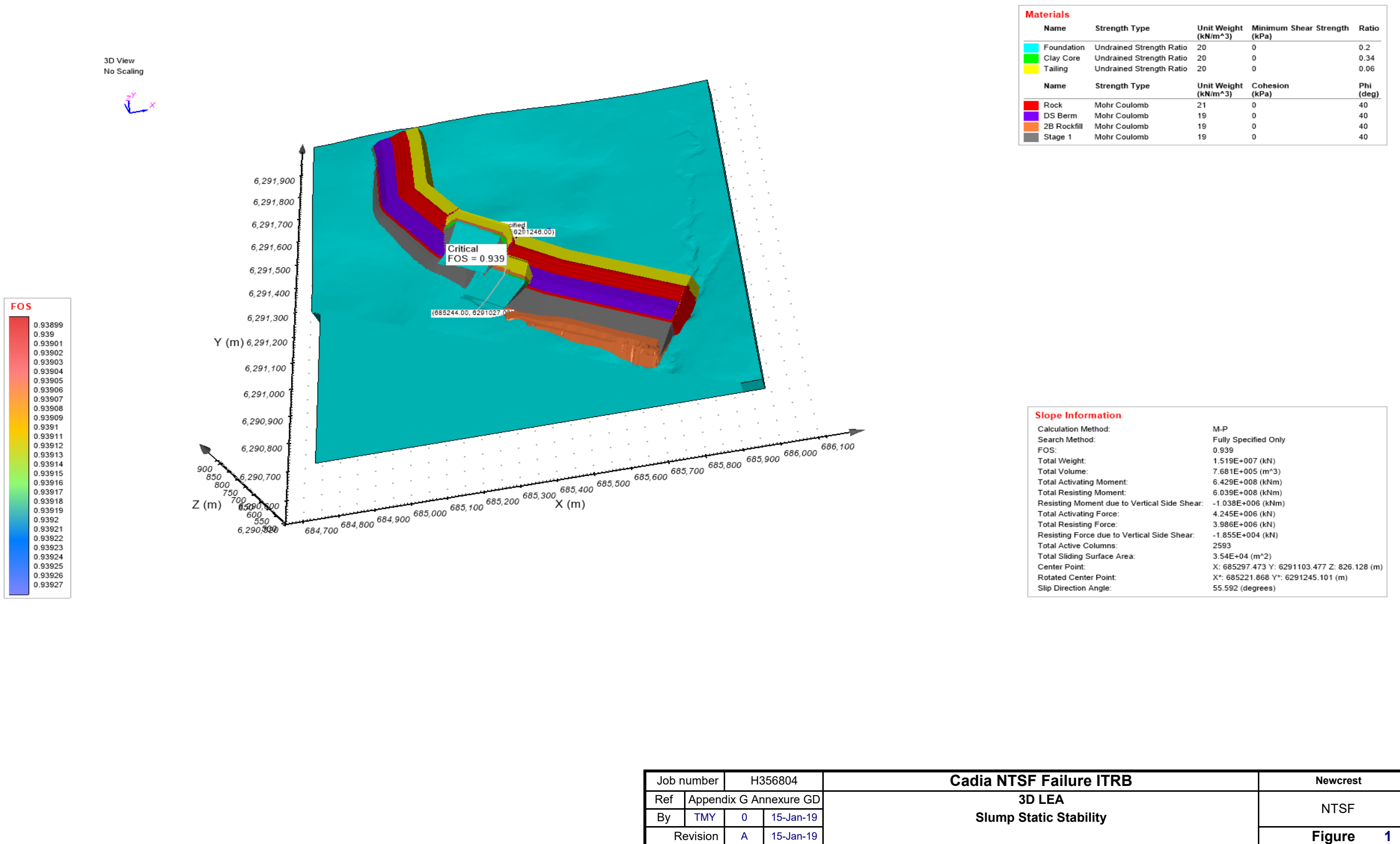


Figure 1 | 15-01-19 2:06 PM | P:\NEWCREST\356804\SPECIALIST_APPS\Reports\ITRB\Appendix G\Annexure GD\3D LEA.xlsx

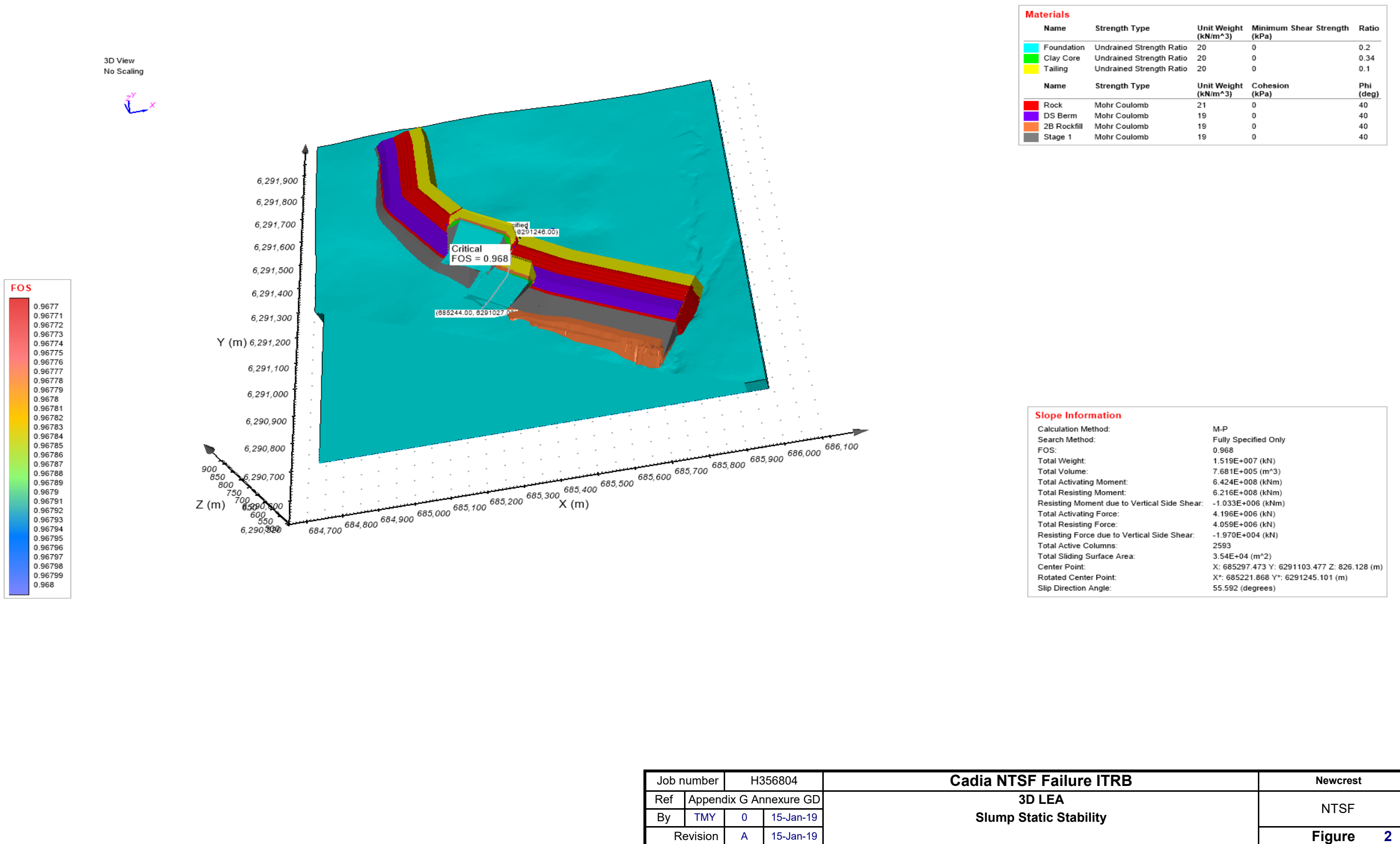


Figure 2 | 15-01-19 2:06 PM | P:\NEWCREST\356804\SPECIALIST_APPPS\Reports\ITRB\Appendix G\Annexure GD\3D LEA.xlsx

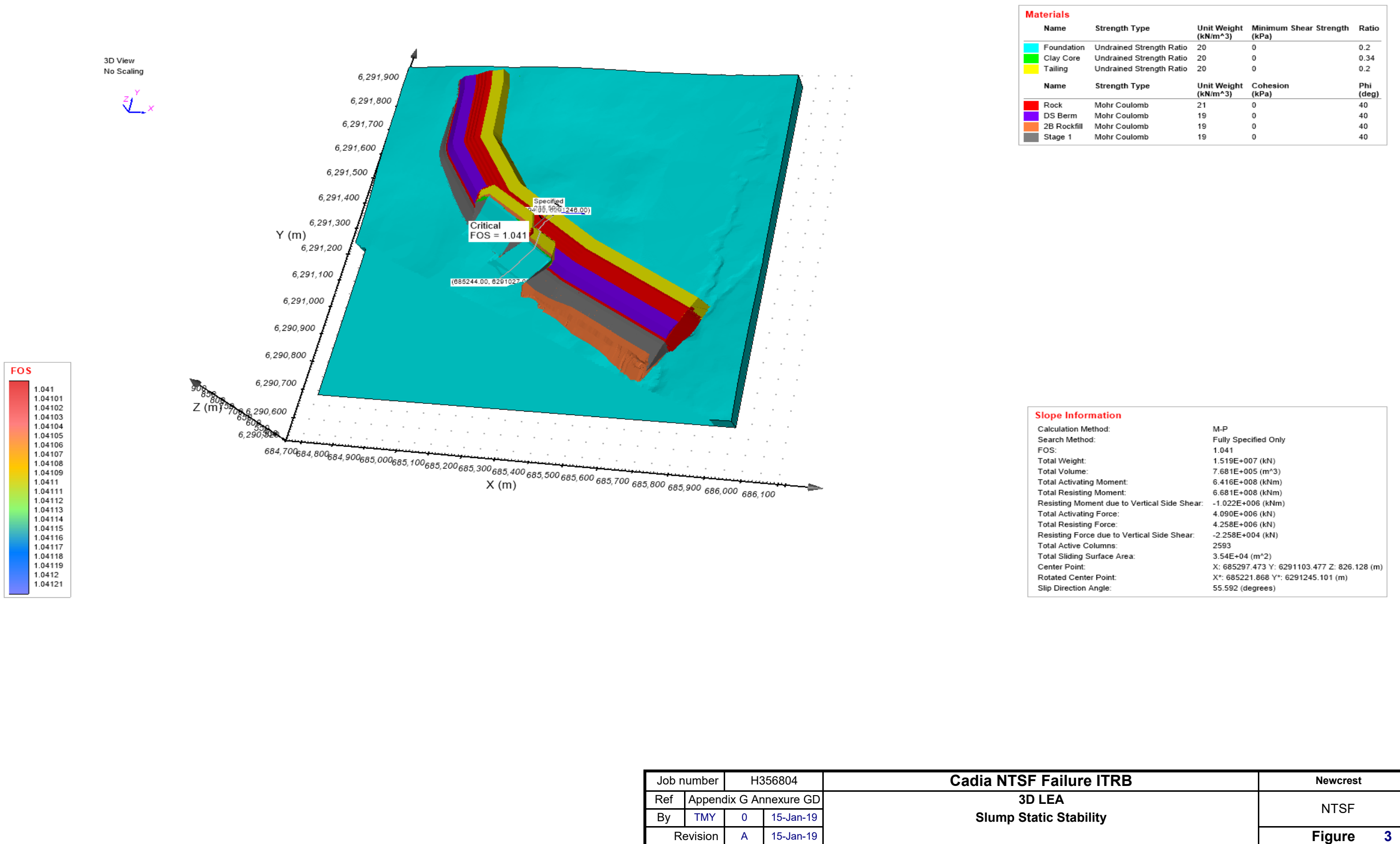


Figure 3 | 15-01-19 2:06 PM | P:\NEWCREST\356804\SPECIALIST_APPS\Reports\ITRB\Appendix G\Annexure GD\3D LEA.xlsx

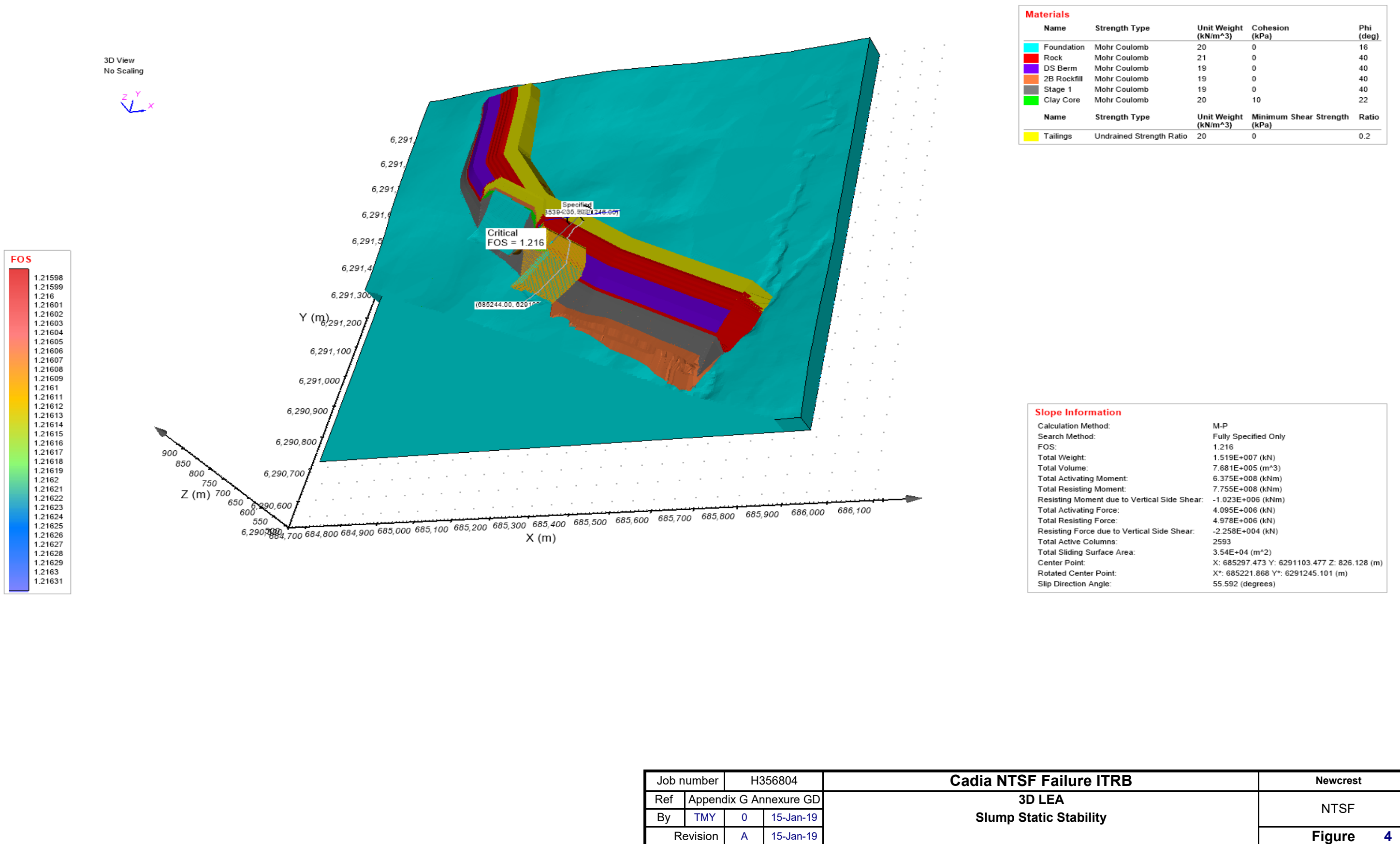
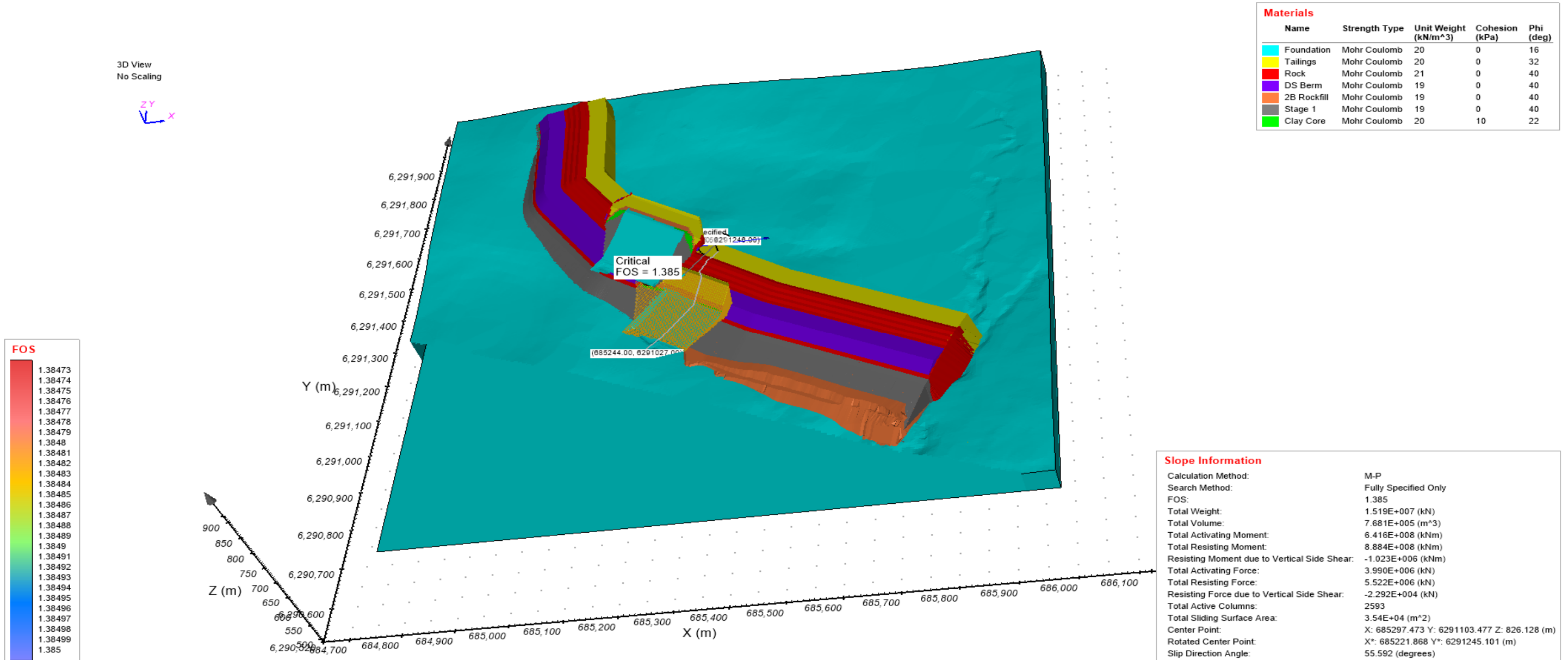


Figure 4 | 15-01-19 2:06 PM | P:\NEWCREST\356804\SPECIALIST_APPS\Reports\ITRB\Appendix G\Annexure GD\3D LEA.xlsx



Job number	H356804			Cadia NTSF Failure ITRB			Newcrest
Ref	Appendix G Annexure GD			3D LEA			NTSF
By	TMY	0	15-Jan-19	Slump Static Stability			
Revision	A	15-Jan-19		Figure 5			

Figure 5 | 15-01-19 2:06 PM | P:\NEWCREST\356804\SPECIALIST_APPS\Reports\ITRB\Appendix G\Annexure GD\3D LEA.xlsx

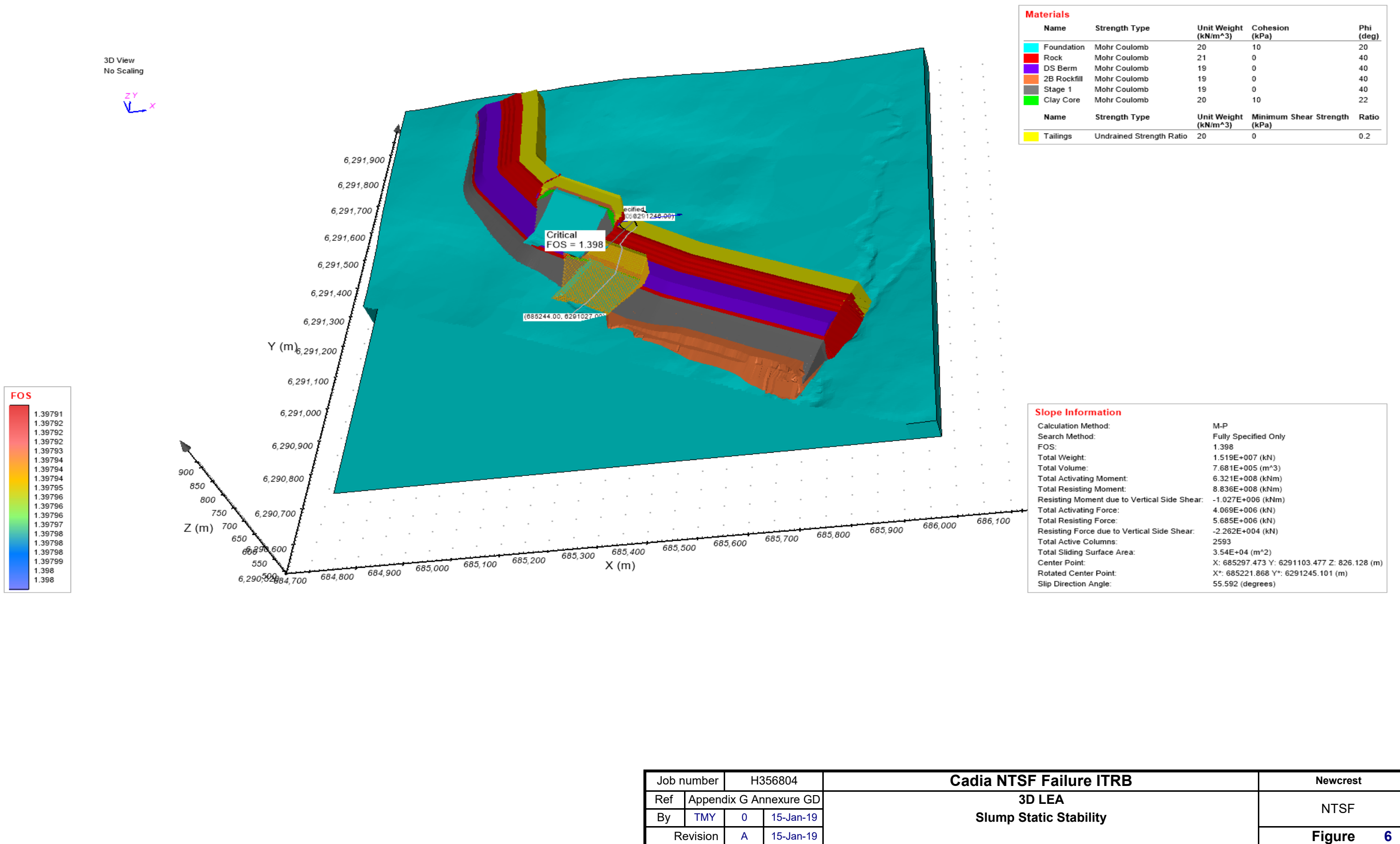
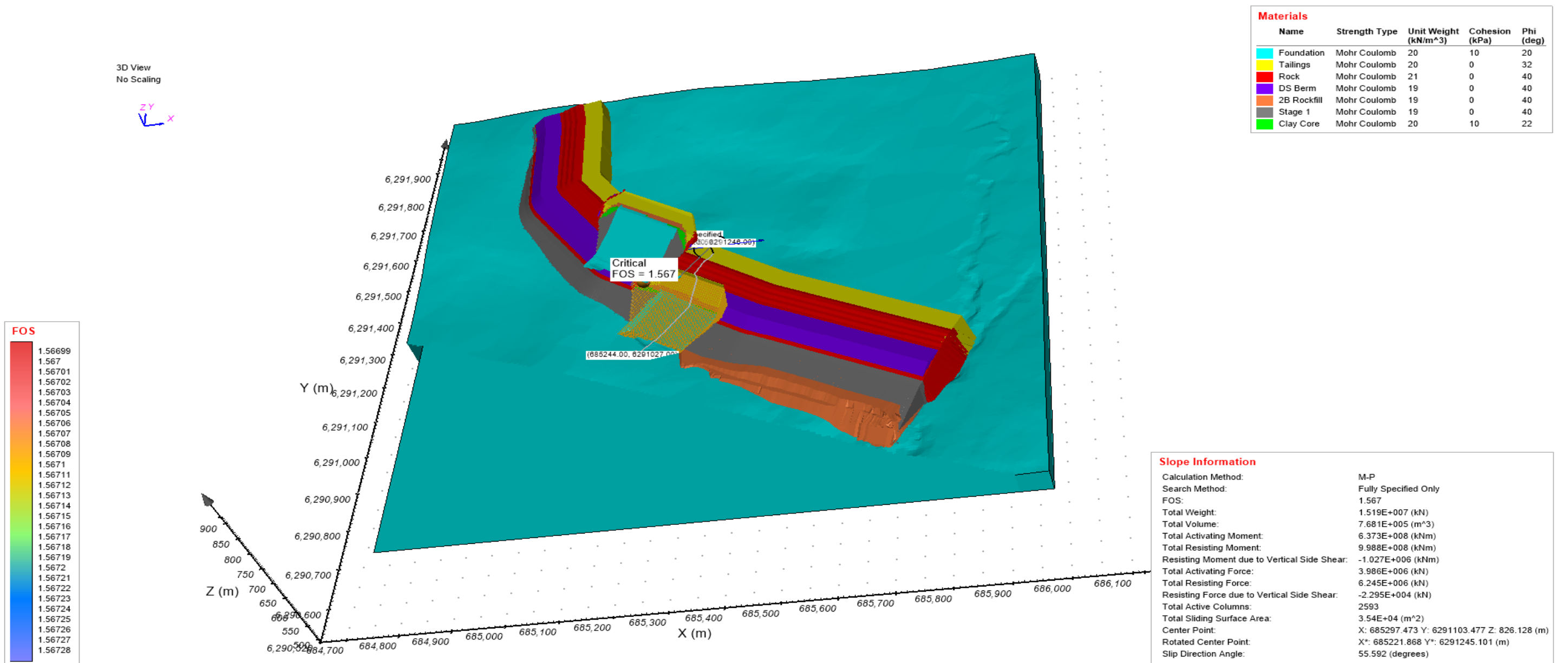


Figure 6 | 15-01-19 2:06 PM | P:\NEWCREST\356804\SPECIALIST_APPS\Reports\ITRB\Appendix G\Annexure GD\3D LEA.xlsx



Job number	H356804			Cadia NTSF Failure ITRB			Newcrest
Ref	Appendix G Annexure GD			3D LEA			NTSF
By	TMY	0	15-Jan-19	Slump Static Stability			
Revision	A	15-Jan-19		Figure 7			

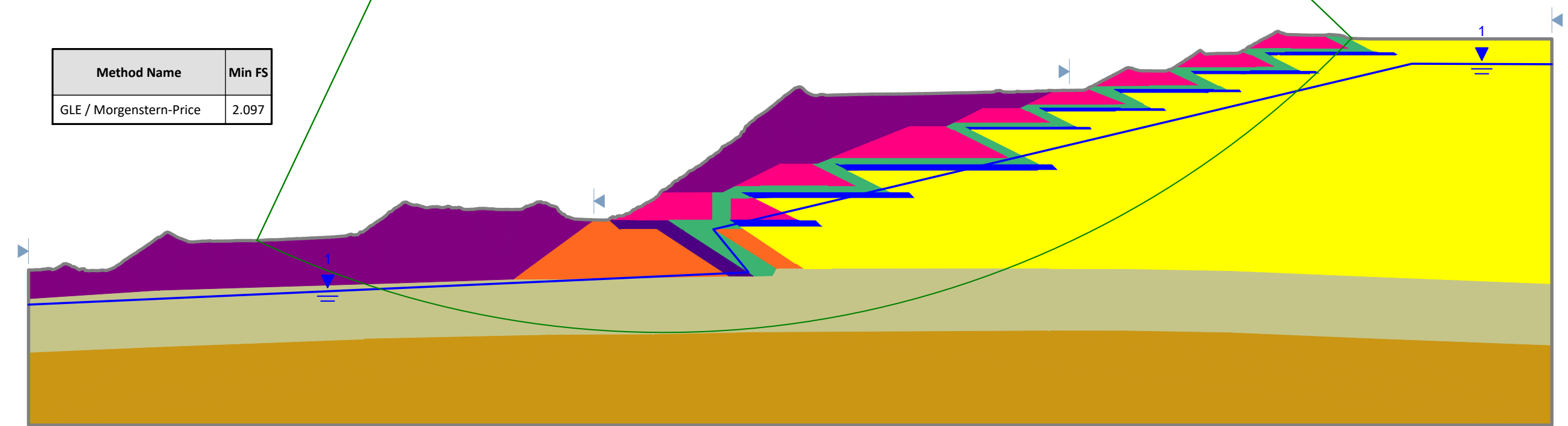
Figure 7 | 15-01-19 2:06 PM | P:\NEWCREST\356804\SPECIALIST_APPS\Reports\ITRB\Appendix G\Annexure GD\3D LEA.xlsx

Annexure GE

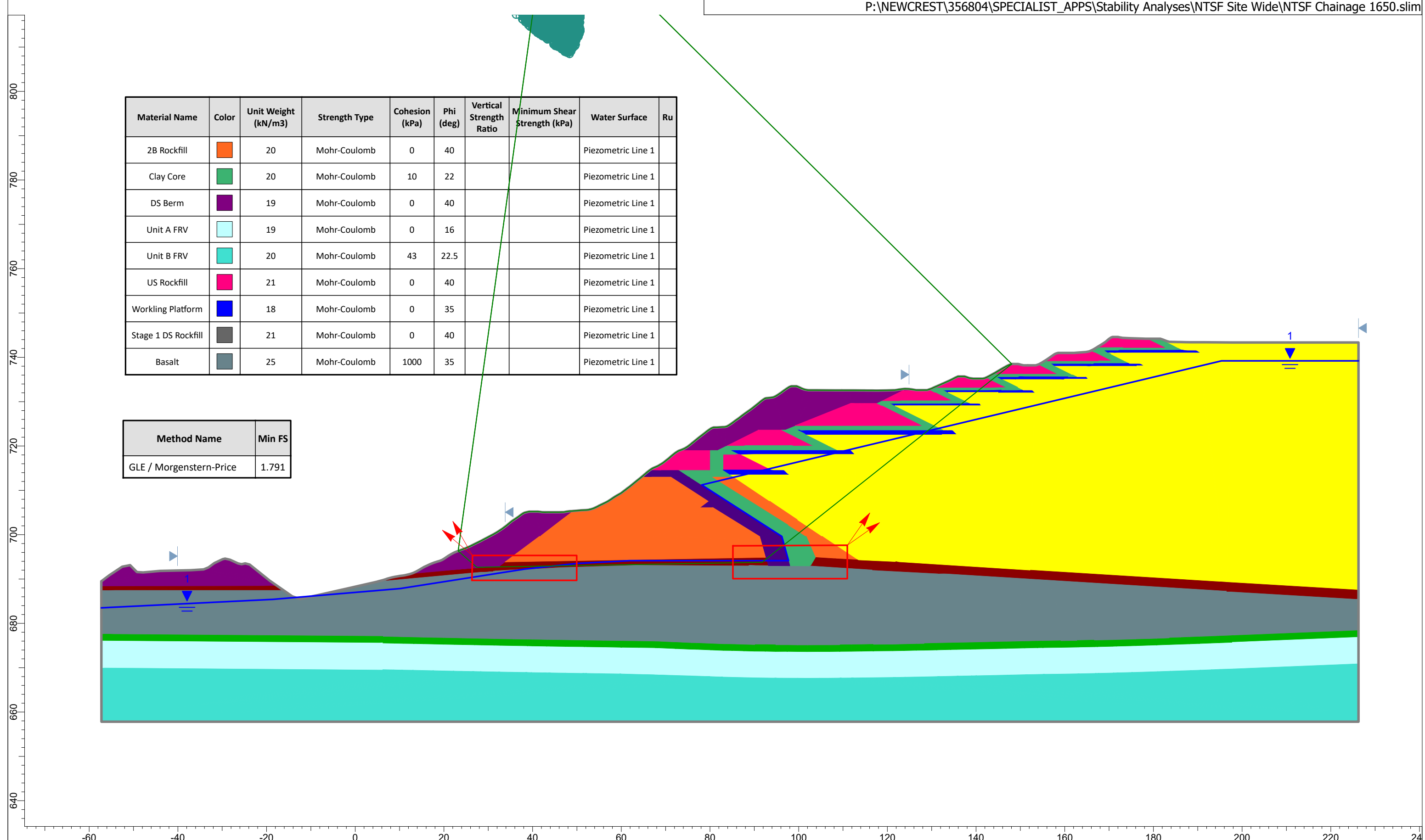
Site Wide – 2D LEA

Material Name	Color	Unit Weight (kN/m³)	Strength Type	Cohesion (kPa)	Phi (deg)	Water Surface	Ru
2B Rockfill	Orange	20	Mohr-Coulomb	0	40	Piezometric Line 1	
Clay Core	Green	20	Mohr-Coulomb	10	22	Piezometric Line 1	
DS Berm	Purple	19	Mohr-Coulomb	0	40	None	0
US Rockfill	Magenta	21	Mohr-Coulomb	0	40	Piezometric Line 1	
Working Platform	Blue	18	Mohr-Coulomb	0	35	Piezometric Line 1	
Zone 2A Transition	Purple	20	Mohr-Coulomb	0	42	Piezometric Line 1	
Tailings	Yellow	20	Mohr-Coulomb	0	32	Piezometric Line 1	
Silurian Sediments (weathered)	Light Green	20	Mohr-Coulomb	4	23	Piezometric Line 1	
Silurian Sediments	Brown	20	Mohr-Coulomb	4	27	Piezometric Line 1	

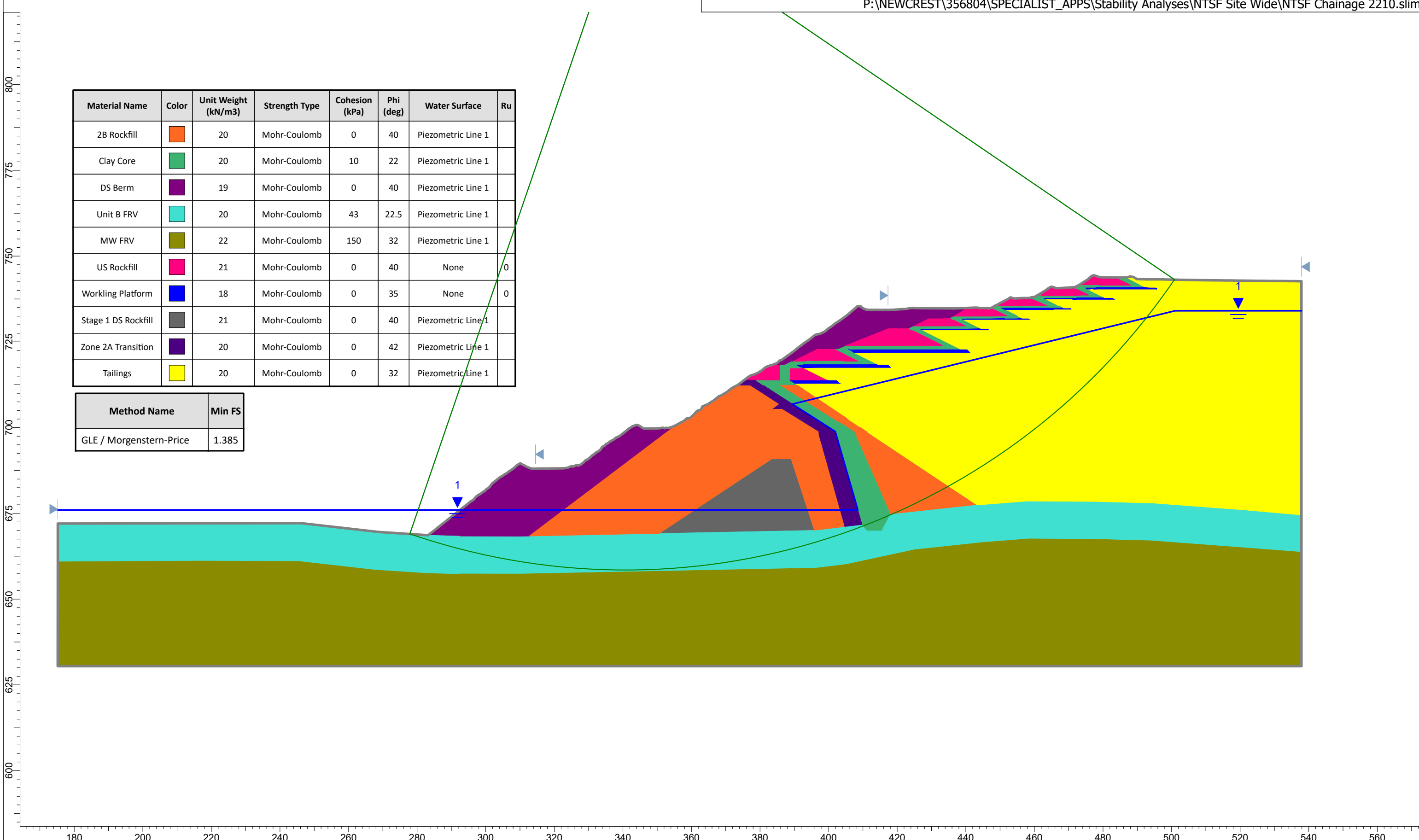
Method Name	Min FS
GLE / Morgenstern-Price	2.097



HATCH <small>SLIDEINTERPRET 8.018</small>	Project	Cadia NTSF Slump ITRB Investigation	
	Analysis Description	Chainage 990	
	Drawn By	TMY	Company
	Date	04-Oct-18, 3:22:07 PM	File Name



HATCH

**HATCH**

Project

Cadia NTSF Slump ITRB Investigation

Analysis Description

Chainage 2210

Drawn By

TMY

Company

Hatch

Date

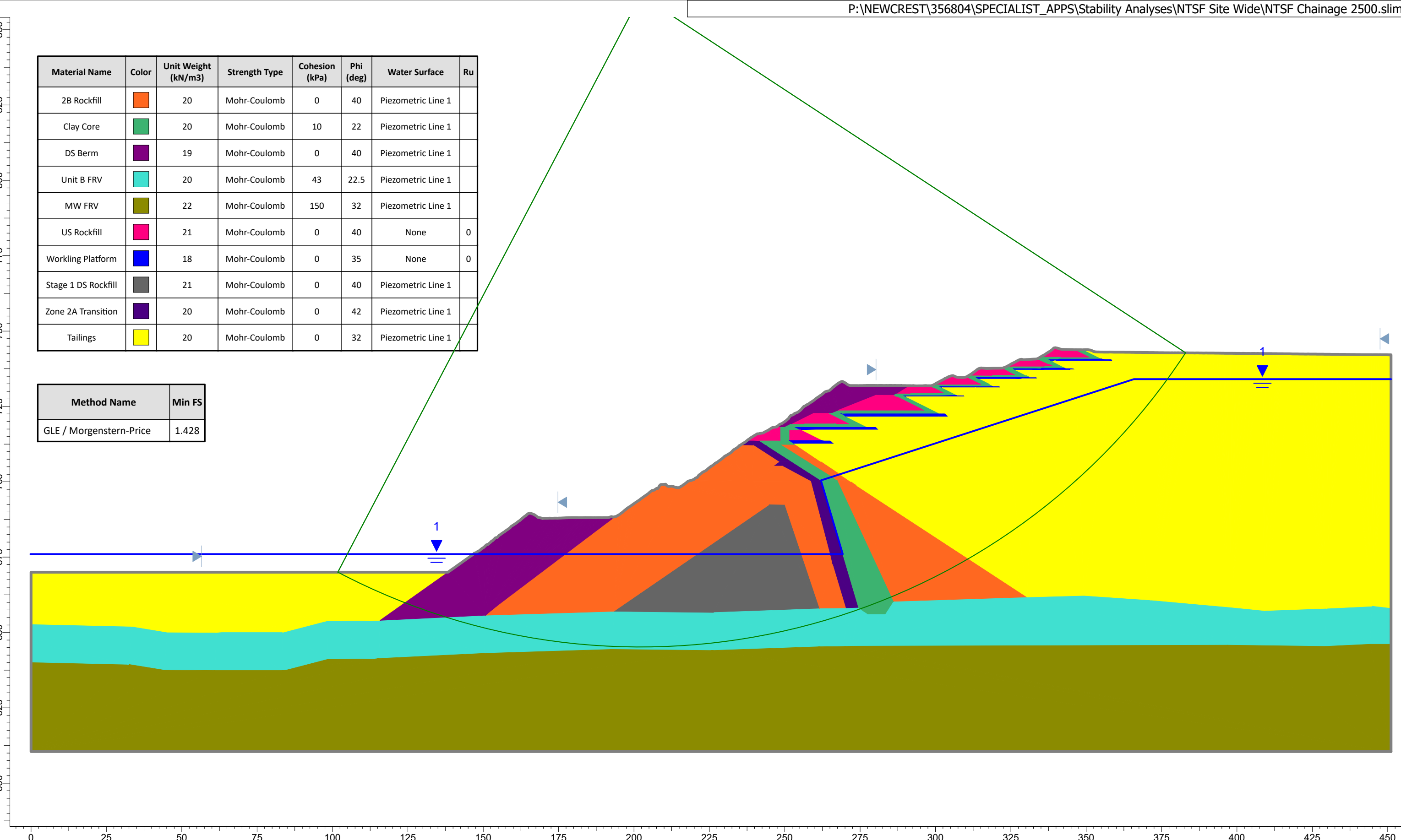
04-Oct-18, 3:22:07 PM

File Name

NTSF Chainage 2210.slim

Material Name	Color	Unit Weight (kN/m³)	Strength Type	Cohesion (kPa)	Phi (deg)	Water Surface	Ru
2B Rockfill	Orange	20	Mohr-Coulomb	0	40	Piezometric Line 1	
Clay Core	Green	20	Mohr-Coulomb	10	22	Piezometric Line 1	
DS Berm	Purple	19	Mohr-Coulomb	0	40	Piezometric Line 1	
Unit B FRV	Cyan	20	Mohr-Coulomb	43	22.5	Piezometric Line 1	
MW FRV	Yellow-Green	22	Mohr-Coulomb	150	32	Piezometric Line 1	
US Rockfill	Magenta	21	Mohr-Coulomb	0	40	None	0
Working Platform	Blue	18	Mohr-Coulomb	0	35	None	0
Stage 1 DS Rockfill	Grey	21	Mohr-Coulomb	0	40	Piezometric Line 1	
Zone 2A Transition	Purple	20	Mohr-Coulomb	0	42	Piezometric Line 1	
Tailings	Yellow	20	Mohr-Coulomb	0	32	Piezometric Line 1	

Method Name	Min FS
GLE / Morgenstern-Price	1.428



HATCH

Project

Cadia NTSF Slump ITRB Investigation

Analysis Description

Chainage 2500

Drawn By

TMY

Company

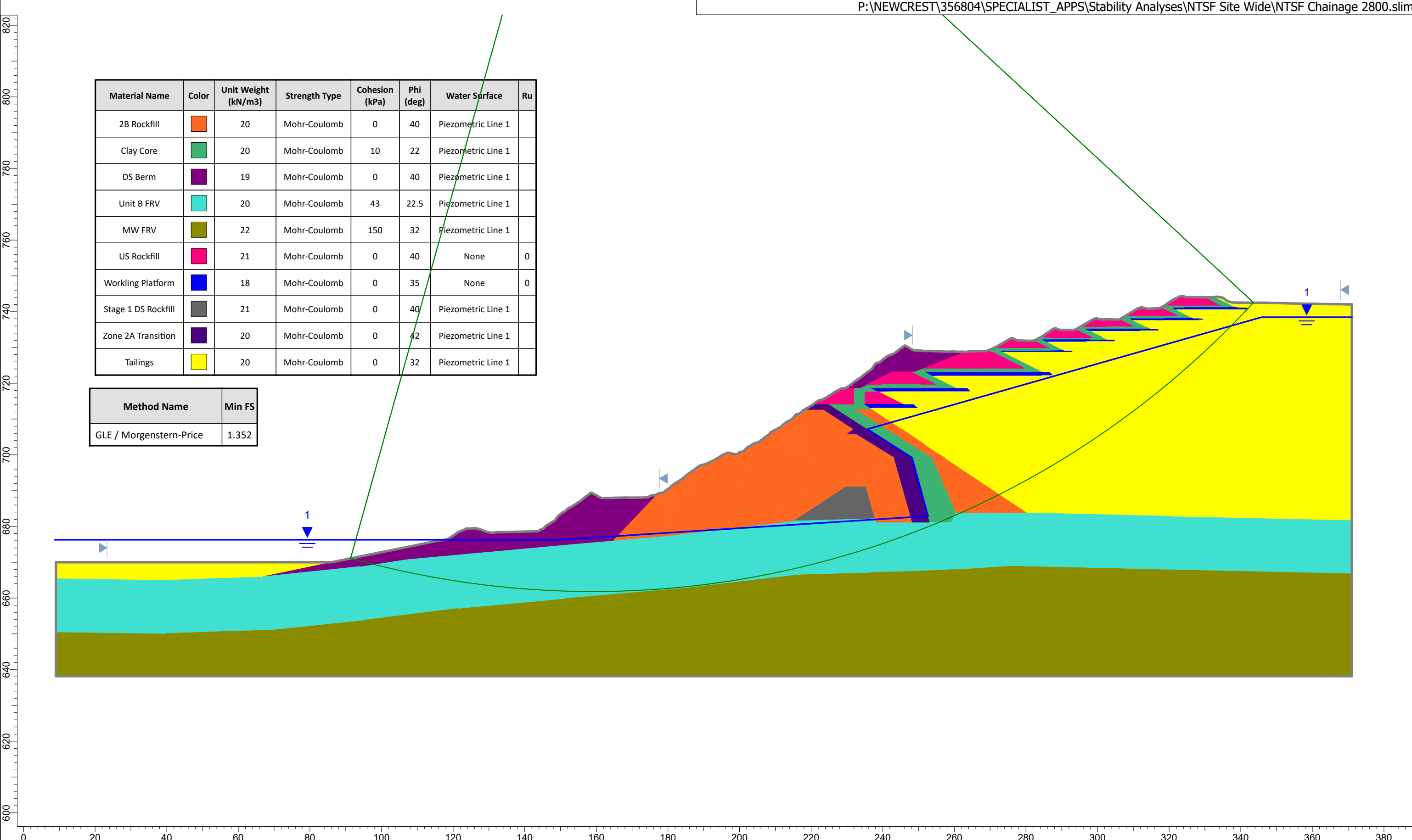
Hatch

Date

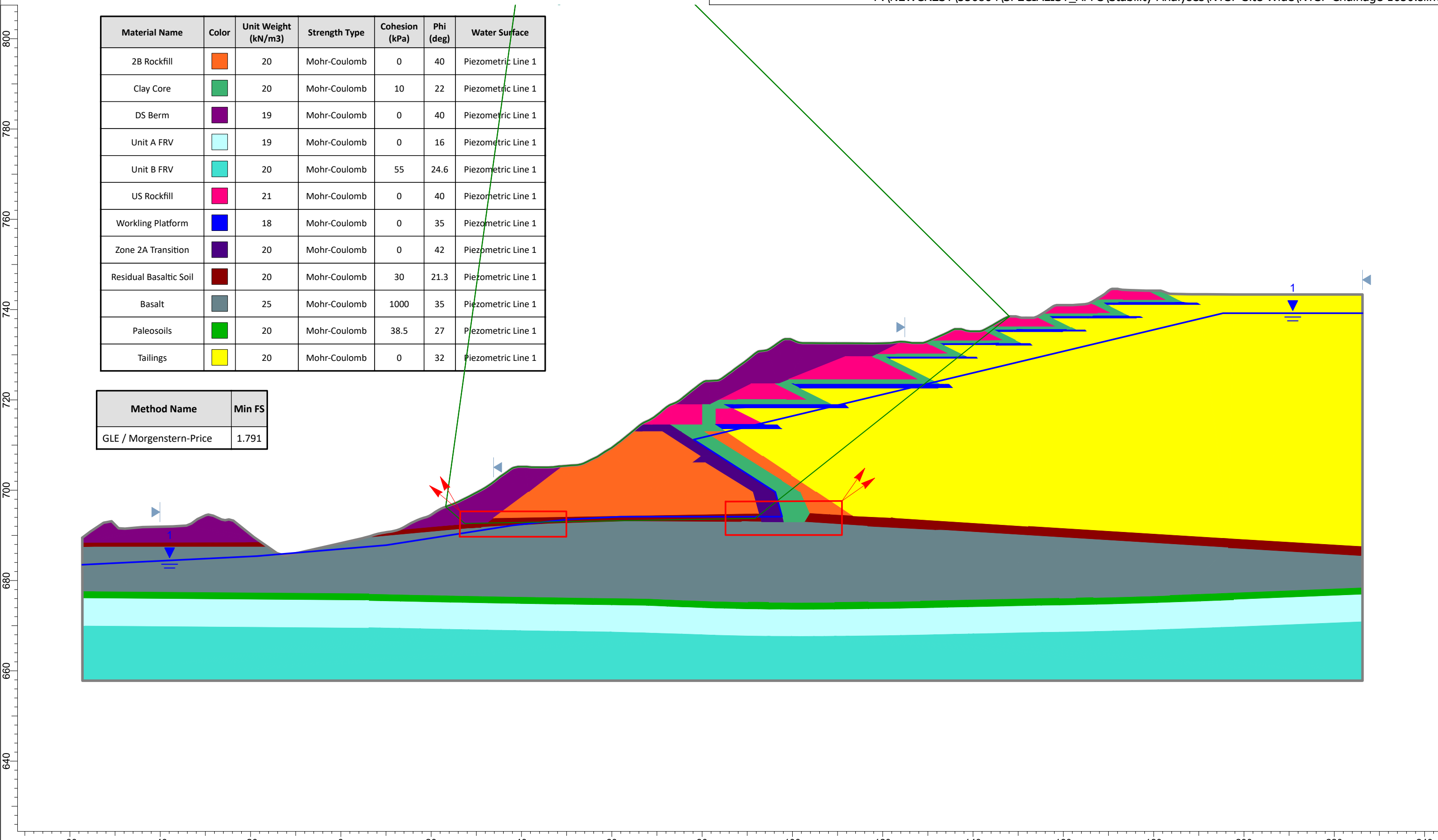
04-Oct-18, 3:22:07 PM

File Name

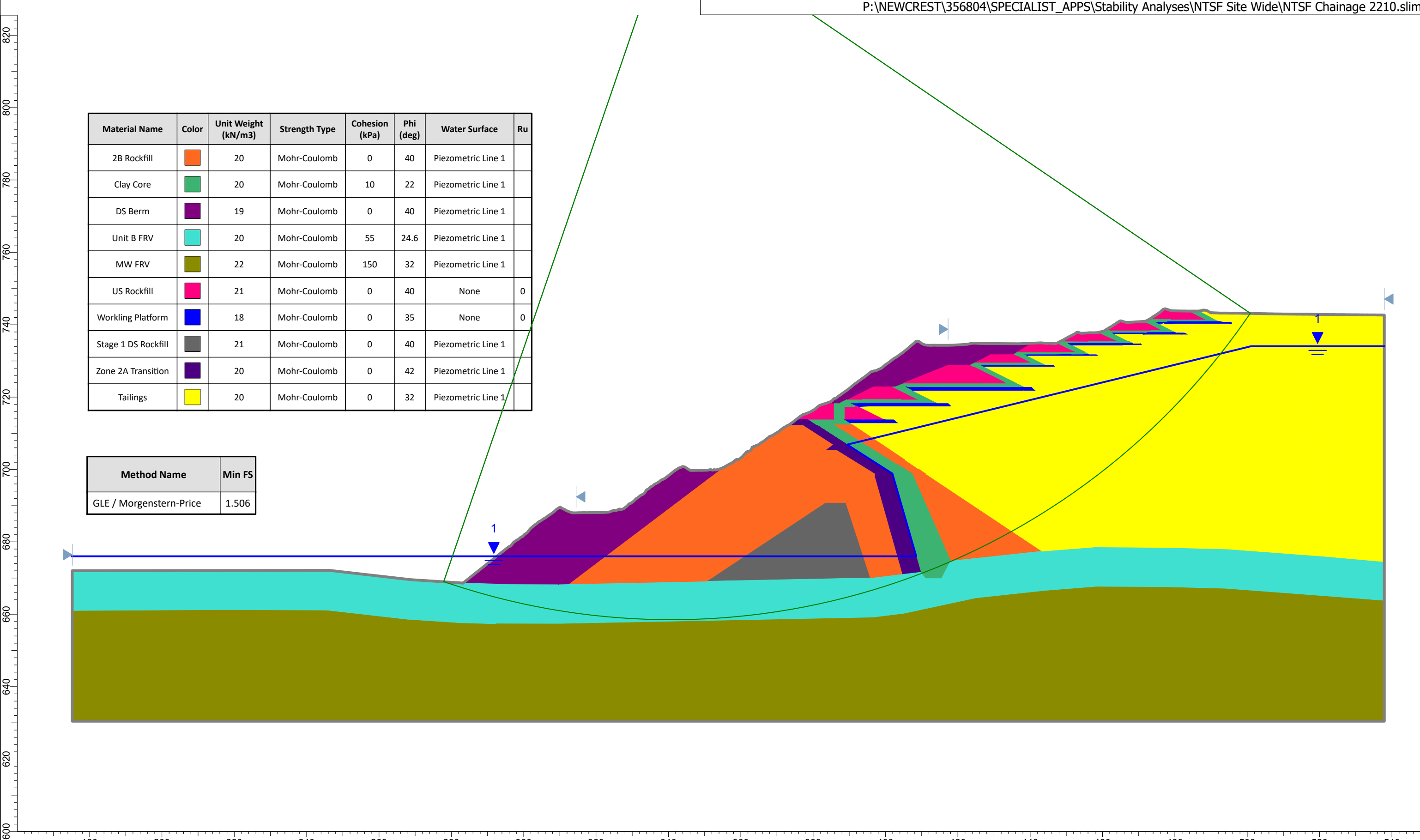
NTSF Chainage 2500.slim

**HATCH**

Project		Cadia NTSF Slump ITRB Investigation	
Analysis Description		Chainage 2800	
Drawn By	TMY	Company	Hatch
Date	04-Oct-18, 3:22:07 PM	File Name	NTSF Chainage 2800.slim



HATCH



HATCH

Project

Cadia NTSF Slump ITRB Investigation

Analysis Description

Chainage 2210

Drawn By

TMY

Company

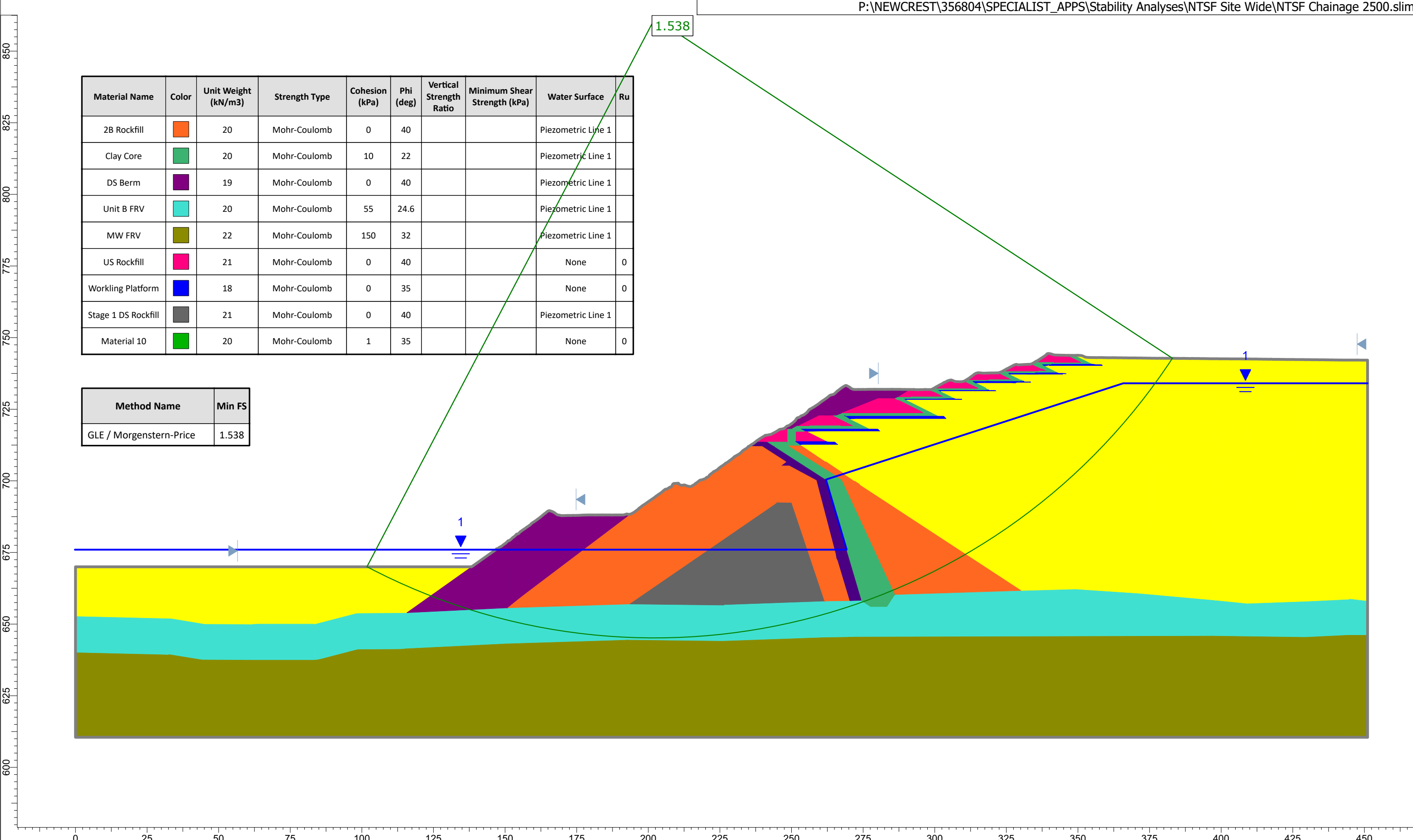
Hatch

Date

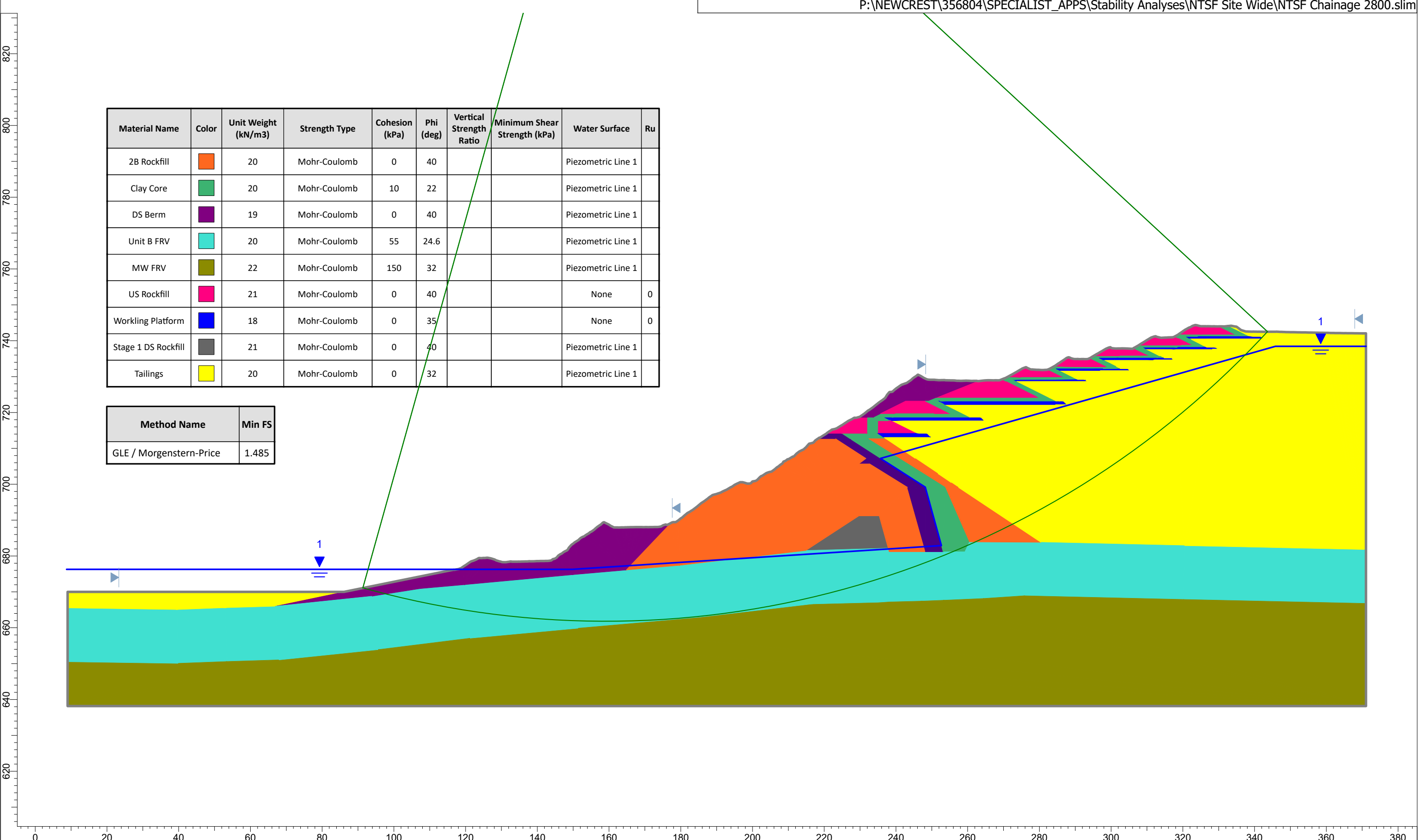
04-Oct-18, 3:22:07 PM

File Name

NTSF Chainage 2210.slim

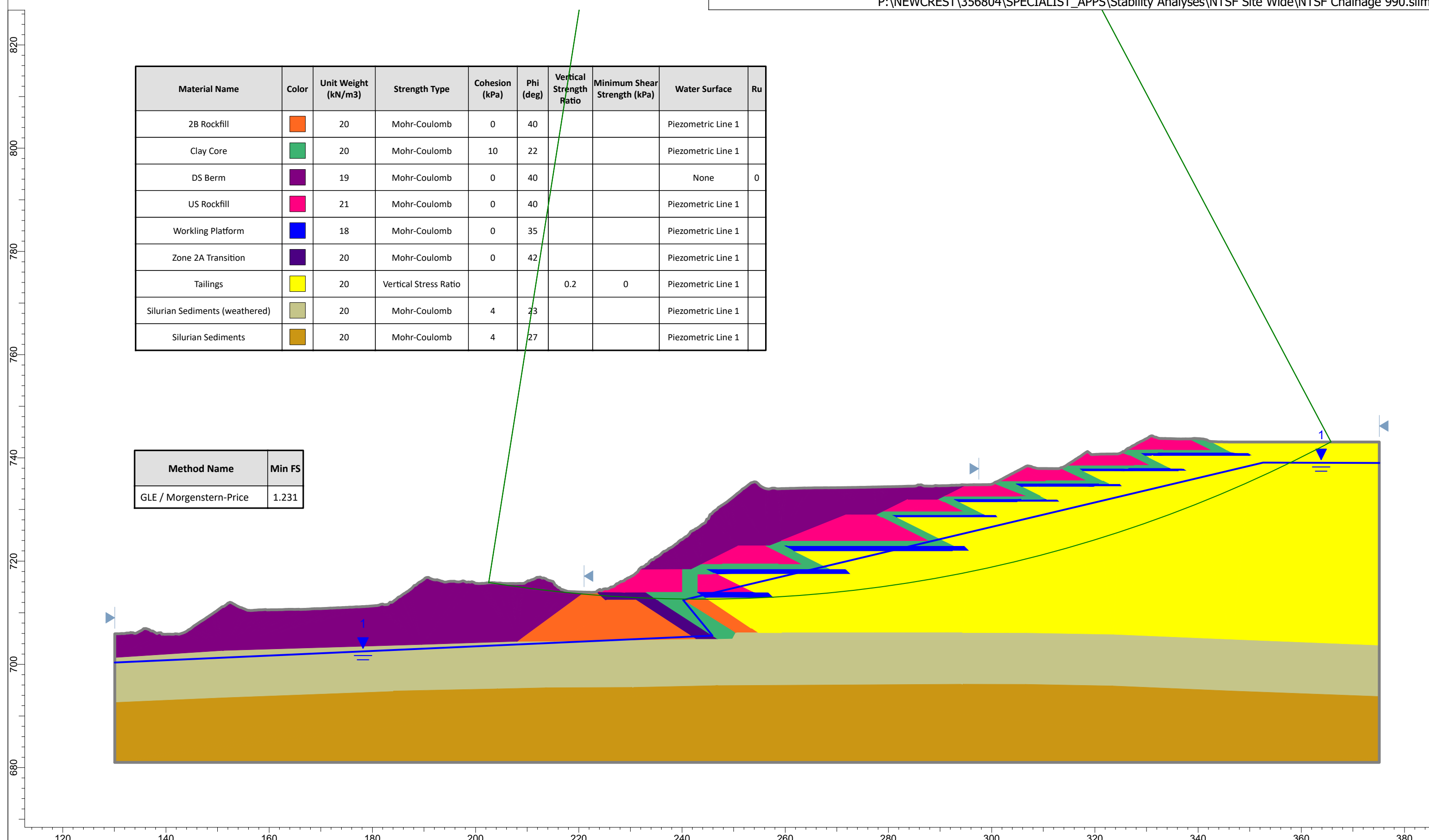
**HATCH**

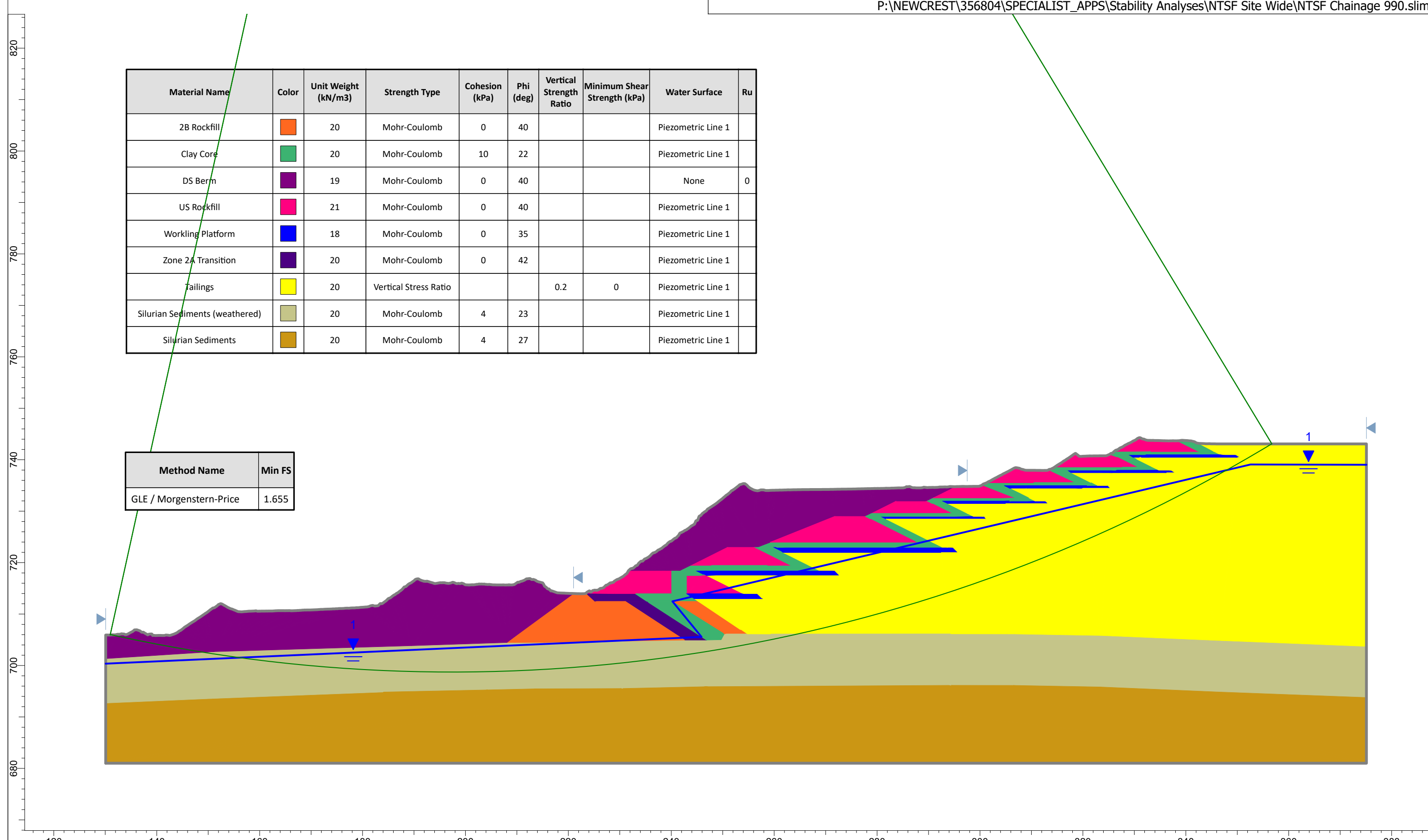
Project	Cadia NTSF Slump ITRB Investigation		
Analysis Description	Chainage 2500		
Drawn By	TMY	Company	Hatch
Date	04-Oct-18, 3:22:07 PM	File Name	NTSF Chainage 2500.slim

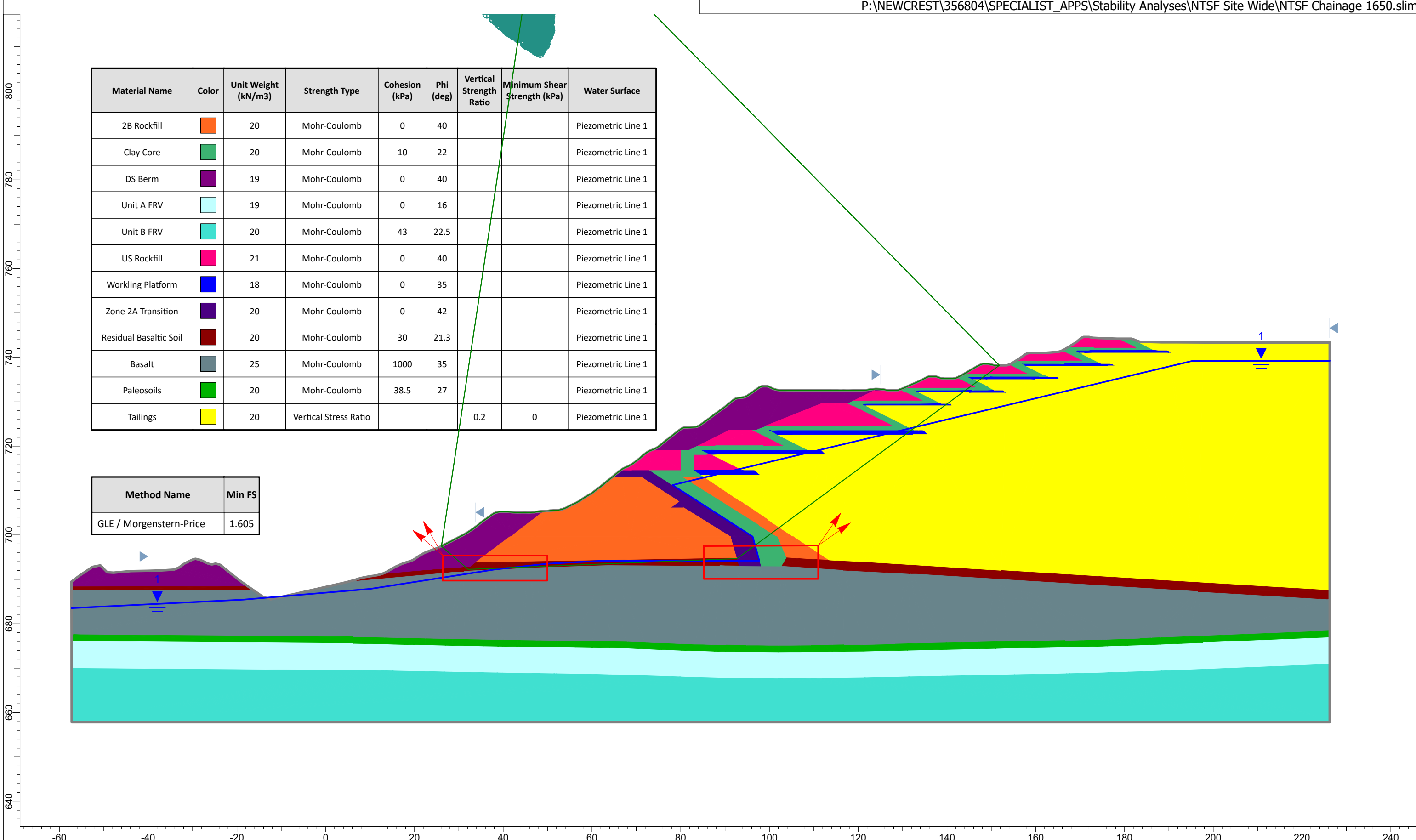


HATCH

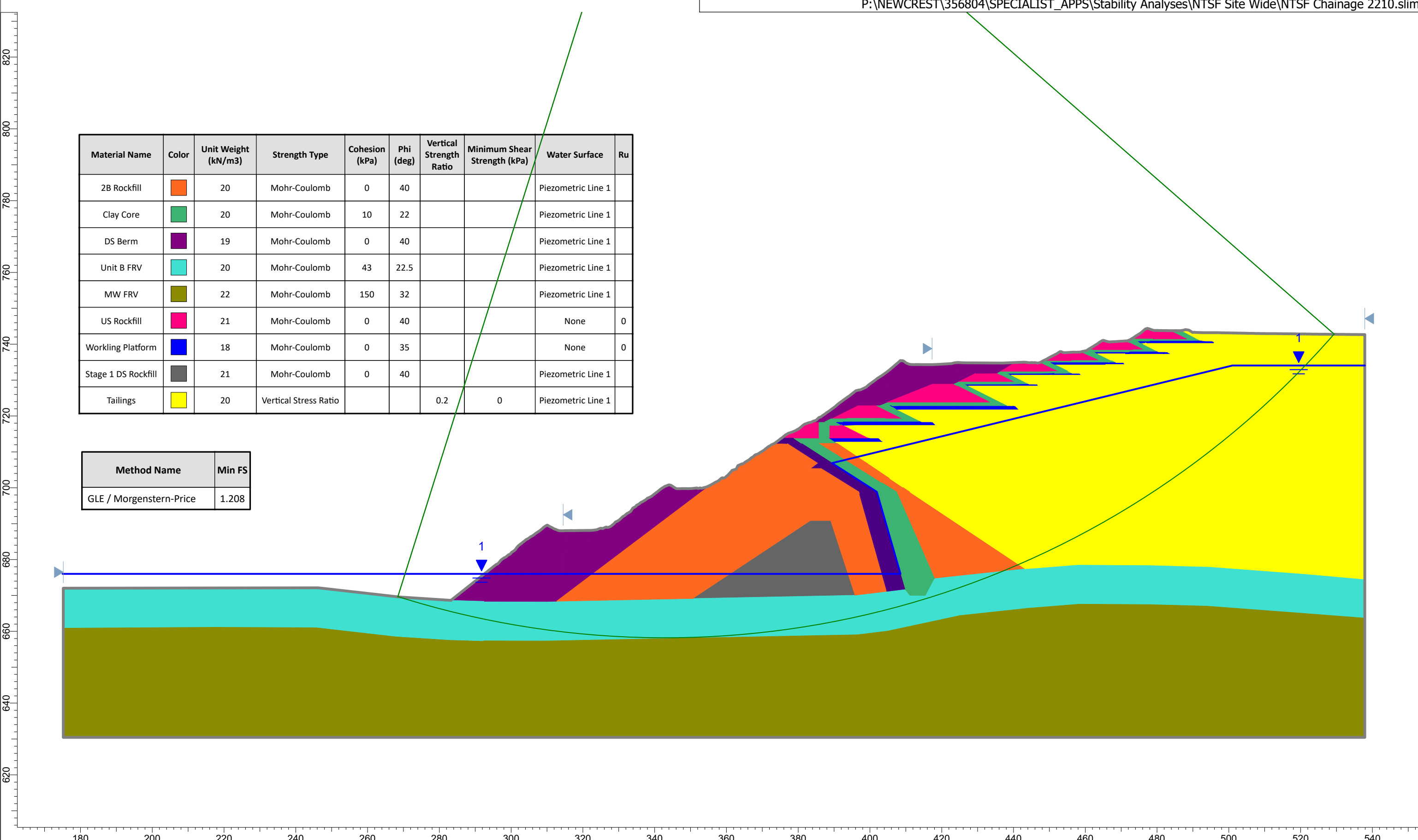
Project		Cadia NTSF Slump ITRB Investigation	
Analysis Description		Chainage 2800	
Drawn By	TMY	Company	Hatch
Date	04-Oct-18, 3:22:07 PM	File Name	NTSF Chainage 2800.slim

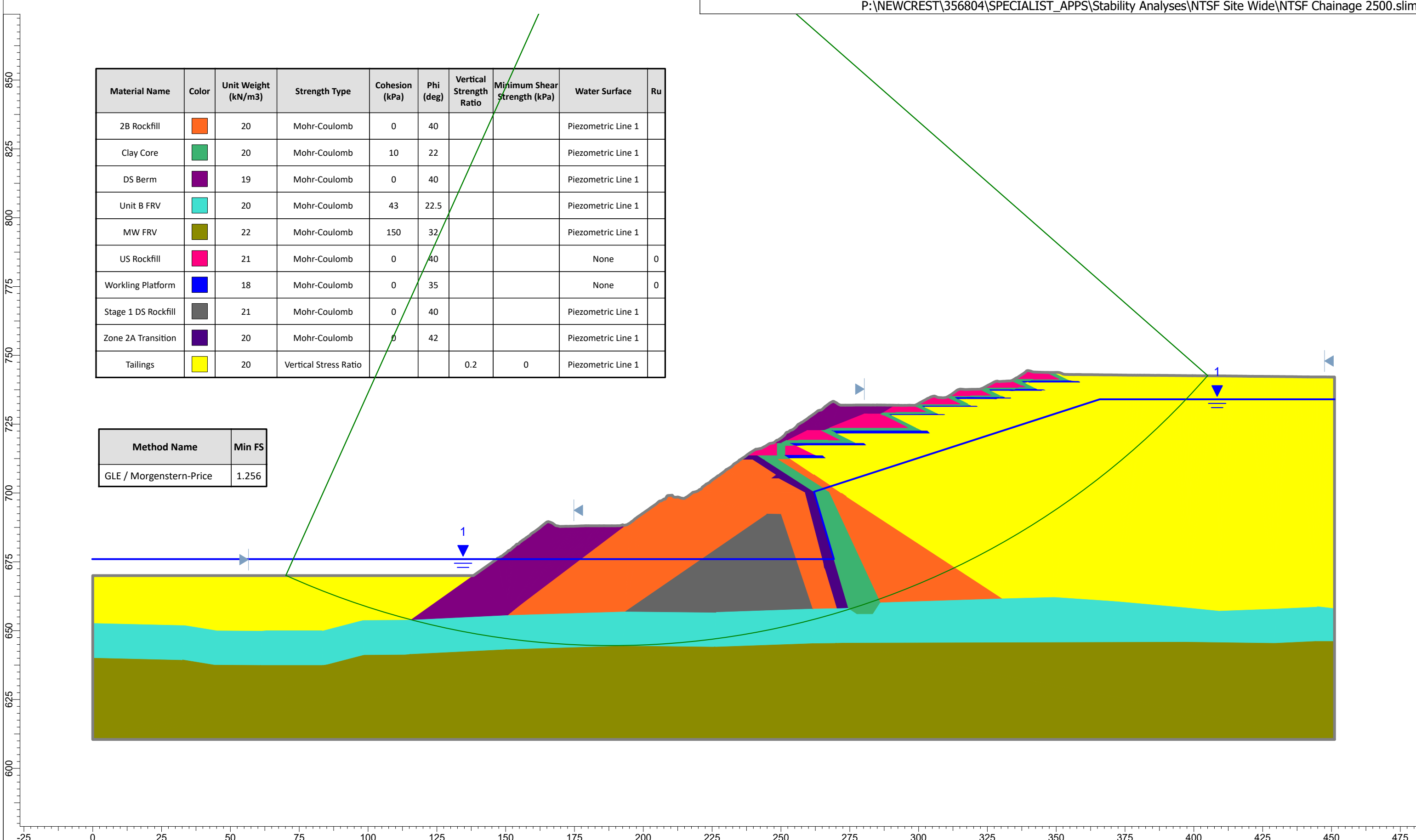




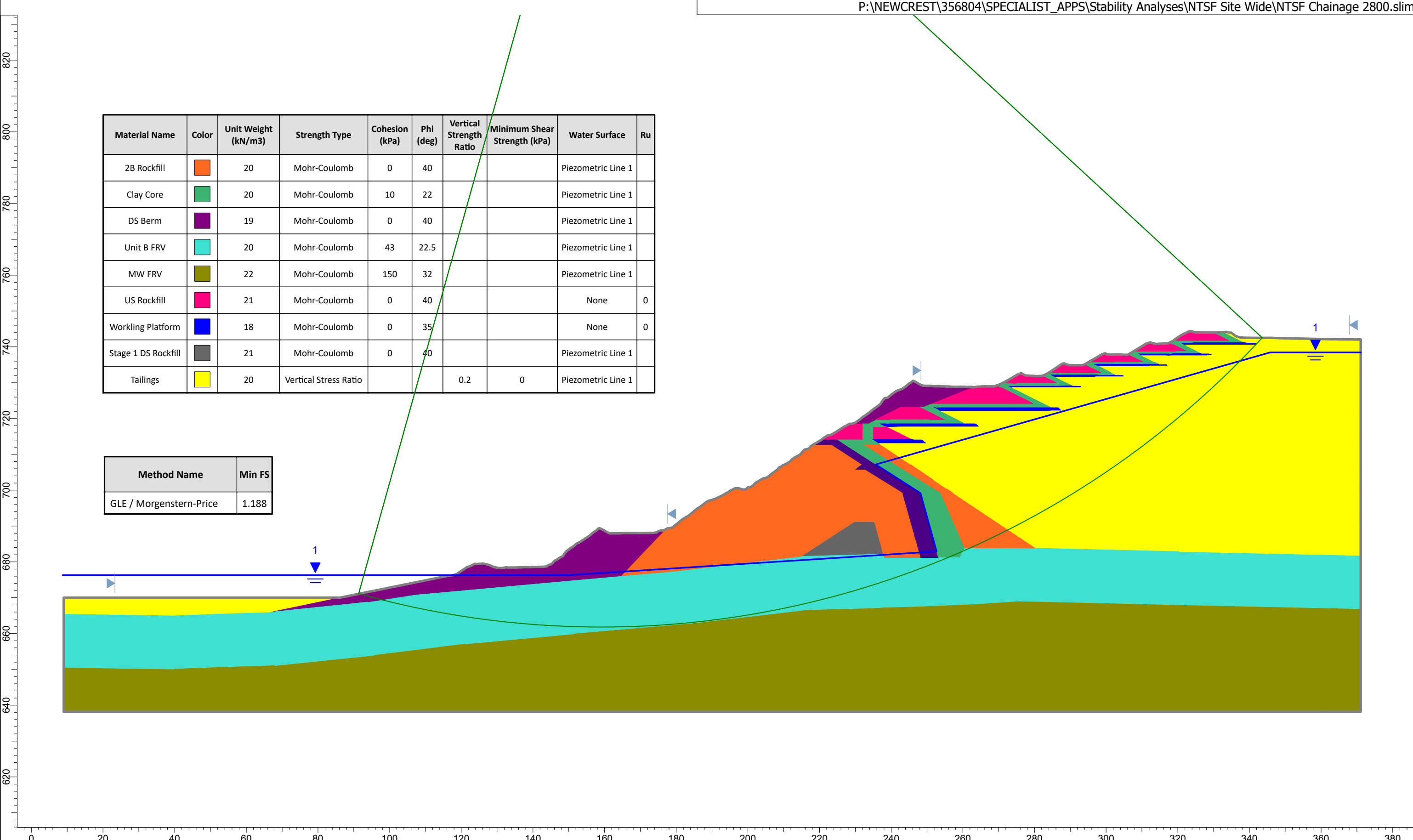
**HATCH**

Project		Cadia NTSF Slump ITRB Investigation	
Analysis Description		Chainage 1650	
Drawn By	TMY	Company	Hatch
Date	04-Oct-18, 3:22:07 PM	File Name	NTSF Chainage 1650.slim





HATCH



HATCH

Project

Cadia NTSF Slump ITRB Investigation

Analysis Description

Chainage 2800

Drawn By

TMY

Company

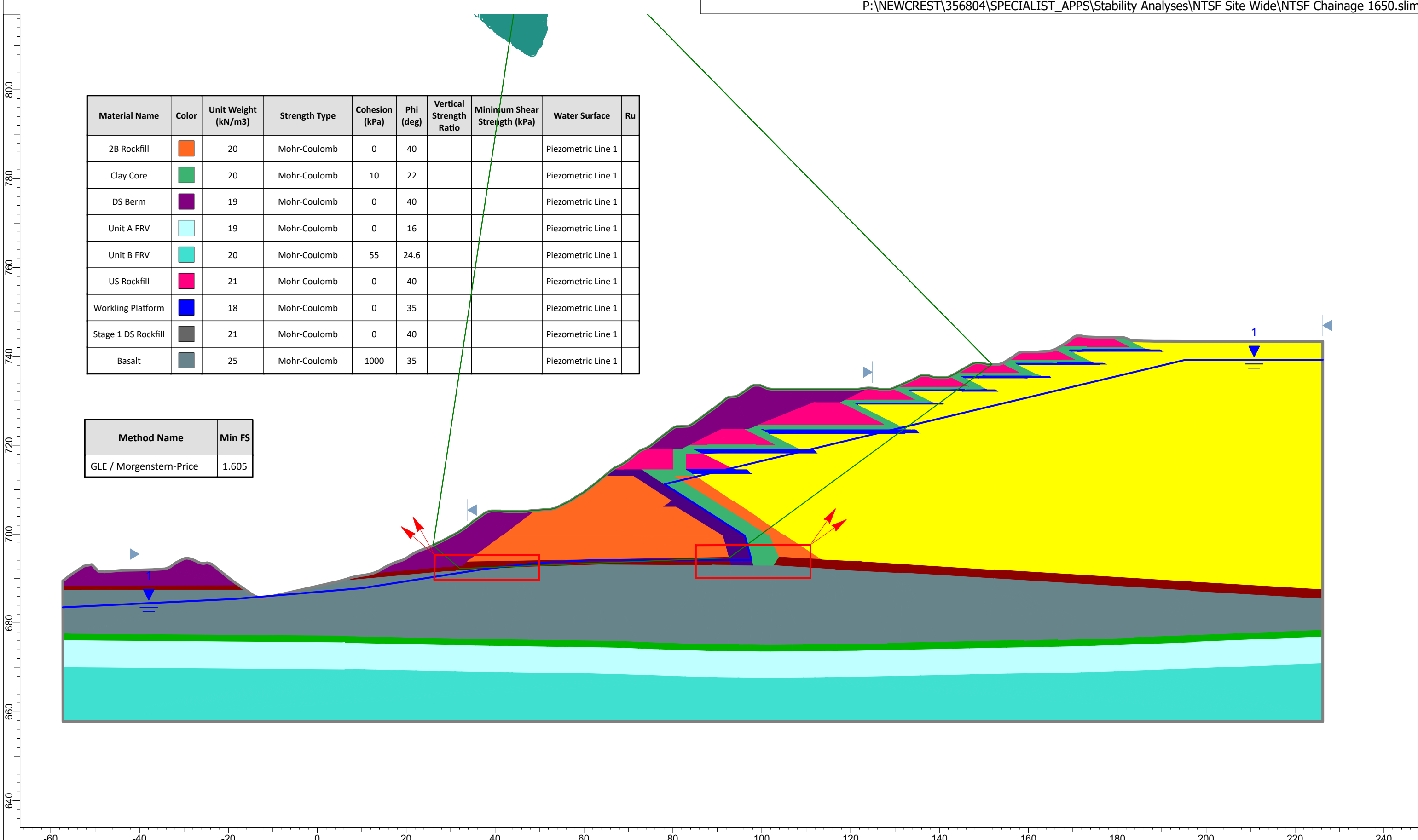
Hatch

Date

04-Oct-18, 3:22:07 PM

File Name

NTSF Chainage 2800.slim

**HATCH**

Project

Cadia NTSF Slump ITRB Investigation

Analysis Description

Chainage 1650

Drawn By

TMY

Company

Hatch

Date

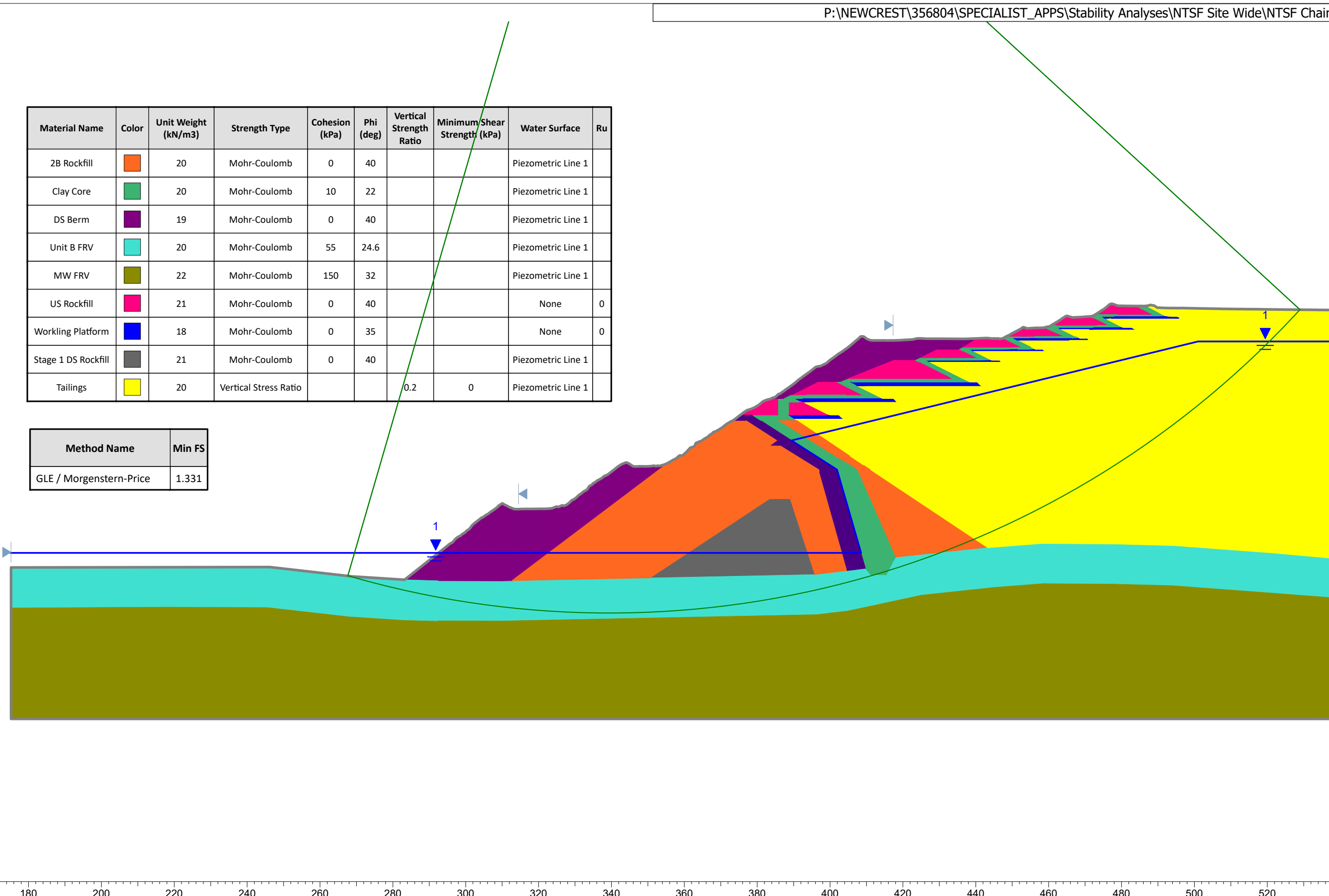
04-Oct-18, 3:22:07 PM

File Name

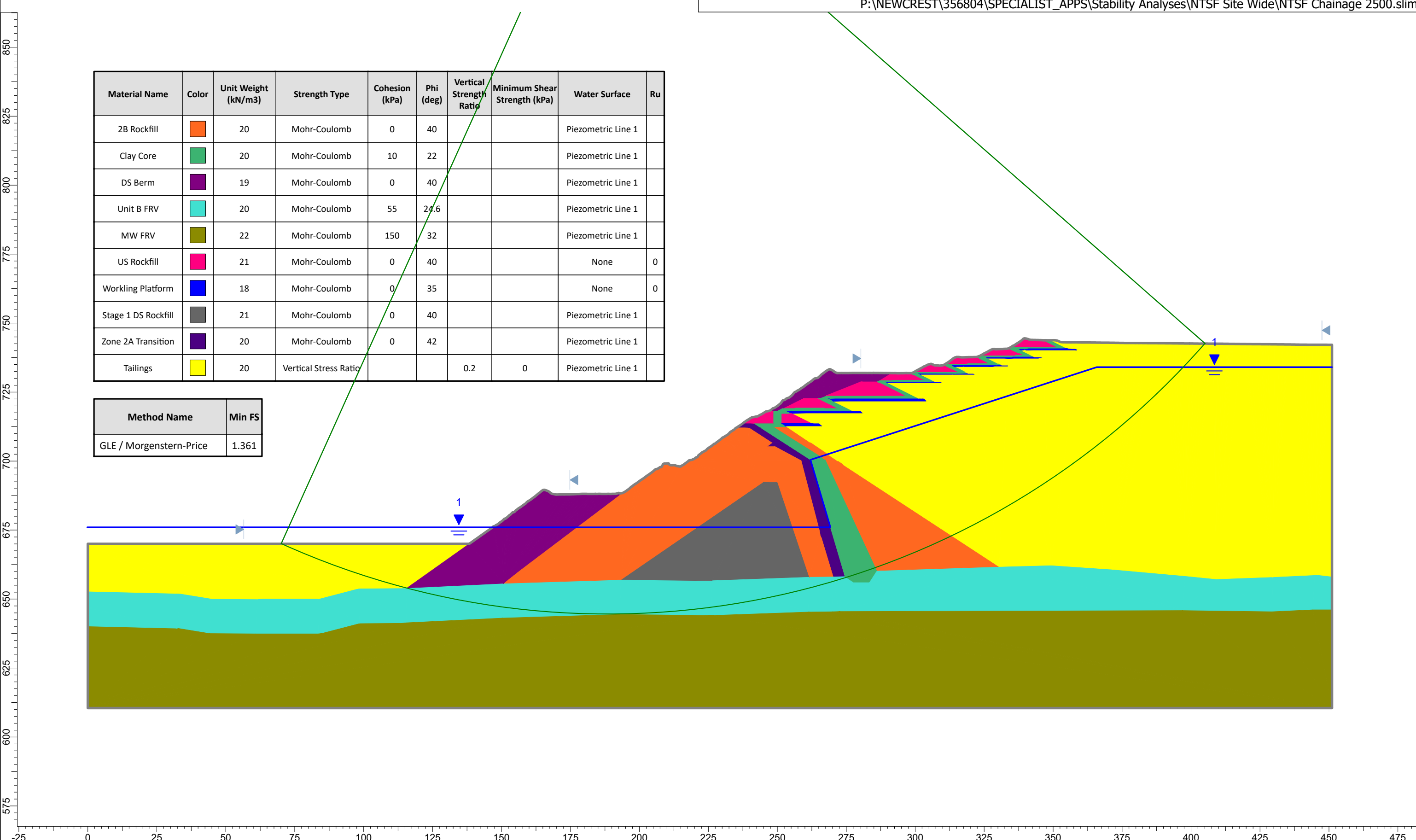
NTSF Chainage 1650.slim

Material Name	Color	Unit Weight (kN/m³)	Strength Type	Cohesion (kPa)	Phi (deg)	Vertical Strength Ratio	Minimum/Shear Strength (kPa)	Water Surface	Ru
2B Rockfill	Orange	20	Mohr-Coulomb	0	40			Piezometric Line 1	
Clay Core	Green	20	Mohr-Coulomb	10	22			Piezometric Line 1	
DS Berm	Purple	19	Mohr-Coulomb	0	40			Piezometric Line 1	
Unit B FRV	Cyan	20	Mohr-Coulomb	55	24.6			Piezometric Line 1	
MW FRV	Yellow-Green	22	Mohr-Coulomb	150	32			Piezometric Line 1	
US Rockfill	Pink	21	Mohr-Coulomb	0	40			None	0
Working Platform	Blue	18	Mohr-Coulomb	0	35			None	0
Stage 1 DS Rockfill	Grey	21	Mohr-Coulomb	0	40			Piezometric Line 1	
Tailings	Yellow	20	Vertical Stress Ratio			0.2	0	Piezometric Line 1	

Method Name	Min FS
GLE / Morgenstern-Price	1.331

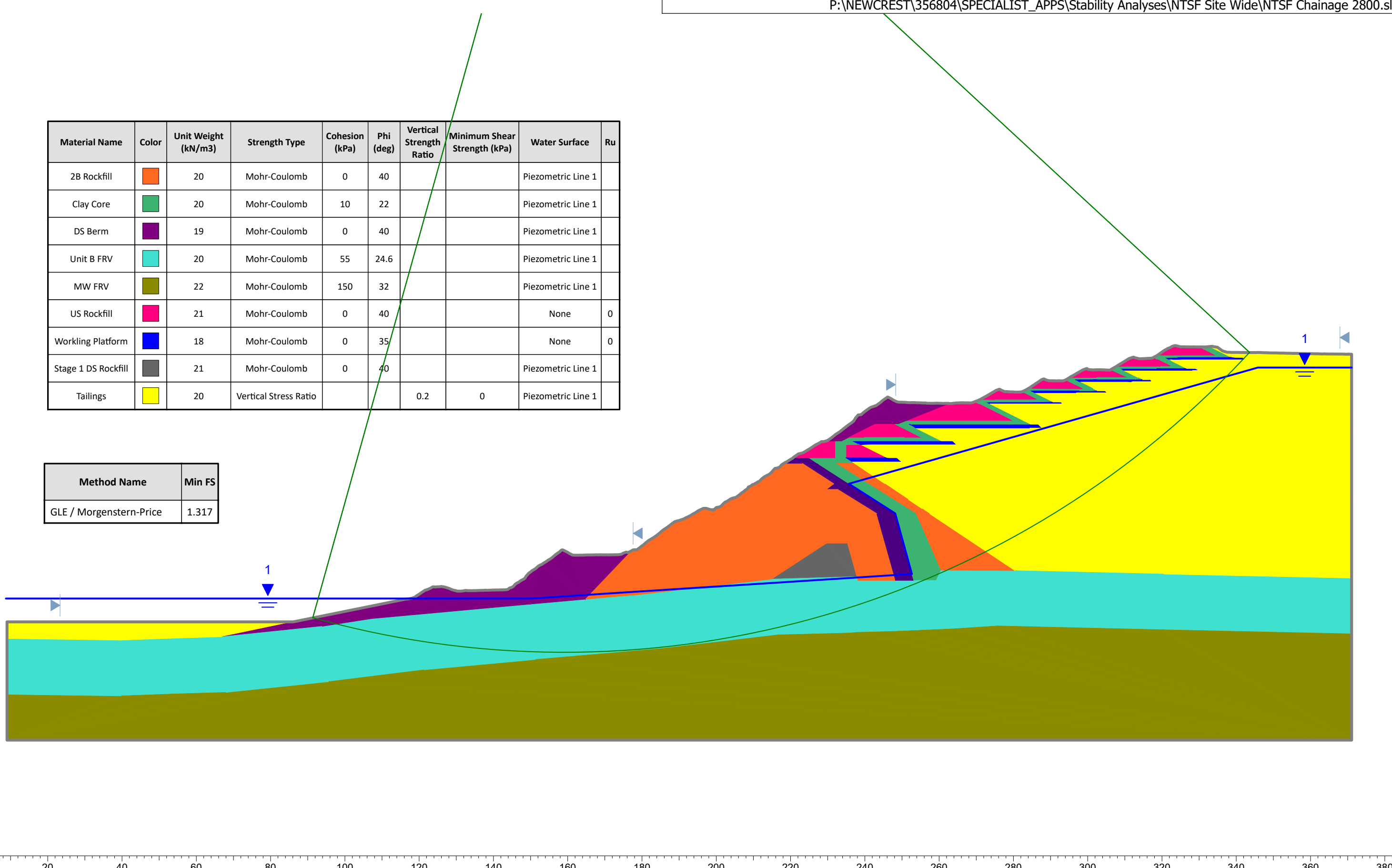


HATCH <small>SLIDEINTERPRET 8.018</small>	Project	Cadia NTSF Slump ITRB Investigation	
	Analysis Description	Chainage 2210	
	Drawn By	TMY	Company
	Date	04-Oct-18, 3:22:07 PM	File Name



Material Name	Color	Unit Weight (kN/m³)	Strength Type	Cohesion (kPa)	Phi (deg)	Vertical Strength Ratio	Minimum Shear Strength (kPa)	Water Surface	Ru
2B Rockfill	Orange	20	Mohr-Coulomb	0	40			Piezometric Line 1	
Clay Core	Green	20	Mohr-Coulomb	10	22			Piezometric Line 1	
DS Berm	Purple	19	Mohr-Coulomb	0	40			Piezometric Line 1	
Unit B FRV	Cyan	20	Mohr-Coulomb	55	24.6			Piezometric Line 1	
MW FRV	Yellow-Green	22	Mohr-Coulomb	150	32			Piezometric Line 1	
US Rockfill	Magenta	21	Mohr-Coulomb	0	40			None	0
Working Platform	Blue	18	Mohr-Coulomb	0	35			None	0
Stage 1 DS Rockfill	Grey	21	Mohr-Coulomb	0	40			Piezometric Line 1	
Tailings	Yellow	20	Vertical Stress Ratio			0.2	0	Piezometric Line 1	

Method Name	Min FS
GLE / Morgenstern-Price	1.317



Project

Cadia NTSF Slump ITRB Investigation

Analysis Description

Chainage 2800

Drawn By

TMY

Company

Hatch

Date

04-Oct-18, 3:22:07 PM

File Name

NTSF Chainage 2800.slim

HATCH

Appendix H

Deformation Analysis



Klohn Crippen Berger

Ashurst Australia

Cadia North Tailings Storage Facility Slump

Deformation Analysis



A03353A01

ISO 9001
ISO 14001
OHSAS 18001

March 2019

TABLE OF CONTENTS

1	INTRODUCTION	1
2	PHASE 1 – MODELLING EVENTS PRIOR TO FAILURE	4
2.1	2D Deformation Analysis	4
2.1.1	General	4
2.1.2	Engineering Properties	6
2.1.3	Instrumentation Data & Visual Observations.....	14
2.1.4	Results.....	16
2.2	Seismic Response Analysis.....	30
2.2.1	General	30
2.2.2	1D Analysis.....	31
2.2.3	2D Analysis.....	36
2.3	Newmark Displacement Analyses	44
2.4	3D Deformation Analysis	45
2.4.1	Model Setup.....	45
2.4.2	Modeling Sequence	46
2.4.3	Results – Final 3D Deformation Model.....	48
3	PHASE 2 – MODELLING POST-FAILURE RESPONSE	64
3.1	General	64
3.2	2D Assessment – Mohr-Coulomb Analysis	64
3.3	2D Assessment – NorSand	65
3.4	FLAC 3D Post-Liquefaction Factor of Safety	67
4	SUMMARY	69
5	CLOSURE	71
REFERENCES.....		72

List of Tables

Table 2.1	NorSand Parameters Provided by the ITRB.....	14
Table 2.2	Summary of Input Time Histories.....	32

List of Figures

Figure 1.1	A) Plan View and B) Oblique View of 2D Section Location and 3D Model Extent Overlain on Pre-Failure Topography	2
Figure 1.2	A) Plan View and B) Oblique View of 2D Section Location and 3D Model Extent Overlain on Post-Failure Topography	3
Figure 2.1	Model Setup.....	5
Figure 2.2	Tailings shear modulus and depth relationship	7
Figure 2.3	Calibration to Clay Core DSS Test Data (Simulated Data shown as Solid Lines) ...	8

TABLE OF CONTENTS

(continued)

Figure 2.4	Calibration to Foundation DSS Test Data (Simulated Data Shown as Solid Lines).....	8
Figure 2.5	Strength-Stress Function for Rockfill Incorporated in the 2D Model (modified after Leps 1970). The Function is Represented with the Solid Red Line.....	9
Figure 2.6	Strength-Stress Function for Rockfill Incorporated in the Early 2D models (modified after Indraratna et al. 1993). The Function is Represented with the Solid Red Line.	10
Figure 2.7	Unit A Calibration Step 1. Simulated Data Shown as Dashed Lines. DSS Test Data Shown as Solid Lines.	11
Figure 2.8	Unit A Calibration Step 2. Simulated Data Shown as Dashed Lines using ITRB's Strength Parameters. DSS Test Data Shown as Solid Lines.	11
Figure 2.9	Unit A Calibration Step 3. Simulated Data Shown as Dashed Lines using ITRB's Strength Parameters. DSS Test Data Shown as Solid Lines.	12
Figure 2.10	Unit A Calibration Step 3. Simulated Data Shown as Dashed Lines using KCB's Alternate Variable Strength Parameters. DSS Test Data Shown as Solid Lines.	12
Figure 2.11	Element Test Calibration of Unit B. Simulated Data Shown as Dashed Lines. CIU Test Data Shown as Solid Lines.	13
Figure 2.12	Survey Prism 5 (Stage 5 crest) Displacement Monitoring Record.....	15
Figure 2.13	InSAR surface movement measurements at CH 20+00.....	16
Figure 2.14	Comparison of Calculated Displacements using A) Board Parameters and B) Alternate KCB Parameters with Monitoring Data at Survey Prism 5	18
Figure 2.15	Calculated Displacement at the Crest of Stage 9 Compared with InSAR Data....	19
Figure 2.16	Horizontal Displacement along Dam Surface Calculated using; A) Board Parameters, B) Alternate KCB Parameters.	20
Figure 2.17	Heave Measurements at the Dam Toe.....	21
Figure 2.18	Development of Strain -Weakening in Foundation Unit A throughout Construction Loading using Board Parameters	22
Figure 2.19	Development of Strain -Weakening in Foundation Unit A throughout Construction Loading using Alternate KCB Parameters	23
Figure 2.20	Distribution of Instability Ratio (η/M_{tc}) Alternate KCB Parameters.....	24
Figure 2.21	Simulated Stress Paths using Board Parameters.....	25
Figure 2.22	Simulated Stress Paths using Alternate KCB Parameters.....	26
Figure 2.23	Change of State Parameter with Time Through Construction Sequence	27
Figure 2.24	Plots showing Difference in Displacement with and without Strain Weakening (SW) of Unit A; (i) Using Board's Parameters, (ii) Using Alternate KCB Parameters.	28
Figure 2.25	Simulated Stress Paths using Board Parameters without Strain Weakening of Unit A	29
Figure 2.26	Simulated Stress Paths using Alternate KCB Parameters without Strain Weakening of Unit A.....	30
Figure 2.27	Column Locations for the 1D Site Response Analyses	31

TABLE OF CONTENTS

(continued)

Figure 2.28	Modulus Reduction and Damping Relationships Applied in the 1D Site Response Analyses.....	33
Figure 2.29	Shear Wave Velocity Relationships used in 1D Site Response Analyses.....	34
Figure 2.30	Example Input Earthquake Time History for the 1D Site Response Analyses.....	34
Figure 2.31	Peak Acceleration and Cyclic Stress Ratio Results for 1D Columns with Two Pulses of Magnitude 4.3 Earthquake Time Histories.....	36
Figure 2.32	Calibration of Hysteretic Damping Parameters for the 2D Analysis to the 1D Modulus Reduction and Damping Relationships	38
Figure 2.33	Comparison of 1D and 2D Site Response Analysis Results for Stress Path Monitoring location 1 (1D Results = SHAKE, 2D Results = FLAC)	39
Figure 2.34	Comparison of 1D and 2D Site Response Analysis Results for Stress Path Monitoring location 2 (1D Results = SHAKE, 2D Results = FLAC)	40
Figure 2.35	Comparison of 1D and 2D Site Response Analysis Results for Stress Path Monitoring location 3 (1D Results = SHAKE, 2D Results = FLAC)	41
Figure 2.36	Comparison of 1D and 2D Site Response Analysis Results for Stress Path Monitoring location 4 (1D Results = SHAKE, 2D Results = FLAC)	42
Figure 2.37	Comparison of 1D and 2D Site Response Analysis Results for Stress Path Monitoring location 5 (1D Results = SHAKE, 2D Results = FLAC)	43
Figure 2.38	Pre-Earthquake Static Shear Stress Ratio (τ/σ'_v ; Static Bias) Calculated in 2D Analysis	44
Figure 2.39	Illustration of 3D Model Setup	45
Figure 2.40	3D Model Foundation Stratigraphy	46
Figure 2.41	Horizontal Displacement Results at End of Buttress Construction Stage – Initial 3D Model	47
Figure 2.42	Peak Strength Variations Applied to Unit A in 3D Sensitivity Analyses.....	48
Figure 2.43	State Parameter Comparison	49
Figure 2.44	Unit A Strength Relationship that Bounded the Observed Behaviour.....	50
Figure 2.45	Plan View Comparison of FLAC3D Displacements with Observed Extent of Failure/ Runout. A) Tailings State Parameter = +0.06; B) Tailings State Parameter = +0.08	51
Figure 2.46	Horizontal Displacement Development: Tailings State Parameter = + 0.06	52
Figure 2.47	Horizontal Displacement Development: Tailings State Parameter = + 0.08	53
Figure 2.48	Comparison of Deformation Modeling Results with Survey Prism Data: Tailings State Parameter = + 0.06	54
Figure 2.49	Comparison of Deformation Modeling Results with Survey Prism Data: Tailings State Parameter = + 0.08	54
Figure 2.50	Comparison of FLAC Surface Displacement Trends with InSAR Results: Tailings State Parameter = +0.06	55
Figure 2.51	Comparison of FLAC Surface Displacement Trends with InSAR Results: Tailings State Parameter = +0.08	55
Figure 2.52	Development of Strain Weakening: Tailings State Parameter = + 0.06	56
Figure 2.53	Development of Strain Weakening: Tailings State Parameter = + 0.08	57

TABLE OF CONTENTS

(continued)

Figure 2.54	Instability Ratio Development: Tailings State Parameter = + 0.06.....	58
Figure 2.55	Instability Ratio Development: Tailings State Parameter = + 0.08.....	59
Figure 2.56	Heave Development: Tailings State Parameter = + 0.06.....	60
Figure 2.57	Development of Surface Horizontal Displacement: Tailings State Parameter = + 0.06	61
Figure 2.58	Comparison of Stress Path Development in FLAC 2D and FLAC 3D: Tailings State Parameter = +0.06	63
Figure 3.1	Displacement Pattern Due to Undrained Strength Mobilization in Tailings Behind the Stage 1 Embankment	65
Figure 3.2	Instability Ratio Contours from Undrained Response Assessment of Tailings ...	67
Figure 3.3	Displacement Results from the 3D Shear Strength Reduction Factor of Safety Analysis	68

1 INTRODUCTION

This appendix documents the 2D and 3D deformation analyses, and 1D and 2D seismic response analyses, undertaken on the failed section of the Cadia North Tailings Storage Facility (NTSF). Analyses were done under direction from the Independent Technical Review Board (ITRB) to help understand the failure mechanism. The analyses have been completed in a series of stages where learnings from each preceding stage have informed the direction of the next stage. The analyses have been grouped broadly into the following two Phases:

- Phase 1 – Modelling of events prior to failure
 - ◆ This Phase was focused on determining the likely conditions immediately prior to failure, as well as how these conditions developed, with the aim of identifying potential mechanism(s) that would lead a dam in this condition to fail.
 - ◆ This involved simulating the construction sequence of the NTSF, and typically involved assignment of drained (i.e. effective stress) strength parameters to each fill, tailings and foundation unit. The only exception to this was the parameters for the extremely weathered Forest Reef Volcanics (FRV, termed ‘Unit A’) that were derived from undrained laboratory tests.
 - The parameters were assigned based on laboratory testing and then varied within the range of the laboratory test data to ‘history match’ the model to observations at the NTSF throughout its construction history, and particularly those shortly before failure.
 - This simulation of the NTSF construction sequence was completed in 2D and 3D.
 - ◆ This Phase also involved a series of 1D and 2D seismic response analyses to determine the potential impact of the earthquake loading on the NTSF dam, tailings and foundation. Earthquake inputs were provided by the ITRB.
- Phase 2 – Modelling the post failure response
 - ◆ Having identified candidate mechanisms for triggering the failure in Phase 1, the aim of this Phase was to implement these failure mechanisms and observe if the resulting failure in the model provided a good representation of the field observations.

The Phase 1 analyses are described in Section 2 of this appendix and the Phase 2 analyses are described in Section 3.

The 2D deformation analyses were conducted on a section through CH19+50 (Figure 1.2). The 3D deformation analyses were done on an 825 m length of the NTSF between CH16+18 to CH24+43. The failure occurred between roughly CH18+50 and CH21+50.

Key inputs to the analyses included foundation stratigraphy and strength, strength and stiffness of the construction materials, internal zonation of the NTSF dam and pore pressures at the end of each construction stage.

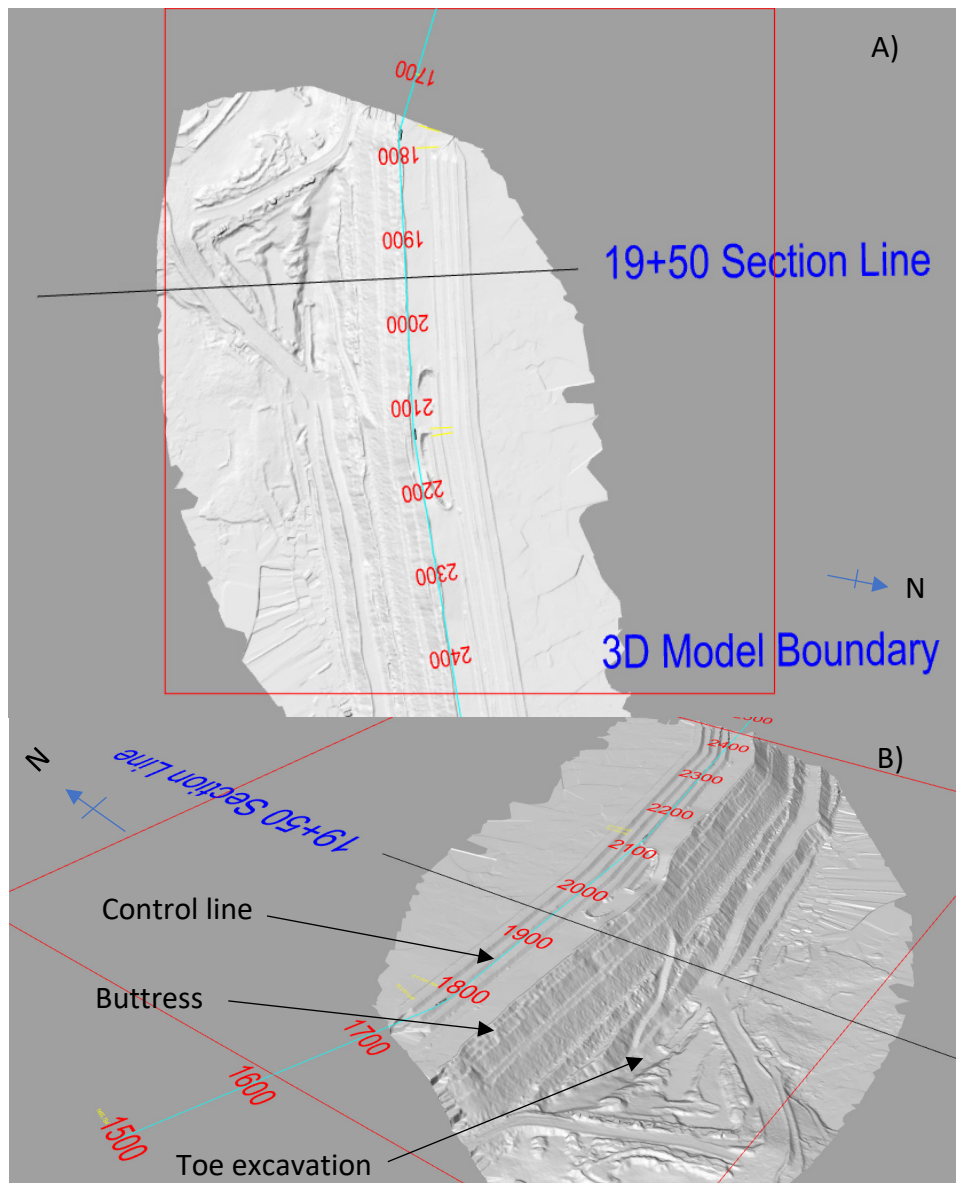


Figure 1.1 A) Plan View and B) Oblique View of 2D Section Location and 3D Model Extent Overlain on Pre-Failure Topography

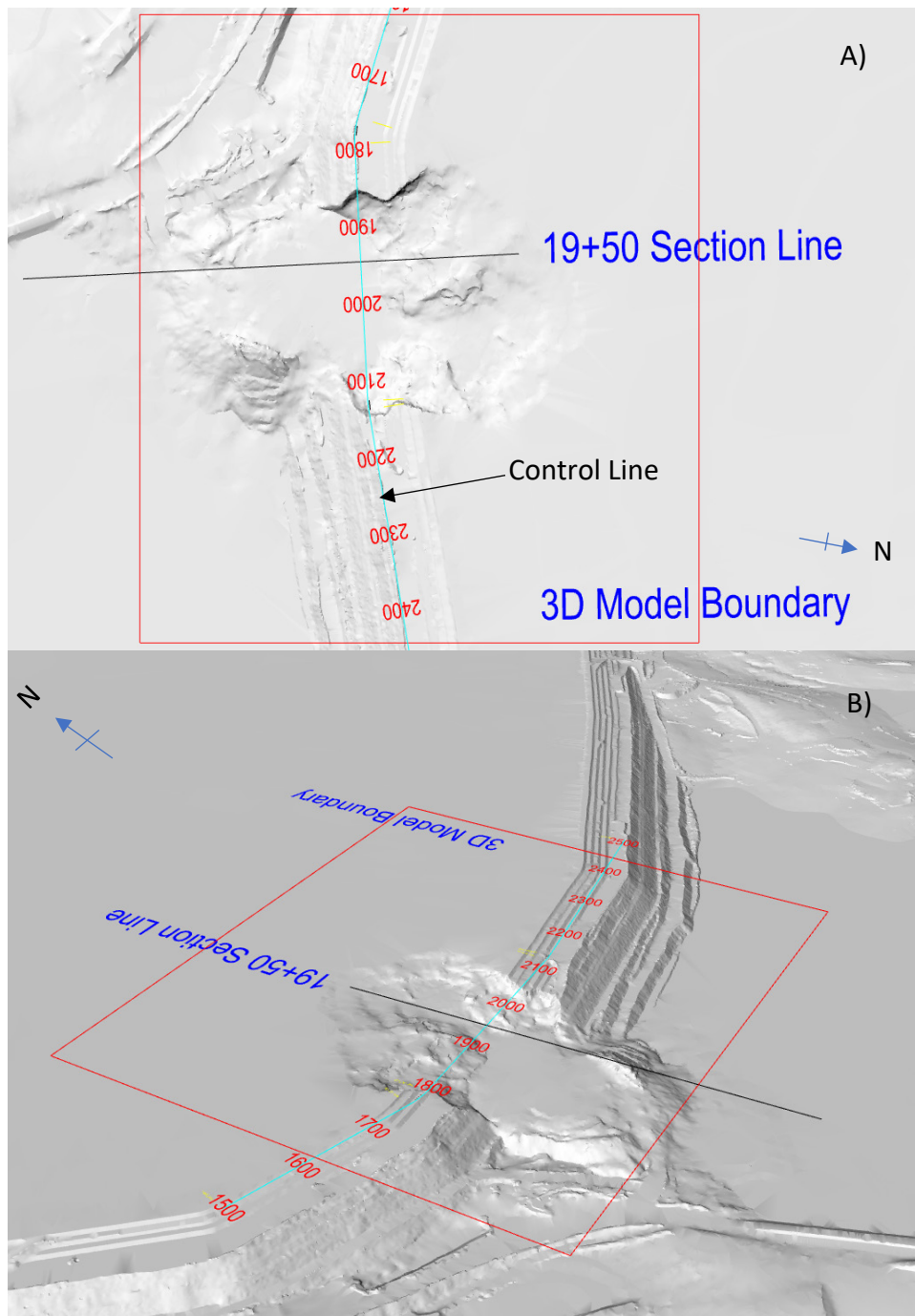


Figure 1.2 A) Plan View and B) Oblique View of 2D Section Location and 3D Model Extent Overlain on Post-Failure Topography

2 PHASE 1 – MODELLING EVENTS PRIOR TO FAILURE

2.1 2D Deformation Analysis

2.1.1 General

The 2D analyses were completed using the finite difference software Fast Lagrangian Analysis of Continua (FLAC) version 8.0.443. The analyses were conducted in a series of iterations, with each iteration increasing the complexity of material behavior to enable evaluation of the influence of different factors. The models were initially constructed using an elastic parameter set for all materials to identify the elastic distribution of deformations within the dam. The models were further developed using Mohr-Coulomb constitutive models with variation of shear stiffness assigned to the rockfill and tailings, and then developed further to include strain-weakening behavior in the weathered foundation units and coupling of volumetric and shear behavior in the tailings. This strain-weakening behavior was implemented by initially assigning the hyperbolic-elastic ‘CHSoil’ soil model in FLAC and then switching to the ‘strain-softening’ soil model in any zone that exceeded roughly 6 % shear strain. The updated behavior of the tailings was implemented using the critical state constitutive model NorSand (after Jefferies and Been 2016). The NorSand analysis was performed to analyze the influence of density-dependent strength and stiffness variations on the response of the tailings. The NorSand constitutive model was implemented as a user-defined model (UDM) dll file.

Before using the CHSoil, strain-softening and NorSand constitutive models in the 2D analyses, 1D ‘element tests’ were completed to either develop the parameters required for these models or to confirm that the parameters supplied by the ITRB were providing the intended response when used in FLAC.

A series of sensitivity analyses was also completed to assess the effect of variations such as not implementing strain weakening in the Unit A foundation unit after the peak shear strain was reached, and adding increments of pore pressure that could potentially have been generated by the earthquakes.

The models were developed to reflect the sequential construction stages of the NTSF. The staged-construction was simulated in the model by sequentially activating the dam components and tailings layers and updating the model pore pressures. Internal zonation details of the NTSF dam, comprising rockfill, clay core and the transition zone were included in the original downstream-constructed Stage 1 and 2 construction layers. For the Stage 3 to 10 construction layers, the whole containment berm portion of the dam raise was modelled as rockfill, thereby reducing the complexity in the model construction. In all these upper layers, the dimensions of the transition zones were insignificant compared to the rockfill and would not have a significant impact on the model results.

2.1.1.1 Model Geometry and Stratigraphy

The model geometry was developed using the topographical survey and geological site characterization data supplied by the ITRB in the form of 3D AutoCAD surfaces, as well as historical pond elevation data and interpretation of subaerial beach width from GoogleEarth time-lapse aerial photographs. The fill and foundation elements were grouped to allow sequencing of

staged-construction and to include inter-stage excavation or deposition downstream of the dam toe. This grouping of materials is shown in Figure 2.1.

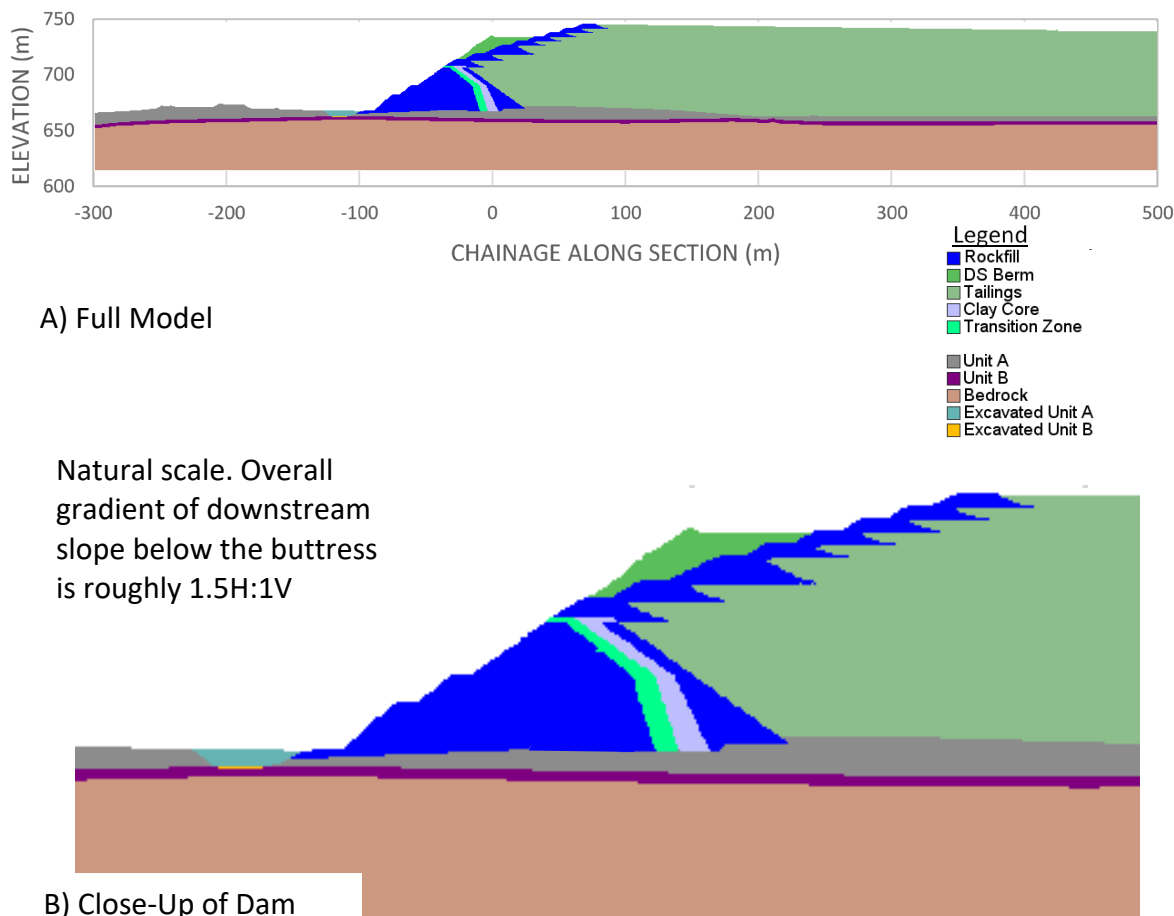


Figure 2.1 Model Setup

The following nomenclature was used for different areas of the model:

- Foundation: material between the pre-construction ground surface and the upper surface of the less weathered/fresh bedrock was referred to as 'Foundation' throughout the modeling. This was updated throughout the course of the investigation as additional data were collected allowing the unit to be subdivided. In the ultimate model, the Foundation was discretized into the following two units:
 - ◆ Unit A – An extremely weathered, intermediate plasticity clay, layer of the Forest Reef Volcanic (FRV) bedrock present immediately below the prepared ground surface along Section 19+50. The thickness of this unit was defined based on the top and bottom 3D AutoCAD surface files provided by the ITRB, which were based on the findings of the post-failure site investigation.
 - ◆ Unit B – A highly weathered layer of the FRV that is more extensive than Unit A. Along Section 19+50, this layer is sandwiched between Unit A and the less weathered/fresh FRV bedrock. A uniform thickness of 2.5 m was assigned to Unit B in the 2D model. The

thickness of 2.5 m was defined based on the drill hole logs collected approximately 80 m downstream of the control line shown on Figure 1.2.

- Bedrock – FRV from the base of Unit B to the base of the model.
- Rockfill – Comprises the general fill for the downstream-constructed stages (Stages 1 and 2), the containment berm for the following stages and the buttress.
- Clay core – The region downstream of the upstream rockfill and upstream of the transition zone in Stage 1 and 2 construction.
- Transition zone – The zone downstream of the clay core and upstream of the downstream rockfill in Stage 1 and 2 construction.
- Tailings – Material contained upstream of the dam and above the original (prepared) ground surface.

2.1.1.2 Other Model Inputs

In addition to the geometry discussed in the preceding section and the parameters discussed in the following section, it was necessary to specify boundary and initial conditions in the deformation models.

The lateral model boundaries were specified as ‘roller’ boundary conditions, which were free to move vertically but fixed horizontally. The base boundary was fixed in the horizontal and vertical directions. These boundaries were set a sufficient distance from the dam to avoid influence on the model results in the region of interest.

The initial stresses in the model were set at an assumed horizontal stress ratio (K_0) of 1 in the foundation and 0.7 in the tailings. The lateral stress in the other units was not specified and was determined by assigning an elastic parameter set and switching on gravity in these units before changing the constitutive model to the intended Mohr-Coulomb relationship or other constitutive model.

2.1.2 Engineering Properties

2.1.2.1 Elastic

Tailings

For the initial analyses, the elastic properties of the tailings were defined using the seismic dilatometer (SDMT) data collected close to the slump area on Jan 21, 2017. The small strain shear modulus (G_0) was calculated from the shear wave velocity (V_s) and density (ρ) of the tailings, which was then converted to an approximate large strain shear modulus (G) by dividing G_0 by a factor of three. A trend of G versus depth was then defined for the data (Figure 2.2), which was implemented in the model. The bulk modulus (K) of the tailings was defined in the models by using an assumed Poisson’s ratio (v) of 0.2 and calculating K from G and v using the following equation:

$$K = \frac{2G(1+v)}{3(1-2v)}$$

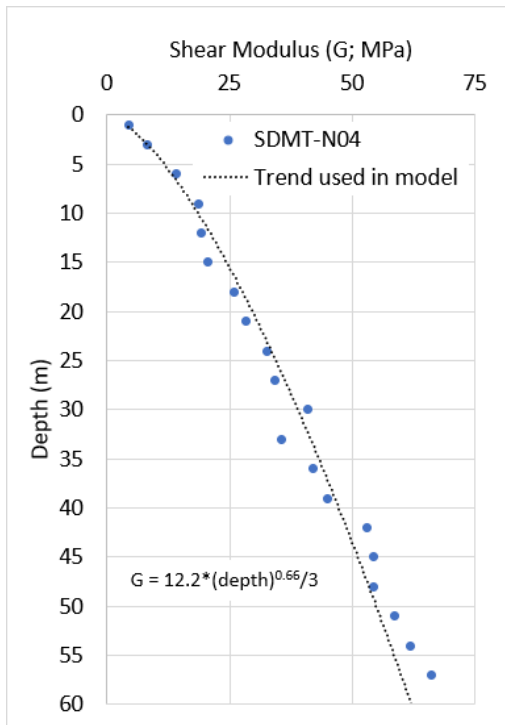


Figure 2.2 Tailings shear modulus and depth relationship

Rockfill

In early stages of the modeling, sensitivity analyses were completed with different values of stiffness, which led to values of $G = 17$ MPa and $K = 37$ MPa being used, which were in the range of rockfill values with a similar construction methodology documented by Hunter and Fell (2002) and Hunter (2003). The stiffness values in the ultimate model were adopted from the ITRB interpretation. The ultimate model was assigned a slightly higher G of 22 MPa and K of 65 MPa.

Transition zone

The transition zone was modelled with a G of 30 MPa and K of 65 MPa. A slightly larger shear modulus was selected for the transition zone compared to the rockfill due to its finer particle size and method of construction.

Clay Core

In early analyses, the clay core was modelled with a G of 15 MPa and K of 27 MPa based on element test simulations of limited laboratory data available at the time (see Figure 2.3). Since the analysis was not sensitive to this material, these parameters were not reviewed in later analyses.

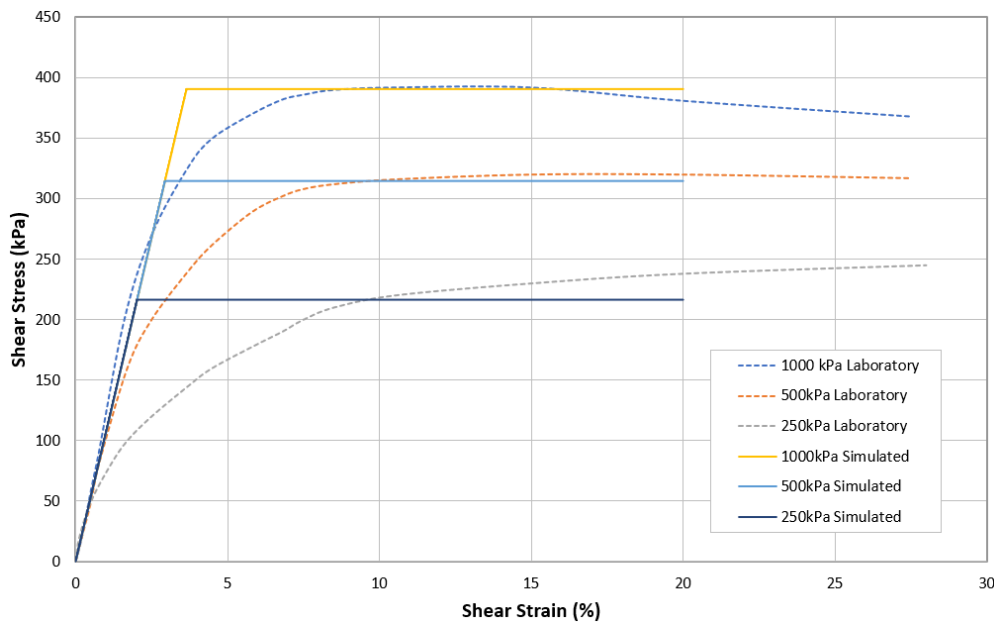


Figure 2.3 Calibration to Clay Core DSS Test Data (Simulated Data shown as Solid Lines)

Foundation

In early analyses, the foundation was modelled as a single unit overlying the bedrock and was assigned $G = 15 \text{ MPa}$ and $K = 33 \text{ MPa}$ based on element test simulations of limited laboratory data available at the time (see Figure 2.4). These parameters were later updated using the CHSoil and strain-softening constitutive models in FLAC based on additional laboratory data.

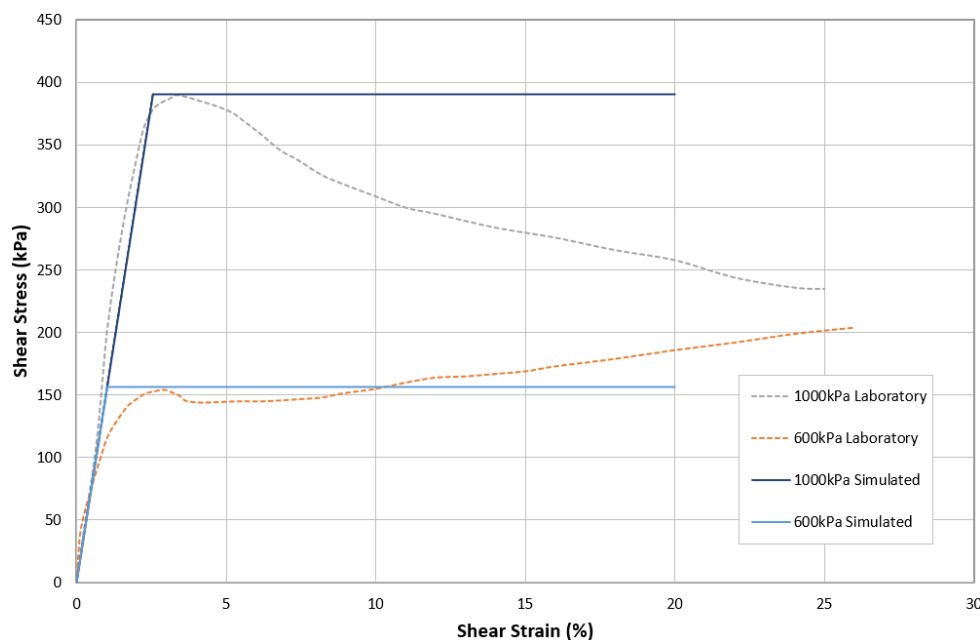


Figure 2.4 Calibration to Foundation DSS Test Data (Simulated Data Shown as Solid Lines)

Bedrock

The less weathered/fresh bedrock unit was modelled as a linear elastic material in all analyses. This unit was modelled with a G of 130 MPa and K of 215 MPa to represent a very stiff material and impose a clear stiffness contrast between the bedrock and overlying Foundation.

2.1.2.2 Mohr-Coulomb

Rockfill

Due to limited information available on the rockfill, the strength of this unit was initially assigned a strength-stress function based on empirical relationships (Figure 2.5). The function was based on the lower bound strength corresponding to a rockfill with low density, poor grading and weak particles, with a minimum friction angle of 40°. The defined function is also within the strength bounds suggested by Indraratna et al. 1993 (Figure 2.6). This was later simplified to an effective friction angle of 40° for consistency with other analyses, and then updated again to a strength function of $\tau = 1.9 \sigma_n^{0.85}$, as instructed by the ITRB.

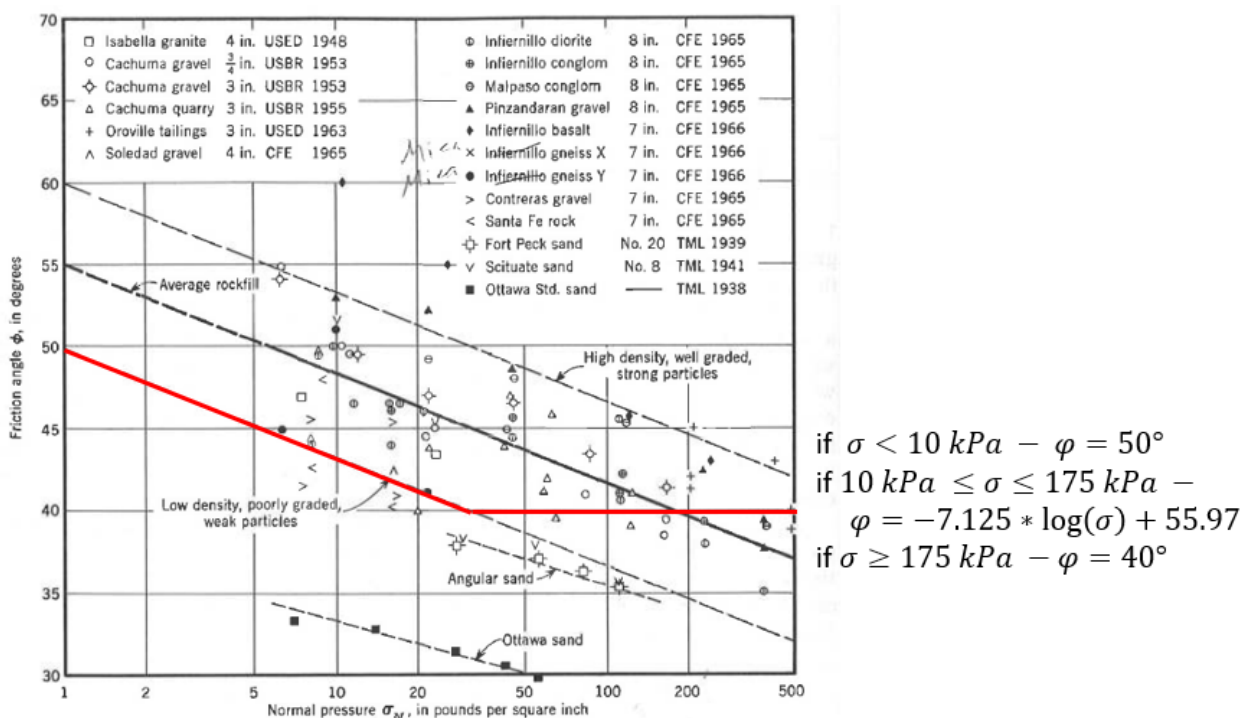


Figure 2.5 Strength-Stress Function for Rockfill Incorporated in the 2D Model (modified after Leps 1970). The Function is Represented with the Solid Red Line.

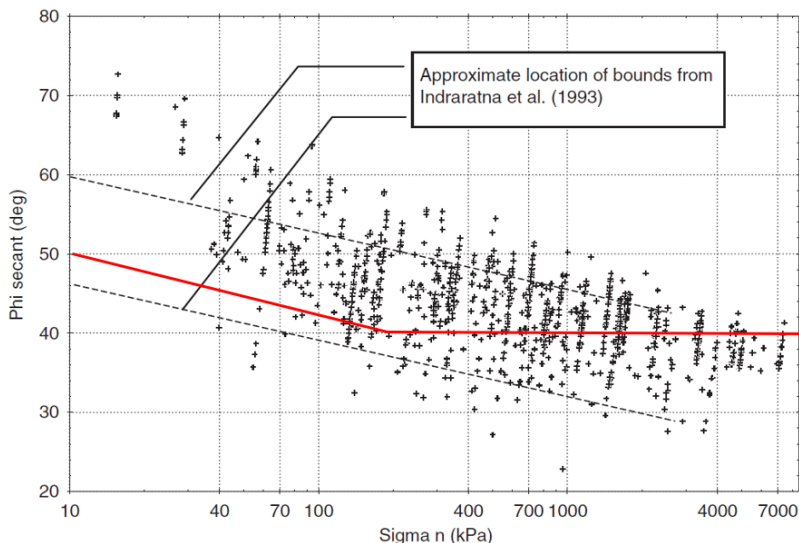


Figure 2.6 Strength-Stress Function for Rockfill Incorporated in the Early 2D models (modified after Indraratna et al. 1993). The Function is Represented with the Solid Red Line.

Transition Zone

The transition zone was modelled with a peak effective friction angle of $\phi' = 42^\circ$ to impose a slightly higher strength than the rockfill due to its finer particle size and higher compaction.

Clay Core

The clay core unit was modelled with an effective friction angle of $\phi' = 26^\circ$ based on the laboratory data shown in Figure 2.3.

2.1.2.3 CHsoil

For the final analysis, the direct simple shear (DSS) and triaxial test data for the Unit A and Unit B foundation units were used for calibration of those units using the CHsoil constitutive model. The CHsoil model was selected to capture the loss in stiffness with shear strain observed in the laboratory test data.

Unit A

The calibration to laboratory test data was completed in three steps:

- Step 1: The CHsoil parameters were selected to match the elastic portion of the individual DSS laboratory test datasets (Figure 2.7).
- Step 2: The stiffness parameters obtained from the first step were then combined with the strength parameters that the ITRB requested ($\phi = 20^\circ$ and $c = 10$ kPa; Figure 2.8).
- Step 3: A relationship was developed incorporating the post-peak strain weakening behavior (Figure 2.9).

Two sets of parameters were determined from this approach: one termed 'Board parameters', which used the strength parameters specified by the ITRB; and one termed 'KCB parameters', which used a stress-dependent friction angle calculated in the element tests shown in Figure 2.7.

The full stress-strain curves for these two relationships are shown in Figure 2.9 and Figure 2.10 for the 'Board parameters' and 'KCB parameters', respectively.

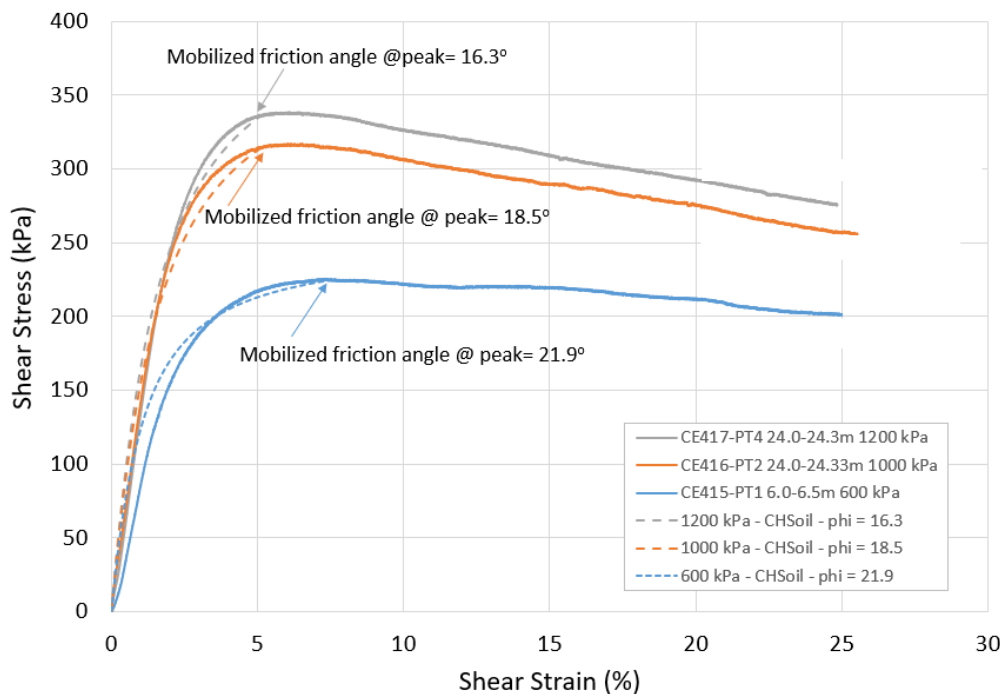


Figure 2.7 Unit A Calibration Step 1. Simulated Data Shown as Dashed Lines. DSS Test Data Shown as Solid Lines.

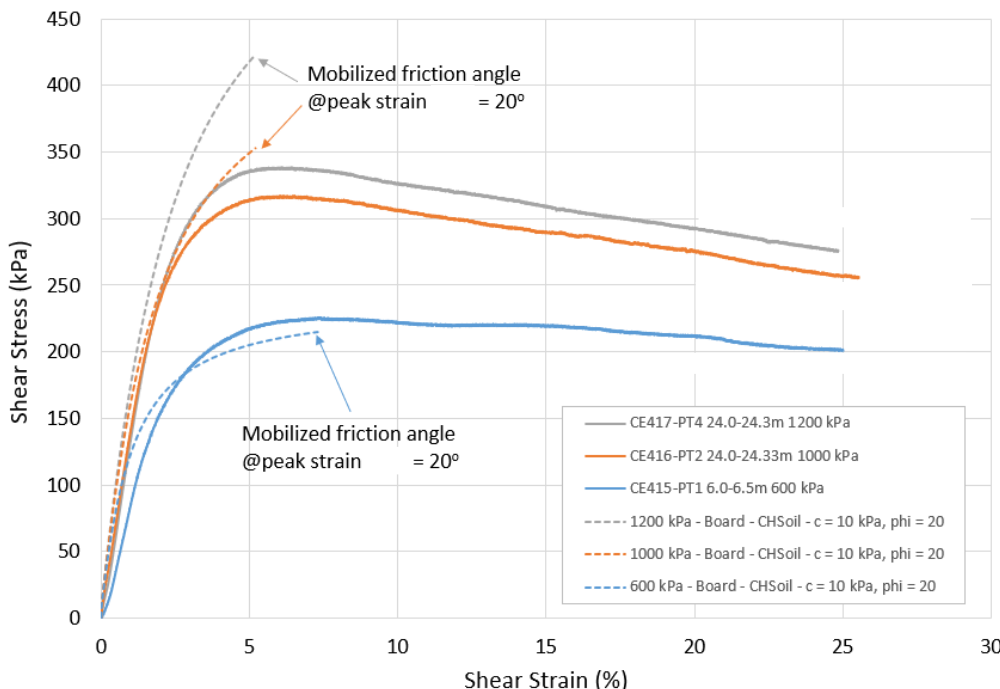


Figure 2.8 Unit A Calibration Step 2. Simulated Data Shown as Dashed Lines using ITRB's Strength Parameters. DSS Test Data Shown as Solid Lines.

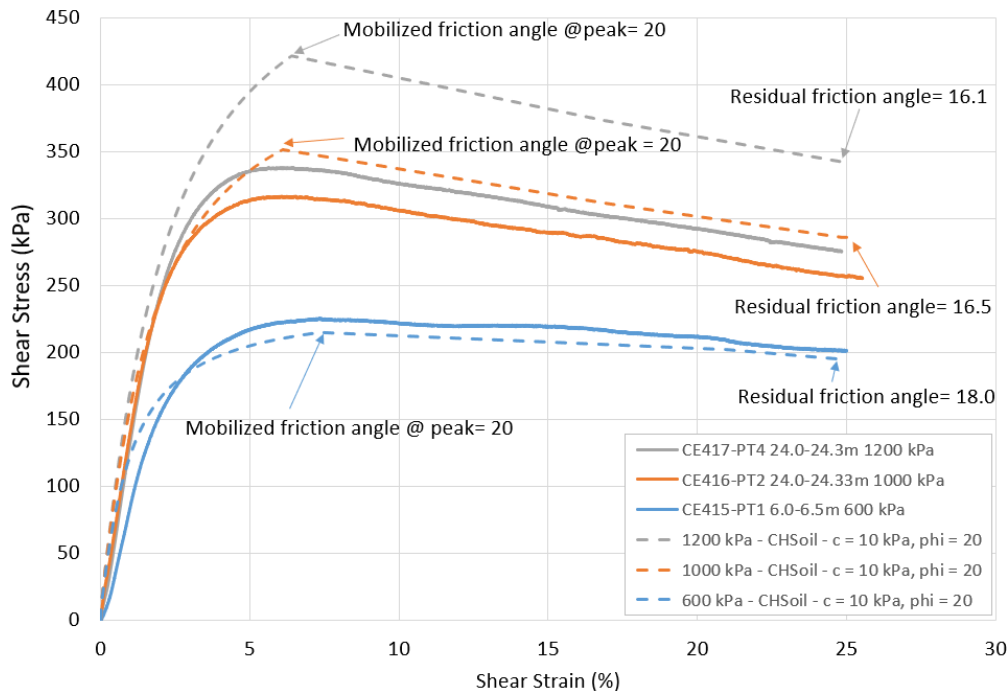


Figure 2.9 Unit A Calibration Step 3. Simulated Data Shown as Dashed Lines using ITRB's Strength Parameters. DSS Test Data Shown as Solid Lines.

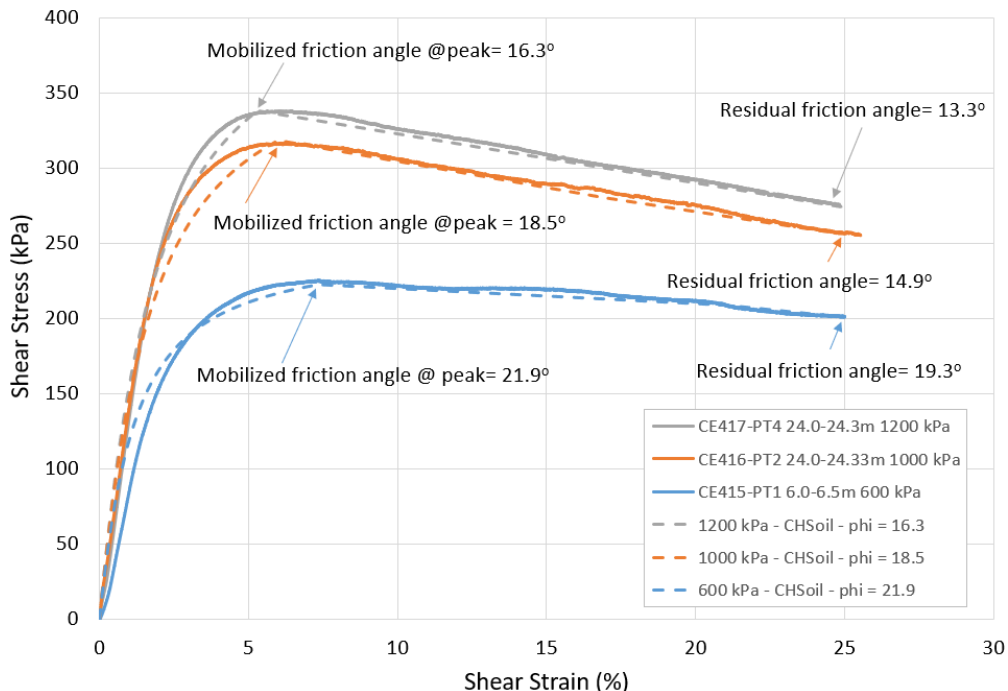


Figure 2.10 Unit A Calibration Step 3. Simulated Data Shown as Dashed Lines using KCB's Alternate Variable Strength Parameters. DSS Test Data Shown as Solid Lines.

Unit B

Unit B was calibrated in a similar manner to Unit A but was based on isotropically consolidated undrained (CIU) triaxial test data rather than DSS data due to a lack of DSS data for this unit. The elastic portion of the triaxial laboratory data was first fitted using a common stiffness parameter

then strength parameters were varied to match the post-peak behavior. Strain-weakening behavior was not observed for tests at confining stresses less than 400 kPa. This unit was modeled with a peak friction angle of 30° and no post-peak strength loss for confining stresses less than 400 kPa. The strain-weakening option was included for confining stresses larger than 400 kPa. A single set of parameters was used for Unit B in all analyses, and the resulting stress-strain relationship is shown in Figure 2.11.

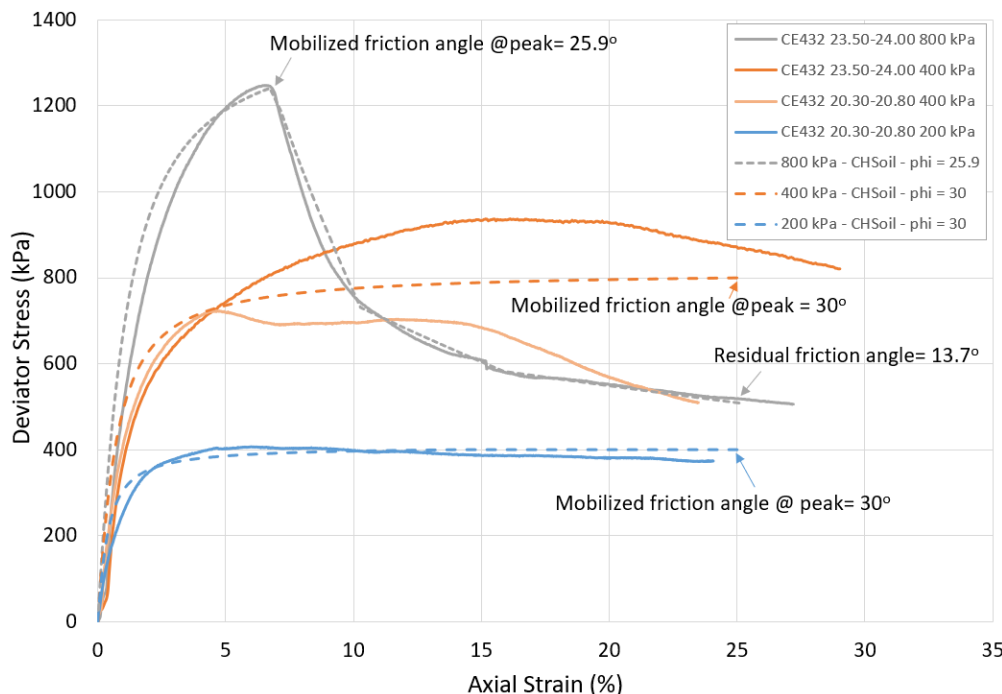


Figure 2.11 Element Test Calibration of Unit B. Simulated Data Shown as Dashed Lines. CIU Test Data Shown as Solid Lines.

2.1.2.4 Critical-State Properties – NorSand

The parameters for the NorSand constitutive model were provided by the ITRB (see Table 2.1); however, additional element test simulations of triaxial laboratory tests were completed as part of this work to confirm the FLAC implementation of NorSand was performing in the same manner as the Visual Basic for Applications (VBA) version used by the ITRB to derive the parameters. These element tests showed good agreement between the FLAC and VBA implementation for the drained tests and the parameters were carried forward into the 2D and 3D simulations.

Table 2.1 NorSand Parameters Provided by the ITRB

Parameter	Value
λ_{10}	0.046
Γ	0.75
M_{tc}	1.5
N	0.3
χ	8
H	50-450 ψ
G_{max}	17 MPa * $(p':\text{kPa}/100)^{0.76}$
v	0.2
CSL Locus (Curved)	$e_c = 0.906 - 0.355 * (p':\text{kPa}/100)^{0.119}$
ψ	Test specific. $\psi = +0.06$ used in 2D analysis based on field data.
OCR	

2.1.3 Instrumentation Data & Visual Observations

Instrumentation data were used to either prepare input parameters or to calibrate the model to the documented archival records.

2.1.3.1 Piezometer Records and Historical Pond Levels

Phreatic surface

The pore pressures for the end of each construction stage were defined using three data sources: the historical piezometric records available close to the upstream edge of the dam; pond elevation; and subaerial beach length. The piezometer records were available for the pneumatic piezometers from the end of Stage 5 construction (year 2011) and for the Vibrating Wire Piezometers (VWP) from the end of Stage 9 construction (Year 2016). Pond level records were available from the end of Stage 4 construction (year 2008). For Stages 1 to 3, where the data were not available, the pond level was calculated with a freeboard of 7 m. This freeboard was selected based on the observed trend from Stages 4 to 9. The phreatic surface at the end of Stage 10 and Buttress 1 construction was taken at 4 m below the tailings surface. Beach length information was inferred based on historical time-lapse photography sourced from GoogleEarth. The GoogleEarth images for the site were available from Dec 2003. For the end of construction periods where the beach length was not available, the beach length was obtained by linear interpolation between the available photographs. The phreatic surface was defined by connecting the piezometer levels to the pond level located at the calculated beach length distance.

At the direction of the ITRB, underdrainage at the site observed in Cone Penetration Test (CPT) pore pressure dissipation test data was honoured by using a sub-hydrostatic gradient of 7.8 kPa/m for calculating pore pressures in the tailings.

2.1.3.2 Surface Survey Prisms

Horizontal and vertical deformation records from surface survey prisms installed on the Stage 4 and Stage 5 crests were used for comparison with the calculated displacements in the deformation models. Prism 5 was located closest to Station 19+50 (see Figure 2.12). The Prism 5 displacement records were only available to April 2017 as the prisms were progressively removed to facilitate Buttress 1 construction.

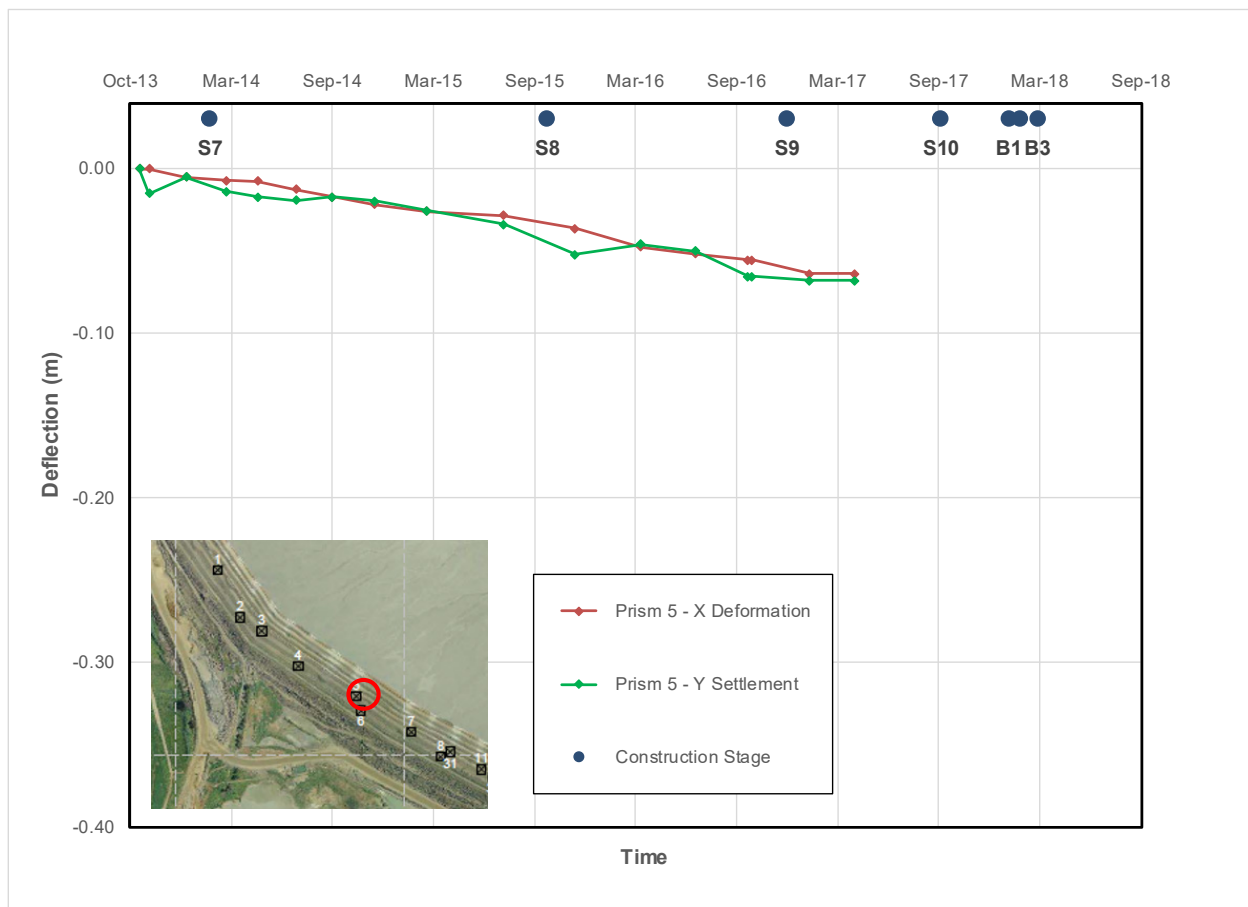


Figure 2.12 Survey Prism 5 (Stage 5 crest) Displacement Monitoring Record.

2.1.3.3 Satellite Monitoring – Surface Movement

A surface displacement time series taken with Synthetic Aperture Radar Interferometry (InSAR) was available and is shown in Figure 2.13. Due to concerns of the ITRB over the accuracy of the InSAR data because they did not match the surface survey data where these datasets overlapped and because the direction of displacement these results represented was not clear, these surface monitoring results were used for calibration of the deformation model in an indicative manner only. The main use of these data was to illustrate a significant increase in displacement rate in the three months prior to failure.

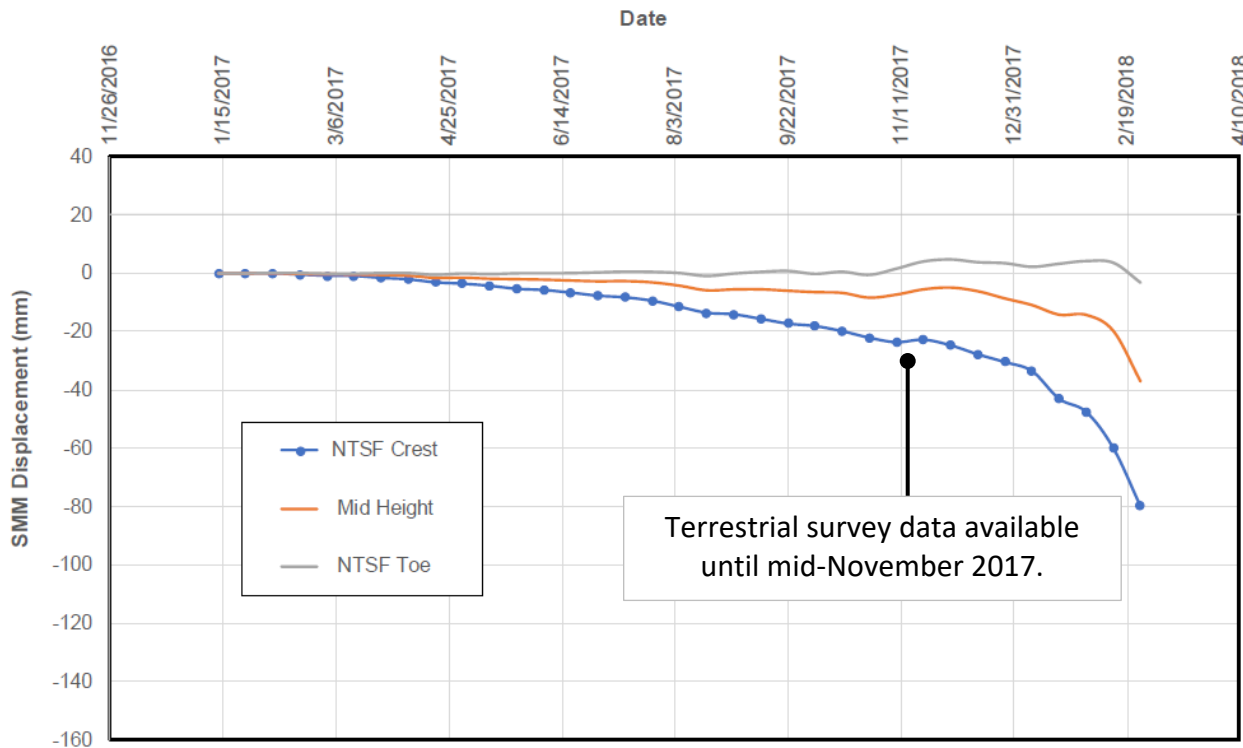


Figure 2.13 InSAR surface movement measurements at CH 20+00.

2.1.3.4 Visual Observations

In addition to the surface deformation data discussed in the preceding sections, visual observations were also used in a qualitative manner in the model calibration. The main observations used were the heaving observed at the dam toe following excavation in preparation for buttress construction and cracking observed on the buttress crest ahead of the failure.

2.1.4 Results

Whilst various model iterations were ran throughout this assessment, only results from the final models are included in this report. The results in this section relate to models with the following variations:

- NorSand constitutive model applied to the tailings using a drained modelling approach and the parameters described in Section 2.1.2.4.
- Combination of CHSoil and strain-softening constitutive models assigned to the Unit A and Unit B foundation units.
 - ◆ Two sets of results are presented: one relating to the ‘Board Parameter’ set and another relating to the alternate ‘KCB Parameter’ set discussed in Section 2.1.2.3.
- Mohr-Coulomb constitutive model assigned to all other units with the parameters discussed in Section 2.1.2.2.

2.1.4.1 Summary

Overall, the results showed a very similar response for the two parameter sets that were used for the Foundation. They both showed a trend of strain weakening developing in the Unit A foundation layer beneath the dam toe at around the Stage 5 construction and spreading upstream throughout the following construction stages. Prior to the buttress construction, the zone of weakened Unit A had spread to roughly the centreline of the downstream-raised portion of the dam, and the buttress construction caused the zone of strain weakening to form a contiguous zone from the rockfill at around this location to the dam toe. The rate of horizontal displacements increased significantly when this occurred. This displacement in the foundation was felt in the tailings adjacent to the Stage 1 and 2 rockfill as a reduction in confining stress and an increase in deviator stress.

This change of stress in the tailings caused the stress ratio in the tailings to increase, making them more susceptible to liquefaction. The stress path followed by these tailings has been used as an input to a series of laboratory tests completed by the ITRB to investigate the triggers needed to cause liquefaction of this material in this stress state and help determine the cause of the dam failure mechanism.

These observations are discussed in more detail in the following sections.

2.1.4.2 Surface Deformation

A comparison of the displacements at the survey prisms with those of the FLAC model is shown in Figure 2.14. In general, there is little difference between the two parameter sets used in this assessment. The horizontal displacements calculated by FLAC are generally close to the measured values

When the trends of displacements in the models are compared with the InSAR data (see Figure 2.15) the displacements in the model can be seen to follow a similar trend as the measured data.

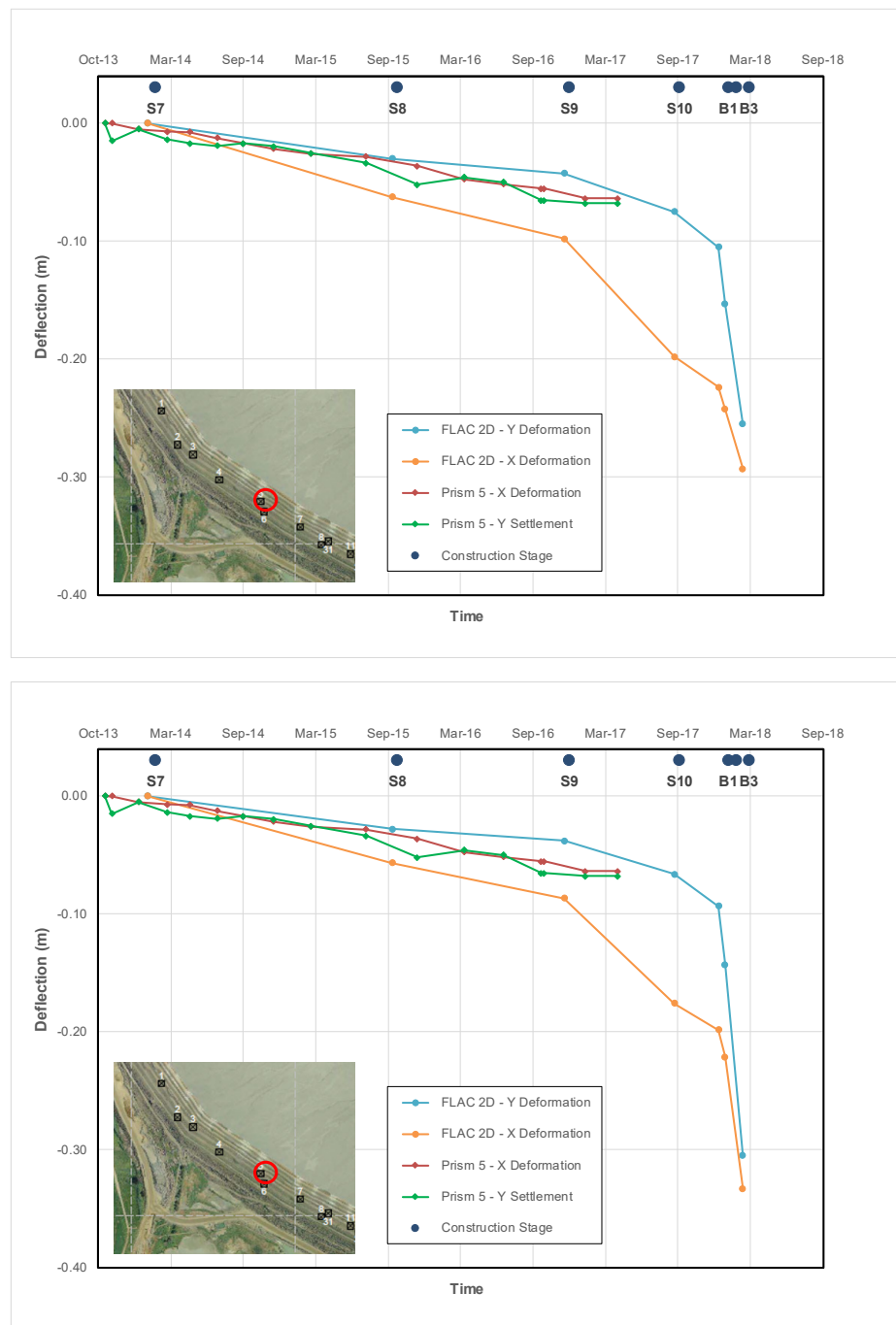


Figure 2.14 Comparison of Calculated Displacements using A) Board Parameters and B) Alternate KCB Parameters with Monitoring Data at Survey Prism 5

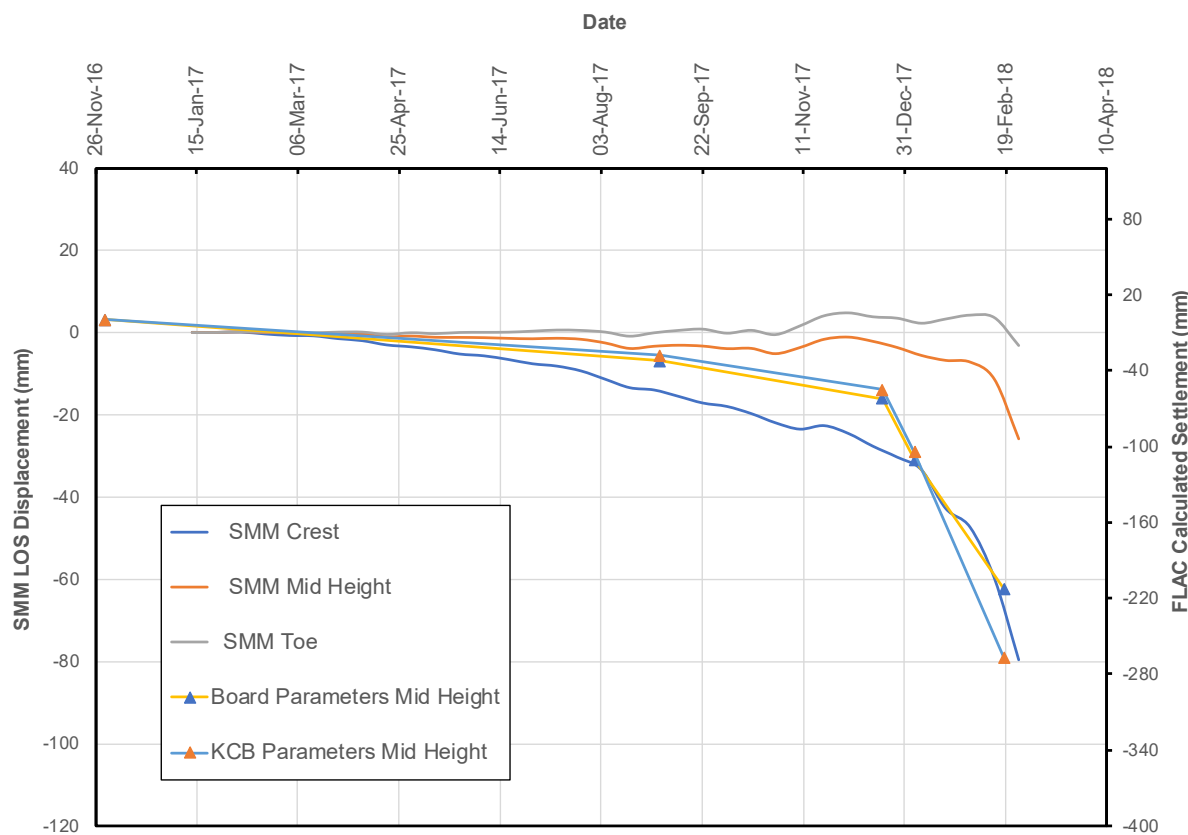


Figure 2.15 Calculated Displacement at mid-height Compared with InSAR Data

2.1.4.3 Surface Cracking

Horizontal displacements were tracked along the model surface throughout construction to identify areas where a distinct break in displacements occurs that would be indicative of an area where a crack would develop. These horizontal displacements are shown in Figure 2.16. It can be seen from this figure that the most distinct change in rate of displacements occurs at roughly chainage 0 m along the section. This corresponds to a region close to the centre of the buttress crest. Whilst cracking was observed on the buttress crest, it was generally located towards the upstream edge of the crest; therefore this break in the displacement profile is occurring slightly further downstream than observed in the field.

Whilst this change of displacements trend was observed to occur in roughly the location of surface cracking, the change of trend is not sufficiently distinct to conclusively attribute the observed cracking to these displacements. It is possible that the observed cracking was a consequence of early onset liquefaction, as discussed in Section 3.2.

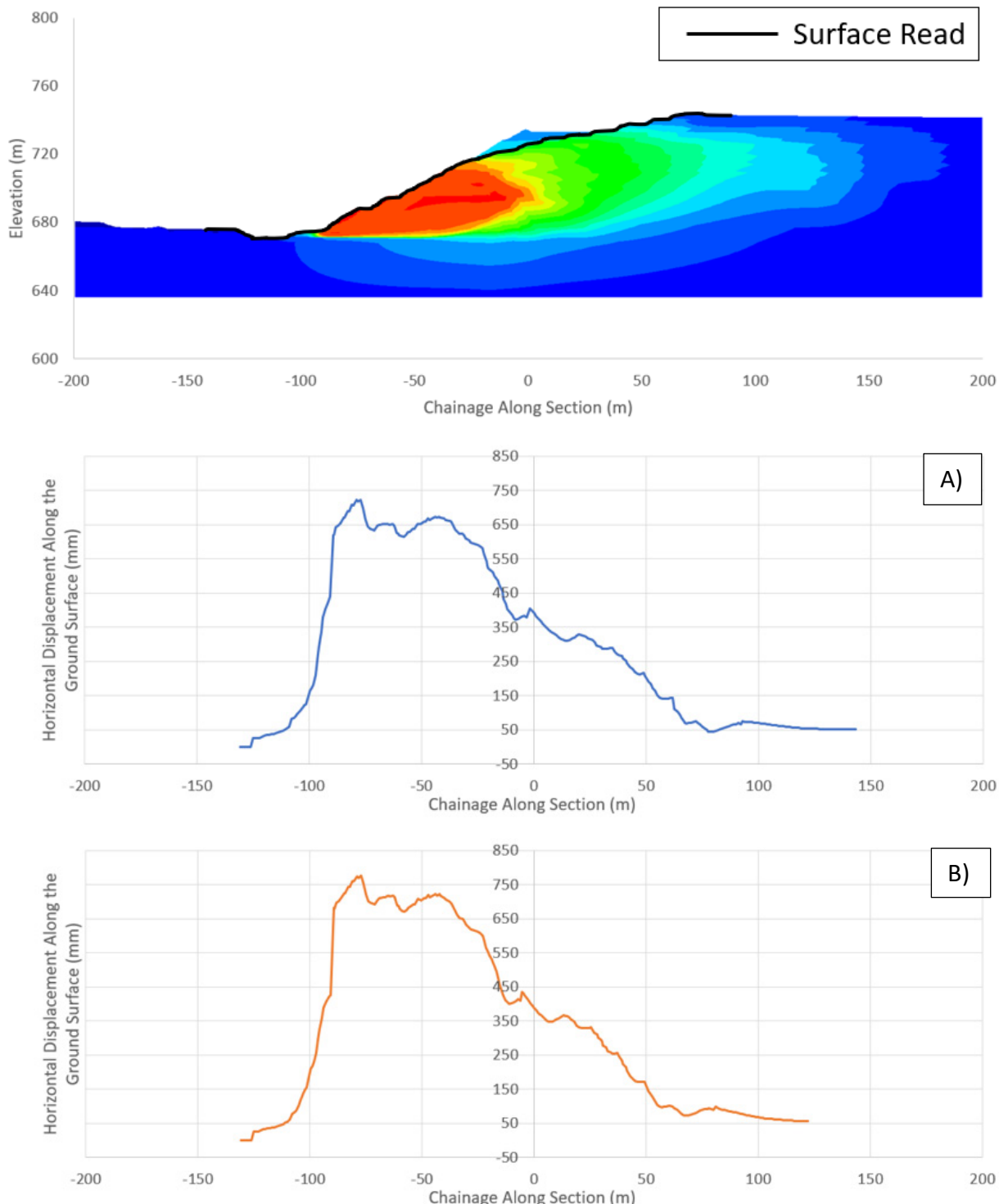


Figure 2.16 Horizontal Displacement along Dam Surface Calculated using; A) Board Parameters, B) Alternate KCB Parameters.

2.1.4.4 Heave at the Toe

Prior to failure, cracking along the toe due to heaving was observed. The dimension of the heave was not measured in the field. Heave was also observed at the dam toe in the FLAC model. The maximum heave calculated in the model was roughly 13 cm (see Figure 2.17).

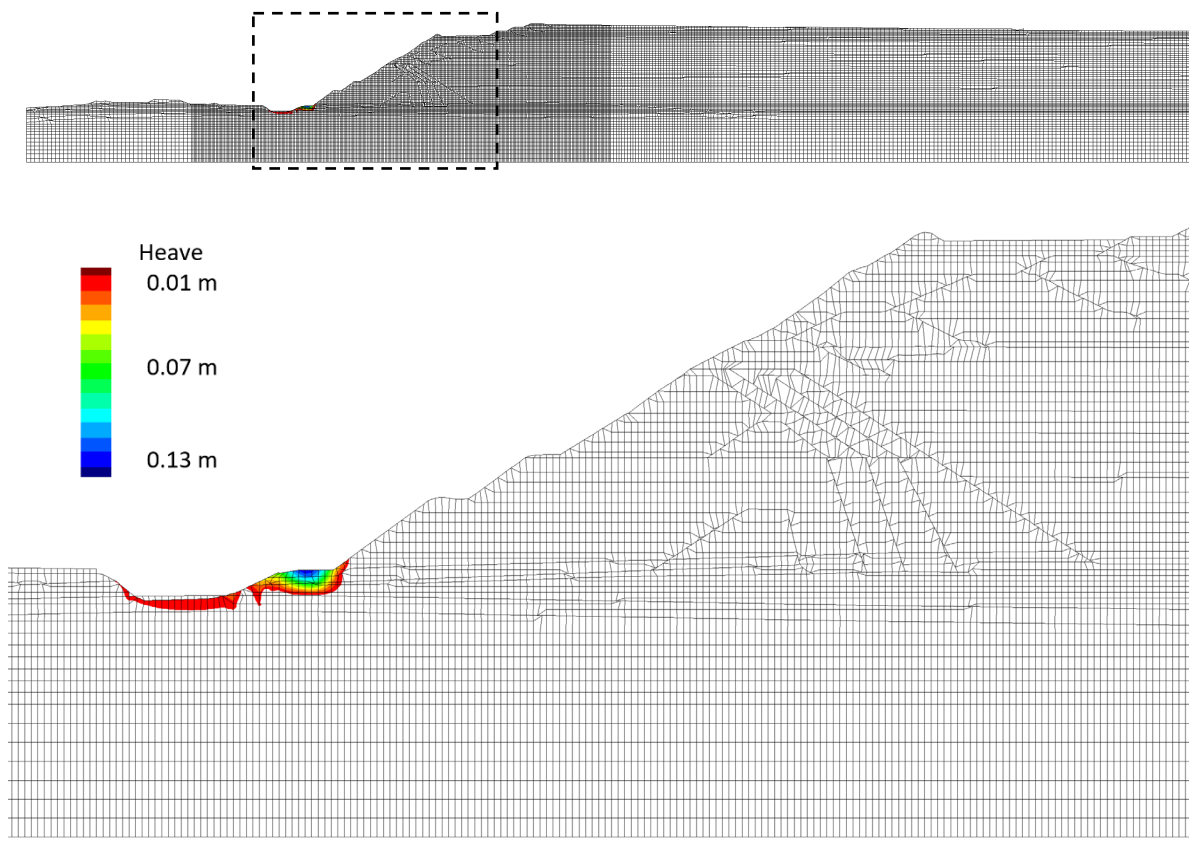
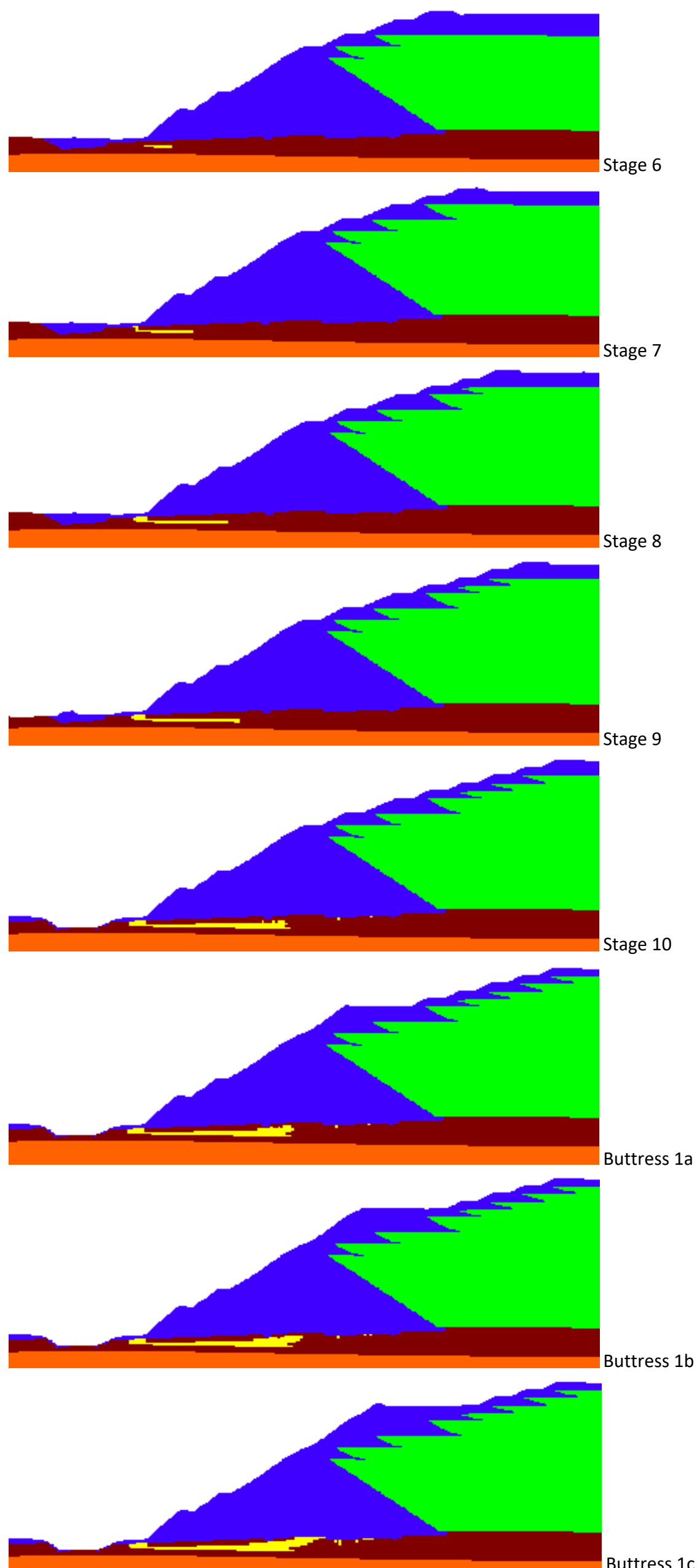


Figure 2.17 Heave Measurements at the Dam Toe

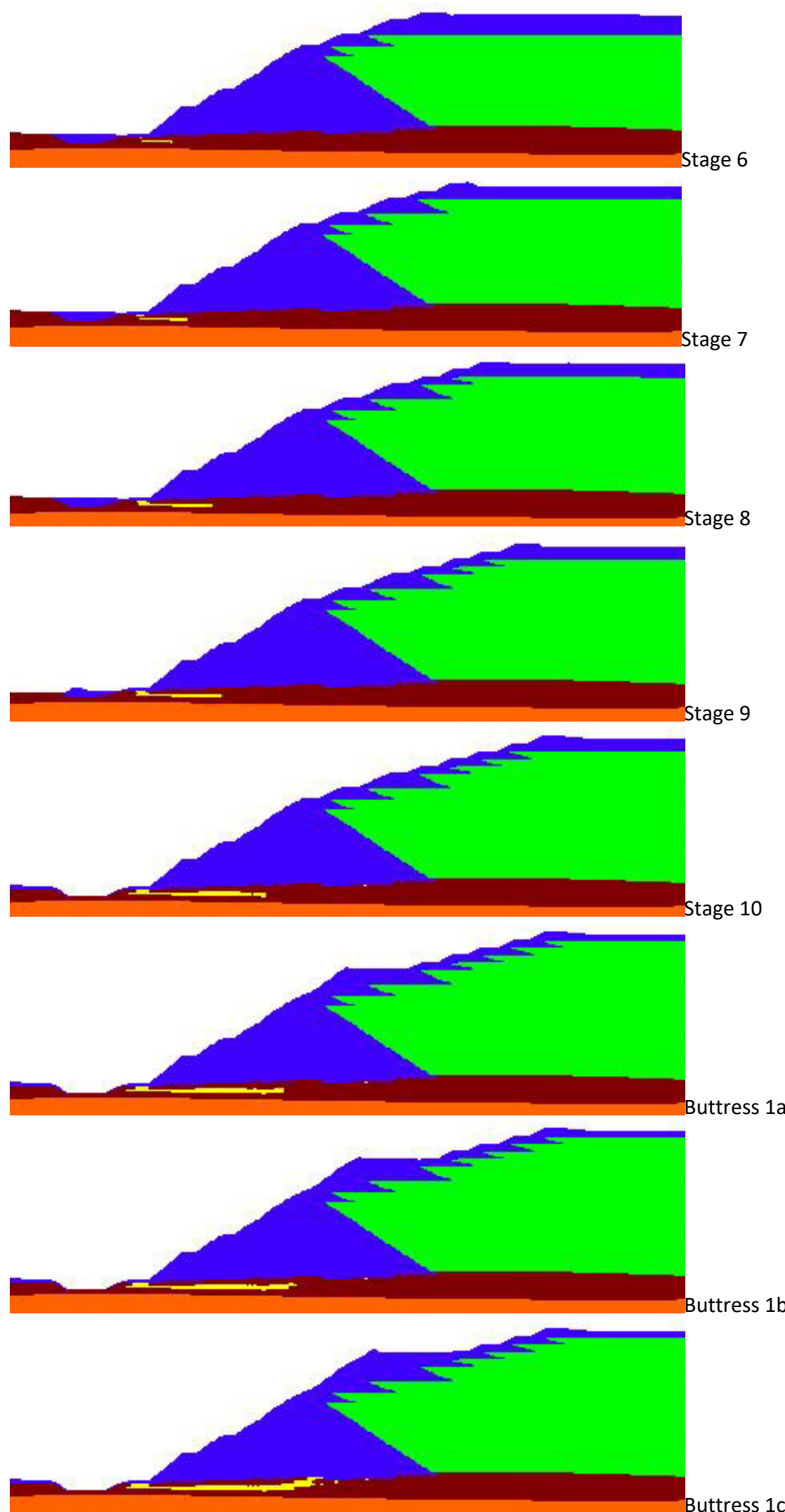
2.1.4.5 Strain Weakening

Illustrations of the development of strain weakening through the Foundation are shown in Figure 2.18 and Figure 2.19. These figures show a similar pattern of behaviour with the two parameter sets. The first onset of strain weakening began at the dam toe in Stage 5 (the figures illustrate the response from Stage 6 onwards) and developed upstream beneath the dam throughout the following construction stages. Excavation at the dam toe during Stage 10 and construction of the buttress caused this zone of strain weakening to develop into a contiguous zone between roughly the centreline of the Stage 1 rockfill and the dam toe.



Note: Zones of strain weakening in Unit A are shown as yellow

Figure 2.18 Development of Strain -Weakening in Foundation Unit A throughout Construction Loading using Board Parameters



Note: Zones of strain weakening in Unit A are shown as yellow

Figure 2.19 Development of Strain -Weakening in Foundation Unit A throughout Construction Loading using Alternate KCB Parameters

2.1.4.6 Stress Paths

To identify the effect of the construction loading and resulting foundation displacement on the impounded tailings, the ratio of the mobilized stress ratio (q/p') to the critical state stress ratio (M_{tc}) was tracked throughout the model loading stages. This ratio, termed the instability ratio (η/M_{tc}), is a measure of the distance of any tailings zone in the model from the critical state line; where an instability ratio of 1 indicates that the stress state of the zone is on the critical state line. The distribution of this ratio at the end of construction is shown in Figure 2.20, which indicates that the most highly-stressed areas of tailings were immediately upstream of the Stage 1 and 2 rockfill and adjacent to the overlying containment berms. As a result, these are the areas of tailings that would be most susceptible to liquefaction.

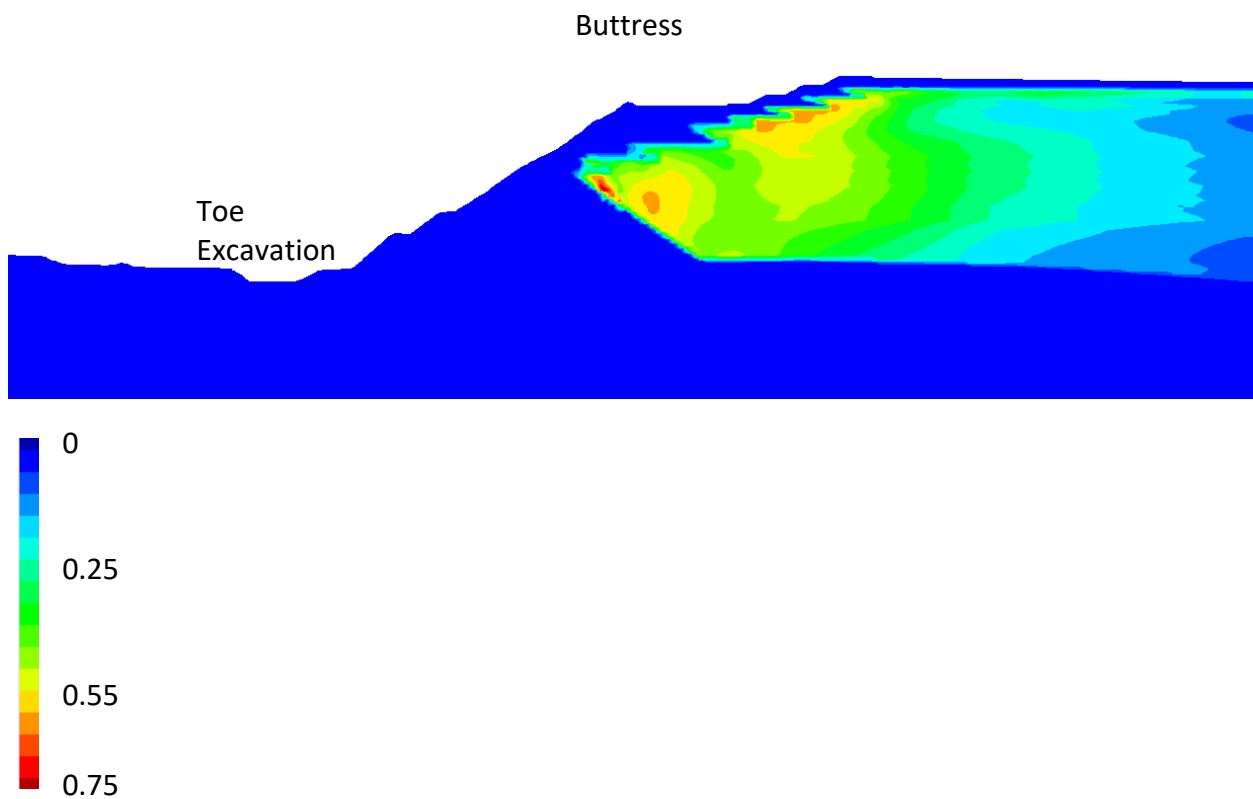


Figure 2.20 Distribution of Instability Ratio (η/M_{tc}) Alternate KCB Parameters

As well as tracking the instability ratio, stress paths were also monitored in these highly stressed regions, and other regions in the tailings, to observe how the stresses developed throughout the dam construction. These stress paths are shown in Figure 2.21 and Figure 2.22. It can be seen from these figures that the final loading stages lead to a reduction in mean effective stress in the region immediately upstream of the Stage 1 and 2 rockfill, annotated as Point 1 in these figures. This reduction in stress is a result of the loss of strength and increase in displacements occurring in the underlying Unit A foundation layer, and it would have an effect of increasing the susceptibility of this region to liquefaction triggering.

The stress path monitored at Point 1 has been used as an input to a laboratory testing program to identify the amount of disturbance that would be required to initiate liquefaction in a tailings sample at this stress state.

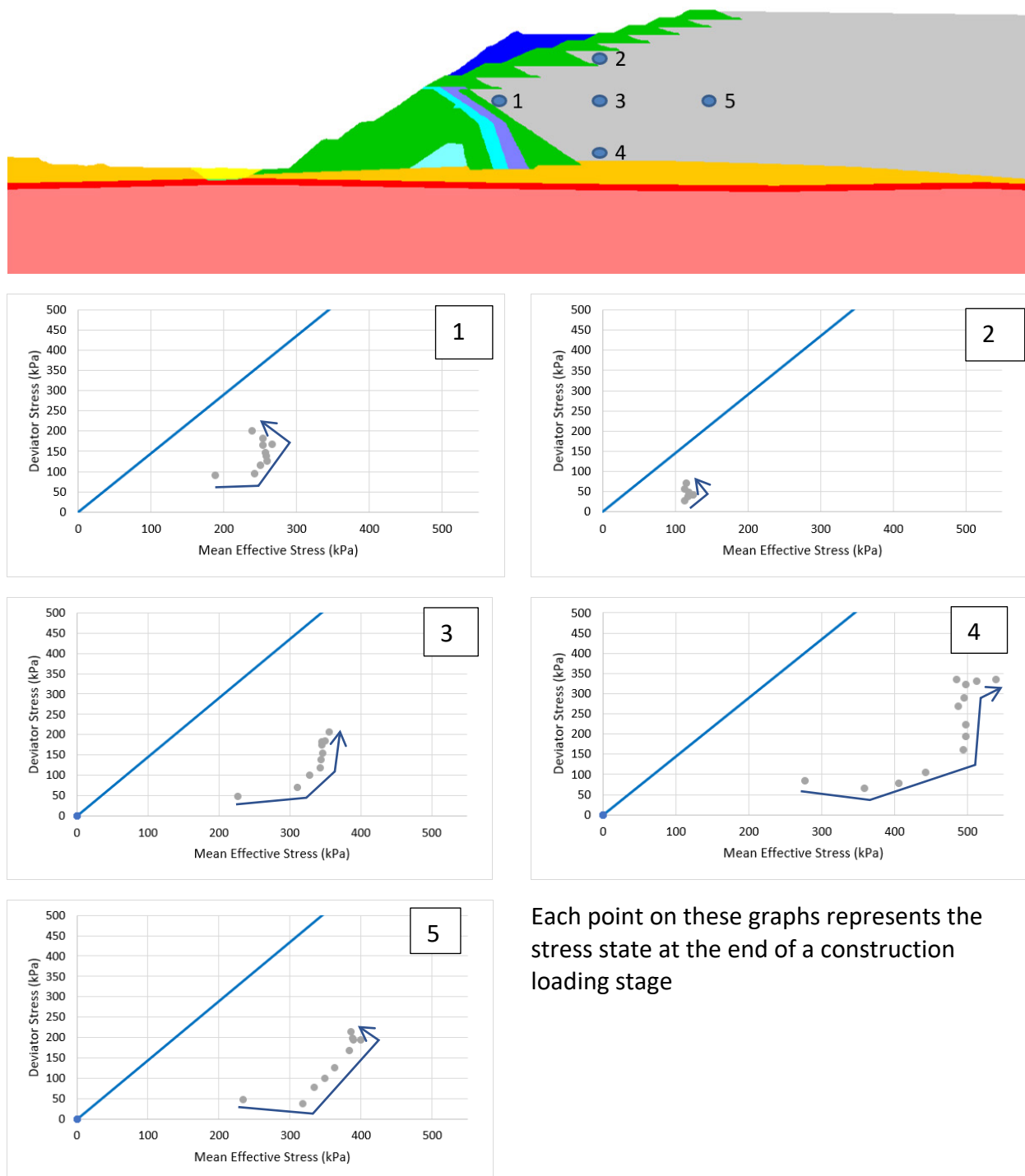


Figure 2.21 Simulated Stress Paths using Board Parameters

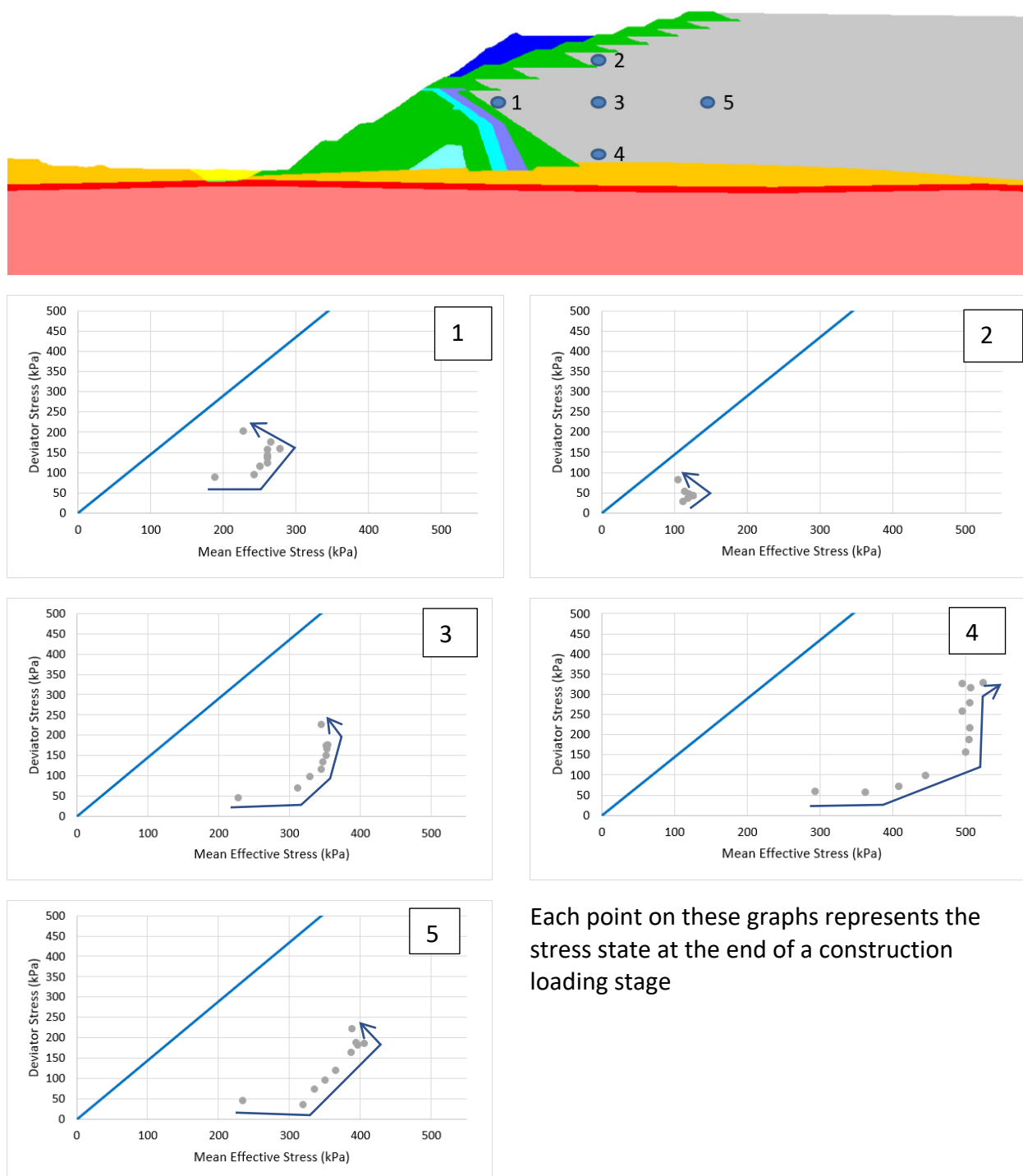


Figure 2.22 Simulated Stress Paths using Alternate KCB Parameters

2.1.4.7 Change of State Parameter with Time

In addition to tracking the stresses and displacements with time throughout the dam construction in the model, the changes in the tailings' state parameter were also monitored. A series of images showing the evolution of state parameter with construction stage are shown in Figure 2.23, which show that the state parameter in the region of tailings adjacent to the rockfill changed significantly throughout the construction loading in response to the shear stresses developed in

this region. This shear-induced densification of the tailings in this region is an expected response and has been incorporated into the laboratory testing of the tailings.

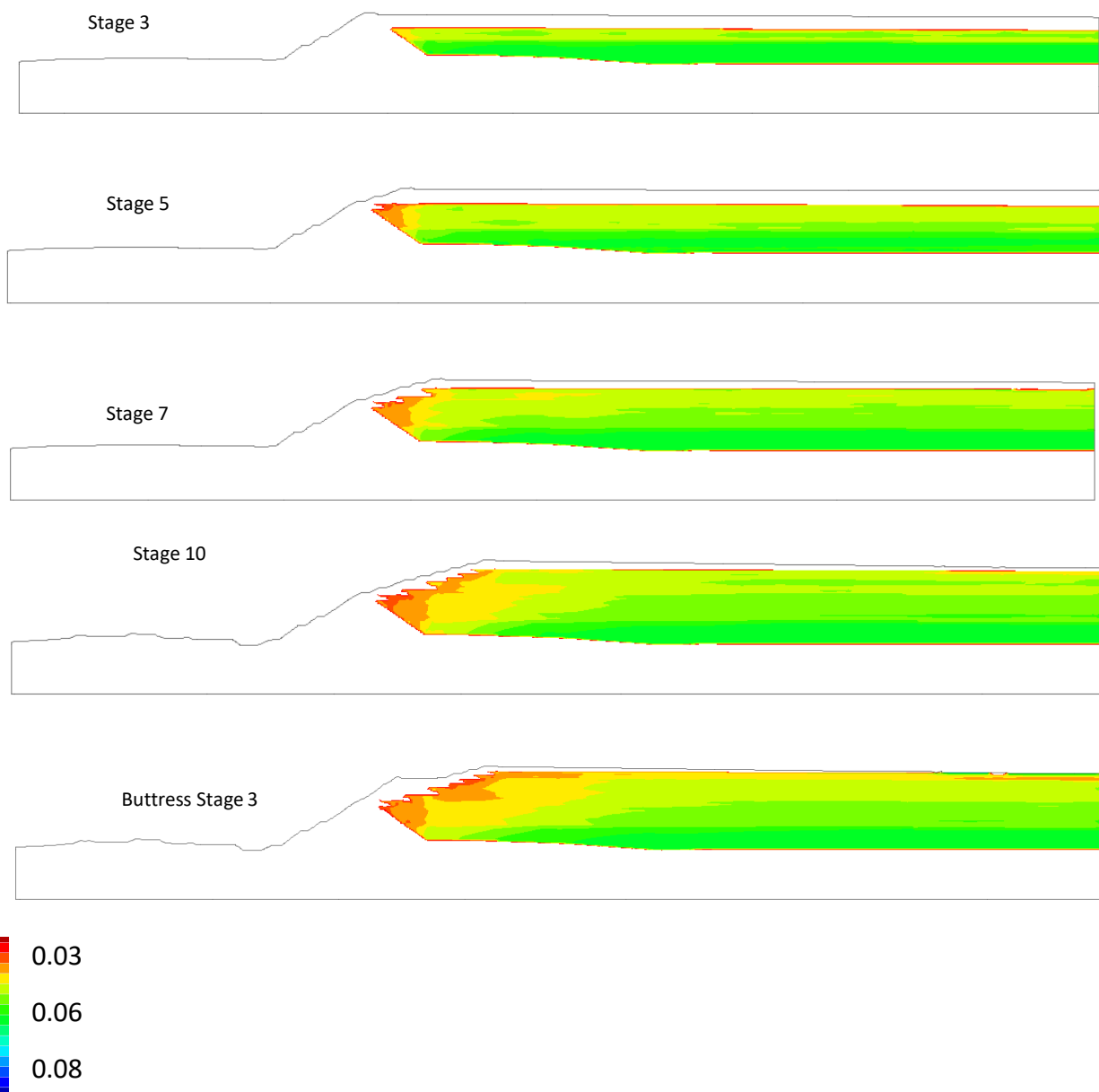


Figure 2.23 Change of State Parameter with Time Through Construction Sequence

2.1.4.8 Sensitivity Analyses

Without strain weakening

To isolate the effect that the strain weakening in the Unit A foundation was having on deformation patterns and stress paths in the tailings, a sensitivity analysis was completed in which the models described in the preceding sections were re-run without strain weakening enabled in the Unit A.

The calculated displacements for this sensitivity analysis are shown in Figure 2.24 and the stress paths are shown in Figure 2.25 and Figure 2.26. These figures show that the calculated displacements without strain weakening are significantly less than those with strain weakening and are, therefore, less representative of the monitoring results. They also show that without strain weakening the reduction in mean effective stress in the tailings discussed in Section 2.1.4.6 does not occur, confirming that this response in the tailings is a result of this strength loss in the Unit A.

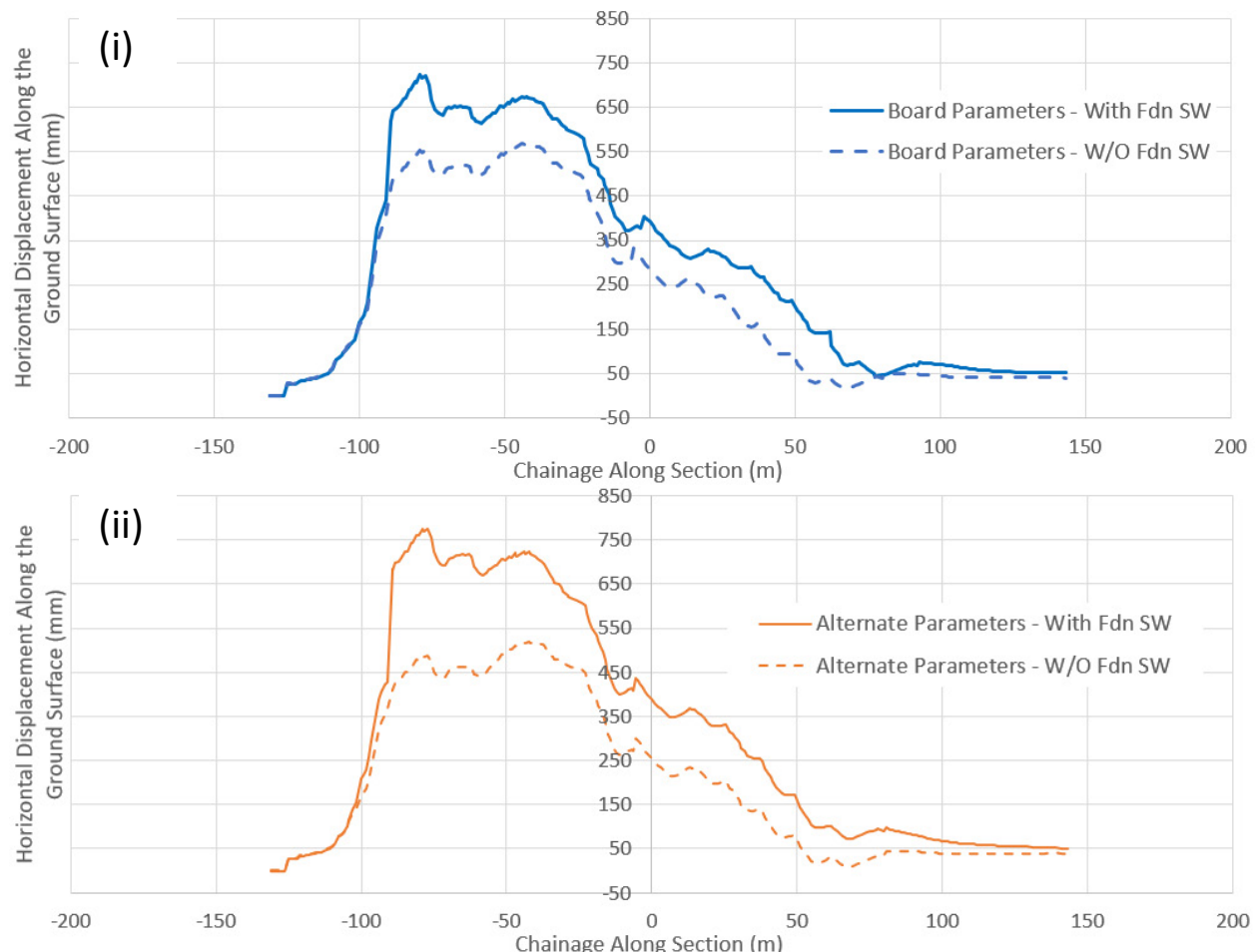


Figure 2.24 Plots showing Difference in Displacement with and without Strain Weakening (SW) of Unit A; (i) Using Board's Parameters, (ii) Using Alternate KCB Parameters.

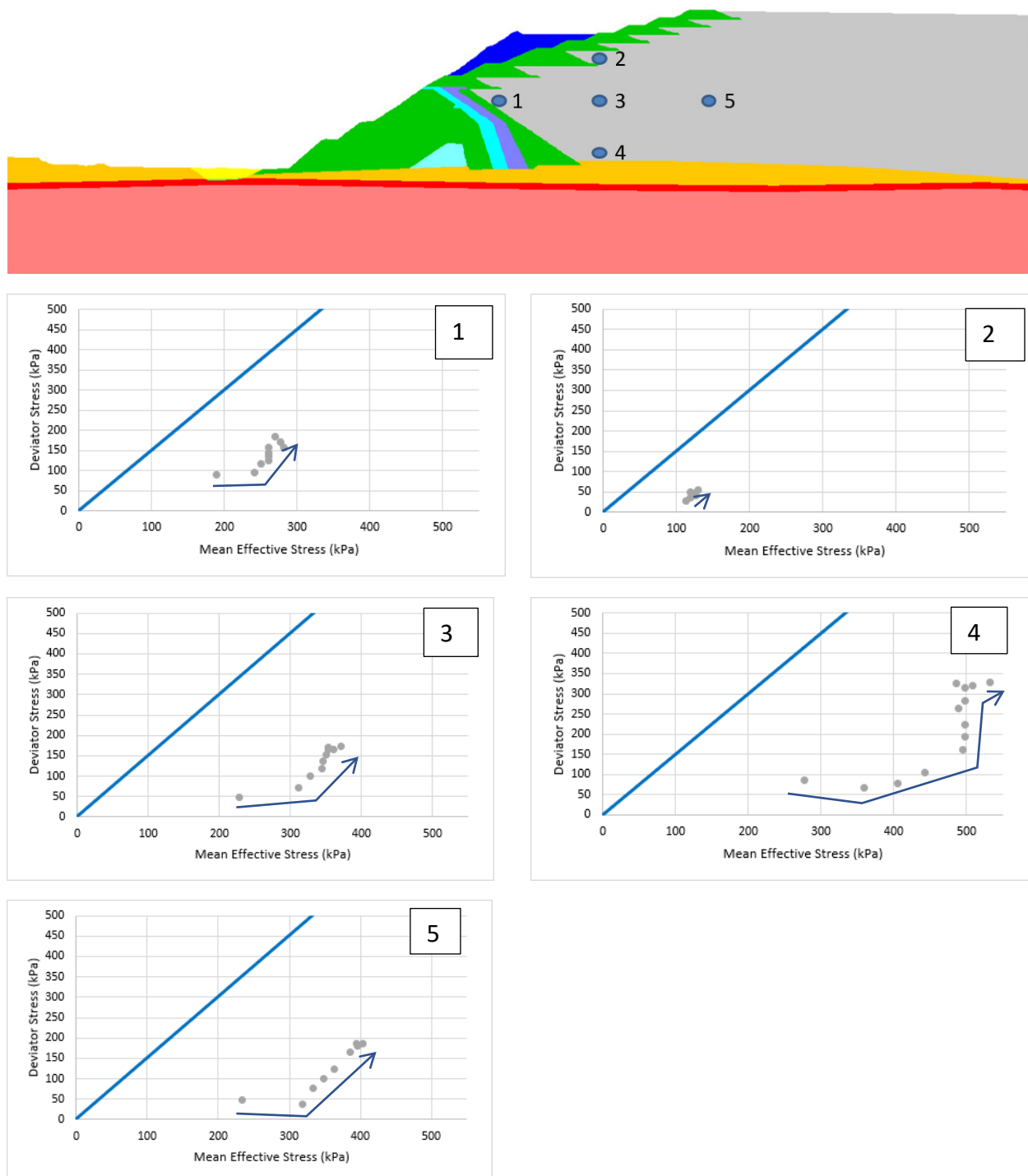


Figure 2.25 Simulated Stress Paths using Board Parameters without Strain Weakening of Unit A

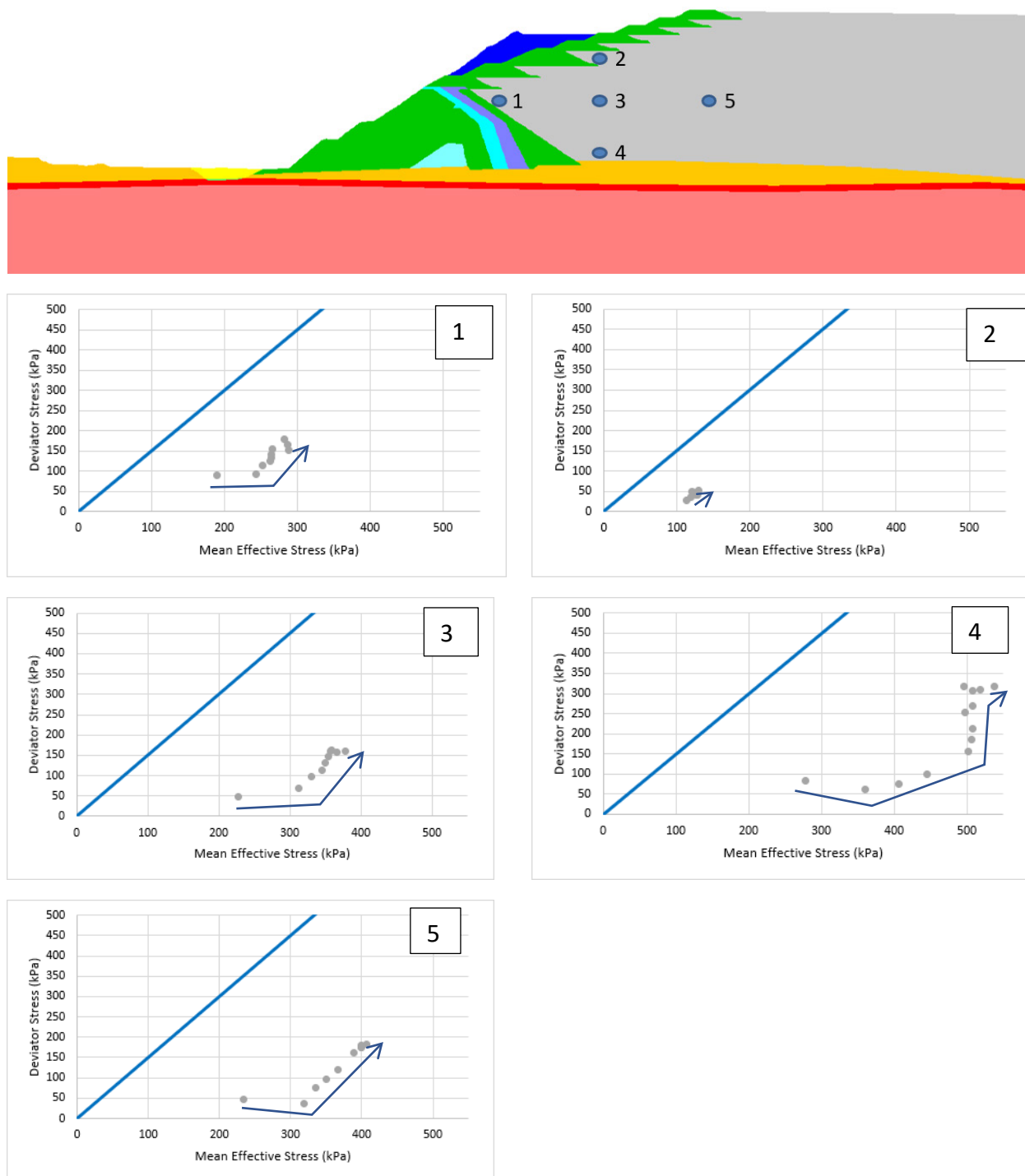


Figure 2.26 Simulated Stress Paths using Alternate KCB Parameters without Strain Weakening of Unit A

2.2 Seismic Response Analysis

2.2.1 General

A series of 1D and 2D seismic (site) response analyses was completed using the earthquake time histories provided by the ITRB as an input. The purpose of these analyses was to determine

potential amplification of the ground motions within the tailings so that the resulting amplified ground motions could be used as an input to the laboratory tests and Newmark-type displacement analyses.

2.2.2 1D Analysis

2.2.2.1 Methodology and Inputs

The 1D analyses were completed using the equivalent-linear analysis method in the software Strata. These analyses were completed at the column locations shown in Figure 2.27 to identify the response in the region of tailings identified in the 2D deformation analyses as being most highly stressed.

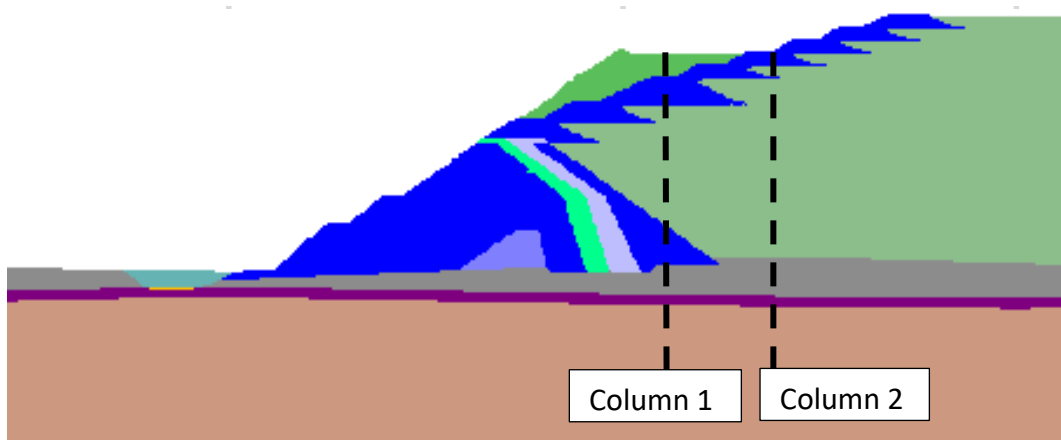


Figure 2.27 Column Locations for the 1D Site Response Analyses

The main inputs required for an equivalent-linear site response analysis include:

- Modulus reduction and damping relationships.
- Shear wave velocity (v_s).
- Earthquake time histories.

The modulus reduction and damping relationships used in these analyses were based on empirical relationships developed for similar materials documented in the published literature. The relationships used in this analysis are shown in Figure 2.28.

The v_s of the rockfill and foundation was determined from multichannel analysis of surface waves (MASW) data provided by the ITRB, and the v_s of the tailings was obtained from the seismic CPT data provided by the ITRB. The relationships used in this assessment are shown in Figure 2.29.

The earthquake time histories used in this assessment were documented in a memorandum prepared by Dr. Gail Atkinson, provided by the ITRB. The earthquake time histories documented in that memorandum include events of roughly magnitude 3 that occurred roughly a day before the failure and a set of records for a larger magnitude 4.3 event that occurred in April 2017. An example time history is shown in Figure 2.30 and a summary of the input ground motions is listed in Table 2.1.

Table 2.2 Summary of Input Time Histories

Time History Filename	Moment Magnitude	Date of event	PGA (g)	PGV (cm/s)	Significant Duration (5-95%) (s)
f1x.M4d3.csv	4.3	April 14, 2017	0.311	2	0.6
f5x.M4d3.csv			0.265	2.2	0.4
f7x.M4d3.csv			0.236	2	0.6
f8x.M4d3.csv			0.252	2.4	0.7
f10x.M4d3.csv			0.346	1.7	0.6
f24x.M4d3.csv			0.304	1.5	1.2
f46x.M3d0.csv	3	March 8, 2018	0.085	0.4	1.8
f81x.M3d0.csv			0.102	0.4	0.3
f82x.M3d0.csv			0.1	0.4	0.5
f83x.M3d0.csv			0.079	0.5	0.4
f90x.M3d0.csv			0.094	0.4	0.2
f91x.M3d0.csv			0.08	0.4	0.1
f92x.M3d0.csv			0.083	0.4	0.4

As recommended in the memorandum of Dr. Atkinson, all these time histories were used in this assessment to assess the range of responses that the tailings and dam may have experienced from seismic loading at this site. The events that are most directly relevant to the failure are the magnitude 3 events of March 8, 2018; however, most of the results presented in this appendix relate to the larger magnitude 4.3 event, which were completed to assess the response to the upper-bound ground motions experienced at this site. These results were subsequently used as inputs to a series of laboratory tests to assess if they had the potential to trigger liquefaction of the tailings. Those tests found that these ground motions would not trigger liquefaction of the tailings or generate excess pore pressures, and it was unnecessary to consider the effect of the magnitude 3 events.

As outlined in Dr. Atkinson's memorandum, analyses were completed with a single earthquake pulse, and with two pulses applied immediately after one another to reflect the range of potential ground motions.

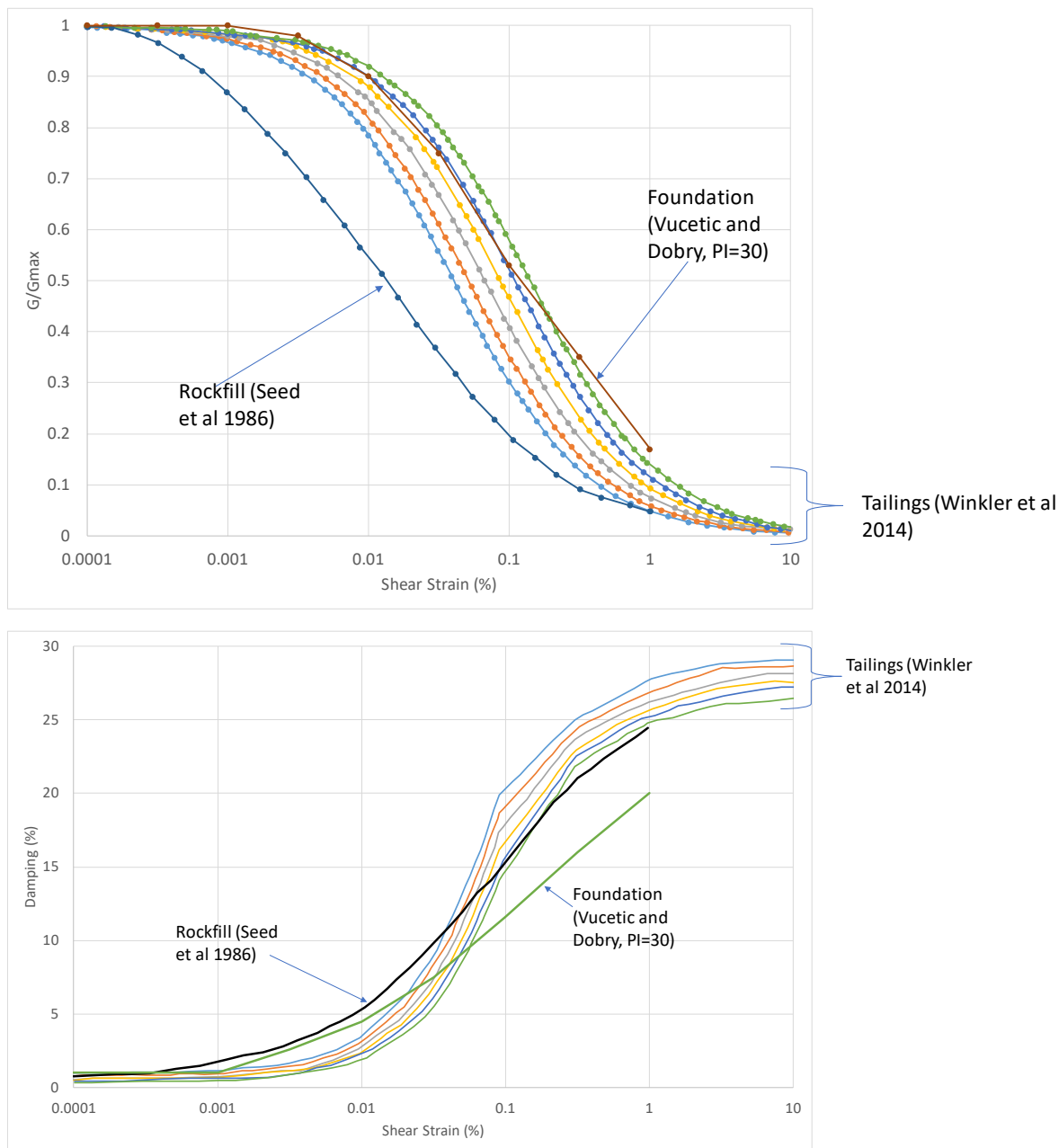


Figure 2.28 Modulus Reduction and Damping Relationships Applied in the 1D Site Response Analyses

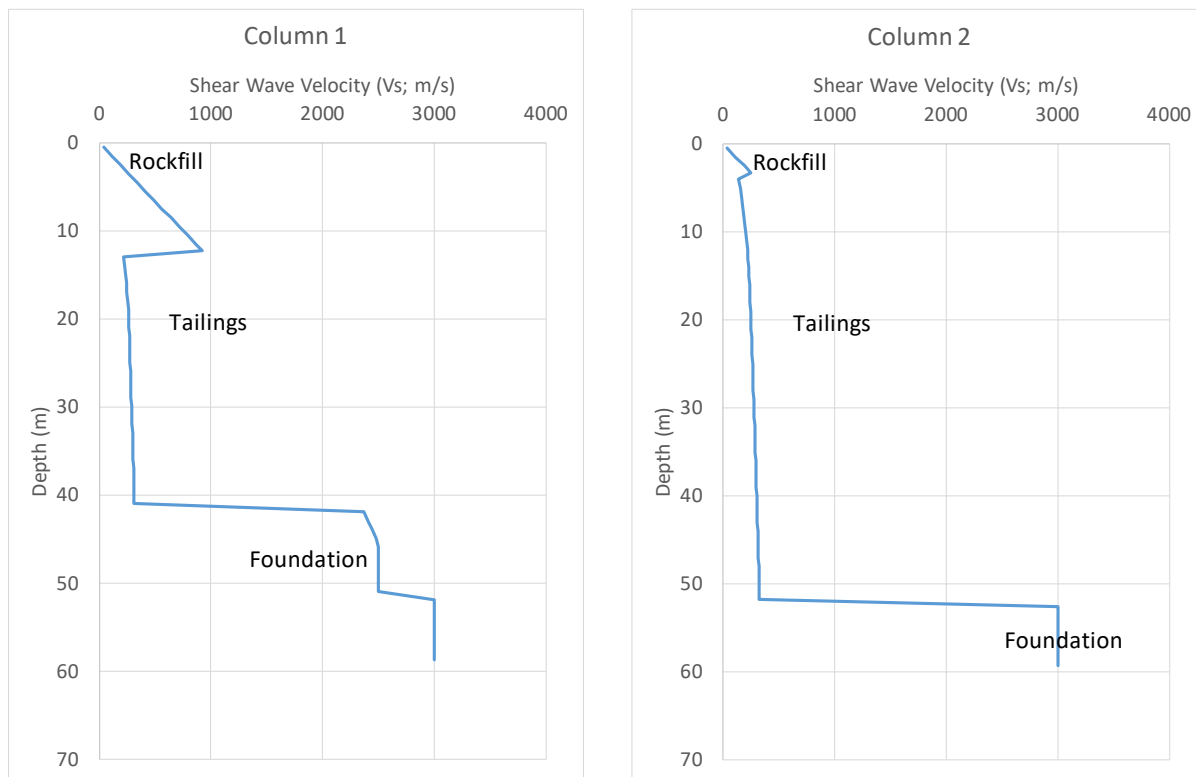


Figure 2.29 Shear Wave Velocity Relationships used in 1D Site Response Analyses

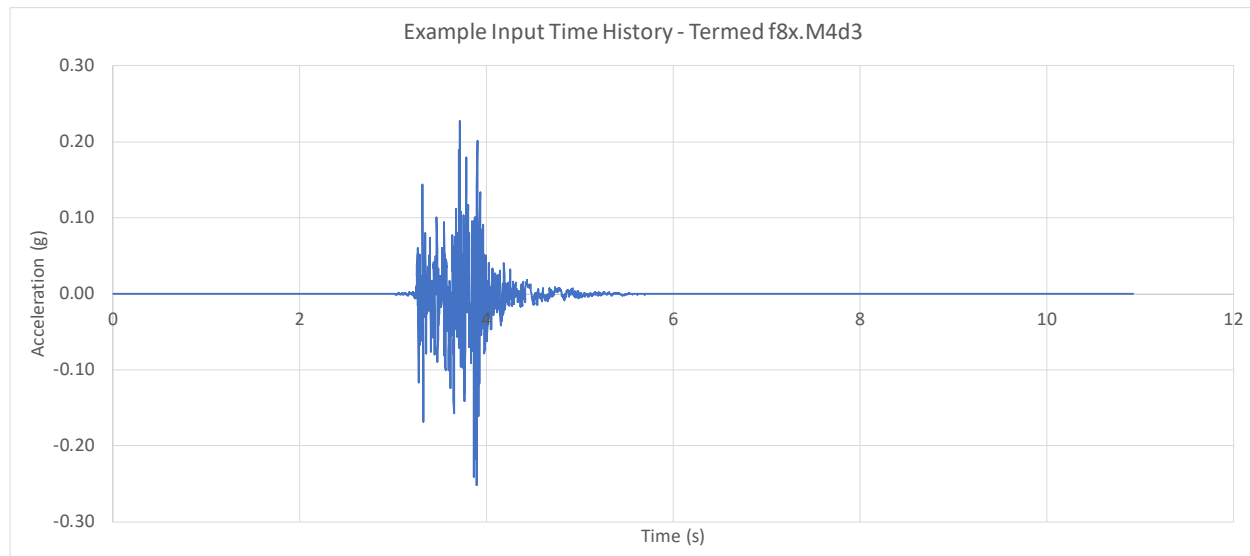


Figure 2.30 Example Input Earthquake Time History for the 1D Site Response Analyses

2.2.2.2 Results

Results of the analyses with two pulses of the magnitude 4.3 earthquake ground motions provided by the ITRB are shown in Figure 2.31. These results show a general trend of acceleration amplification as the motions pass from the foundation units into the tailings, which then show a steady trend of reduction within the tailings and then amplify again towards the ground surface. This acceleration trend is reflected in the trend of cyclic stress ratio (CSR), which shows an increasing trend towards the ground surface. These CSR values were used as inputs to laboratory tests to assess whether they would be sufficient to trigger liquefaction of the tailings.

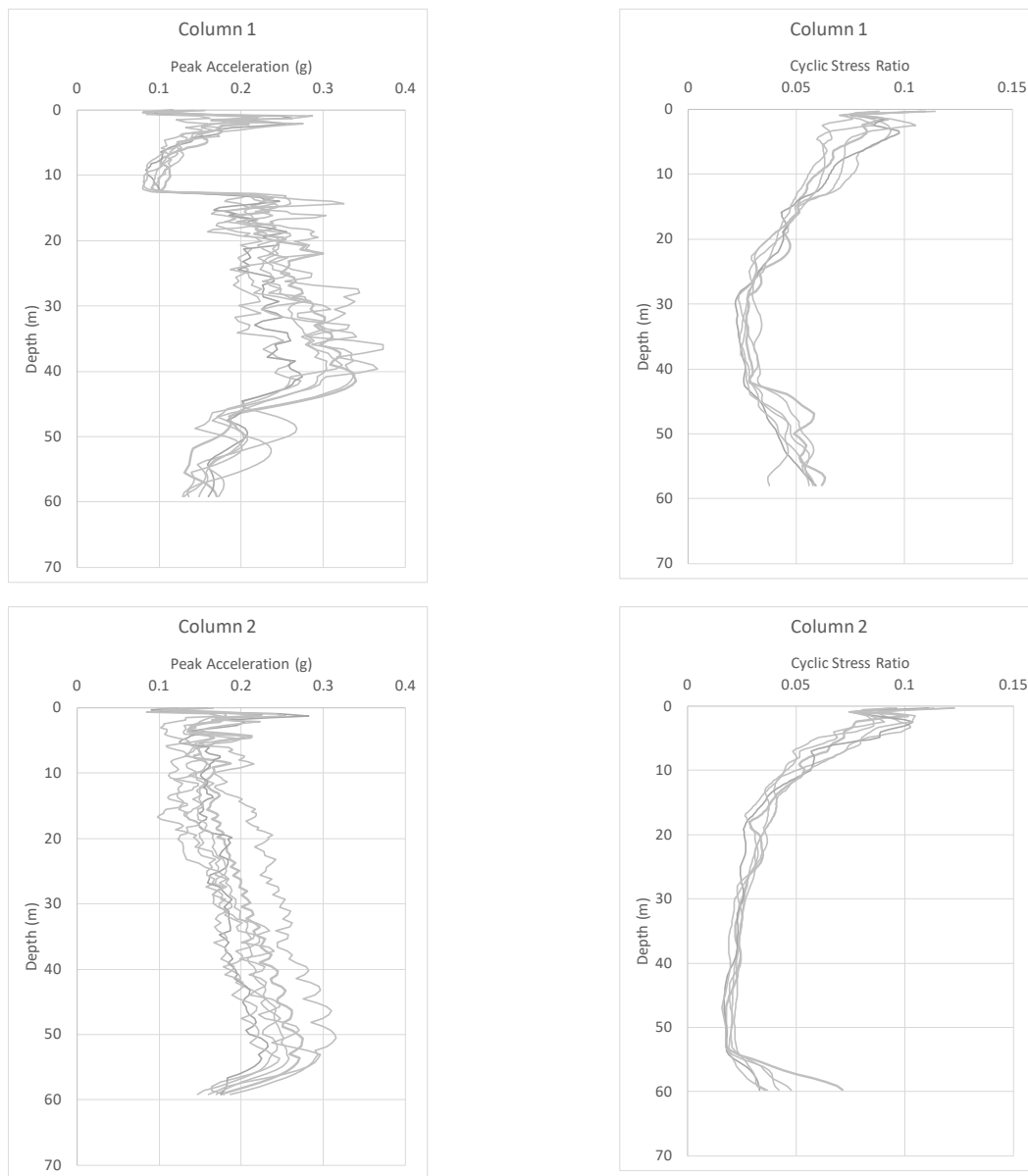


Figure 2.31 Peak Acceleration and Cyclic Stress Ratio Results for 1D Columns with Two Pulses of Magnitude 4.3 Earthquake Time Histories

2.2.3 2D Analysis

2.2.3.1 Methodology and Inputs

Given the potential significance of the ground motions to the failure mechanism, a 2D site response analysis was completed as a check on the reliability of the 1D results for this assessment. The 2D analysis was completed in FLAC2D using the same 2D model described in Section 2.1. In this analysis, the constitutive models of all soil units were switched to elastic after completion of the buttress construction stage and the stiffness was modified to match the small-strain trend used in the 1D analysis. Damping parameters were then applied to each soil unit to reflect the modulus reduction and damping curves selected for the 1D analyses.

A hysteretic damping relationship was used in the 2D analyses. It is not possible to exactly replicate the equivalent linear curves with this relationship; however, a series of simulated resonant column element tests were completed at the outset of this 2D assessment to identify the combination of parameters that would generate the closest match to the 1D curves. Example results from these element test simulations are shown in Figure 2.32.

After modifying the constitutive models and parameters of the 2D FLAC model from Section 2.1 for this seismic response analysis, the boundary conditions were modified for application of the seismic loading. The deconvolved seismic ground motion from the base of the 1D analysis was applied to the base of the 2D model and free-field boundary conditions were applied to the lateral model boundaries.

These 2D analyses were only ran for the magnitude 4.3 events, with two ground motion pulses applied immediately after one another, outlined in the memorandum by Dr. Atkinson.

Ground motions were monitored throughout the 2D analyses and compared with the results from the 1D analyses.

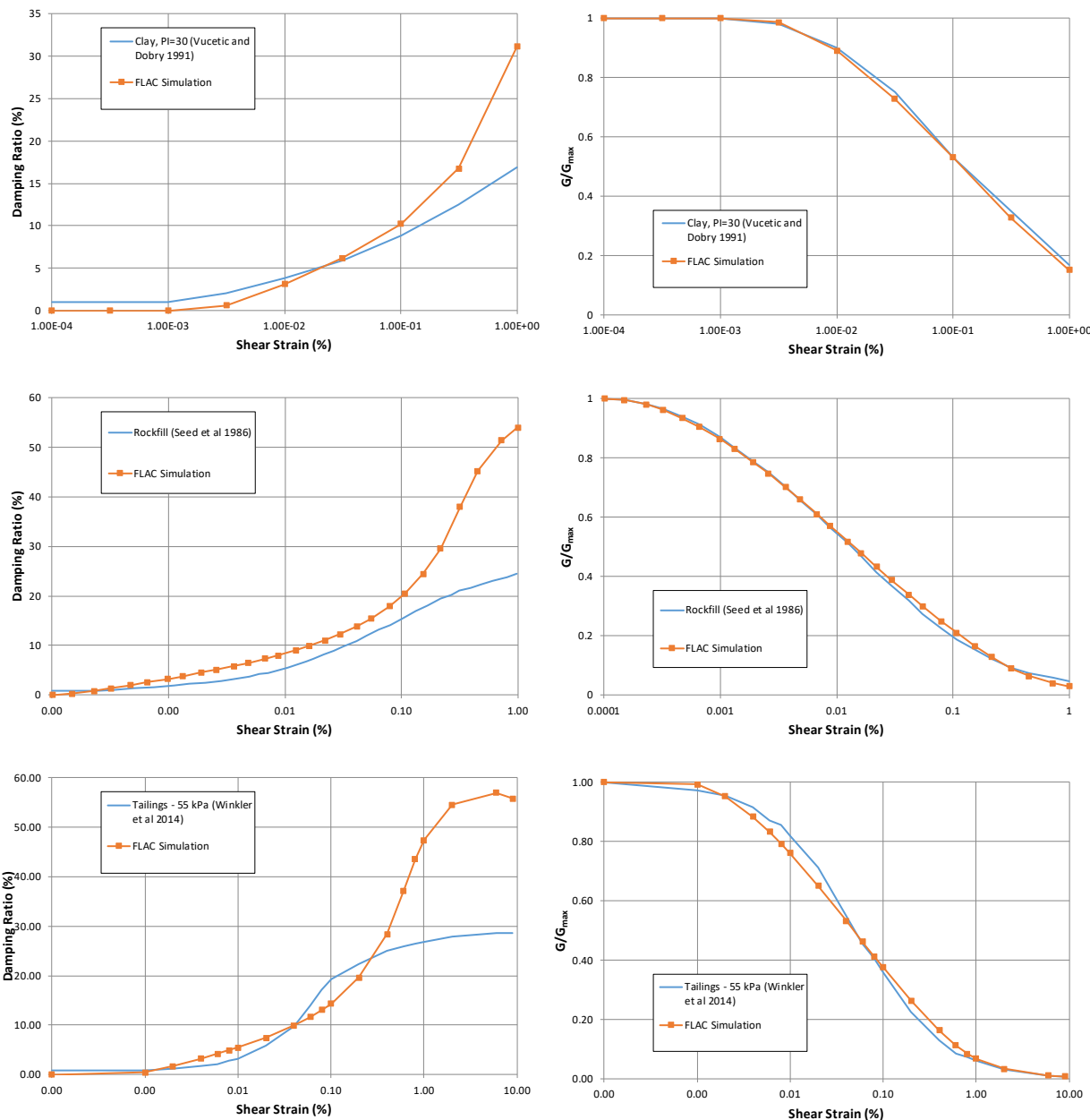


Figure 2.32 Calibration of Hysteretic Damping Parameters for the 2D Analysis to the 1D Modulus Reduction and Damping Relationships

2.2.3.2 Results

A comparison of the 1D and 2D analysis results was made at each of the five monitoring points at which the stress paths were monitored in the 2D static analyses, documented in Section 2.1.4.6. This involved identifying the location on either Column 1 or Column 2 from the 1D analyses that was closest to the stress path monitoring location and comparing those results with the results from the 2D analysis.

Comparisons of shear stress and acceleration between these two analyses are presented in Figure 2.33 to Figure 2.37. These results show that the 2D results were very similar to the 1D analysis. Based on this assessment, it was concluded that there was no significant 2D influence on

the site response results, and the 1D results were carried forward for use in the specification and interpretation of laboratory testing.

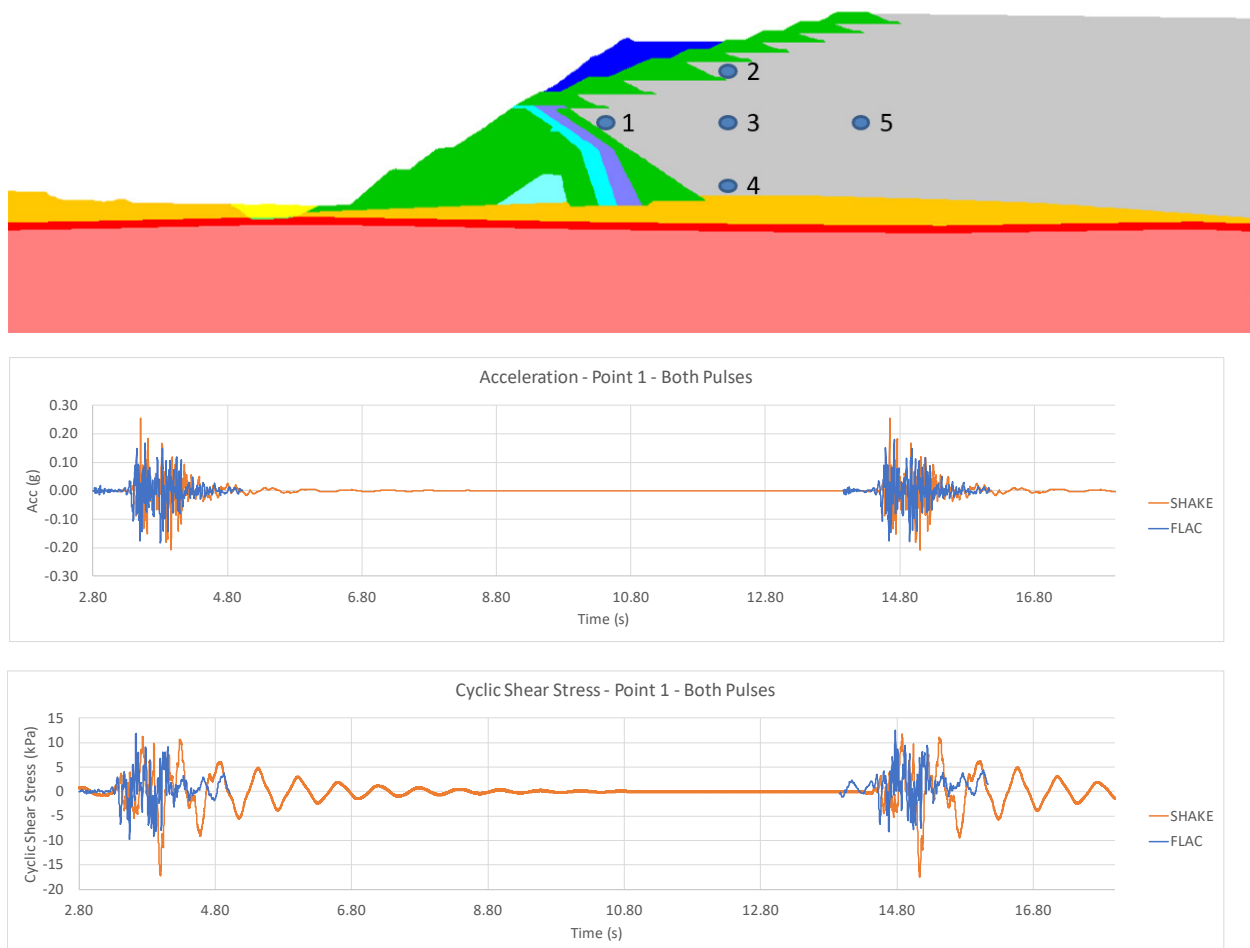


Figure 2.33 Comparison of 1D and 2D Site Response Analysis Results for Stress Path Monitoring location 1 (1D Results = SHAKE, 2D Results = FLAC)

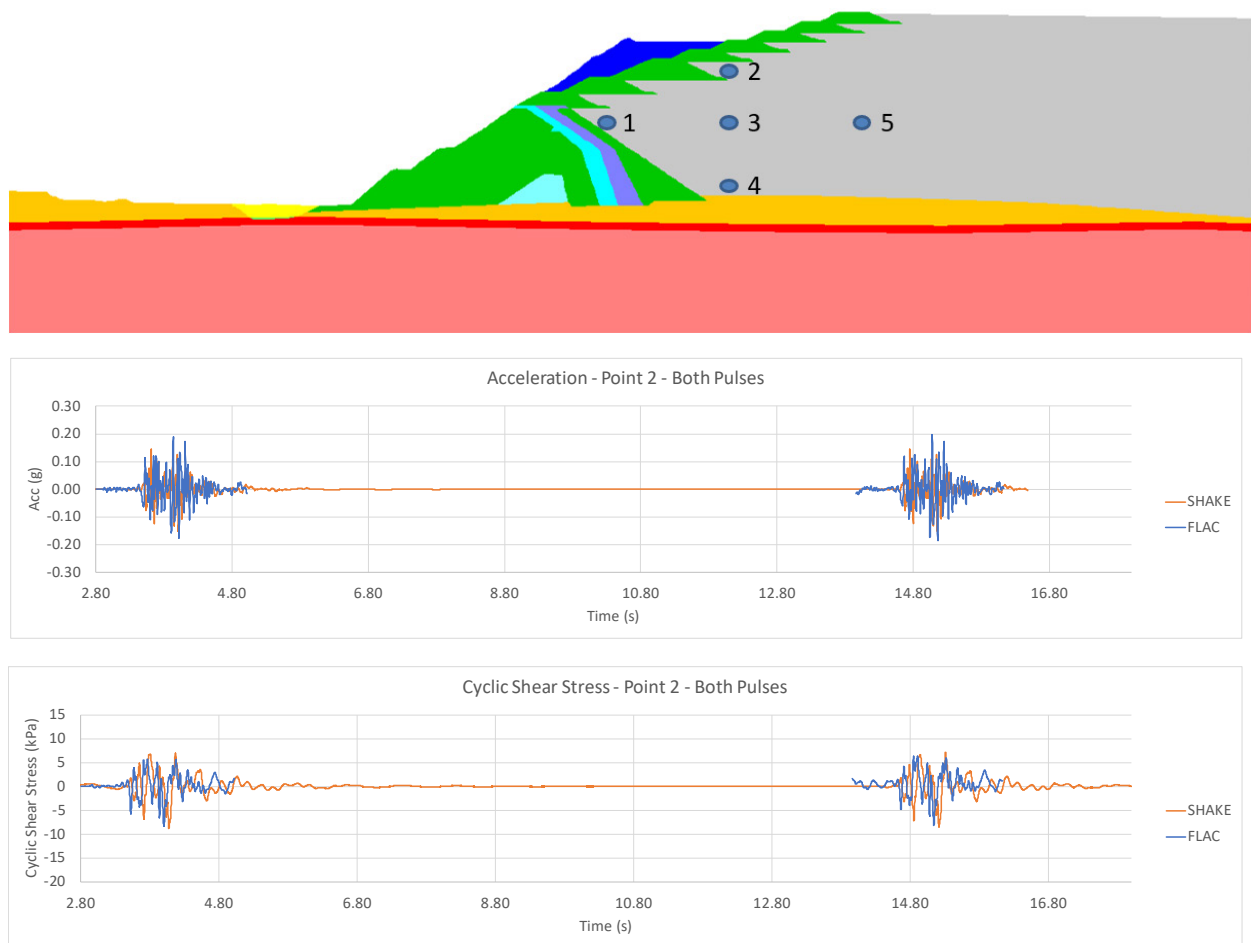


Figure 2.34 Comparison of 1D and 2D Site Response Analysis Results for Stress Path Monitoring location 2 (1D Results = SHAKE, 2D Results = FLAC)

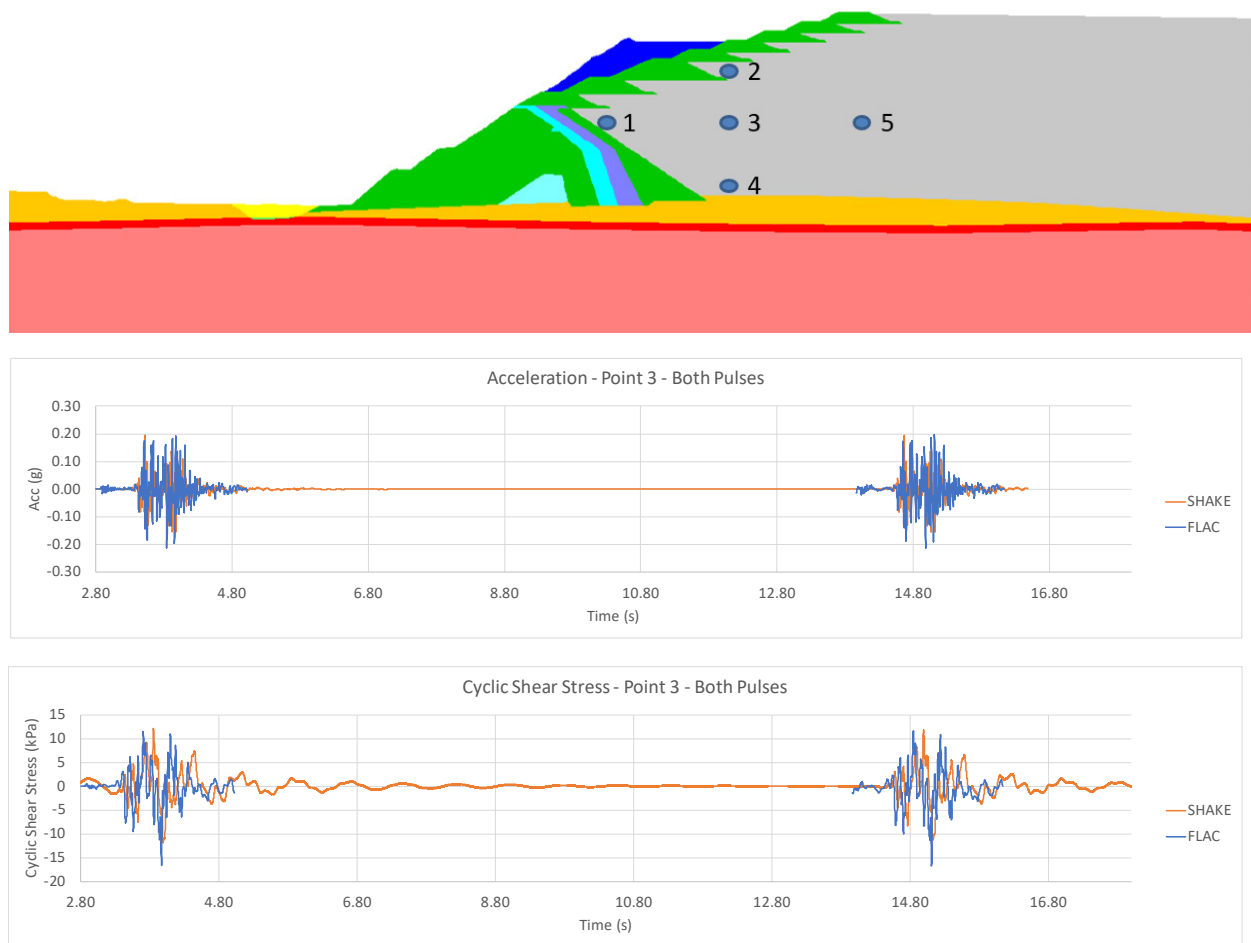


Figure 2.35 Comparison of 1D and 2D Site Response Analysis Results for Stress Path Monitoring location 3 (1D Results = SHAKE, 2D Results = FLAC)

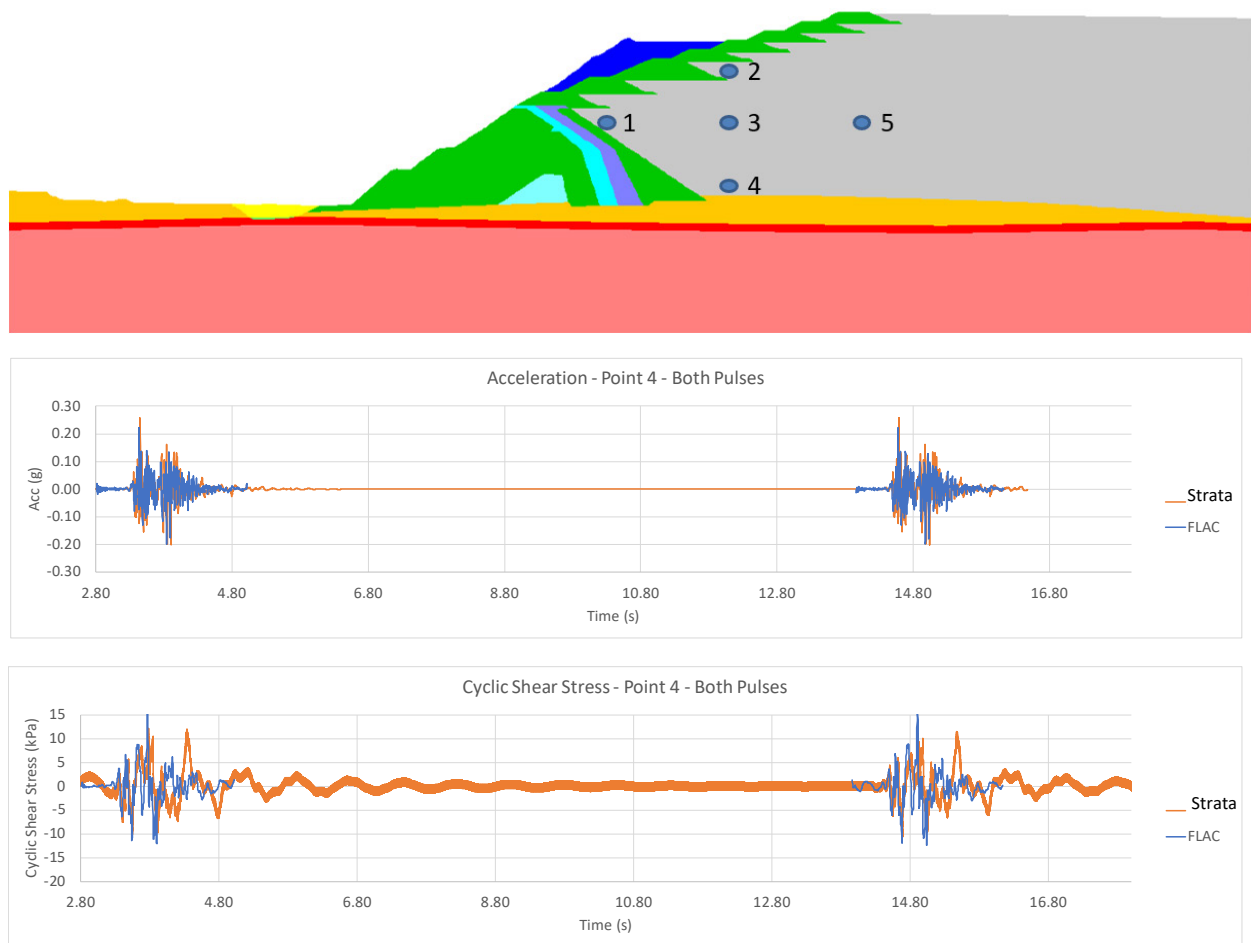


Figure 2.36 Comparison of 1D and 2D Site Response Analysis Results for Stress Path Monitoring location 4 (1D Results = SHAKE, 2D Results = FLAC)

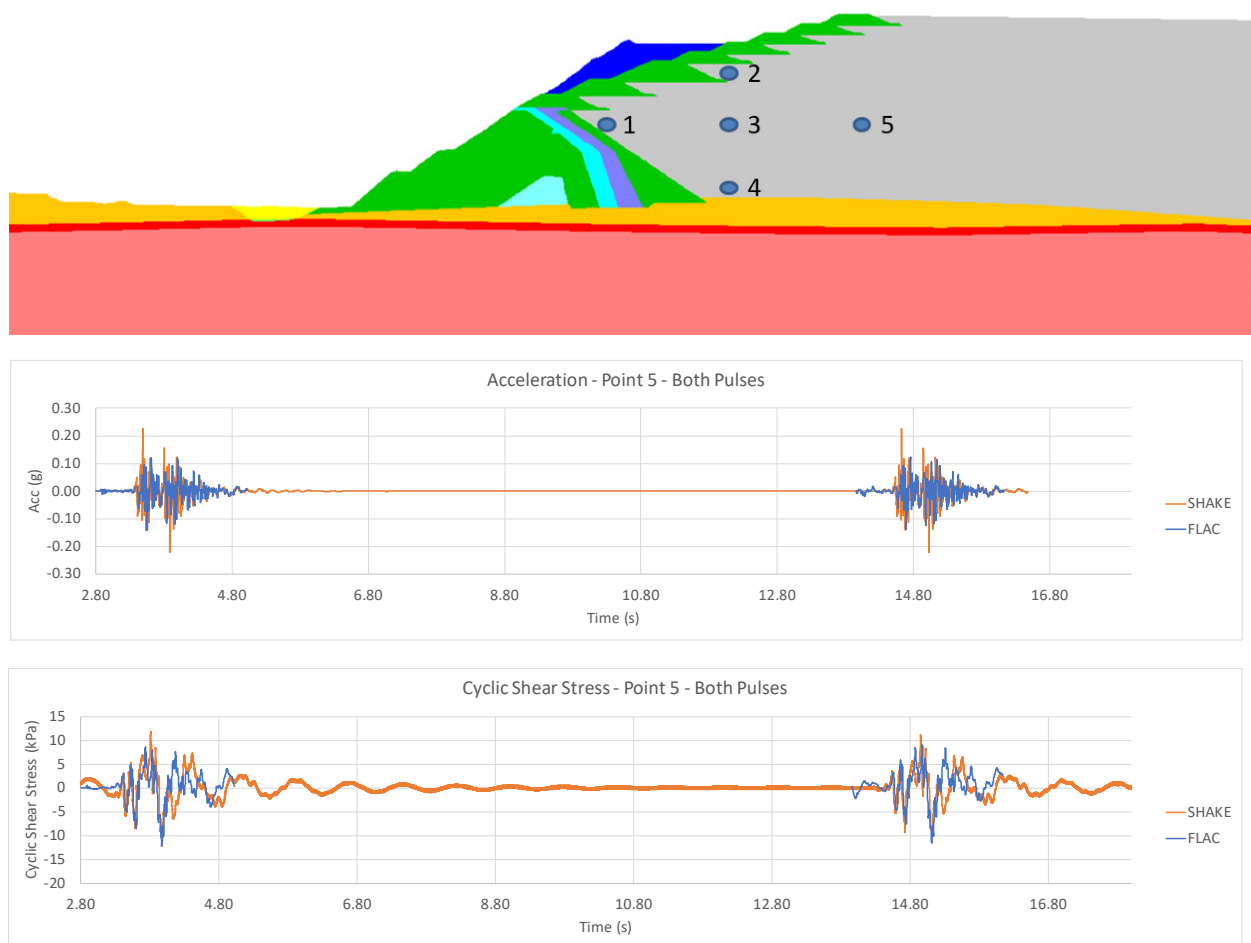


Figure 2.37 Comparison of 1D and 2D Site Response Analysis Results for Stress Path Monitoring location 5 (1D Results = SHAKE, 2D Results = FLAC)

2.2.3.3 Initial Static Bias

In addition to the ground motions calculated in the site response analyses, it was also necessary to identify the initial (pre-earthquake) static shear stress ratio (τ/σ'_v), termed static bias, for input to the laboratory testing program to identify if these ground motions could potentially generate excess pore pressures or liquefy the tailings. The variation of static bias throughout the 2D section was calculated in the 2D deformation model, and the results are presented in Figure 2.38. These results showed that the static bias at the location with the highest instability ratio (see Section 2.1.4.6) was roughly 0.32.

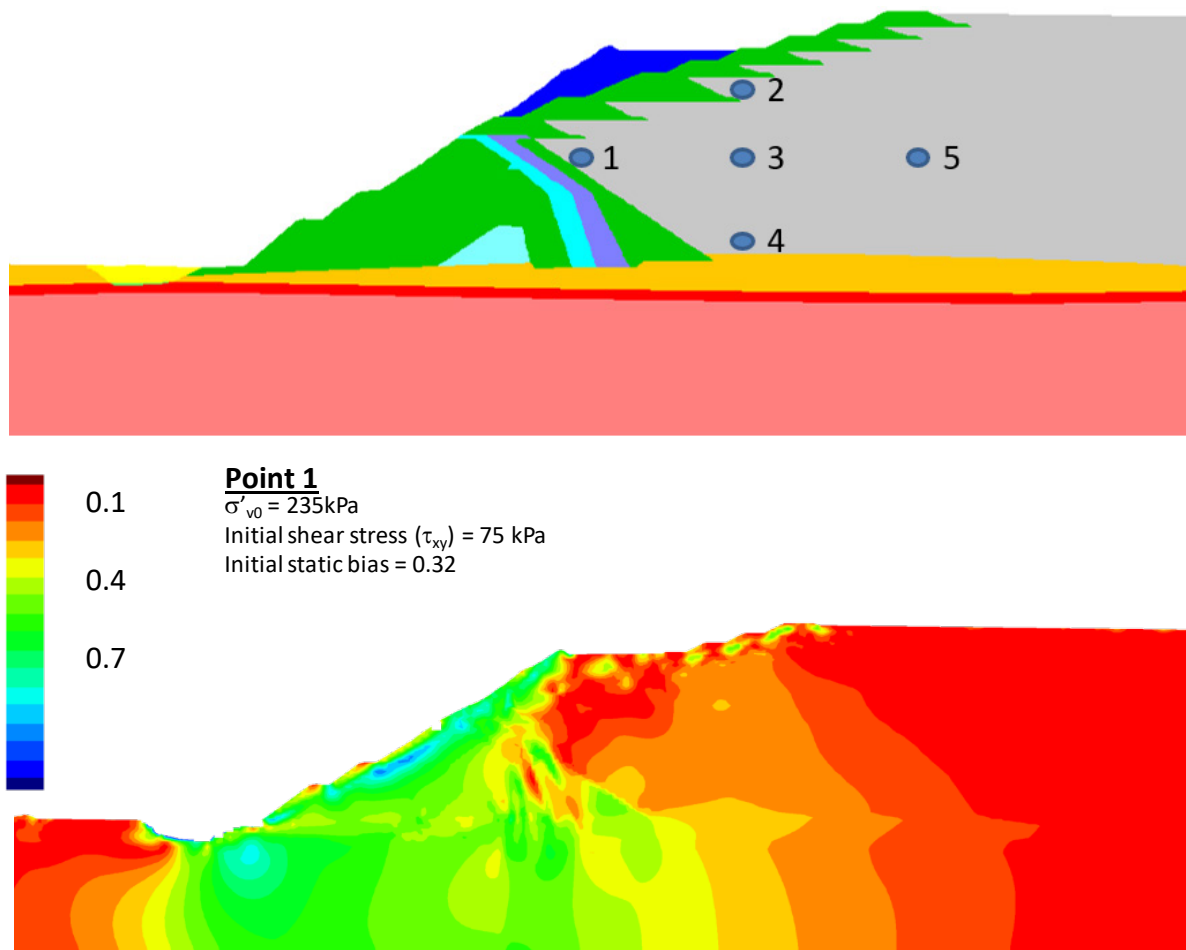


Figure 2.38 Pre-Earthquake Static Shear Stress Ratio (τ/σ'_v ; Static Bias) Calculated in 2D Analysis

2.3 Newmark Displacement Analyses

The laboratory tests that were used to assess the potential effects of these ground motions found that they would be unlikely to trigger liquefaction or generate excess pore pressures in the tailings. To conclude this assessment of the ground motions, the acceleration time histories from the 1D analyses were used as inputs to a series of Newmark sliding block-type analyses to help understand if these ground motions could have caused additional displacements in the foundation.

The ground motions were extracted from the base of the tailings and applied to the software ‘Slammer’, which was used for the Newmark-type calculations.

The analysis was completed as a sensitivity assessment in which the analysis was repeated with different values of yield acceleration. This analysis showed that even with a very low yield acceleration of 1 % g, the calculated displacements were less than 1 cm. On this basis, it was concluded that the earthquake loading would not have a significant impact on the foundation displacements in the event that they would not cause liquefaction of the tailings, which was later confirmed by laboratory testing.

2.4 3D Deformation Analysis

2.4.1 Model Setup

A 3D FLAC model was developed, covering an area 825 m long by 724 m wide, as shown on Figure 1.2. The model was a maximum of 114 m high. The basal model boundary was fixed in all three orthogonal directions. The lateral boundaries were fixed in the perpendicular direction and free to move both vertically and parallel to the boundary.

The 3D model comprised 506,006 quadrilateral ‘zones’ that were generated and grouped around geological, fill and tailings boundaries. The greatest concentrations of zones were created in the region of the failure and the Unit A foundation layer, and the size of the zones was gradually increased with distance from these regions.

Having generated the model and grouped the zones within the material boundaries, the model was used to simulate the dyke construction sequence in the same manner as the 2D model (see Section 2.1.1). An illustration of the model setup is shown in Figure 2.39 and Figure 2.40.

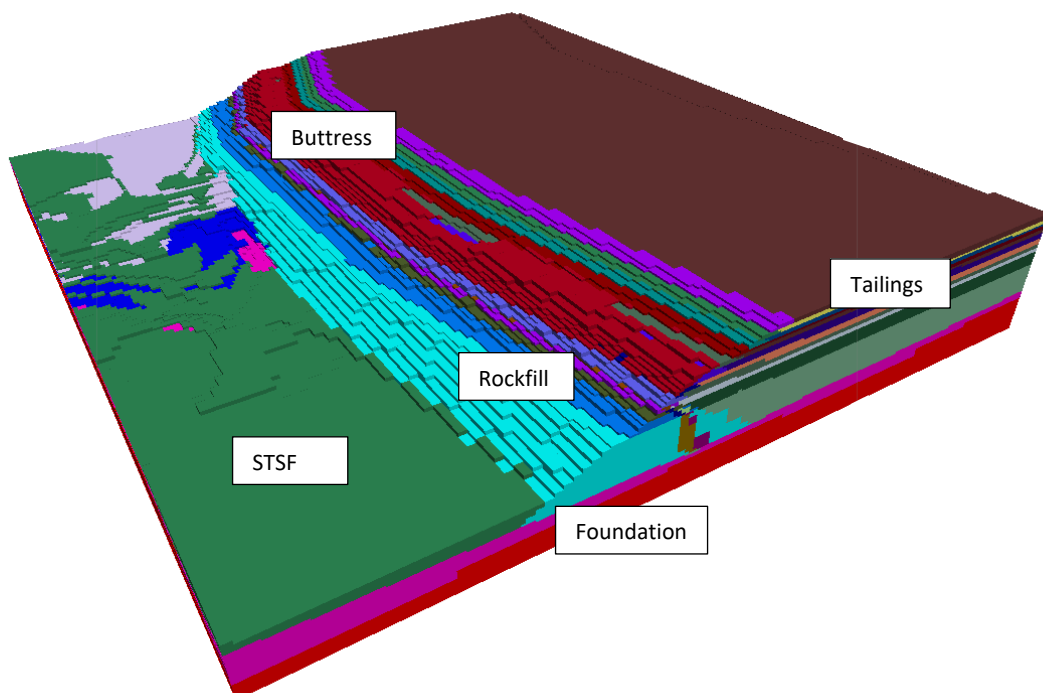


Figure 2.39 Illustration of 3D Model Setup

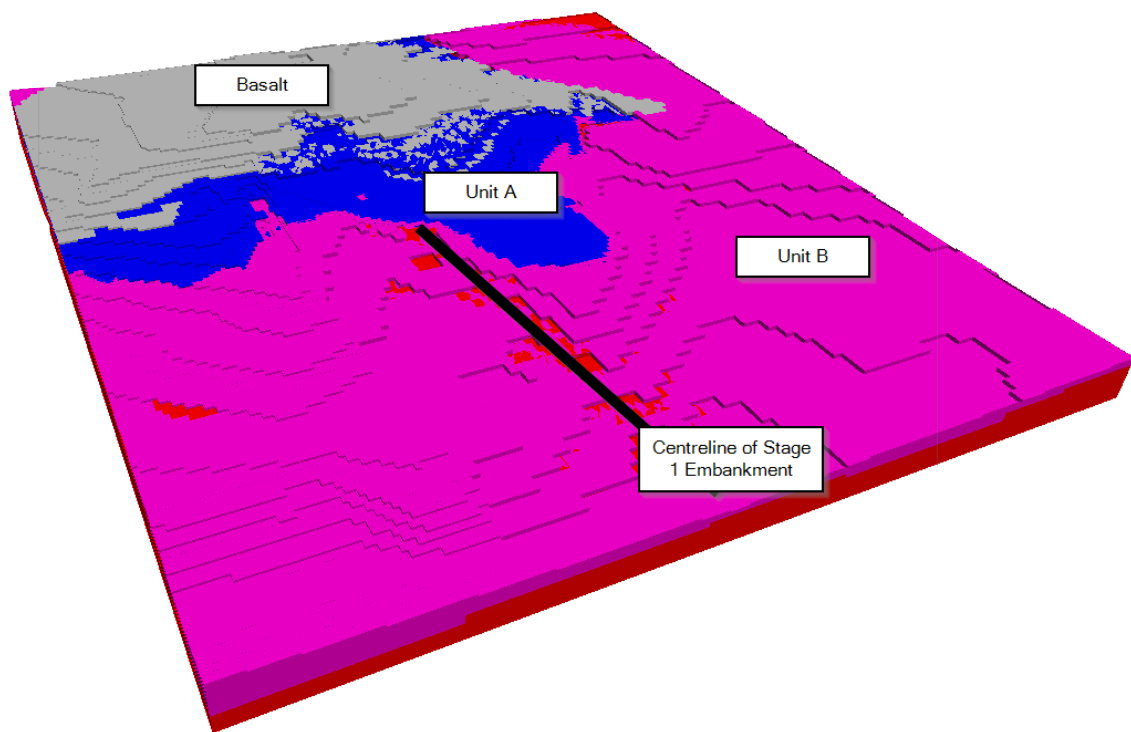


Figure 2.40 3D Model Foundation Stratigraphy

2.4.2 Modeling Sequence

The 3D modeling assessment was completed in a trial-and-improvement manner, where the results of each iteration were compared to the monitoring observations discussed in Section 2.1.3, and used to inform the next model iteration.

The first iteration of the 3D model was set up with the same parameters as the final 2D model except that in this initial 3D model the tailings were modeled using Mohr-Coulomb parameters to simplify the analysis. The deformations calculated in this initial analysis were significantly lower than the 2D results and monitoring observations throughout the construction sequence and concentrated at the toe of the dam after the excavation in that region during the Stage 10 construction. Example results for the buttress construction stage of this model are shown in Figure 2.41.

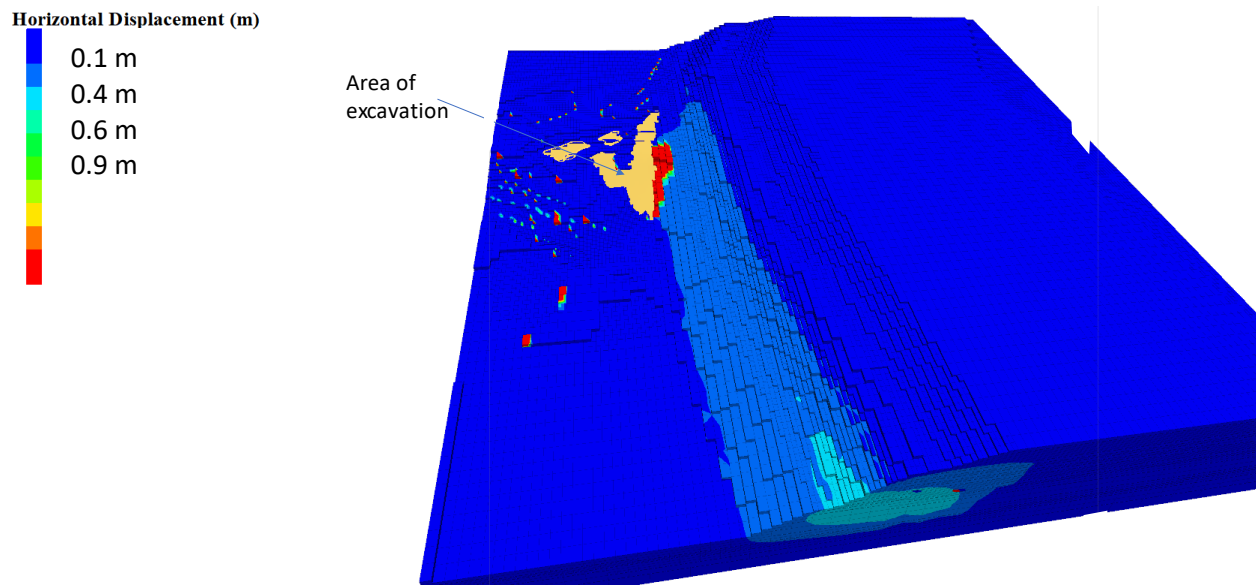


Figure 2.41 Horizontal Displacement Results at End of Buttress Construction Stage – Initial 3D Model

Given that the initial model displacements were less than the observations, a series of sensitivity analyses was completed that included the following variations:

- Testing the model response to variations in the Unit A strength within the range of laboratory test data interpretations for this unit. The range of strength values assessed was provided by the ITRB and is shown in Figure 2.42. Combinations of these trends were also assessed.
- Testing the model response to variations in the Unit A extent to assess the impact of uncertainty in this aspect. Variations on this included assigning the Unit A parameters to the Foundation in a) the area shown on Figure 2.40; b) the upper 2.5 to 3 m of Foundation (depending on zone size in this area) in the region underlying the excavation shown in Figure 2.41; and c) the upper 2.5 to 3 m of Foundation throughout the entire model.
- Assigning the NorSand constitutive model to the tailings to assess the impact of the tailings on the model response.

These variations were applied sequentially over roughly 34 model iterations.

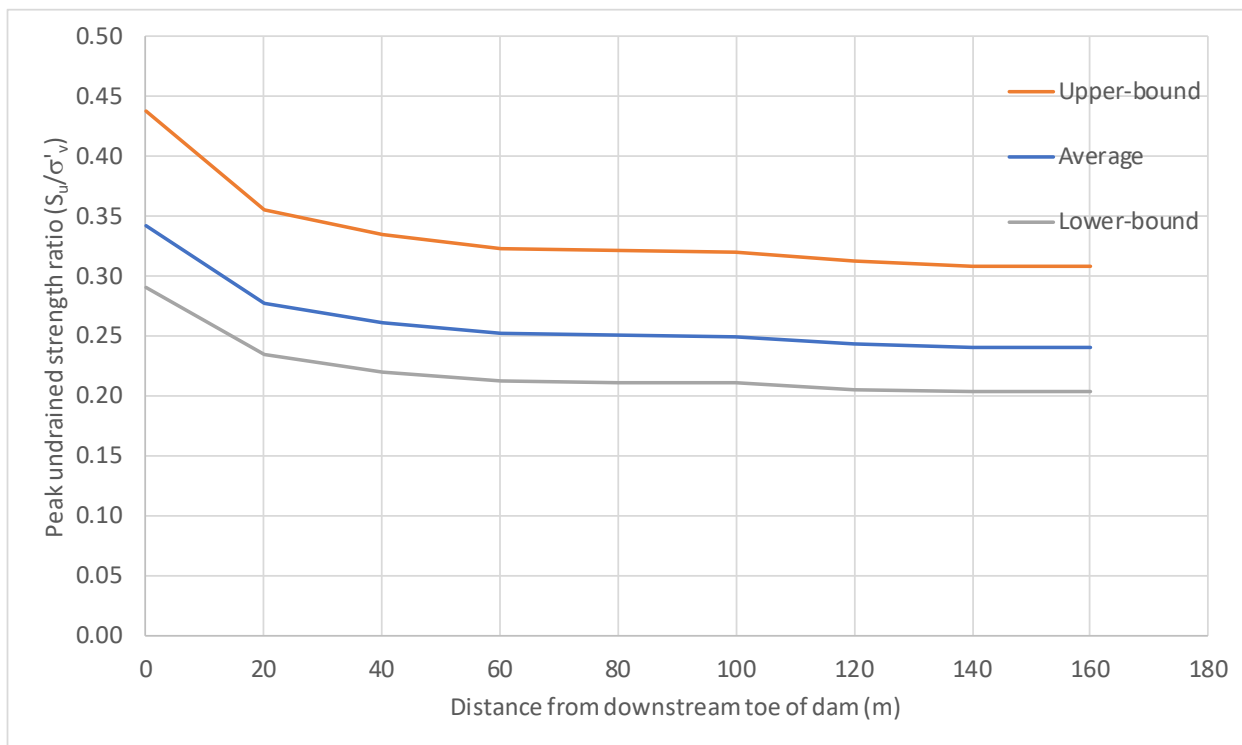


Figure 2.42 Peak Strength Variations Applied to Unit A in 3D Sensitivity Analyses

A key finding from this process was that changing the constitutive model of the tailings from Mohr-Coulomb to NorSand made a significant difference to the pattern and magnitude of the calculated displacements. The pattern of displacements when NorSand was assigned to the tailings aligned better with the field observations than the Mohr-Coulomb iterations. The reason for this is that this change in constitutive model allowed ongoing volumetric strain and yielding of the loose tailings throughout the dam construction, leading to a transfer of stresses to the foundation and increased straining and yielding of Unit A.

The models from this process that produced the most representative results are discussed in Section 2.4.3.

2.4.3 Results – Final 3D Deformation Model

The two model variants that produced the closest match to the field observations had the Unit A properties assigned to the upper 2.5 to 3 m of the entire Foundation and NorSand properties assigned to the tailings; one variant used an initial tailings state parameter (ψ) of +0.06 and the other used +0.08. Figure 2.43 shows that both of these initial tailings state parameter values lead to state parameter distributions that plot within a similar range compared with the measured 2017 values at CPT location N04 because of the process of shear densification described in Section 2.1.4.7.

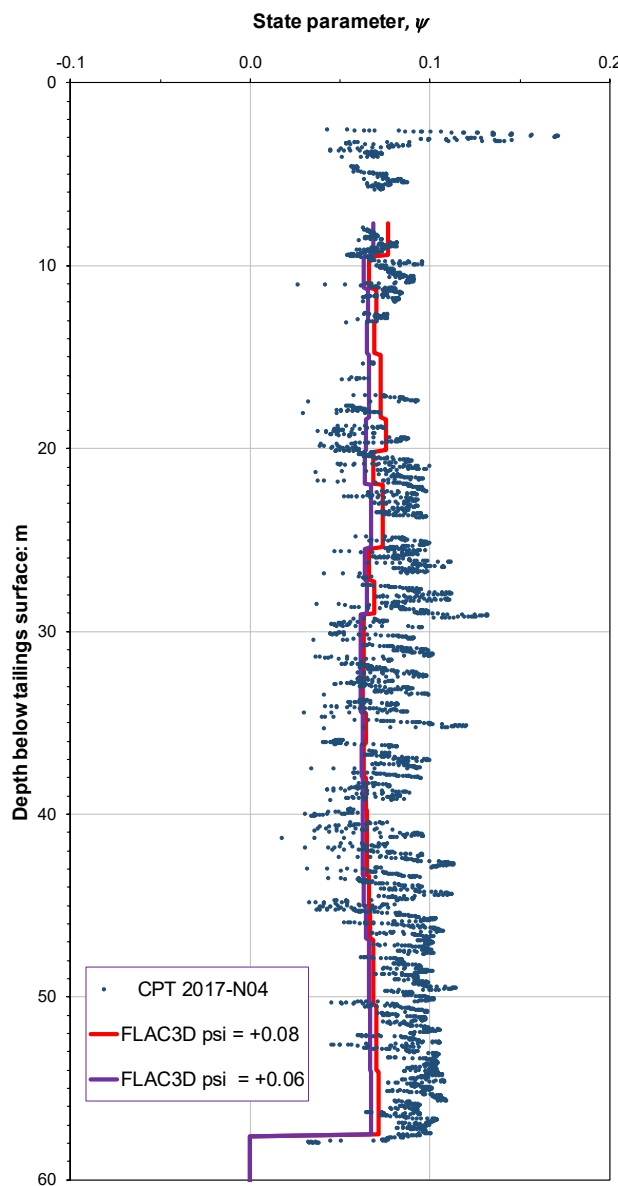
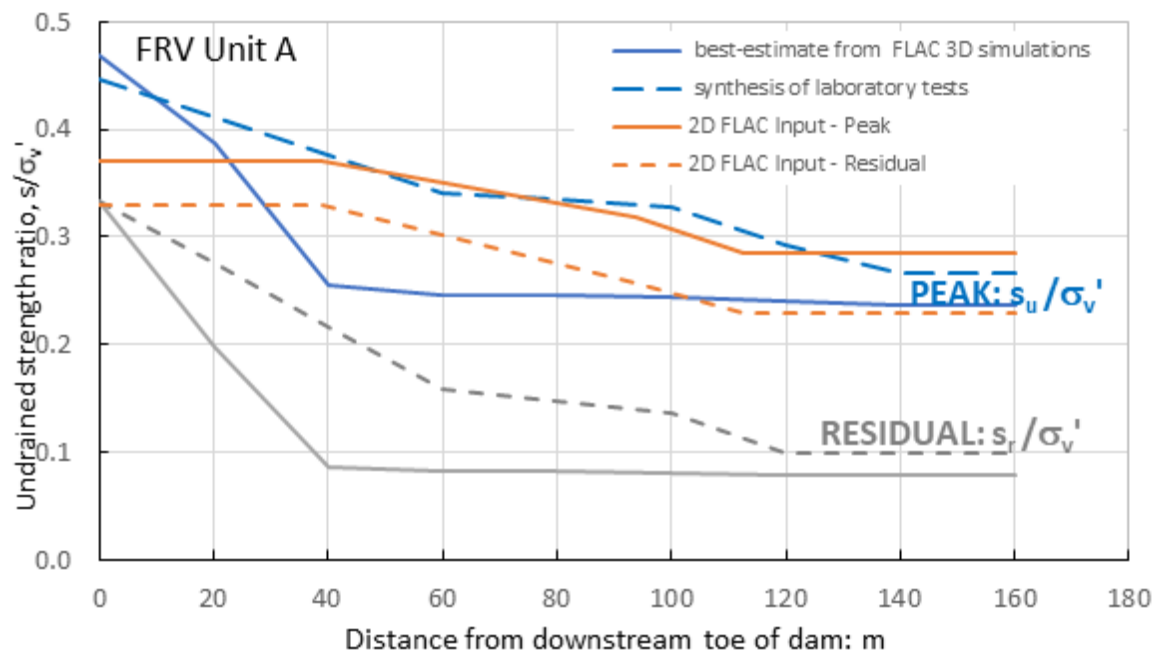


Figure 2.43 State Parameter Comparison

The Unit A strength assigned in these analyses is shown and compared with the strengths used in the 2D analyses in Figure 2.44. The response of the models with these two tailings state parameters bounded the observed field behaviour.



Note: 2D FLAC inputs shown are the 'Alternate KCB Parameters'.

Figure 2.44 Unit A Strength Relationship that Bounded the Observed Behaviour

When the tailings state parameter was set to $\psi=+0.06$ this model was able to complete the simulation of the entire construction sequence; however, when the tailings were assigned $\psi=+0.08$, the dam failed in the model during the buttress construction. This difference in response highlights the significant role that the tailings yielding had on the overall model response and pattern of displacements. The horizontal displacements from these two model variants are shown in plan view in Figure 2.45 and on a plane cut through the 3D model at Station 19+50 in Figure 2.46 and Figure 2.47. It can be seen in these figures that both model variants led to a concentration of displacements within the region where the failure occurred and that the displacements developed through the foundation, beneath the Stage 1 rockfill and into the tailings beneath the buttress. The main difference in the displacement patterns is that the displacements in the $\psi=+0.08$ model were more widespread.

The patterns of displacements from these two model variants are compared with the prism monitoring data discussed in Section 2.1.3.2 in Figure 2.48 and Figure 2.49. These results show that both models matched well to the survey data until Stage 9. After Stage 9 the displacements in the $\psi=+0.08$ model increase significantly more quickly than was observed, whereas the $\psi=+0.06$ model continued to replicate the observed trend reasonably well. This same pattern can be seen when the model displacements are compared with the InSAR data in Figure 2.50 and Figure 2.51; the overall trend of the InSAR data is matched more closely with the $\psi=+0.06$ model than the $\psi=+0.08$ model. The reason for the difference in response at this stage in the construction sequence can be seen in Figure 2.52 and Figure 2.53, which show that strain weakening began occurring in the foundation during Stage 9 in the $\psi=+0.08$ model and during Stage 10 in the $\psi=+0.06$ model. Figure 2.54 and Figure 2.55 also show that the effect of this earlier displacement in the $\psi=+0.08$ model was to increase the stress (instability) ratio in the tailings, making them more susceptible to liquefaction at an earlier stage. Based on these results, it was concluded that

the $\psi=+0.06$ model represented a closer match to the field observations and that the $\psi=+0.08$ model provided an estimate of how the drained (Phase 1) response would transition into the undrained (Phase 2) response in the tailings.

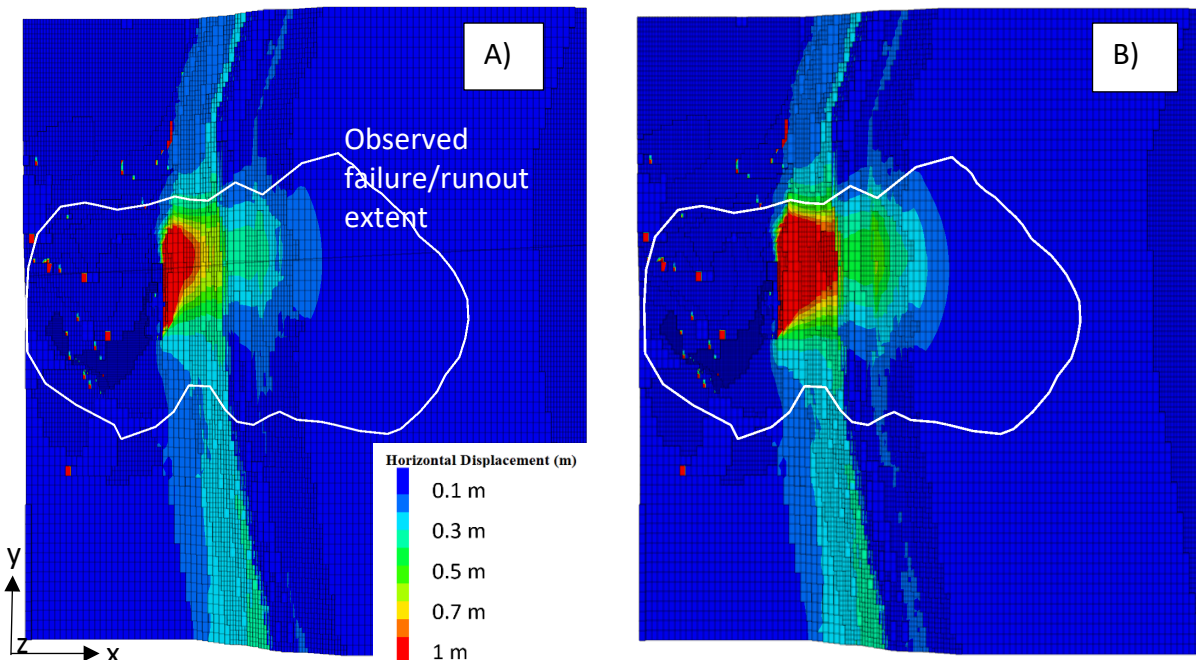


Figure 2.45 Plan View Comparison of FLAC3D Displacements with Observed Extent of Failure/Runout. A) Tailings State Parameter = +0.06; B) Tailings State Parameter = +0.08

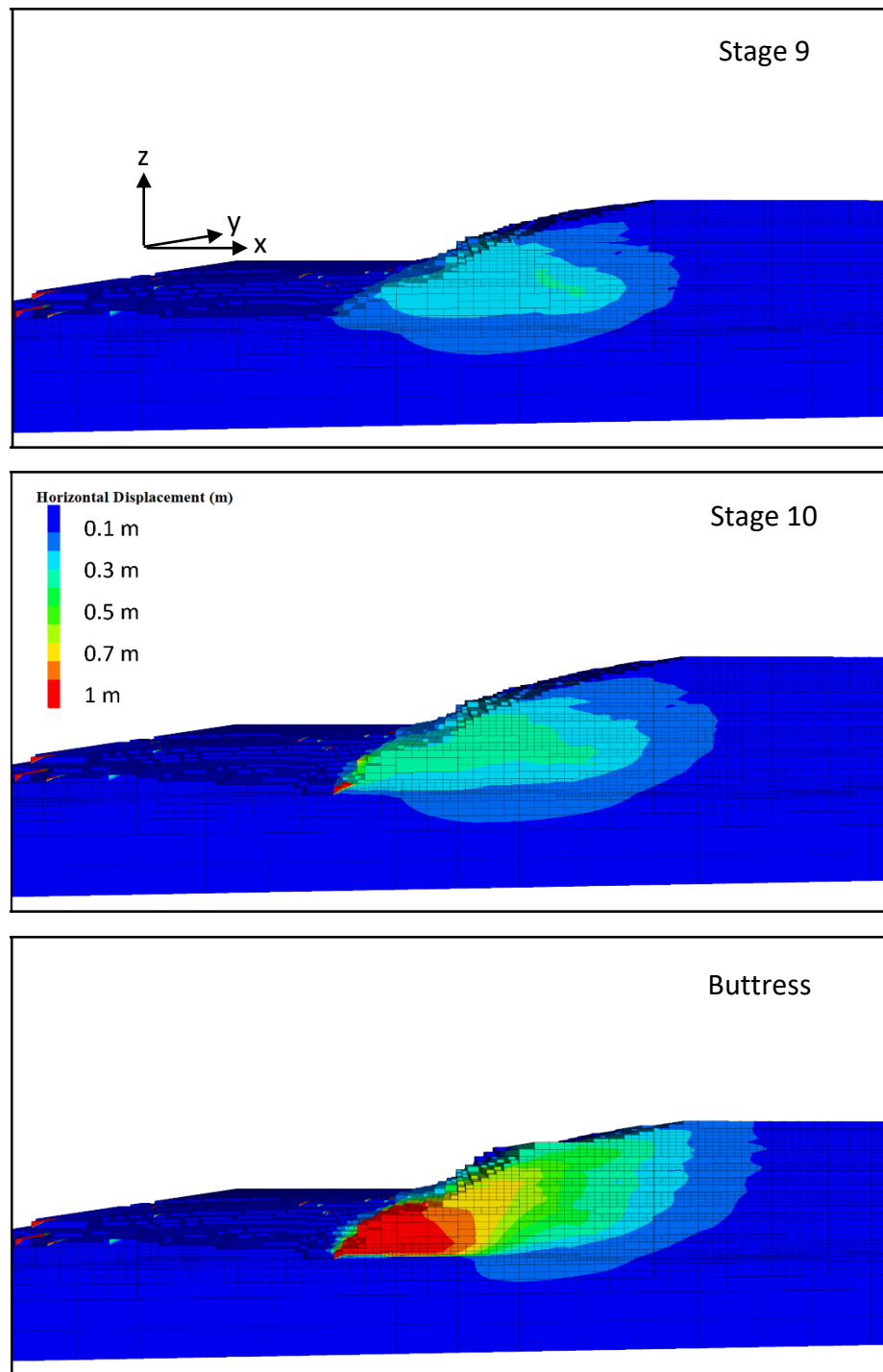


Figure 2.46 Horizontal Displacement Development: Tailings State Parameter = + 0.06

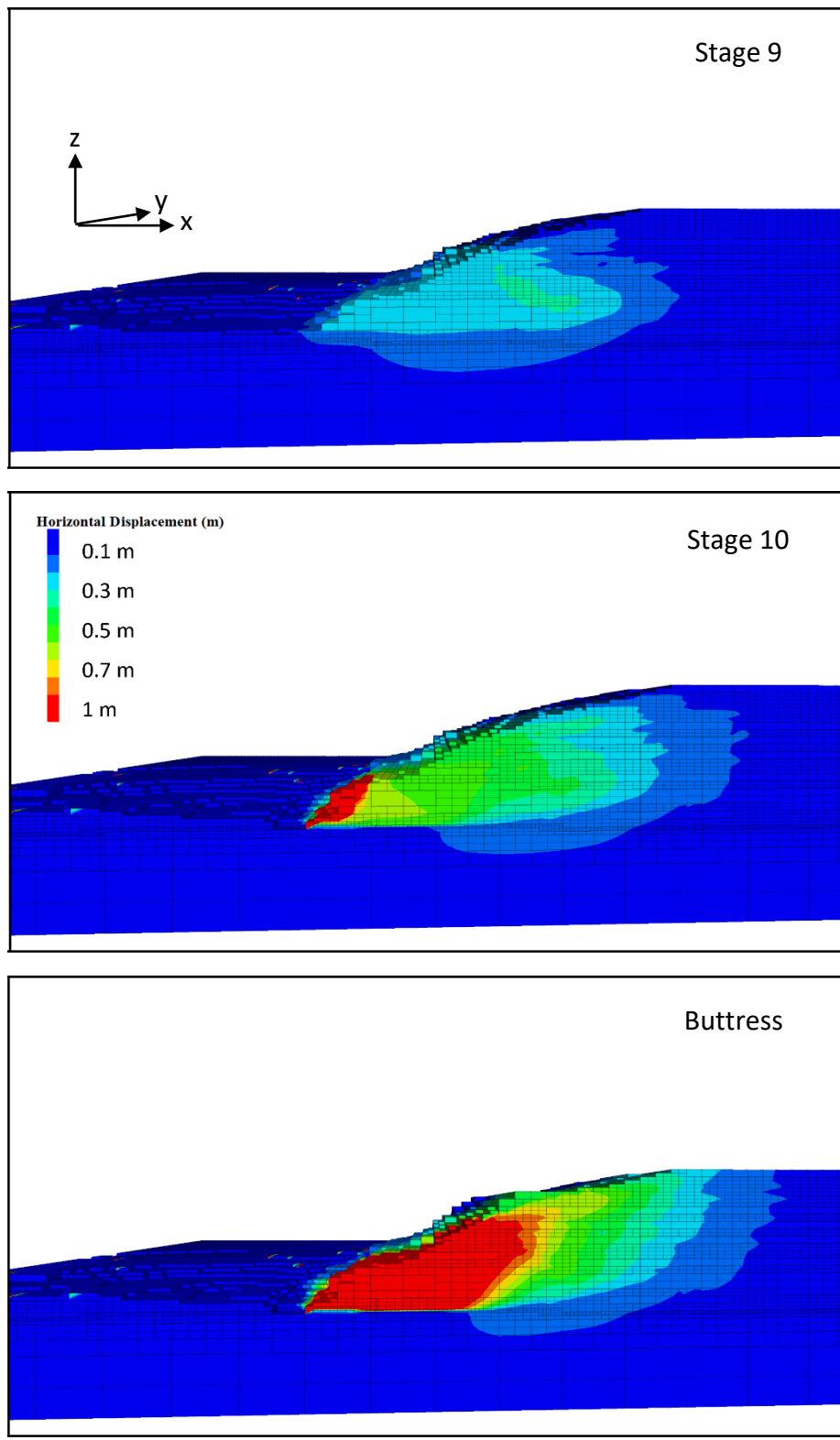


Figure 2.47 Horizontal Displacement Development: Tailings State Parameter = + 0.08

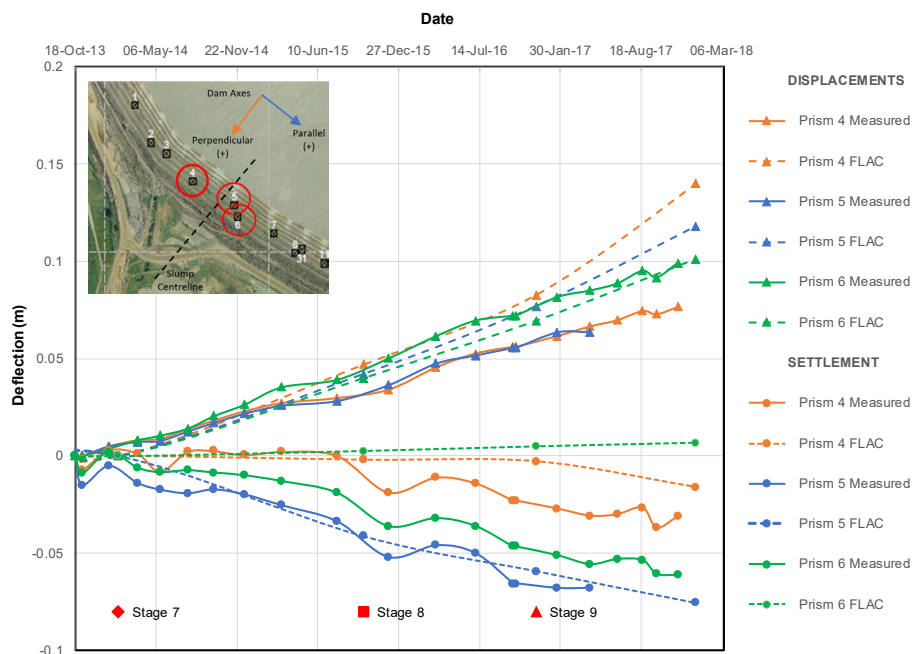


Figure 2.48 Comparison of Deformation Modeling Results with Survey Prism Data: Tailings State Parameter = + 0.06

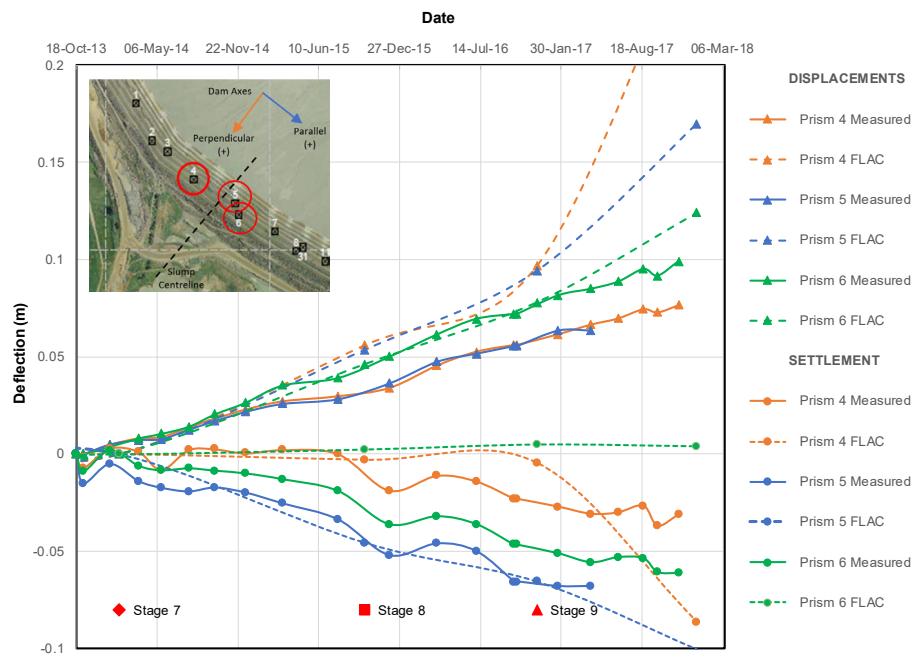


Figure 2.49 Comparison of Deformation Modeling Results with Survey Prism Data: Tailings State Parameter = + 0.08

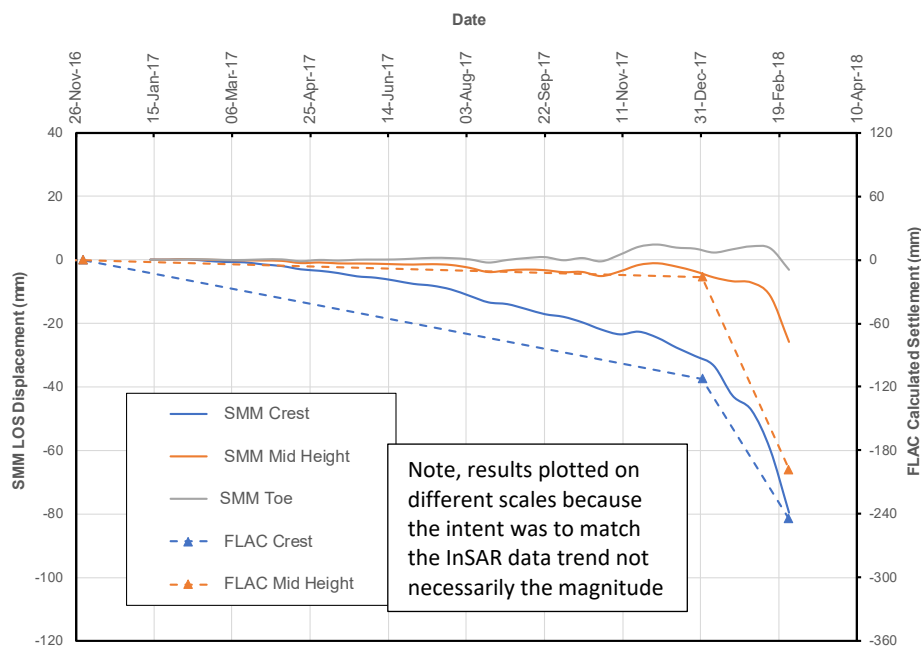


Figure 2.50 Comparison of FLAC Surface Displacement Trends with InSAR Results: Tailings State Parameter = +0.06

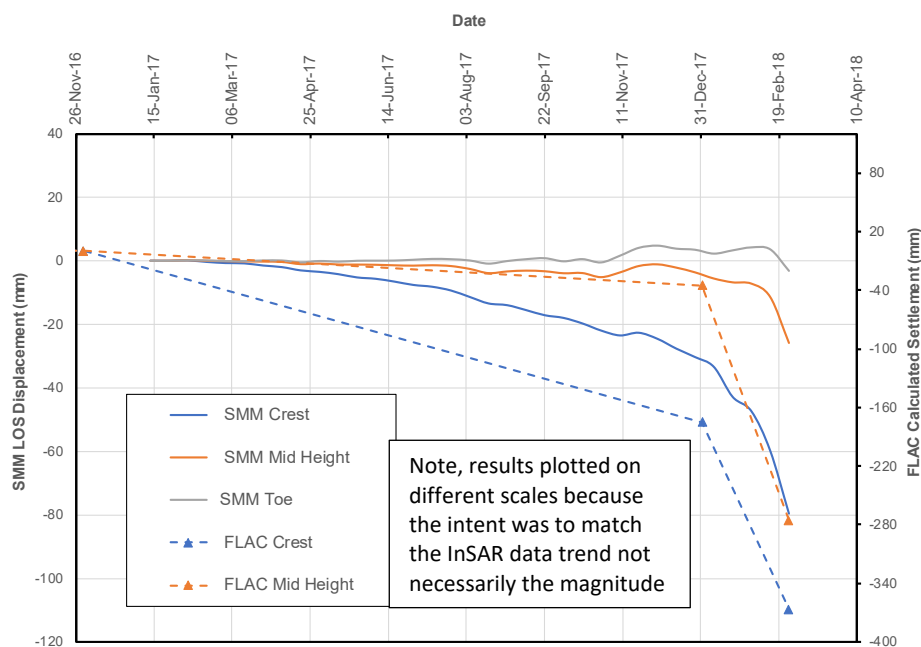


Figure 2.51 Comparison of FLAC Surface Displacement Trends with InSAR Results: Tailings State Parameter = +0.08

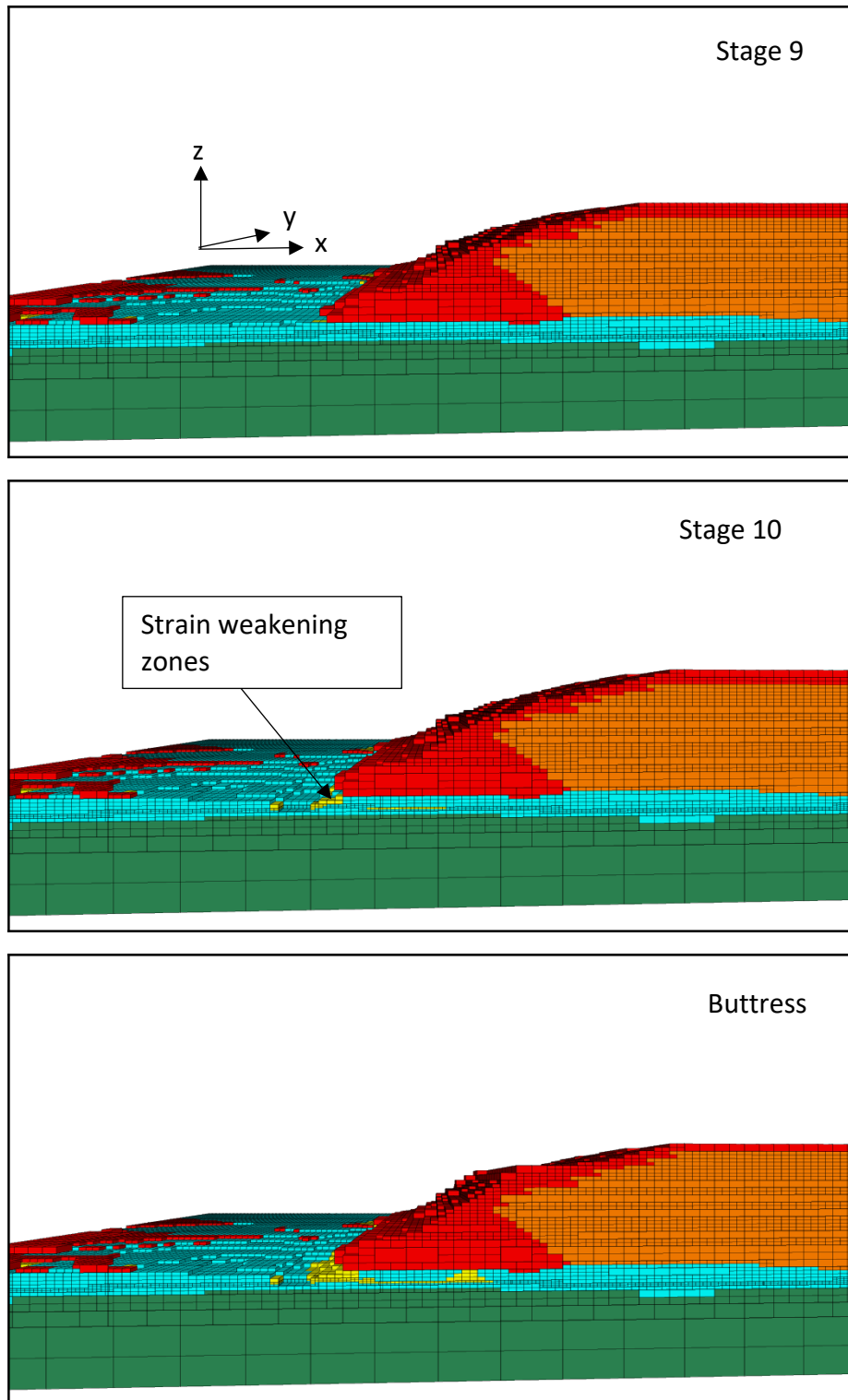


Figure 2.52 Development of Strain Weakening: Tailings State Parameter = + 0.06

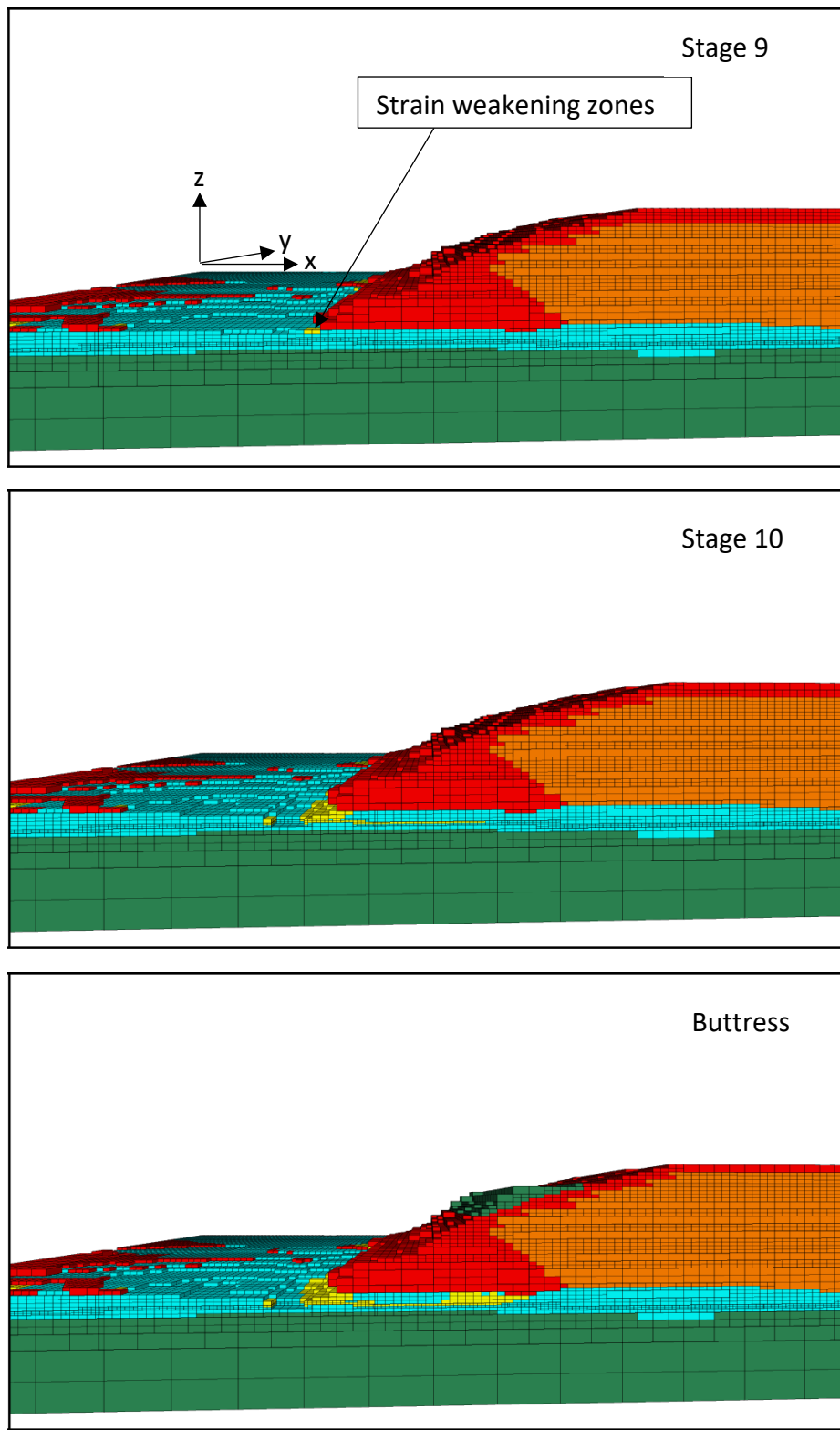


Figure 2.53 Development of Strain Weakening: Tailings State Parameter = + 0.08

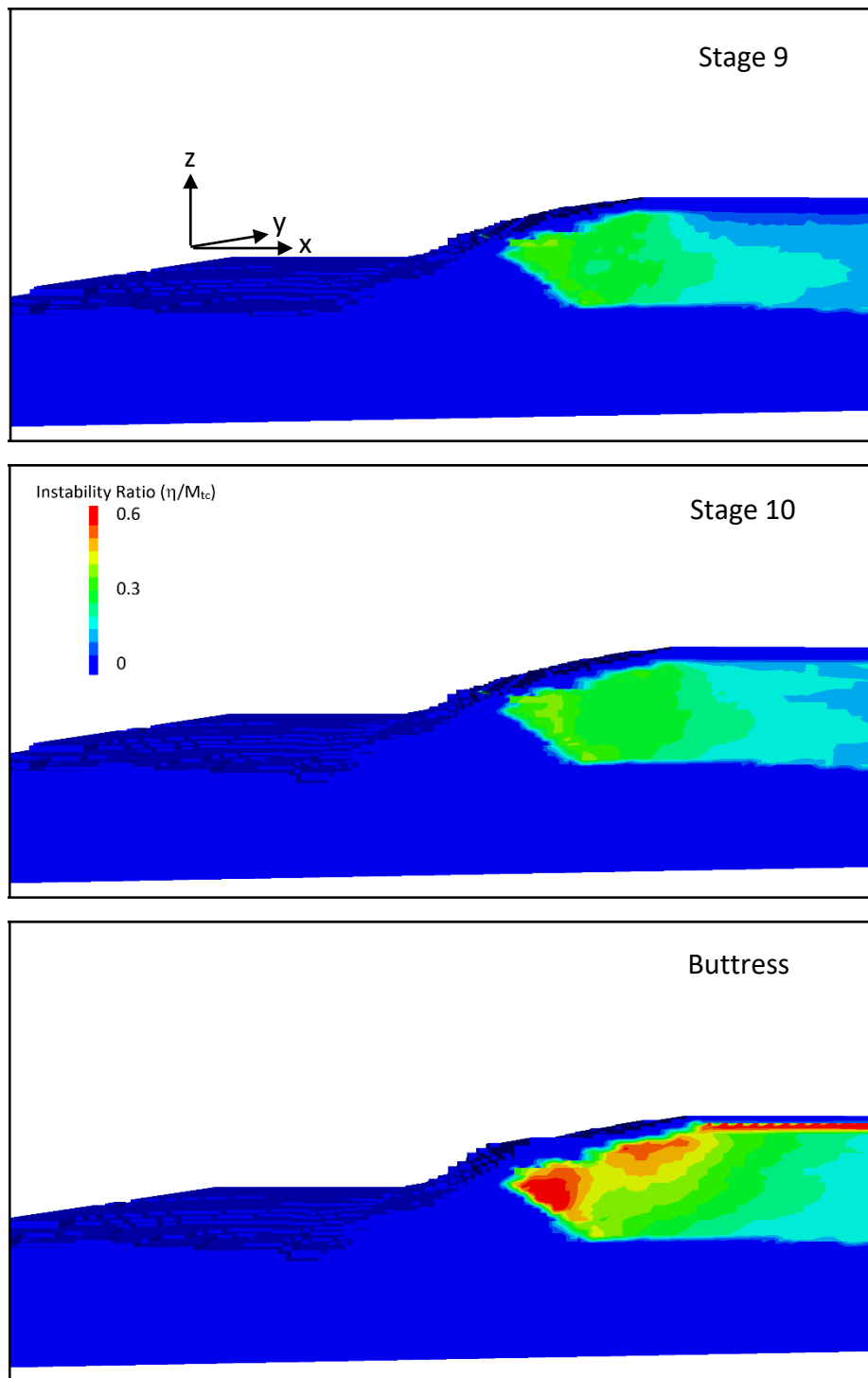


Figure 2.54 Instability Ratio Development: Tailings State Parameter = + 0.06

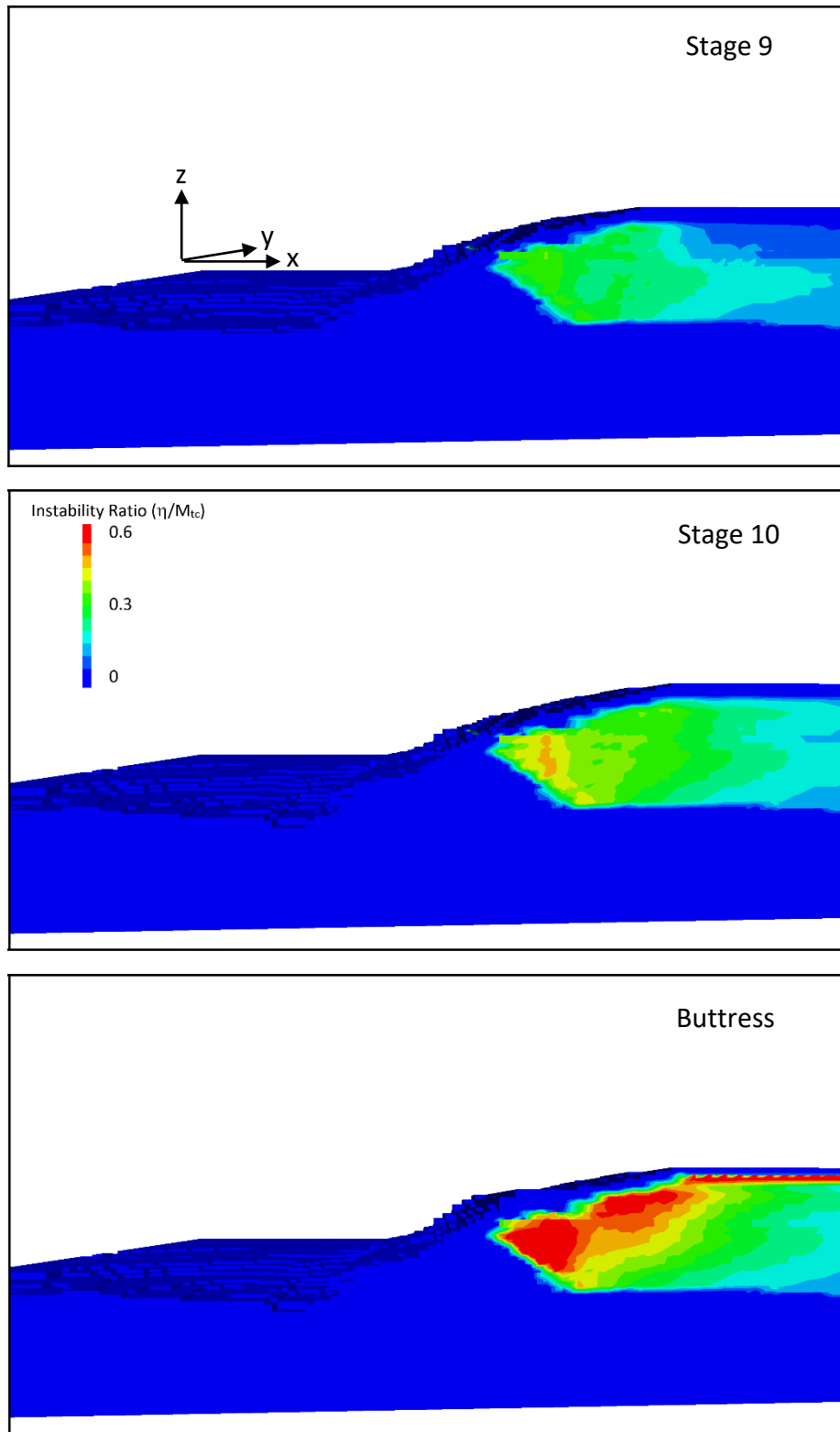


Figure 2.55 Instability Ratio Development: Tailings State Parameter = + 0.08

In addition to comparing the model results against the prism displacement measurements and InSAR displacement trends, the $\psi=+0.06$ model was reviewed for evidence of heave at the toe of the excavation and cracking on the buttress crest. Figure 2.56 shows how a zone of heave was

observed to develop in the model between the Stage 9 and 10 construction stages, thereby honouring the observation that heaving was observed in this region. Figure 2.57 shows two regions of potential cracking indicated by the surface horizontal displacement trends; one on the buttress crest and one towards the toe of the dam. As discussed in Section 2.1.4.3, this observation is roughly in accordance with the observations but not conclusive, suggesting that some of the observed cracking could have been a result of early onset liquefaction in the tailings.

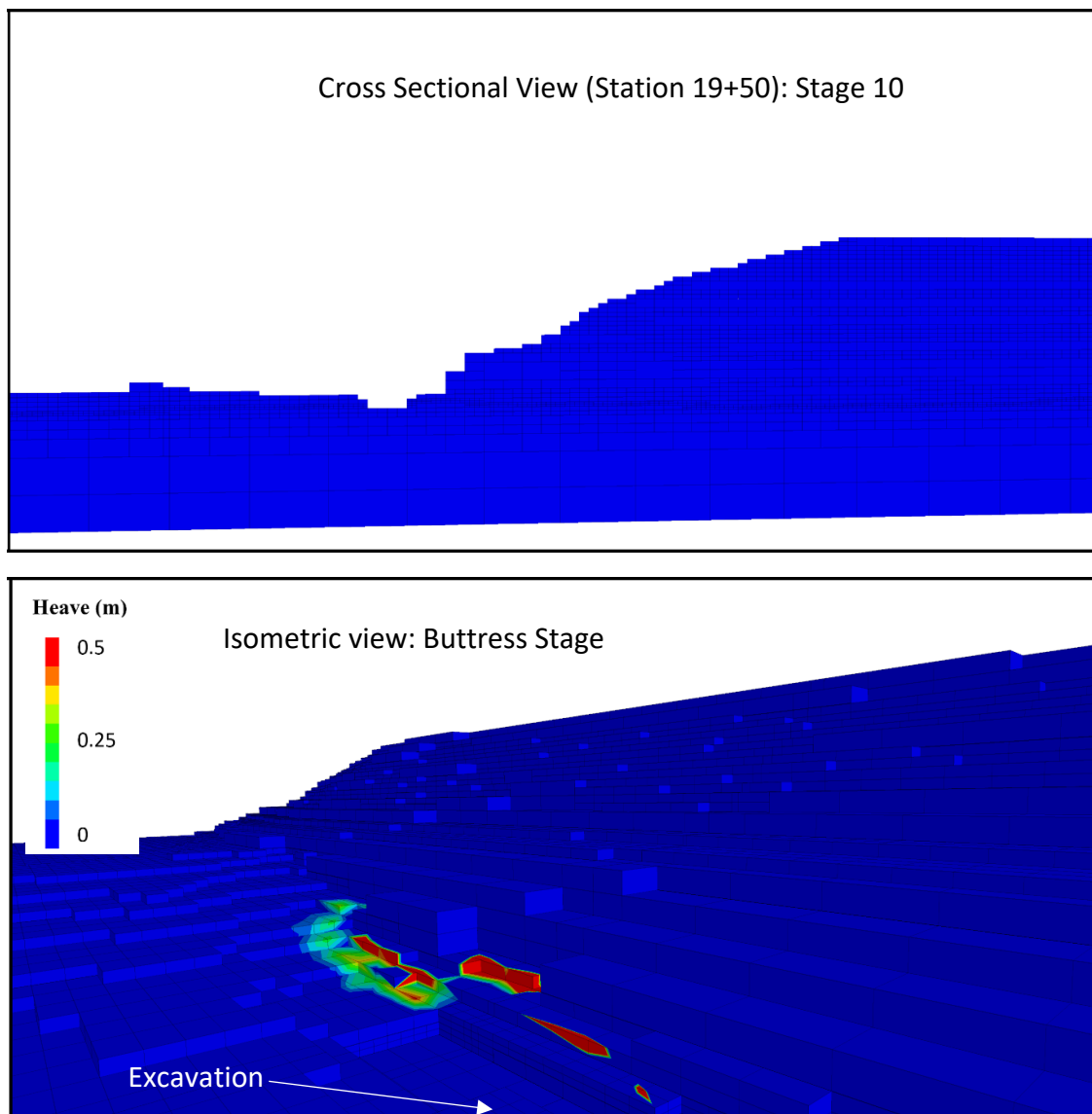


Figure 2.56 Heave Development: Tailings State Parameter = + 0.06

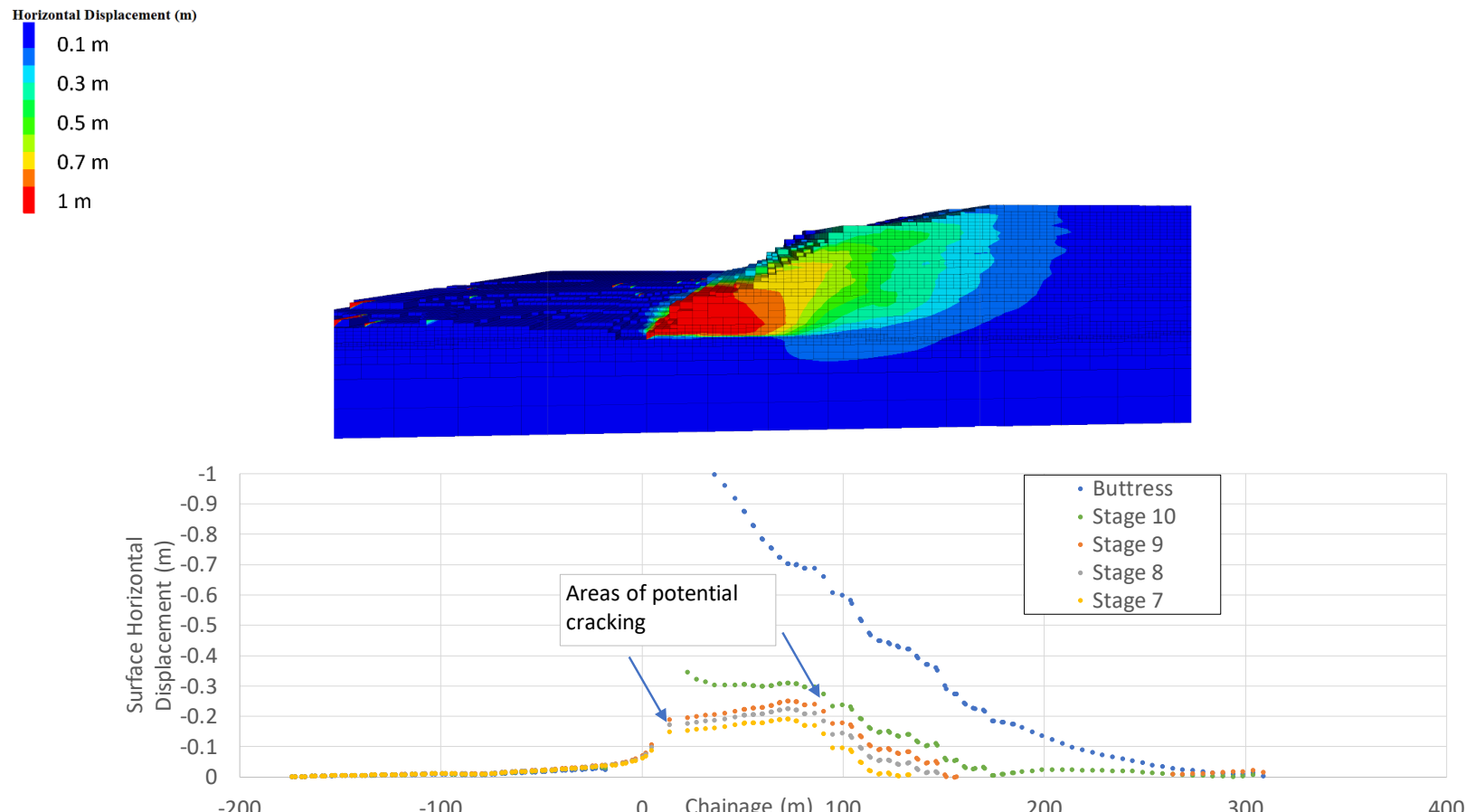


Figure 2.57 Development of Surface Horizontal Displacement: Tailings State Parameter = + 0.06

A final stage in this assessment was to compare the stress path that developed in the 3D model with that observed in the earlier 2D models to enable a comparison with the laboratory testing that was completed using the stress paths from the 2D results. This comparison is shown in Figure 2.58 for two of the monitoring points used in the 2D analysis (Point 1 and Point 3). Both of these monitoring points show that in 3D the mean effective stress increased to a higher value than in the 2D analysis before developing a reducing trend once strain weakening started to occur in the foundation; however, once strain weakening started to develop in the 3D model the direction of the reducing portion of the stress path was similar to that observed in 2D. The reason for this difference is that the strain weakening started at Stage 5 in the 2D model, but did not occur until Stage 9 or 10 in the 3D models. Because it is the strength loss in the foundation that leads to the stress reduction in the tailings, this later onset of strength reduction in the 3D model allowed the stresses in the tailings to continue increasing; however, once strain weakening occurred the resulting instability ratio would be similar to the 2D model.

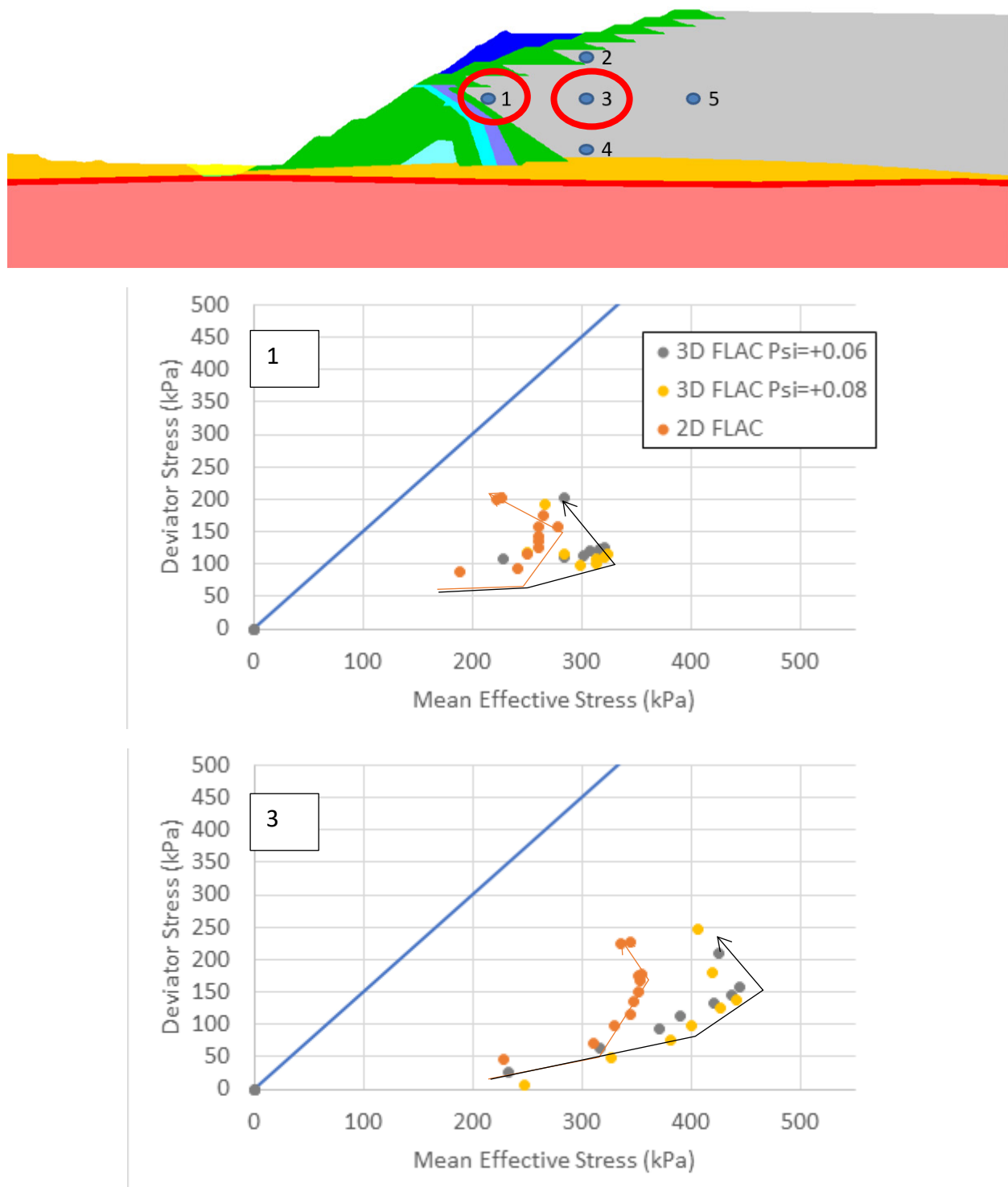


Figure 2.58 Comparison of Stress Path Development in FLAC 2D and FLAC 3D: Tailings State Parameter = +0.06

3 PHASE 2 – MODELLING POST-FAILURE RESPONSE

3.1 General

The 2D and 3D deformation modelling identified that the mechanisms occurring in the dam prior to failure likely involved a combination of ongoing yielding of the tailings, leading to stress transfer to the foundation and progressive yielding of the foundation. These mechanisms have been shown to increase the stress ratio/ instability ratio in the tailings in the region of failure and increase their susceptibility to liquefaction.

Results of the static deformation analyses have been used as inputs to laboratory testing programs to assess the degree of disturbance that would be required to cause soil with this stress state to liquefy. Separately, results from the seismic analyses have been used as inputs to laboratory tests to identify if the seismic loading could cause tailings in this state to liquefy.

The purpose of the analyses documented in this section of this report were to assess the likely effect of liquefaction on the deformation patterns to assess how the resulting failure in the model would compare with the observed failure.

3.2 2D Assessment – Mohr-Coulomb Analysis

In the first instance, the effect of liquefaction was reviewed by assigning an undrained strength to the region of tailings adjacent to the Stage 1 rockfill that was identified in the Phase 1 analyses to be affected by the yielding in the Unit A Foundation layer. Vectors illustrating the displacement pattern that would result from this mechanism are shown in Figure 3.1.

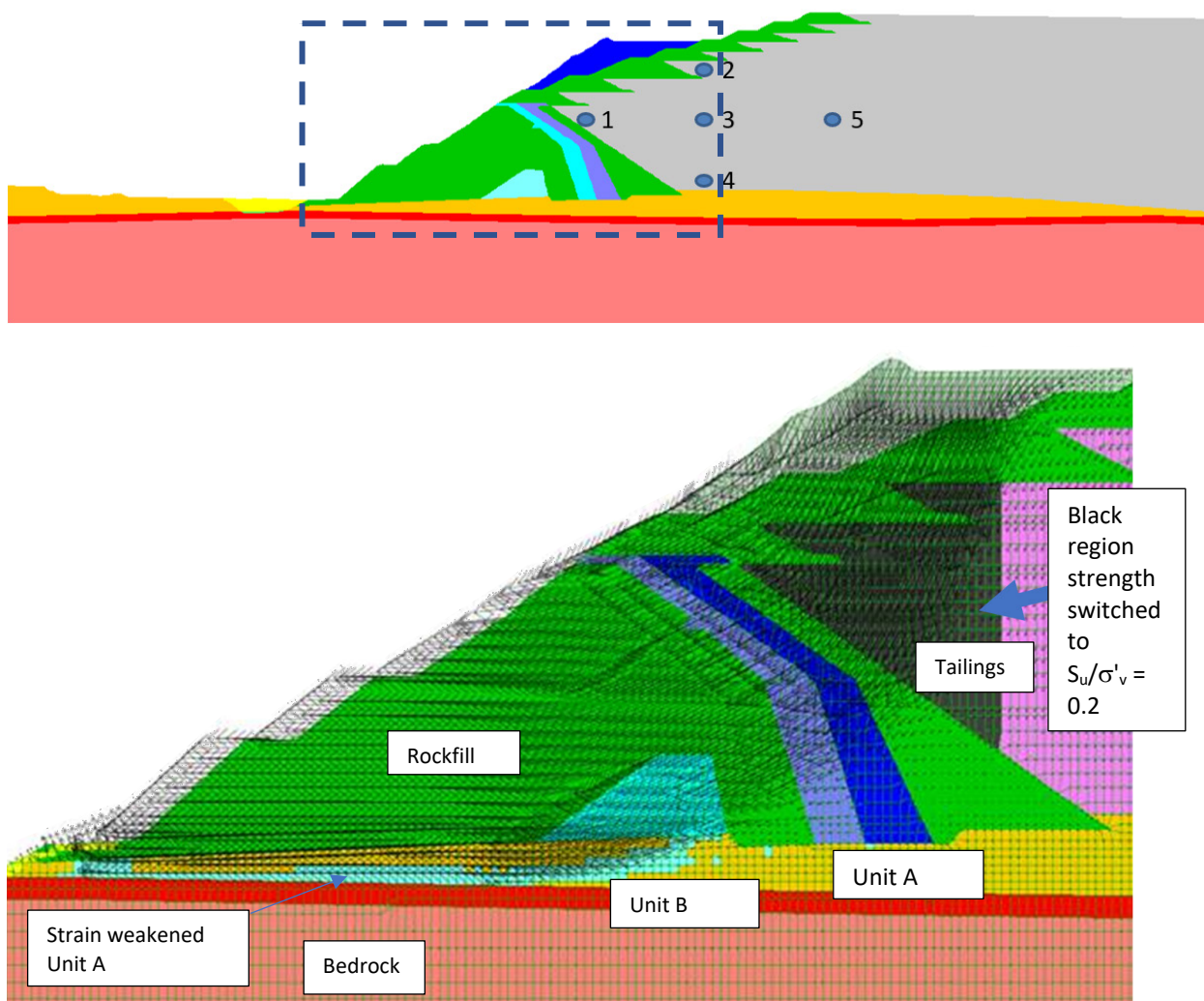


Figure 3.1 Displacement Pattern Due to Undrained Strength Mobilization in Tailings Behind the Stage 1 Embankment

Figure 3.1 shows a distinct concentration of displacements in the region of undrained strength mobilization, indicative of a slip surface developing in this region. The slip surface (i.e. zone of concentrated displacements) originates at the upstream side of the buttress and passes through the tailings and into the strain-weakened zone of the foundation. This distinct break in displacement pattern would lead to cracking of the dam surface at roughly the location where it was observed in the field and leads to a failure that is consistent with the observed mechanism. Given that this mechanism lead to results that were consistent with the failure observations, an additional analysis was completed to confirm that this is the area where undrained strengths would likely be mobilized in the tailings if the tailings were disturbed (see Section 3.2).

3.3 2D Assessment – NorSand

Given that the results of Section 3.2 showed that localized undrained strength mobilization would lead to a displacement pattern that was consistent with the field observations, the undrained

response of the tailings was reviewed using the NorSand constitutive model through the following steps:

- Enable undrained behavior of the tailings by switching the bulk modulus of the pore fluid in the tailings zones from the value of zero that was assigned throughout the drained construction loading stages to 2GPa. This change causes pore pressures to be generated during shear for any contractive tailings.
- Create a minor disturbance to the model to identify how the undrained response of the tailings would develop. In this model, this disturbance was created by extending the upstream side of the toe excavation towards the dam by removing one row of zones.
- Observing the undrained response in the tailings.

Figure 3.2 shows contours of instability ratio after running this undrained response analysis. This model did not reach numerical convergence, indicating that the model could not determine a stable solution during this analysis; however, the partial results that were obtained showed that the region of tailings immediately upstream of the Stage 1 embankment (in the region of monitoring Point 1 from the earlier analyses) would generate a very high instability ratio (> 1) and be the region most-likely to mobilize undrained strengths from a similar undrained disturbance. This analysis complements the Mohr-Coulomb analysis (Section 3.2) and indicates the area where undrained strengths were applied in that analysis is the area where these strengths were most likely to develop.

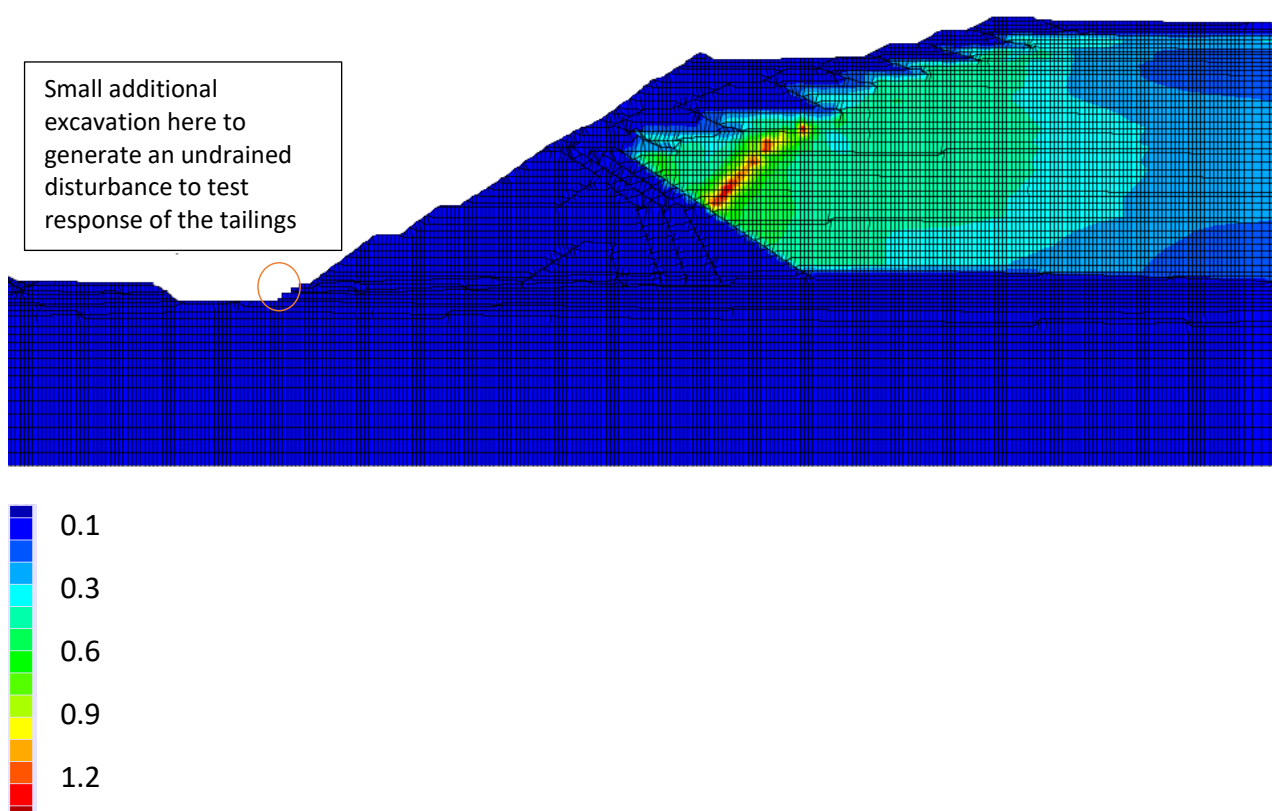


Figure 3.2 Instability Ratio Contours from Undrained Response Assessment of Tailings

3.4 FLAC 3D Post-Liquefaction Factor of Safety

As a final step to the analysis, a factor of safety calculation was completed using the 3D FLAC model for comparison with the limit equilibrium analyses and the failure runout observations. These analyses were completed by assigning an undrained strength ratio (S_u/σ'_v) of 0.22 to the Unit A Foundation layer and a liquefied strength ratio ($S_{u(liq)}/\sigma'_v$) of 0.06 to the tailings for consistency with the inputs used in separate limit equilibrium calculations completed by the ITRB. This strength ratio for Unit A is lower than the peak value of 0.24 used at high stresses in the final FLAC 3D analysis (see Figure 2.44) of Phase 1 and, therefore, represents a slightly weakened strength. The liquefied tailings strengths in this analysis were applied to the tailings upstream of the observed failure. The results of this assessment are shown Figure 3.3. These results show that if liquefaction developed in this region, the factor of safety for a slip surface of roughly the extent observed would be approximately 1 using this slightly reduced strength in the foundation. The displacement contours indicate that two slip surfaces would develop with similar factors of safety; one in the foundation and one in the tailings. Given the inter-dependency of the Unit A strength on that of the tailings and vice versa shown in the Phase 1 analyses, it can be assumed that this liquefaction triggering would have an effect of reducing the strength of the Unit A further and cause both failures to occur simultaneously.

It is of interest to note that the factor of safety calculated in this analysis was roughly equal to that calculated by the ITRB in the 3D limit equilibrium analyses, thereby demonstrating consistency between these two approaches.

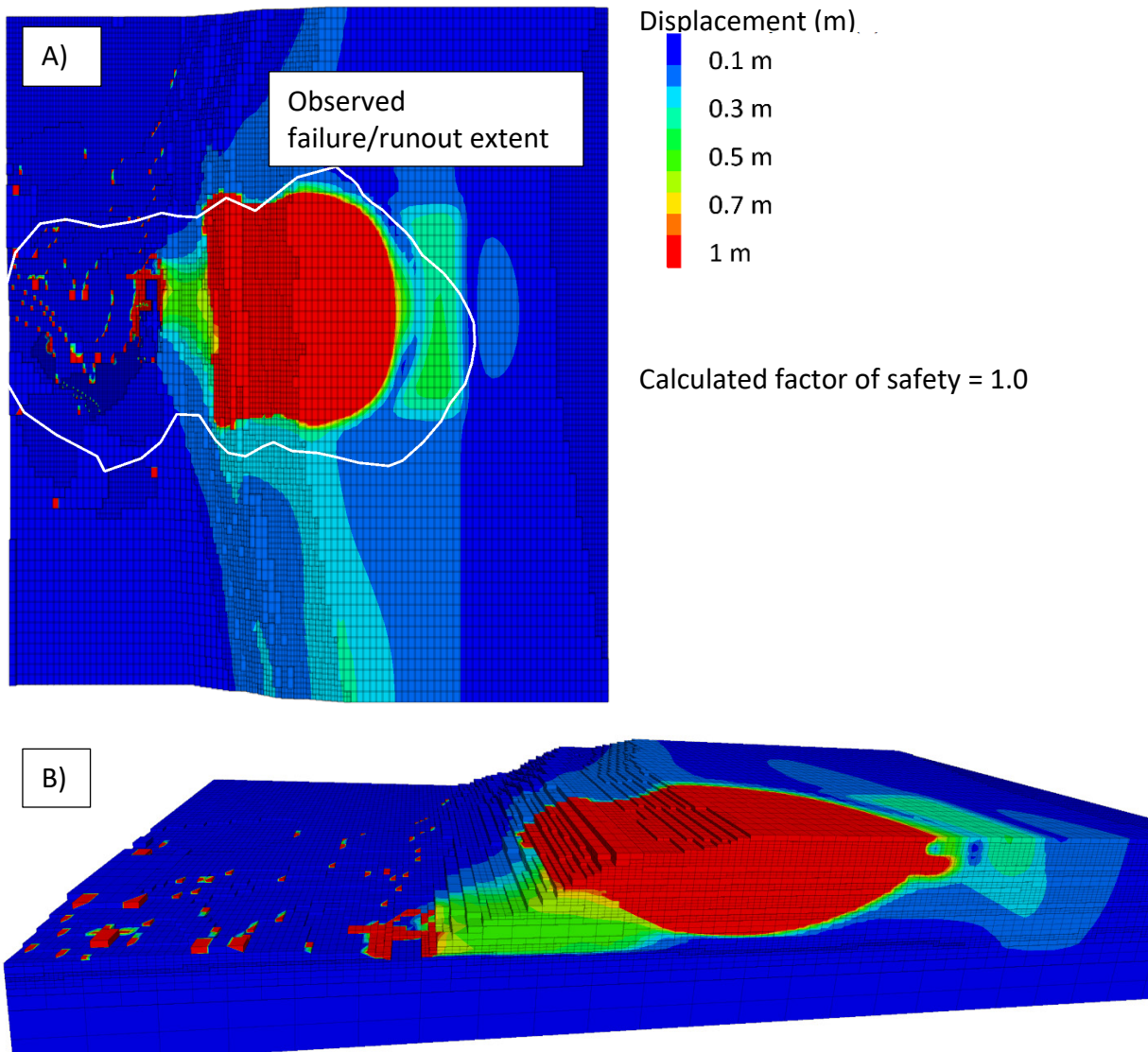


Figure 3.3 Displacement Results from the 3D Shear Strength Reduction Factor of Safety Analysis

4 SUMMARY

A series of 2D and 3D deformation analyses has been completed with the aim of replicating the field observations at the Cadia NTSF prior to failure. By replicating these displacements and honoring the field and laboratory test data it was possible to gain insight into the mechanism of the failure. The analyses were divided into two Phases: Phase 1 captured events up to the onset of failure and Phase 2 captured the post-failure response. The mechanism that provided the best match to the field observations included the following sequence of events:

- A combination of dam construction, excavation at the toe in the failure area and construction of the Stage 1 Buttress led to progressive yielding in the tailings, stress transfer to the Unit A Foundation layer and subsequent strain weakening of the Unit A layer.
- This strain weakening in the Unit A had a reciprocal effect on the tailings, leading to a reduction in confining stress in the tailings and increasing their susceptibility to liquefaction.
- Liquefaction of the tailings would lead to additional stress transfer to the Unit A Foundation layer and additional strength loss.
- This combination of strength loss in the Foundation and liquefaction of the tailings lead to a response in the model that is consistent with the observations prior to failure and the observed extent of the failure runout.

A summary of key observations from the various analysis stages is:

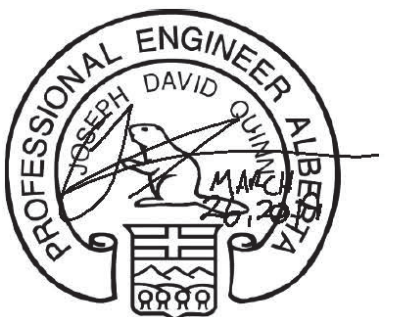
- The 2D analyses showed that it is necessary to account for strain weakening in the Unit A Foundation layer to generate representative displacements. If strain weakening develops in this unit it has an effect of causing the tailings adjacent to the Stage 1 embankment to progress along a reducing mean effective stress path. Development of this stress path would increase the liquefaction susceptibility of the tailings in this region.
- The 3D analyses showed that, because of the various stabilizing factors in 3D, the strength of Unit A would need to be lower than that used in the 2D analyses to develop a similar response. Results of sensitivity analyses showed that the strength required to generate these displacements is within the range of values from the laboratory testing.
- The 3D sensitivity analyses also highlighted the important role that the loose tailings had on developing displacements and transferring stress to the strain weakening foundation unit. These analyses showed that including strain weakening behavior in the Unit A foundation is not enough on its own to generate representative displacement; it must be combined with yielding of the tailings.
- The Phase 2 (post-liquefaction) analyses showed that mobilization of undrained strengths in the region that was following a reducing mean effective stress path in the Phase 1 analyses would lead to a pattern of displacements and failure mechanism that is consistent with the observed failure.
 - ◆ The 2D liquefaction triggering analysis using NorSand indicated that this is the zone where liquefaction was most likely to develop.

- Results of 1D and 2D seismic site response analyses were very similar to each other and showed amplification of ground motions towards the base of the tailings and close to the ground surface; nonetheless, the cyclic shear stresses generated by these ground motions were low (typically < 10 kPa).
- The stress paths and cyclic stresses identified in these analyses were used as inputs to the laboratory testing program to assess whether static or cyclic loading was most likely to have caused the undrained disturbance of the tailings adjacent to the Stage 1 embankment, leading to liquefaction of this material. These laboratory tests confirmed that the effect of the seismic loading on the tailings was negligible and that the trigger for liquefaction would likely relate to the ongoing change of stresses and displacements from the foundation weakening.

5 CLOSURE

This report is an instrument of service of Klohn Crippen Berger Ltd. The report has been prepared for the exclusive use of Newcrest Mining Ltd. (Client) for the specific application to the Cadia NTSF Slump. The report's contents may not be relied upon by any other party without the express written permission of Klohn Crippen Berger. In this report, Klohn Crippen Berger has endeavoured to comply with generally-accepted professional practice common to the local area. Klohn Crippen Berger makes no warranty, express or implied.

KLOHN CRIPPEN BERGER LTD.



Joseph D. Quinn, Ph.D., P.Geo., P.Eng
Senior Geotechnical Engineer, Associate

APEGA Permit to Practice No. P09196

REFERENCES

- Hunter, G. 2003. The Deformation Behaviour of Embankment Dams and Landslides in Natural and Constructed Soil Slopes. PhD Thesis, School of Civil and Environmental Engineering, The University of New South Wales
- Hunter, G. and Fell, R. (2002). The Deformation Behaviour of Rockfill. UNICIV Report No. R405, School of Civil and Environmental Engineering, The University of New South Wales. www.engineering.unsw.edu.au/civil-engineering/uniciv-reports
- Indraratna, B., Wijewardena, L.S.S. and Balasubramaniam, A.S. (1993). Large-scale triaxial testing of greywacke rockfill. *Geotechnique*, 43(1), 37–51.
- Leps T.M. (1970) Review of Shearing Strength of Rockfill. *Journal of the Soil Mechanics and Foundations Division*, 1970, Vol. 96, Issue 4, Pg. 1159-1170.
- Seed, H.B., Wong, R.T., Idriss, I.M., and Tokimatsu, K. 1986. Modulus Reduction and Damping factors for dynamic analysis of cohesionless soils. *Journal of Geotechnical Engineering, ASCE*, 112(11), 1016-1032
- Vucetic, M. and Dobry, R. 1991. Effect of soil plasticity on cyclic response. *Journal of Geotechnical Engineering (ASCE)*. Vol. 117, No. 1, pp. 89-117.
- Winkler, C., Davidson, R., Yenne, L. and Pilz, J. (2014). CPTu based characterization of tailings liquefaction susceptibility. Proceedings 34th USSD Annual Meeting, San Francisco, April 10th 2014. USSD, Denver Co.